THE UNIVERSITY OF HULL

Can Tufa Mg/Ca Ratios be Used
as a Palaeoclimate Proxy?

being a Thesis submitted for the Degree of

Doctor of Philosophy

in the University of Hull

by

Paul Saunders
BSc (Hons) PGcert MSc

July 2012

Abstract

The reliability of the $(Mg/Ca)_{calcite}$ palaeotemperature proxy requires that the partitioning of Mg^{2+} into the calcite deposit be controlled by thermodynamics. The $(Mg/Ca)_{calcite}$ ratios of marine carbonates have proven to be effective archives of past sea surface temperatures. In a freshwater setting the use of $(Mg/Ca)_{calcite}$ ratios has been less convincing. This could be due to the presence of microbial biofilms whose metabolic processes and secretory products such as extracellular polymeric substances (EPS) may be able to alter the Mg/Ca ratio of the precipitating solution. Tufas are a freshwater carbonate generally deposited in streams fed by waters from a limestone aquifer. They have been proposed as a potential source of high resolution palaeotemperature data due to their annually laminated structure. A series of laboratory experiments were conducted at temperatures of $12 - 20$ °C to determine whether the presence of microbial biofilms and/or isolated EPS would override the expected thermodynamic control on Mg^{2+} partitioning into freshwater calcite. Additional experiments examined the role of varying concentrations of isolated EPS and also salinity variations on calcite precipitation rate and its $(Mg/Ca)_{calcite}$ ratios.

The results reveal that in the presence of a living biofilm, $(Mg/Ca)_{calcite}$ values in a freshwater setting are not thermodynamically controlled. Mg/Ca ratios of the solution at the precipitating surface appear to be strongly influenced by the chemoselective chelation of Ca^{2+} over Mg^{2+} by anionic functional groups within the EPS resulting in the precipitation of low $(Mg/Ca)_{calcite}$ at faster precipitation rates. Precipitates generated in the presence of isolated EPS exhibited the expected thermodynamic control on Mg^{2+} partitioning in the temperature range of $12 - 18$ °C. At 20 °C it appears that precipitation rate is the dominant control. These results strongly suggest that it is microbial metabolism, rather the mere presence of EPS molecules that causes the thermodynamic control in Mg^{2+} partitioning to be overridden. The results also confirm that salinity variations are significantly correlated with $(Mg/Ca)_{calcite}$ ratios when organic molecules are present and that increasing amounts of EPS acts as an inhibitor to calcite precipitation.

The results described here indicate that freshwater tufa $(Mg/Ca)_{calcite}$ ratios are not a reliable source of high resolution palaeotemperature data.

Acknowledgements

I would firstly like to thank my supervisors from the department of chemistry, Dr Jay Wadhawan and Professor Gillian Greenway for their assistance throughout the project and for their valuable advice on analytical approaches. I am extremely appreciative of my supervisor in the department of Geography, Dr Martyn Pedley for his continual advice on experimental design and all aspects of tufas. I am especially grateful to my lead supervisor Dr Mike Rogerson for his academic advice and assistance in the many phases of the experimental design and also for his patience and support when things weren't going well! I also thank Dr John Adams, who although not my supervisor, offered support and advice on the biological aspects of the project. I gratefully acknowledge the funding granted to me through the University of Hull's 80th anniversary scholarship scheme.

I am very grateful to the technical staff of the department of Geography, Mark Anderson and Mike Dennett for their advice and assistance throughout the project. I would also like to thank Bob Knight from the department of chemistry for teaching me how to operate the ICP – OES instrument and for granting me ready access to it at unsociable hours. I am very appreciative of the company and support given to me by Biccie and Miccie, you've been fantastic! I would never have started a career in academia had it not been for the fact, that at work one day, a friend showed me a textbook from an Open University course he was undertaking. I was so impressed I signed up for a degree with the Open University and so began the long journey to the submission of this PhD thesis. I thank Tim Cross for showing me that text book. My most sincere thanks go to my wife, without her continuous encouragement and emotional support I would never have reached the end of the project. Words cannot describe how amazing you have been throughout this process, thank you!

This work is dedicated to both my mother in law, Patricia Jones and to my father Vic Saunders who both sadly passed away before this PhD was completed.

List of abbreviations

BFD	Biofilm in the dark
BFL	Biofilm exposed to light
CLSM	Confocal scanning laser microscopy
DBL	Diffusive boundary layer
DIC	Dissolved inorganic carbon
EDTA	Ethylenediamine tetraacetic acid
EDX	Energy dispersive X-Ray
EPS	Extracellular polymeric substances
FISH	Fluorescence in situ hybridization
ICP – MS	Inductively coupled plasma mass spectrometry
ICP – OES	Inductively coupled plasma optical emission spectroscopy
LOD	Limit of detection
PCP	Prior calcite precipitation
PWP	Plummer-Wigley-Parkhurst rate equation
RF	Radio frequency
RSD	Relative standard deviation
SEM	Scanning electron microscopy
SI	Saturation index
SRB	Sulphate reducing bacteria
TEA	Terminal electron acceptor
TIMS	Thermal ionization mass spectrometry
UHQ	Ultra high quality

Table of Contents

List of Figures

Figure 2.10 A model for biofilm development. Plankton cells (1) approach and attach to a surface (2). Through interaction with the substratum with a pole, cells become reversibly attached (3). Cells become laterally attached (4). During this time, the attachment of cells begins to create a two-dimensional biofilm (5). The biofilm grows in thickness as more cells are incorporated. Extracellular polysaccharides and other substances are produced, resulting in more firmly attached cells with an extracellular matrix. The architecture of the biofilm may be modified by production of surfactant and release of cells (6). In response to environmental or physiological stimulants, cells may be released from the matrix and return to the planktonic state,

List of Tables

1 Rationale and aims

1.1 Rationale

The increasing level of concern regarding anthropogenically induced climate change, not only amongst the scientific community but also within the media, public and political arenas has resulted in a substantial increase in the amount of research conducted on climate related issues (Burroughs, 2001). Research on climate change relies heavily on computer models in which a number of variables can be altered to see what effect they have on future global mean surface temperatures (Wilson *et al*., 2000). Before the results of these models can be viewed with any degree of certainty they need to be tested against known scenarios, this requires high quality and highly resolved palaeoclimate data. Instrumental records of climate data only extend to 150 years before present, though anecdotal observations of previous crop types and the extent of lake and river freezing can extend climate estimates to about 1500 before present (Wilson *et al*., 2000). Before this time it is necessary to use climatically relevant "proxy" records archived within natural settings. A proxy can be considered as a quantity which can be measured from a natural archive (Henderson, 2002), examples being tree ring widths in fossil trees and the chemical composition of gases trapped in ice cores.

Increasingly, chemical measurements are being exploited as climate proxies in a variety of settings, notably the ocean (Henderson, 2002). For example, the substitution of magnesium into the lattice of calcite is dependent on temperature (Mucci and Morse, 1983). There are several calibrations of the $(Mg/Ca)_{calcite}$ palaeothermometer in the marine environment including planktonic foraminifera (e.g. Nurnberg *et al*., 1996, Anand *et al*., 2003, Regenberg *et al*., 2009), benthic foraminifera (e.g. Rosenthal *et al*., 1997, Martin *et al*., 2002, Elderfield *et al*., 2006) and corals (e.g. Mitsuguchi *et al*., 1996, Wei *et al*., 2000, Reynaud *et al*., 2007). The success of $(Mg/Ca)_{calcite}$ palaeothermometry in the marine setting has not thus far been matched by that in a freshwater setting. The study of $(Mg/Ca)_{calcite}$ ratios in speleothems (cave calcite deposits e.g. stalagmites and stalactites) was initially seen as a potential source of palaeotemperature data (Fairchild and Treble, 2009).

However, the realisation that factors such as variations in drip water trace element composition, drip rate and prior calcite precipitation (PCP) along the flow path (Gascoyne, 1983, Fairchild *et al*., 2006, Wong *et al*., 2011) may also exert a significant control over the trace element ratios of cave carbonates has made it difficult to isolate the temperature induced component on speleothem $(Mg/Ca)_{calcite}$.

Tufa carbonates are ambient temperature freshwater deposits that are generated under the influence of flowing stream waters. Given that tufas are precipitated under the ambient temperatures of the time it is reasonable to assume that any temperature controlled trace element ratios such as $(Mg/Ca)_{calcite}$ held within fossil tufas will reflect the temperature at the time the deposit was precipitated. To date very few studies have investigated the potential of $(Mg/Ca)_{calcite}$ in tufas as a palaeothermometer. Its potential was first realised when a study by Chafetz (1991) showed that the incorporation of Mg^{2+} into tufas deposited in the summer was found to be higher than in winter. Additionally, a seasonal temperature change in stream water of ~ 10 °C appeared to be the dominating influence on Mg^{2+} incorporation into a 14 year (1985 – 1999) tufa record from Queensland Australia (Ihlenfeld *et al*., 2003).

A potential and serious complicating factor in freshwater $(Mg/Ca)_{calcite}$ palaeothermometry is the presence of benthic microbial biofilms in the stream waters. Studies are beginning to show that both the metabolism and secretory products of the microorganisms within the biofilm may exert a significant control on trace element incorporation in tufas (Rogerson *et al*., 2008) and as such may mask the expected thermodynamic control on tufa $(Mg/Ca)_{calcite}$.

1.2 Thesis aims

This thesis has the following main aims:

1) To develop a microcosm environment in which freshwater calcite can be precipitated under controlled temperatures from a solution with a constant Mg/Ca ratio and in the presence of a biofilm that contains no contaminating calcite. The developed method will be used to determine

whether it is possible to derive an $(Mg/Ca)_{calcite}$ palaeothermometer calibration equation for tufa carbonates

2) To investigate the role of biofilms in tufa precipitation with respect to both precipitation rates and $(Mg/Ca)_{calcite}$ ratios under varying environmental conditions

3) To determine the specific impact of isolated microbial extracellular polymeric substances on calcite precipitation rates and $(Mg/Ca)_{calcite}$ ratios under varying environmental conditions.

4) To investigate the influence of salinity variations on precipitation rate and $(Mg/Ca)_{calcite}$ ratios both in the presence and absence of isolated microbial extracellular polymeric substances.

1.3 Thesis outline

Chapter 2 outlines the background to this project including a summary of $(Mg/Ca)_{calcite}$ palaeothermometry in other carbonate deposits along with a description of the mechanisms behind carbonate precipitation. It also describes the theory behind partition coefficients and the thermodynamic principles that control the partitioning of magnesium into calcite. Microbial biofilms are discussed along with a review of extracellular polymeric substances and their ability to chelate cations.

Chapter 3 describes the generic (i.e. non original) methods used throughout the project.

Chapter 4 details the experimental design along with a description of the methods used in extracting the samples for analysis. Supporting evidence obtained analytically is presented and discussed which highlights the effectiveness and validity of the method development.

Chapter 5 presents the results from the experiments in which calcite was precipitated under multiple ambient temperatures in the presence of biofilm in both a flow through and agitated flask environment. The influence of biofilms on the results is discussed.

Chapter 6 describes the results of experiments where calcite was precipitated in the presence of isolated extracellular polymeric substances of both a constant and varying concentration in the solution. The impact of salinity on precipitates generated in both the absence and presence of extracellular polymeric substances is examined. The impact of extracellular polymeric substances on $(Mg/Ca)_{calcite}$ and its consequences for tufa $(Mg/Ca)_{calcite}$ palaeothermometry is discussed.

Chapter 7 presents the results of the systematic sampling of a Welsh Holocene tufa sample for the trace element ratios (Mg/Ca) and (Sr/Ca). The ratios are examined in relation to the different coloured laminations within the sample.

Chapter 8 provides a summary of the work and describes the opportunities for further studies based on the results of this work.

Chapters 5, 6 and 7 are presented in the format of journal articles with individual sections for the abstract, introduction, results, discussion and conclusion.

2 Background and literature review

2.1 Introduction

This chapter will begin with an introduction to tufas, their geological setting and a basic description of the main precipitation mechanisms. A brief overview of some related carbonate deposits is also given. Microbial biofilms and extracellular polymeric substances are described individually and then related to the chelation of cations and precipitation of calcite. The background chemistry is described in sections on thermodynamics, activity coefficients and solubility products. An overview of trace element partition coefficients is followed by a section on $(Mg/Ca)_{calcite}$ palaeothermometry in relation to foraminiferal calcite, corals, speleothems and tufas. Finally, the impact of salinity on $(Mg/Ca)_{calcite}$ in foraminiferal calcite is discussed.

2.2 Tufas: a definition

The term 'tufa' is believed to have been in use in Great Britain since before the 12th century when it was used to describe both volcanic ash and poorly consolidated freshwater carbonates (Pentecost and Viles, 1994). In modern times its usage has generally been restricted to describing ambient temperature freshwater carbonates (Pedley, 1990). Recent definitions of the term 'tufa' describe it as a highly porous freshwater carbonate formed in cool waters, being rich in microphytic and macrophytic growths as well as leaves and woody tissue (Pedley, 1990), and a calcium carbonate deposit precipitated in ambient but cool waters and which commonly contains the remains of bacteria, invertebrates and micro and macrophytes (Ford and Pedley (1996). The cool water and porous aspects of the definition are also emphasised by other researchers (Zhang *et al*., 2001 and Andrews, 2005).

The use of the term tufa as defined above is not unanimous. The term travertine has been used to describe all freshwater carbonate deposits on plant debris, making no reference to the degree of cementation or precipitation temperature (Julia 1983). However, travertines are frequently differentiated from tufas by two factors, the degree of cementation (Pedley, 1990, Pentecost and Viles, 1994, Ford and Pedley, 1996) and the temperature at which precipitation occurs, (Ford and Pedley, 1996,

Janssen *et al.,* 1999, Andrews, 2005, Boch *et al.,* 2005), with travertine being used for carbonates precipitated under hydrothermal conditions and tufa for those originating under ambient conditions. Additionally, the term travertine has been used to describe precipitation that occurs across a range of temperatures from ambient to near boiling (Chafetz *et al*., 1991). Pentecost (2005) uses the term travertine for all fluvial and lacustrine carbonates but makes sub-distinctions based on temperature. It has been proposed that the terms tufa and travertine can, to a certain extent, be considered interchangeable, describing any distinction between the two as being dependant on the degree of cementation (Pentecost and Viles, 1994). The classification of these deposits clearly requires further refining, but this is beyond the scope of this thesis. Here I follow Pedley *et al.,* (2003, p24) in defining the term 'tufa' as *"...a calcium carbonate deposit, regardless of crystallinity, which has developed under ambient temperature conditions by biomediation and/or physico-chemical processes associated with freshwater discharge."*

2.3 The geological setting of tufas

Tufas are worldwide deposits that develop under the influence of flowing freshwater and their distribution reveals a predominantly late Cenozoic development. Their deposition progressively increased towards the start of the Pleistocene and since this time they have become common deposits during humid episodes and in the Holocene (Ford and Pedley, 1996). Tufa deposits can be extremely localised such as at waterfalls and springs or spread over wide expanses several kilometres in length where lithofacies vary from loose and thinly laminated lime mud deposits to well cemented massive fluvial barriers (Ford and Pedley, 1996). Various growth rates of tufa have been recorded ranging from 0.13 mm a^{-1} (Preece and Day, 1984) to 10 mm a^{-1} (Pazdur *et al*., 1988), however it has been pointed out that the studied profiles may include surfaces of erosion and omission so growth rates may have been substantially greater (Gradzinski, 2010).

In a wider context tufas form part of a group of carbonate deposits known as microbialites. These are organosedimentary deposits which have built up as a result of benthic microbial communities trapping and binding detrital sediment and/or forming the locus of mineral precipitation (Burne and Moore, 1987). Konhauser (2007) uses the phrase *"lithified carbonate bioherms"* as being synonymous with the

term microbialite. These deposits have been an important part of carbonate sediments since the Archaean (3.8 – 2.5 Ga) and are most widely known in the geological record as marine and lake deposits, though they also present an important record in recent fluvial, spring, cave and soil environments (Riding, 2000). In all these settings, when microbialites produce laminated structures they are termed "stromatolites" (Pringault *et al.*, 2004). Geologically, microbialites can range from being the dominant component in rock units such as reefs, to being relatively minor constituents of algal dominated reefs and of allochthonous sediments (Riding, 2000).

Four important processes have been identified as being involved in the formation of calcareous microbialites; 1) trapping and binding of detrital sedimentary particles, 2) biologically influenced calcification, divided by Riding (2000) into cyanobacterial calcification, extracellular polymeric substances (EPS) calcification, other bacterial calcification, organomineralisation and whiting precipitation, 3) skeletal calcification and 4) inorganic calcification (Burne and Moore, 1987). However, many microbialites have a mixed genesis, with the relative importance of each process in the formation of an individual microbialite determining the final composition (Burne and Moore, 1987). The interplay of these processes is controlled by the environmental setting in which precipitation is occurring, the result of which is that deposits are heterogeneous, frequently containing trapped particles, *in situ* invertebrates and algae (Riding, 2000). However, they are generally dominated by micrite, a fine grained lithified lime mud of 1-5μm crystals of calcium carbonate (Konhauser, 2007).

The large scale morphology of carbonate deposits is similarly dependent on the environmental settings, the most important of which include shallow marine environments, hypersaline lakes, caves, ambient temperature rivers and geothermal environments. Secondary factors that influence morphology include depth of formation, sedimentary processes and the diversity and complexity of microbial communities (Laval *et al.*, 2000).

2.4 Carbonate geochemistry

By definition carbonate rocks must consist of at least 50% carbonate minerals of which there are six with the same principle composition, calcite, aragonite, vaterite,

calcium carbonate monohydrate, calcium carbonate hexahydrate and amorphous calcium carbonate (Mann, 2001) (Table 2.1). Volumetrically, the most important are calcite ($CaCO_3$), dolomite ($Ca.Mg(CO_3)_2$) and aragonite ($CaCO_3$) (Tucker and Wright, 1990).

Table 2.1 Formulae, crystal system and density of carbonate minerals.

Mineral	Formula	Crystal system	Density (g cm^{-3})
Calcite	$CaCO_3$	Trigonal - rhombohedral	2.71
Aragonite	$CaCO_3$	Orthorhombic	2.94
Dolomite	$(CaMg)(CO_3)_2$	Trigonal - rhombohedral	2.85
Vaterite	$CaCO_3$	Hexagonal	2.54
Calcium carbonate monohydrate	$CaCO_3$	Trigonal – hexagonal	2.38
Calcium carbonate hexahydrate	$CaCO_3$	Monoclinic	1.8
Amorphous calcium carbonate	$CaCO_3$		

The carbonate group (CO_3^{2-}) is the basic structural unit common to all carbonate minerals. It consists of three oxygen atoms making up the corners of an imaginary equilateral triangle with a carbon atom at its centre (Figure 2.1) (Tucker and Wright, 1990).
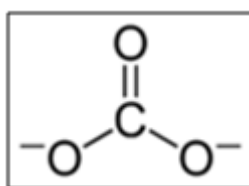
Figure 2.1 Lewis structure of CO$_3^{2-}$

The structural unit of the carbonate ion is strong due to the short C – O bonds, these bonds are stronger than the metal – O (M^{2+} – O) bonds found in any carbonate mineral. The trigonal-rhombohedral crystal structure of calcite is shown in Figure 2.2.
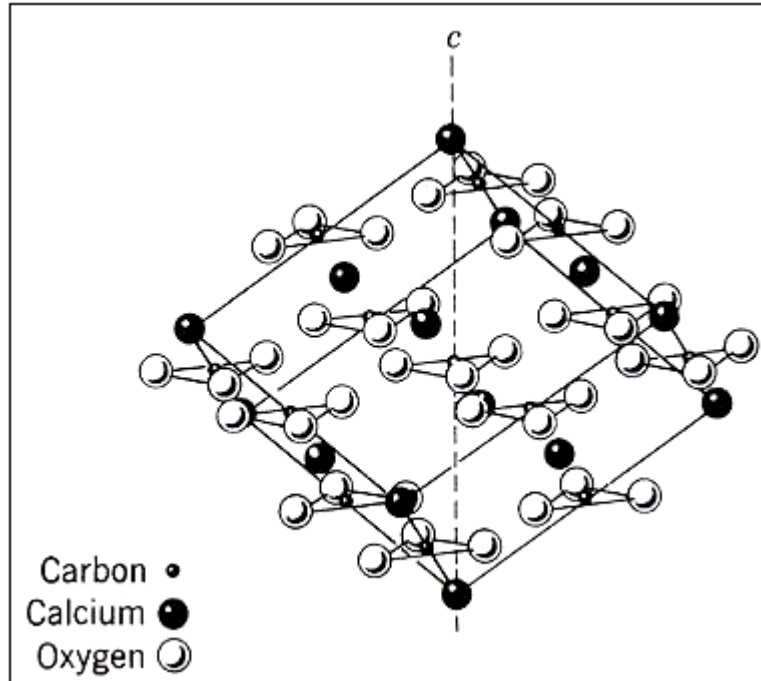
Figure 2.2 Crystal structure of calcite (Hurlbut and Klein, 1977).

The calcite structure consists of alternating layers of CO_3^{2-} ions and Ca^{2+} cations with each Ca^{2+} cation being coordinated with six oxygens from different CO_3^{2-} anions. Each oxygen of the carbonate group is bonded to two Ca^{2+} cations and one carbon from adjacent cation layers (Tucker and Wright, 1990).

2.4.1 Carbonic acid system

One of the most important aspects of carbonate mineral precipitation is the carbonic acid system which includes the ions carbonate and bicarbonate (CO_3^{2-} and HCO_3^-), undissociated carbonic acid (H_2CO_3) and dissolved carbon dioxide ($CO_{2(aq)}$) (Morse and Mackenzie, 1990). Carbonic acid arises from the dissolution of carbon dioxide gas in water, which dissociates to give the dissociation products of a hydrogen ion (H^+) and a HCO_3^- ion, which itself dissociates to the products H^+ and CO_3^{2-}. This series of reactions is summed up by the chemical equation (2.1)

$$CO_{2(aq)} + H_2O_{(l)} \rightleftarrows H_{(aq)}^+ + HCO_3^-{}_{(aq)} \rightleftarrows H_{(aq)}^+ + CO_3^{2-}{}_{(aq)} \qquad (2.1)$$
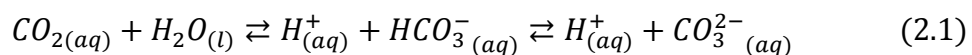
Dissolved CO_2 achieves a state of dynamic equilibrium between its atmospheric concentration and the concentration that is partitioned between the three dissolved carbon compounds of H_2CO_3, HCO_3^- and CO_3^{2-}, which together are known as the

total dissolved inorganic carbon (DIC). The hydrogen ion is an integral part of the reactions between the DIC compounds and this highlights the important role that the carbonic acid system plays in determining the pH and buffering ability of natural waters (Morse and Mackenzie, 1990).

The concentrations of carbonate species in solution is determined by the pH of the solution, the fraction of carbonate species H_2CO_3, HCO_3^- and CO_3^{2-} with respect to solution pH values is shown in Figure 2.3
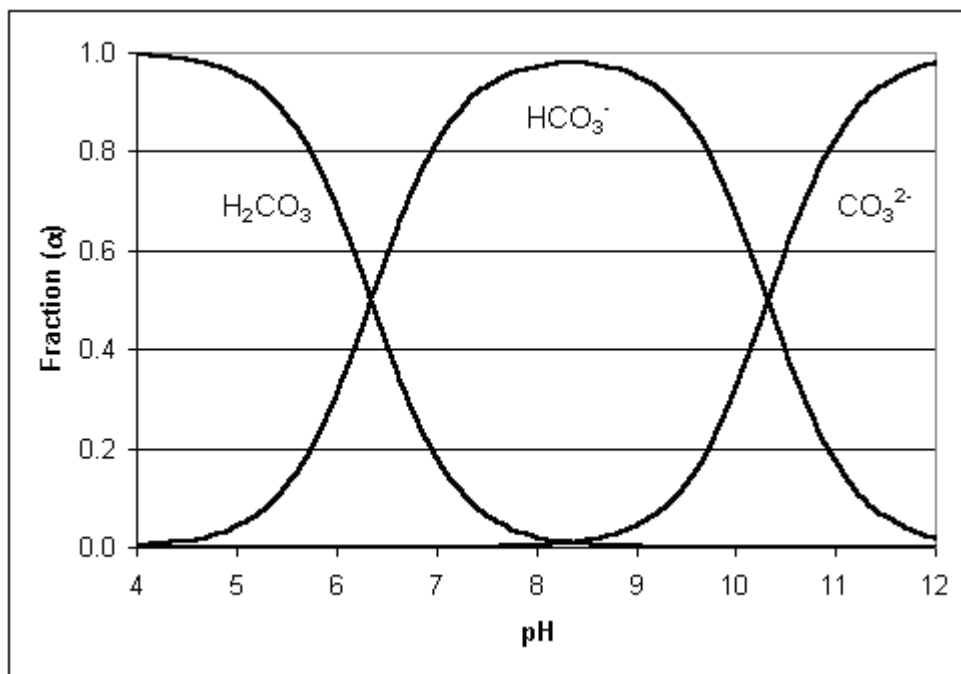
Figure 2.3 Distribution of carbonate species in aqueous solution against pH of the solution at 25 °C (Bosnich, 2012).

The water in most natural fluvial environments has a pH value between 6 and 8.5 (Suarez, 1983) and from Figure 2.3 it can be seen that HCO_3^- will be the predominant carbonate ion in these environments.

2.5 Carbonate precipitation

The precipitation of a substance occurs when the system is saturated with respect to that substance and will continue until a state of equilibrium is achieved. Calcium carbonate precipitation is dependent on both Ca^{2+} availability and carbonate alkalinity which both impact on the saturation index (SI) of the water mass. The tendency to precipitate from a supersaturated solution may be inhibited by kinetic

10

constraints on nucleation (Mann, 2001). Nucleation is divided into two types, homogeneous and heterogeneous. In homogeneous nucleation there is a spontaneous nucleation from the bulk solution. This occurs through the formation of clusters of molecules which become enlarged via continued accretion until they become crystals and settle out of the solution. Homogeneous nucleation rarely occurs in natural systems due to the high energy barrier, it requires a saturation index > 1.5 (Ford and Williams, 2007). Heterogeneous nucleation takes place on the surface of a substrate in the solution, the activation energy is reduce by the presence of the substrate and as a consequence, significant precipitation may begin at a saturation index of 0.3 (Ford and Williams, 2007). Therefore, in geochemical systems nucleation is predominantly heterogeneous (Misra, 2012). The precipitation of calcite is expressed in the balanced equation (2.2):

$$Ca^{2+}{}_{(aq)} + 2HCO_3^-{}_{(aq)} \rightarrow CaCO_{3(s)} + CO_{2(g)} + H_2O_{(l)} \qquad (2.2)$$
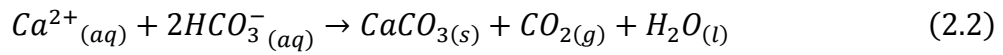
The solubility product of calcite ($K_{sp(calcite)}$) is calculated from equation (2.3) (Misra, 2012):

$$K_{sp(calcite)} = \alpha_{Ca^{2+}} a_{CO_3^{2-}} = \left(c_{Ca^{2+}}\gamma_{Ca^{2+}}\right)\left(c_{CO_3^{2-}}\gamma_{CO_3^{2-}}\right) = 10^{-8.48} \qquad (2.3)$$

where $\alpha_{Ca^{2+}}$ and $a_{CO_3^{2-}}$ represent the activities of Ca^{2+} and CO_3^{2-} respectively. The terms c and γ represent the molar concentrations and activity coefficients of the respective ionic species. The solubility product leads to a definition of a saturation index which is defined by:

$$SI = log_{10} \frac{\left(c_{Ca^{2+}}\gamma_{Ca^{2+}}\right)\left(c_{CO_3^{2-}}\gamma_{CO_3^{2-}}\right)}{10^{-8.48}} \qquad (2.4)$$

A more detailed treatment of these issues is given in sections 2.15 and 2.16.

Three main ideas have been highlighted as the dominant controls on precipitation rates in the system $H_2O - CO_2 - CaCO_3$ (Liu and Dreybrodt, 1997, Ford and Williams, 2007):

- The kinetics at the mineral surface which is given by the Plummer-Wigley-Parkhurst rate equation (PWP) (see below) of Plummer *et al.,* (1978)

- The conversion of HCO_3^- and H^+ to CO_2 due to the stoichiometric requirement that the amount of calcite precipitated must be balanced by the CO_2 that is released.

- The molecular diffusion of the reacting solutes including HCO_3^-, Ca^{2+} and H^+ to and from the mineral surface across a chemical or diffusive boundary layer (see section 2.6) which separates the mineral from the bulk solution.

Although originally derived to describe dissolution rates the PWP equation is believed to be valid for precipitation if the solution is sufficiently distant from equilibrium with respect to calcite (Dreybrodt *et al.*, 1996). The equation is:

$$R = k_1[H^+] + k_2[H_2CO_3^*] + k_3 - k_4[Ca^{2+}][HCO_3^-] \qquad (2.5)$$

Where k_1, k_2, k_3 and k_4 are temperature dependant rate constants and the brackets indicate activities.

2.6 The diffusive boundary layer

Calcite precipitation and dissolution both involve the mass transport of solutes to and from the mineral surface across a diffusive boundary layer (DBL) (Liu *et al.*, 1995, Pentecost, 2005) and this is achieved entirely by molecular diffusion, which is governed by Fick's first law of diffusion; which for one dimensional transport is:

$$J_i \,(diffusion) = -D_i \frac{\delta C_i}{\delta x} \qquad (2.6)$$

where D_i (cm^2 s^{-1}) is the diffusion coefficient and $\delta C_i/\delta x$ the concentration gradient of species *i*. The diffusion coefficient is temperature dependant and generally increases with increasing temperature (Misra, 2012) and is expressed as:

$$D_i = A_D e^{-E_D/RT} \qquad (2.7)$$

where A_D (cm^2 s^{-1}) is the *frequency factor* (which is normally a constant for a diffusing species in a given medium), E_D is the *activation energy of diffusion* (kJ mol^{-1}) for species i and T is the temperature (K). The values of D for Ca^{2+} and Mg^{2+} in water (at 25 °C) are 7.93 and 7.05 cm^2 s^{-1} respectively (Misra, 2012).

The thickness of the diffusive boundary layer varies inversely with water flow velocity but can range from a single molecule to millimetre order thicknesses (Santschi *et al.*, 1983). Therefore faster flow velocities should lead to faster precipitation rates due to the thinning of the DBL as solute transport time from the bulk water to the solid surface will be reduced. However, the rate of diffusion of ions through the DBL is generally orders of magnitude lower than the rate of turbulent or advective transport in the bulk water; therefore the DBL effectively acts as a bottleneck between the bulk water and the solid surface (Brand *et al.*, 2009). A simplified schematic representation of the DBL is shown in Figure 2.4.
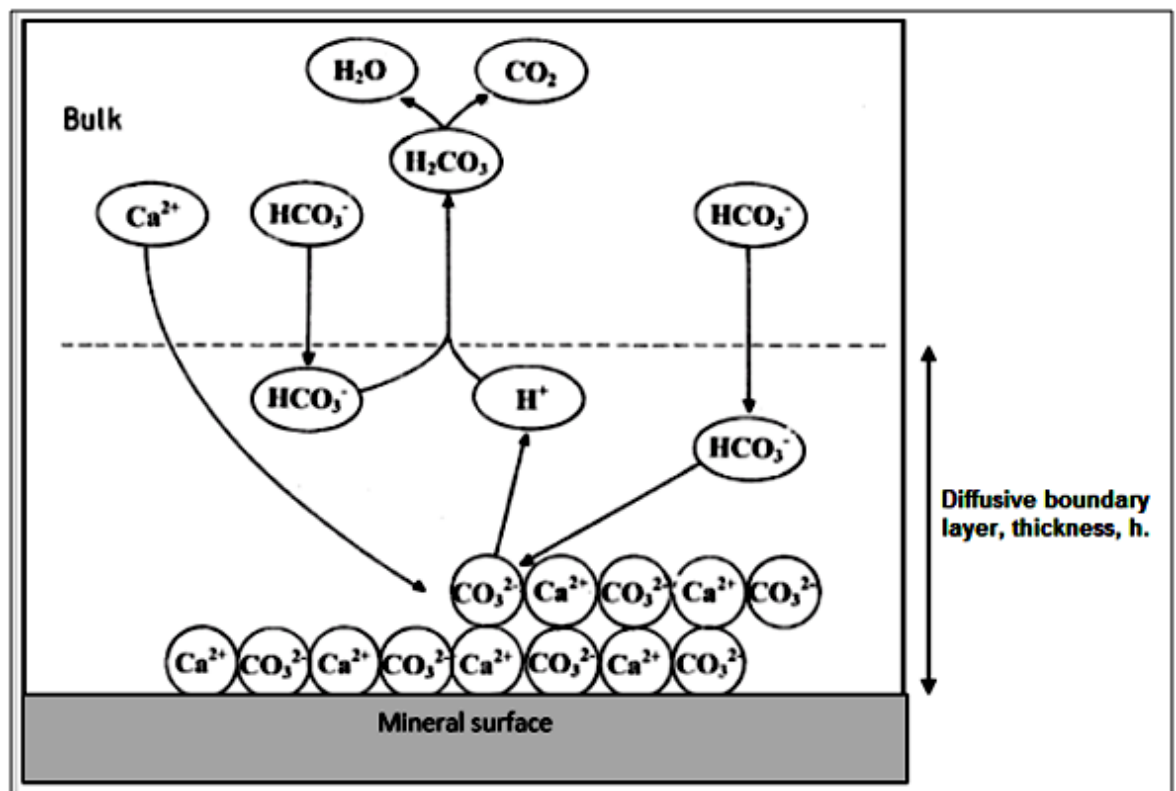
Figure 2.4 Diffusive transport of ions from the bulk water to the crystal surface across the diffusive boundary layer (adapted from Pentecost, 2005).

The bottle neck effect described above will act as a rate limiting step in calcite precipitation rates. Although the PWP rate equation (2.5) is the most widely accepted (Dreybrodt *et al*., 1997), its use can lead to serious errors in calculated precipitation rates if the concentrations used were obtained from the bulk solution, as the activities in the equation relate to those at the calcite surface and not the bulk water (Liu *et al*., 1995). Diffusion across the DBL can cause the activities of the species Ca^{2+}, H_2CO_3, HCO_3^- and H^+ to be significantly different from those of the bulk water (Dreybrodt and Buhmann, 1991). To account for the influence of the DBL it has been suggested that a 10 fold reduction of the rate obtained from the PWP equation gives a good estimation of the actual precipitation rate (Dreybrodt and Buhmann, 1991).

2.7 Tufa precipitation

Tufa precipitation processes have been investigated since the 1980s (Chen *et al*., 2004) when the consensus on precipitation mechanisms was divided into those who considered that all freshwater carbonates were abiotically precipitated and those who believed that biofilms, consisting mainly of cyanobacteria, heterotrophic bacteria and diatoms, had a significant impact on precipitation (Pedley *et al*., 2009). In more recent times it has generally become accepted that biofilms are a key component in the precipitation of fluvial carbonates for the following reasons; their metabolism can cause changes in the aqueous chemistry of their local microenvironment and they provide nucleation sites by secreting extracellular polymeric substances (EPS) which some studies have shown are an aid to calcite precipitation (e.g. Janssen *et al*., 1999; Arp *et al*., 2001; Turner and Jones, 2005; Braissant *et al*., 2007; Dupraz *et al*., 2009; Rogerson *et al*., 2008; Pedley *et al*., 2009). Inorganic tufa precipitation occurs when waters become supersaturated with respect to calcite, a supersaturation level of 5 to 10 times is usually required (Chen *et al*., 2004). In an abiotic system this is achieved by CO_2 outgassing, whereby CO_2 rich groundwater emerges and loses CO_2 to the atmosphere as part of the equilibration with the surface environment (Pentecost, 2005). The following subsections outline the basic processes involved in both inorganic and biotically induced/influenced calcite precipitation.

2.7.1 Physicochemical precipitation of tufa

An early study on inorganic calcite precipitation on a small spring fed stream located over limestone bedrock near Gottingen, West Germany revealed that relatively large

amounts of calcite (~ 12600 kg yr^{-1}) were being precipitated in conditions apparently devoid of organisms (Jacobson and Usdowski, 1975). A profile of the stream is shown in Figure 2.5.
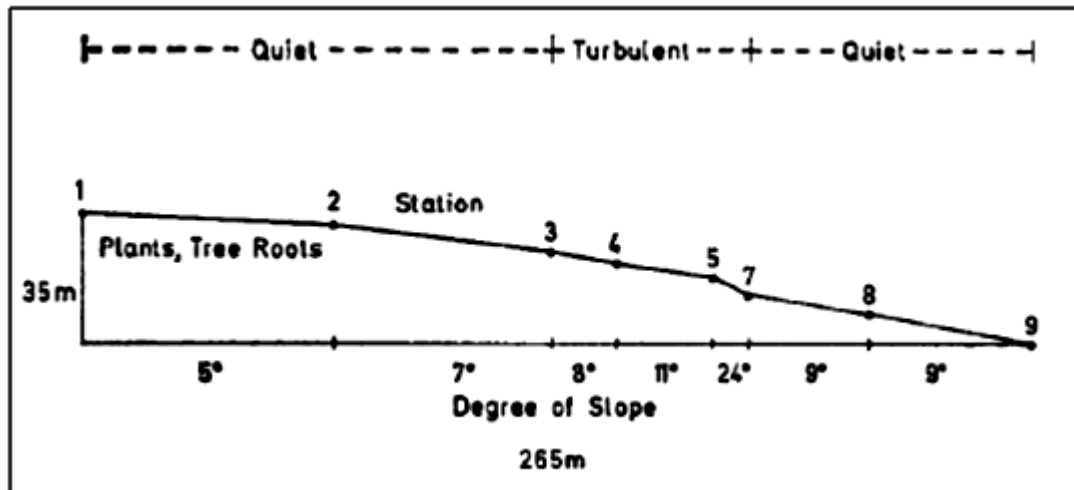
Figure 2.5 Profile of a tufa precipitating stream. The numbers refer to observation points along the stream (Jacobson and Usdowski, 1975).

At its emergence point the stream is 5 times supersaturated with respect to calcite and precipitation was found to occur at this point. The sampling conducted by Jacobson and Usdowski (1975) showed that Ca^{2+} and HCO_3^- concentrations varied with distance from the emergence point (Fig. 2.6), but other ions remained constant, indicating there was no significant influence on water chemistry from evaporation and recharge during the study period.
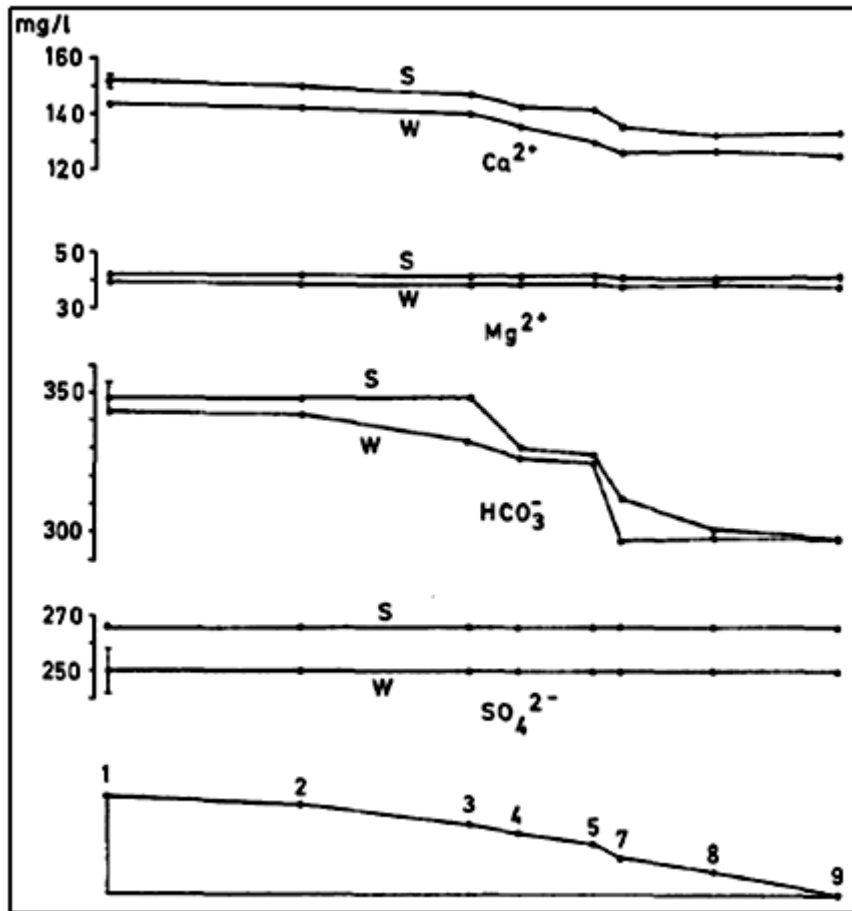
Figure 2.6 Evolution of chemical species along the stream; 'S' is August 1974, 'W' is February 1974. All concentrations are mg L^{-1} (Jacobson and Usdowski, 1975).

The pH value rose until station 3, after which it remained essentially constant indicating that the rate of CO_2 outgassing and calcite precipitation were equal, the loss of CO_2 through outgassing was balanced by the CO_2 produced from the precipitation.

Two main observations arose from the study by Jacobson and Usdowski (1975) on the inorganic precipitation of calcite:

a) precipitation occurred at less than five times supersaturation but was more rapid at greater than ten times supersaturation

b) concentration values for Ca^{2+} changed more rapidly in areas of turbulent flow, argued by the authors to be due to greater CO_2 outgassing which aided the precipitation of calcite.

16

Support for observation b) was provided by the placement of kitchen sponges at two points along the stream, one in the quiet waters between stations 2 and 3 and the other in the turbulent region between stations 5 and 7. After three weeks the sponge in the quiet region contained 2 grams of precipitate whilst the sponge in the turbulent region acquired 300 grams (Jacobson and Usdowski, 1975).

The idea of CO_2 outgassing being a major factor in tufa precipitation rates was assessed by a series of laboratory experiments on calcite precipitation rates under stationary and flowing water conditions and with varying sizes of the air-water interface (Chen *et al*., 2004). It was suggested that CO_2 would degas faster in flowing water as a consequence of the physical properties of a flowing fluid, which are described by the Bernoulli equation:

$$P + \frac{1}{2}\rho v^2 + \rho g h = constant \qquad (2.8)$$

where P is pressure (N m^{-2}), ρ is the fluid density (kg m^{-3}), v is the fluid velocity (m s^{-1}) and h is the elevation above a reference point (m). If the terms ρ, g *and* h are constant then an increase in velocity must result in a decrease in pressure. It has been argued that because the solubility of a gas in water decreases with decreasing pressure (at a constant temperature), CO_2 degassing rates and hence precipitation rates must be higher in flowing water (Chen *et al*., 2004). However, it has been found that even at flow rates as high as 1 m s^{-1} the pressure fall induced by the Bernoulli effect at the air-water interface is only about 0.5%, so under equilibrium conditions the corresponding 0.5% decrease in dissolved gas would not have a major impact on precipitation rates. Instead, it has been proposed that the increased precipitation seen in faster flow regimes is due to a thinning of the diffusive boundary layer which divides the bulk water from the mineral surface (Hammer *et al*., 2008).

2.7.2 Biotic influences on tufa precipitation

Biomineralization has been described as *"the selective extraction and uptake of elements from the local environment and their incorporation into functional structures under strict biological control"* (Mann, 2001, p). This definition refers to

processes such as the building of hard shells by marine organisms where the shell has a specific biological function, but does not include the construction of materials such as tufas, travertines, speleothems, stromatolites and other materials precipitated through a biotic influence. There is evidence of biological processes being involved in inorganic mineralization in the creation of stromatolites, however this is not a controlled precipitation of inorganic material with a specific biological function, but appears to be the result of fortuitous chemical combinations (Mann 2001). Mineral precipitation of this kind was described by Lowenstam (1981) as "*biologically induced mineralization*" and is in contrast to biologically controlled (Konhauser, 2007) mineralization where the products have a precise biological function. The terms *bio-influenced* (Rogerson *et al*., 2008) and *biologically-influenced* (Dupraz *et al*., 2009) mineralisation have also been recently introduced. Differentiating between bio-*induced* or *influenced* precipitation can be achieved by considering bio-induced to be a direct consequence of the metabolic processes of the organisms and bio-influenced to be purely the result of the physical presence of the organisms whereby they act as a trap for detrital material and/or provide nucleation sites for heterogeneous precipitation.

Photosynthesis is often described as the major biological process that induces calcite precipitation (Folk, 1985, Chafetz and Buczynski, 1992, Arp *et al*., 2001, Soetaert *et al*., 2007, Bisset *et al*., 2008, Shiraishi *et al*., 2008a, Gonzalez-Munoz *et al*., 2010, Rogerson *et al*., 2010). Photosynthesis by microbial mats in a tufa precipitating stream removes CO_2 from the water which increases alkalinity and raises the saturation state with respect to calcite. Other metabolic mechanisms driving calcite precipitation are sulphate reduction (Baumgartner *et al*., 2006), urea degradation (Warren *et al.*, 2001) and denitrification (Novitsky, 1981). Bio-influenced precipitation has been described as a passive process that results from the interactions between extracellular organic molecules and the aqueous geochemical environment (Decho, 2010). The presence of these extracellular molecules can cause favourable conditions for precipitation through the accumulation and concentration of different ions and acting as nucleation sites whose presence can cause a significant decrease in the activation energy of calcite precipitation (Gonzalez-Munoz *et al*., 2010). A more thorough treatment of the role of microbial biofilms and their

secretory products on calcite precipitation and its trace element composition is given in sections 2.10 – 2.12.

2.8 Related carbonate deposits

The following subsections provide a brief overview of some related carbonate deposits. Discussion on their $(Mg/Ca)_{calcite}$ ratios as palaeotemperature archives can be found in section 2.18. Much of the work in developing an understanding of trace element partitioning in calcite has been undertaken in these deposits. By examining the complicating factors highlighted by these studies it is much easier to take a wider overview of the many potential issues that may impact on tufa $(Mg/Ca)_{calcite}$ palaeothermometry.

2.8.1 Speleothems

Speleothems are calcium carbonate deposits frequently seen in caves of karstic environments and consist of three principal types, stalactites, stalagmites and flowstones (Fairchild *et al*., 2006). The precipitation of speleothems was initially believed to be a purely abiotic process due to their location in the dark interiors of caves (Cacchio *et al*., 2004; Jones, 2010), with precipitation resulting from the outgassing of CO_2 from cave drip waters (Figure 2.7) resulting in supersaturation with respect to calcite. However more recent studies have revealed that microbes can play a role in the precipitation of the calcium carbonate minerals that make up speleothems (Cacchio *et al*., 2004; Baskar *et al*., 2006; Jones, 2010). The mechanisms said to be behind this microbial influence are their ability to trap and bind detrital grains and/or induce calcite precipitation by altering the microenvironment as a result of their metabolic processes (Jones, 2010).
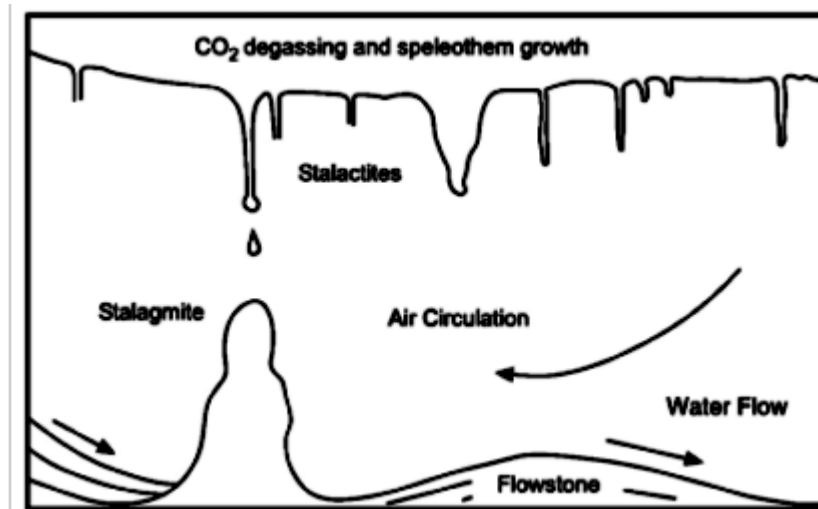
Figure 2.7 Processes in the cave environment which affect speleothem growth (Fairchild *et al*., 2006)

The growth rate of speleothems is usually in the range of $0.01 - 1.00$ mmyr^{-1} and is primarily dependent on the concentration of Ca^{2+} in the dripwaters, temperature, rainfall/drip water rates, cave P_{CO_2} and the thickness of the water film covering the deposit (Genty *et al*., 2001).

2.8.2 Salt water stromatolites

Marine stromatolites have been described as one of the most common and identifiable features of Precambrian carbonate platforms (Andres and Reid, 2006) and although the term '*stromatolite*' is commonly used, no single definition has achieved general acceptance (Riding, 2000). Stromatolite definitions are mainly dependant on the bias of the author, with some preferring to emphasise the biogenic nature while others prefer a definition based on the sedimentological morphology of the structure (Schopf *et al*., 2007). A succinct definition is given by Dupraz and Visscher (2005) as "*Stromatolites are lithifying organosedimentary structures formed by trapping and binding of sediment and/or the net carbonate-precipitating activities of microorganisms, resulting in layered structures*".

Stromatolites date back to approximately 3.5 billion years ago when it is believed that early microbial communities, mainly cyanobacteria and associated heterotrophic bacteria (Decho *et al*., 2005), facilitated the precipitation of calcium carbonate resulting in stromatolite formation (Dupraz and Visscher, 2005). Although stromatolites are commonly domed structures, they also form ridges and can have

20

branching and columnar structures. The final morphology of the stromatolite is dependent on factors such as accommodation space, hydrodynamics and burial by sand (Andres and Reid, 2006). Lamination (Figure 2.8) is a characteristic feature (Andres and Reid, 2006) that arises from an episodic accretion which may be the result of seasonal growth variations and/or periodic sedimentation (Riding, 2000).
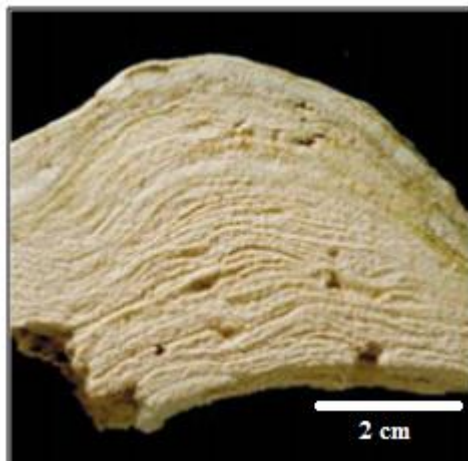
Figure 2.8 Section of stromatolite from Highbourne Cay, Bahamas showing lamination (Reid *et al*., 2000).

Although stromatolites now occur far less frequently than in the Precambrian, there are some scattered extant examples which are considered analogous to the ancient stromatolites of the Archean, notably those in the hypersaline conditions of Shark Bay, Western Australia and in the open marine conditions around the Bahamas, (Riding, 2000). Both these locations exhibit living cyanobacterial surface mats considered to be a critical aspect of ancient stromatolites (Decho *et al*., 2005).

Stromatolites from a shallow subtidal environment at Highborne Cay, Bahamas were studied by Reid *et al*. (2000) and found to be covered with three types of cyanobacterial mats representing a continuum of growth stages. Type 1 mats (70%) are sparsely populated by the filamentous cyanobacterium *Schizothrix* resembling pioneer communities; they are dominant in periods of sediment accretion with the role of the *Schizothrix* being the production exopolymeric secretions which are crucial to the accretion process. Type 2 mats (15%) have calcified biofilms on the upper most surface and an abundance of exopolymeric secretions underlain by a sparse to moderately dense population of *Schizothrix* and represent a more advanced surface community with a continuous exopolymer film. Type 2 mats develop during periods when sedimentation is absent and the lithification process begins. Type 3

mats (15%) are more fully developed with a high population of the coccoid cyanobacterium *Solentia* combined with randomly oriented filaments of *Schizothrix* which underlay a calcified biofilm. The characteristic laminations of fossil stromatolites are representative of a continuous alternation of these mat types. The laminated nature of stromatolites is frequently seen in tufa deposits which can be considered as the freshwater analogue of these marine deposits.

2.8.3 Foraminiferal calcite

Foraminifera are an order of single celled protists which can be divided into benthic and planktonic species, combined with coccoliths they account for greater than 80 % of modern carbonate deposits in the marine environment (Brasier, 1980). The organism's protoplasm is largely enclosed within a solid test which may be composed of secreted minerals (mainly calcite) or agglutinated particles. Foraminiferal classification is divided into two types based on the structure of their tests, miliolid and hyaline (de Nooijer *et al*., 2009). Hyaline species store calcium and carbonate ions within intracellular pools which are used to precipitate new test chambers extracellularly, whilst miliolid species precipitate needle like calcite from within cytoplasmic vesicles (Figure 2.9) (de Nooijer *et al*., 2009).
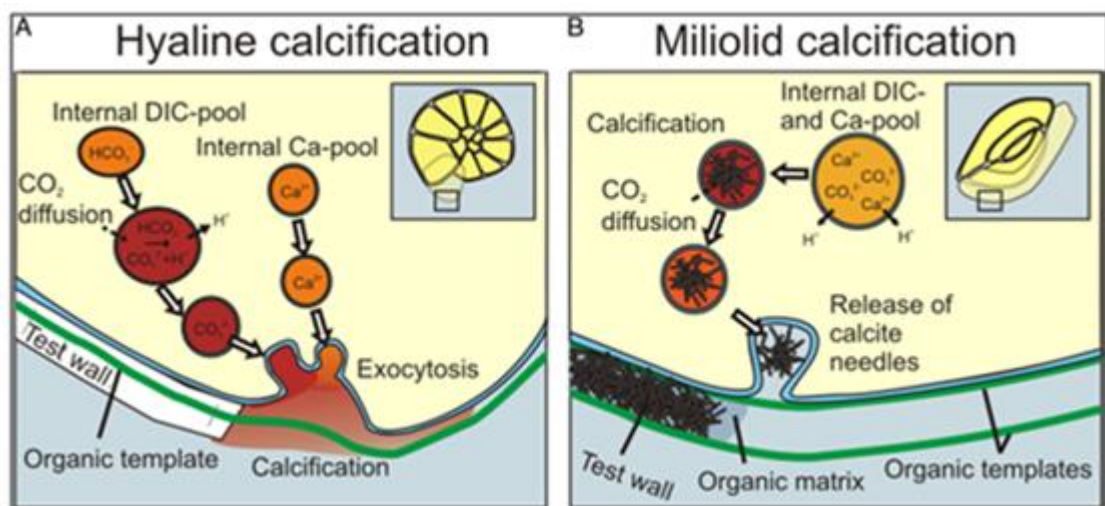
Figure 2.9 Similarities and differences in foraminiferal calcite pathways: (A) Increased pH in the carbonate pool and possible diffusion of metabolic CO$_2$ during chamber formation in a generalised hyaline foraminifera, (B) Elevation of the pH during calcite precipitation and subsequent decrease during chamber formation in the miliolid foraminifera (de Noojer *et al*., 2009).

Foraminiferal calcite is precipitated under a strong biological control by the organism (Elderfield *et al*., 1996). These biological impacts on calcite precipitation have been labelled as 'vital effects' which is used to describe the sum of the biological impacts

without detailing the exact causes (Sen Gupta, 2002). The ratio of magnesium to calcium incorporated into the shells of marine organisms such as foraminifera has been put forward as a method of independently assessing the temperature at which calcification took place (Rosenthal *et al*., 1997; Elderfield *et al*., 1996). It has notable advantages over other temperature proxies in that the oceanic residence times of Ca and Mg are of the order of 10^6 and 10^7 years allowing the reasonable assumption that Mg/Ca ratios in seawater are constant on a glacial-interglacial timescale (Barker *et al*., 2005). The use of foraminiferal $(Mg/Ca)_{calcite}$ ratios as a palaeo sea surface temperature proxy is discussed in section 2.18.1.

2.9   Microbial biofilms

Biofilms thrive in an enormous number of environments whether natural or artificial, provided adequate water is present (Sutherland, 2001). They are found in aquatic and soil environments, on plants, pipes and filtration systems and even on the tissues of animals and humans (Bradding *et al*., 1995, Wingender *et al*., 1999, Flemming and Wingender, 2001 and Sutherland, 2001). At the simplest level biofilms can be considered as communities of microorganisms attached to a surface (O'Toole *et al*., 2000). A biofilm consists of microorganisms such as bacteria, fungi, protozoa and algae, as well as biogenic and inorganic particles, multivalent cations and dissolved compounds contained within a matrix of extracellular polymeric substances (EPS) (Wingender *et al*., 1999 and Vu *et al*., 2009). The development of a biofilm represents a lifestyle change for the organisms where they switch from a unicellular planktonic existence to a multicellular static state, with further growth of the microbial mass creating structured communities (Lemon *et al*., 2008). Although biofilms can exist as a single species entity, mixed species biofilms dominate in most environments (O'Toole *et al*., 2000). The stages of biofilm formation start with the initial surface attachment followed by a monolayer formation, the development of multilayered microcolonies, the production of an extracellular matrix, finally leading to a mature biofilm with a three dimensional architecture (O'Toole *et al*., 2000). This process is shown schematically in Figure 2.10.

Figure 2.10 A model for biofilm development. Plankton cells (1) approach and attach to a surface (2). Through interaction with the substratum with a pole, cells become reversibly attached (3). Cells become laterally attached (4). During this time, the attachment of cells begins to create a two-dimensional biofilm (5). The biofilm grows in thickness as more cells are incorporated. Extracellular polysaccharides and other substances are produced, resulting in more firmly attached cells with an extracellular matrix. The architecture of the biofilm may be modified by production of surfactant and release of cells (6). In response to environmental or physiological stimulants, cells may be released from the matrix and return to the planktonic state, thus completing the developmental cycle (7). The whole process is dynamic and is influencd by environmental factors (Goller and Romeo, 2008).

In freshwater settings such as tufa precipitating streams the microbial make up of biofilms is dominated by filamentous cyanobacteria which represent the major primary producer (Dupraz *et al*., 2009 and Shiraishi *et al*., 2008b). Other constituents include coccoid cyanobacteria, filamentous green algae, diatoms and heterotrophic bacteria, including sulphate reducers, anaerobes and methanogenic bacteria (Shiraishi *et al*., 2008b). The heterotrophic organisms are usually found in close proximity to the phototrophic community as they are able to thrive on the organic exudates the phototrophs produce. The presence of extracellular polysaccharides within the biofilm matrix allows photosynthetic organisms to thrive in deeper parts of the biofilm than would be expected (Flemming, 2011). Extracellular polysaccharides have a slightly different refractive index than water which results in a forward scattering of photons rather than a back scattering reflection. Light will therefore tend to propagate through a biofilm rather than being reflected off it. Also, the gelatinous nature of the extracellular polysaccharides enables light to scatter photons within deeper layers and therefore increase the chances of absorption by photosynthesising organisms deep in the biofilm (Flemming, 2011).

Living within the matrix framework of a biofilm affords the microorganisms with a number of survival benefits. The majority of the protective features of life in a

biofilm are provided by the extracellular polymeric substances which make up the majority of the biofilm matrix.

2.9.1 Extracellular polymeric substances (EPS)

The term 'EPS' was initially applied to 'extracellular polysaccharides' but has now become widely applied to the more general term 'extracellular polymeric substances' due to the discovery that the biofilm matrix also contains proteins, nucleic acids, humic substances and other biopolymers found in the intracellular regions of biofilms (Flemming and Wingender, 2010). The EPS matrix is highly intricate and complex, even for biofilms formed in the same environment, this complexity and the difficulties in analysing it has led to it being described as the 'dark matter' of biofilms (Sutherland 2001, Flemming *et al*., 2007). The secretion of an EPS matrix is a general property of microorganisms and has been observed in both prokaryotic (Bacteria, Archaea) and eukaryotic (fungi, algae) organisms (Flemming and Wingender, 2001). EPS are produced within the cell and then excreted to the cell surface with physical states ranging from gels through to slime to a fully dissolved state (Decho, 2000 and Dupraz *et al*., 2004).

The EPS generally accounts for between 50 and 90% of the total organic matter of a biofilm (Wingender *et al*., 1999) and in the majority of cases the dried mass of a biofilm is over 90% EPS, with the microorganisms representing less than 10% (Flemming and Wingender, 2010). The amount of EPS and its composition and hence the structure of the biofilm matrix, depends on the type of microorganisms, the age of the biofilm and environmental conditions such as shear forces, temperature and nutrient availability (Sutherland, 2001, Vu *et al*., 2009 and Flemming and Wingender, 2010). As the above factors can change with time the exact nature of EPS within any biofilm is highly heterogeneous in space and time (Flemming, 2011). The heterogeneous nature of biofilms has been confirmed by confocal scanning laser microscopy (CLSM) (Stoodley *et al*., 1999). Examination of both single and multi-taxa natural biofilms has revealed an architecture where slime-enclosed microcolonies are distributed between open cell-free water channels that penetrate all areas of the biofilm (Costerton, 1995). These water channels have been observed to allow both convective water flow and the passage of 0.3 μm polystyrene beads (Costerton, 1995).

Microorganisms are able to alter the EPS matrix after it has been secreted from the cell. For example, the shape and charge can be changed by the addition of substituents to the polysaccharides and programmed cell death can lead to the creation of new pores and channels within the matrix (Flemming, 2011). The nature of the EPS matrix may also be altered by higher organisms such as larvae, protozoa and snails grazing on the matrix resulting in the selective removal of EPS and EPS producing organisms. It has also been noted that the distribution of cells and EPS in a biofilm varies greatly; large areas of biofilm may consist mainly of EPS and actually be devoid of microbial cells (Wolfaardt *et al*., 1999). As a consequence of the multiple means by which EPS can be modified, the variety of states it may take, compositional variations within and between species and environmentally induced changes in rates of production it has been describe as existing in a 'continuum' of compositional and degradation states and molecular sizes (Decho, 2010).

The production of EPS is both energy and carbon intensive (Wolfaardt *et al*., 1999 and Konhauser, 2007) and therefore must serve a beneficial purpose for microbial communities. One of the primary functions of EPS is to facilitate the initial adhesion of microorganisms to a given surface and allow them to exist in close proximity to each other (Sutherland, 1999 and Flemming and Wingender, 2001). The EPS matrix also provides a protective environment, shielding the organisms from adverse biotic and abiotic threats from the outside environment; it also provides a shelter from destructive forces such as shear stress and desiccation (Wingender *et al*., 1999, Romani *et al*., 2008). It is thought that the protection from harmful compounds in the bulk water is achieved by diffusion limitation and/or chemical interactions between the EPS and the harmful substances, thus delaying or preventing them from reaching target microorganisms (Wingender *et al*., 1999).

Some EPS components are able to adsorb substances which would be toxic to the organisms such as Cd, Pb, Cu and Sr (Sutherland, 1999). The EPS are also able to sequester nutrients from the bulk water (Wingender *et al*., 1999) and due to the close proximity of the microbial cells the competition for these nutrients will be fierce (Sutherland, 2001). The existence of channels within the biofilm matrix makes it possible for water to flow convectively through the matrix, helping organisms in the depths of the biofilm to obtain nutrients without having to compete with those

residing at the interface with the bulk water (Flemming, 2011). Under oligotrophic conditions the EPS matrix itself may act serve as a food source, however the complexity of the EPS makes it only slowly biodegradable (Flemming and Wingender, 2010). It has been observed that only a limited number of organisms possess the necessary enzymes to depolymerise their own EPS (Wolfaardt *et al*., 1999 and Flemming and Wingender, 2001), therefore EPS must be able to be degraded by other organisms as a nutrient source otherwise its existence would be permanent (Flemming and Wingender, 2001).

2.10   Cation chelation by EPS molecules

2.10.1   Chelation theory

Chelation occurs when a chelating agent or ligand binds with a metal ion forming a compound called a chelate. During the process of chelation two or more ligands bind to a free metal ion and water molecules from the hydrated metal ion in solution are released (Hanas *et al*., 2005). The stability of the chelate complex is determined by the coordination preferences which are based on Pearson's Hard/Soft Acid/Base Theory. Metals or ligands with a high charge density (z_i^2/r_i) and low polarization are said to be 'hard' resulting in large energy gaps between the highest occupied molecular orbital of the base and the lowest unoccupied orbital of the acid. The large energy gap results in a primarily ionic interaction between the base and the acid. Conversely, 'soft' acids and bases result when charge density is low and polarization high. In this case the energy gap between the highest occupied molecular orbital of the base and the lowest unoccupied orbital of the acid is small so the bonding is much more covalent in nature. The distinction between these two classifications is not sharp, 'borderline' species exist which are able to bind with either hard or soft species (Hanas *et al*., 2005).

 Generally, 'hard' acids (metals can be considered as acids as their positive charge will accept negative species, a base) such as K^+, Na^+ , Ca^{2+} and Mg^{2+} will form chelates with hard bases or ligands such as carboxylates (Hanas *et al*., 2005). Acids such as Cd^{2+}, Pb^{2+} and Hg^{2+} have a larger number of d electrons than hard metals and these d-rich metals most readily form chelates with soft ligands such as sulphydryls (Hanas *et al*., 2005).

The binding preferences of divalent cations for a given ligand have been shown to be related to the ionic radii of the cations. Therefore, large diameter Ca^{2+} and Mg^{2+} chelation complexes are not as stable as those formed by the smaller diameter d-rich metals such as Co^{2+}, Ni^{2+}, and Cu^{2+} (Hanas *et al*., 2005). This behaviour is commonly referred to as the *Irving-Williams effect* (Irving and Williams, 1953) which predicts that stability of metal-ligand complexes increases as ionic radii decreases resulting in stronger metal-ligand bonds as the ionic radii decreases (Lippard and Berg, 1994, Hanas *et al*., 2005). So, binding preferences of a given ligand for some divalent cations will follow the stability series Mn < Fe < Co < Ni < Cu (Lippard and Berg, 1994).

2.10.2 Chelation by EPS of biofilms

The ability of EPS molecules to adsorb substances which are potentially toxic to biofilms such as Cd, Pb, Cu and Sr is due to the fact that most molecules within the EPS have a negative surface charge due to the presence of negatively charged functional groups which deprotonate as pH increases (Konhauser, 2007). Studies on cyanobacteria and sulphate reducing bacteria (SRB) have revealed that the functional groups include carboxylic acids (R-COOH), hydroxyl groups (R-OH), amino groups (R-NH_2), sulphate (R-O-SO_3H), sulphonate (R-SO_3H), and sulphydryl groups (-SH), all of which bind metal ions including Ca^{2+} and Mg^{2+} (Dupraz *et al*., 2009 and references therein). Deprotonation of these functional groups occurs under slightly acidic to alkaline conditions with each functional group having a different pH at which 50% of the group is deprotonated (Dupraz *et al*., 2009). Although several functional groups are involved in creating the negative charge of EPS, the most important are believed to be carboxylic acids and sulphate groups (Dupraz *et al*., 2009).

The stability of some matrix polysaccharides is dependent on the presence of multivalent cations, particularly Mg^{2+} and Ca^{2+}, these allow the formation of ionic bridges by the cross linking of charged compounds, particularly the carboxylic groups of anionic EPS (Flemming and Wingender, 2010) within the matrix. These ionic bridges assist in the maintenance of an ordered and stable structure and are an important factor in the stability of the EPS matrix (Nielsen and Jahn, 1999 and

28

Sutherland, 1999). The configuration and structure of the polysaccharides in the matrix has a very strong influence of ionic bonding. The chelating ability (and its selectivity) has been shown to be greatly reduced in the presence of *O-* acetyl groups (Sutherland, 1999).

The chelation of Ca^{2+} and other M^{2+} ions to the high abundances of EPS associated with microbial biofilms has been suggested as an initial inhibiting factor in carbonate mineral precipitation (Reid *et al*., 2000; Kawaguchi and Decho, 2002). The removal of Ca^{2+} from the surrounding solution reduces its level of supersaturation with respect to calcite and hence inhibits precipitation as evidenced by the type 1 stromatolite mats of Reid *et al*. (2000), (see section 2.8.2) where aragonite precipitation is inhibited by the calcium binding of cyanobacterial EPS. However, the binding of Ca^{2+} and other cations to EPS is not a permanent arrangement. The EPS matrix can be used as an energy and organic carbon source for heterotrophic bacteria (Dupraz *et al*., 2009) and the consequential degradation of the EPS matrix releases the chelated Ca^{2+} ions creating areas of elevated Ca^{2+} concentration which favours precipitation (Baumgartner *et al*., 2006). The molecular structure of EPS is also modified through partial degradation by bacteria and by environmental impacts such as ultraviolet light irradiation (Baumgartner *et al*., 2006). These structural changes produce exposed carboxyl groups whose characteristics may provide nucleation sites which induce precipitation (Baumgartner *et al*., 2006).

Although it is reported that the chelation of Ca^{2+} ions to EPS is initially an inhibiting factor in carbonate mineral precipitation in seawater, *in vitro* experiments have shown this may not be the case in a freshwater setting (Rogerson *et al*., 2008 and Pedley *et al*., 2009). As pointed out by Rogerson *et al*. (2008) the chelation of cations to EPS results in the latter acquiring a net positive charge which can only be balanced by the assembling of anions in an additional solution based layer. This results in an 'electrical double layer' (Rogerson *et al*., 2008), which in seawater, with its high ionic strength, will be in tight association with the charged surface (Rogerson *et al*., 2008). The low ionic strength of karstic freshwaters will result in a weakly associated double layer with the main anion being HCO_3^-, meaning calcite precipitation is more likely in low ionic strength freshwaters as there is a reduced requirement for the degradation of EPS by heterotrophic organisms to release the

chelated cations (Rogerson *et al*., 2008). It has also been proposed that the presence of anionic functional groups may help initiate calcite precipitation. If only one of the positive charges on a Ca^{2+} cation is complexed to an anionic functional group, it leaves the other positive charge free to bind with a carbonate ion and initiate $CaCO_3$ precipitation, providing a nucleation site for further precipitation (Decho, 2010).

In addition to their possible effect on precipitation rates, EPS molecules may also alter the chemical composition of the precipitates. The chelation process appears to be chemoselective, with selectivity being in favour of larger ions with smaller charge densities (z_i^2/r_i), so chelation preferences will follow the order $Ba^{2+} > Sr^{2+} > Ca^{2+} >$ Mg^{2+} (Rogerson *et al*., 2008). Consequently, chemoselectivity by EPS will result in precipitates with different trace element ratios than those expected from precipitation at equilibrium with bulk water. For tufa carbonates this will give a Ba/Ca ratio greater than that expected at equilibrium values and an Mg/Ca ratio lower than expected at equilibrium (Rogerson *et al*., 2008). The observation that chemoselectivity favours larger ions appears to be in contrast to the Irving - Williams effect which states that metal – ligand stability increases as charge density increases. This apparent dichotomy may be explained by the fact that complex formation occurs in two stages (Irving and Williams, 1953):

$$M(H_2O)_n + L \rightleftharpoons M(H_2O)_nL \rightleftharpoons ML(H_2O)_n + (n-m)H_2O \qquad (2.9)$$
$$\text{Ion pair} \qquad\qquad \text{Complex}$$
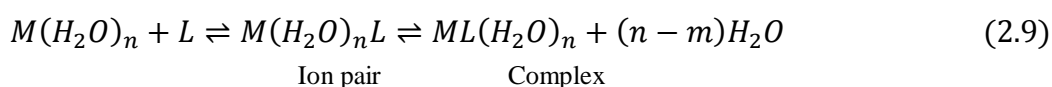
where M is a cationic metal and L a anionic ligand. The stability of the M-L compound may be different at different stages of the reaction in equation (2.47). This has been proposed as a possible reason that the binding stabilities of the alkaline-earth metals do not follow the predicted pattern based on charge density (Irving and Williams, 1953). For example, magnesium may form an ion pair, whilst barium may form a stronger complex (Williams, 1952). It has been argued that there is an increasing *complex* formation, M – L in the order $Ba^{2+} > Sr^{2+} > Ca^{2+} > Mg^{2+}$ (Irving and Williams, 1952). The increased stability of complexes over ion pairs combined with the above stated order of complex formation offers a possible expalanation to the apparent dichotomy between the Irving – Williams effect and the chemoselectivty observed by Rogerson *et al*., (2008).

2.11 Microbial metabolism and its influence of carbonate precipitation

The organisms in microbial mats can be divided into three main groups based on their method of acquiring energy and carbon for biomass (Baumgartner *et al.*, 2006), oxygenic phototrophs, aerobic heterotrophs and anaerobic heterotrophs. The oxygenic phototrophs are the primary producers which reduce CO_2 to organic carbon using H_2O as an electron donor to produce oxygen. The combination of chemical and microbial reactions that lead to $CaCO_3$ precipitation being induced by photosynthesis is (Visscher and Stolz, 2005):

$$HCO_3^- \rightarrow CO_2 + OH^- \quad (chemical) \tag{2.10}$$

$$CO_2 + H_2O \rightarrow CH_2O + O_2 \quad (microbial) \tag{2.11}$$

$$Ca^{2+} + HCO_3^- \rightarrow CaCO_3 + H^+ \quad (chemical) \tag{2.12}$$

$$H^+ + OH^- \rightarrow H_2O \quad (chemical) \tag{2.13}$$

the sum of which gives:

$$2HCO_3^- + Ca^{2+} \rightarrow CH_2O + O_2 + CaCO_3 \tag{2.14}$$
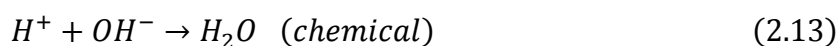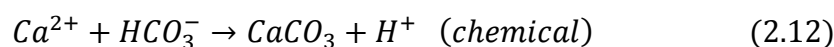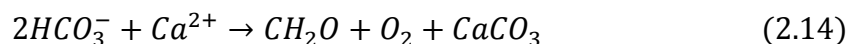
Therefore, photosynthetic carbon fixation creates one mole of $CaCO_3$ for each mole of CO_2 consumed.

The photosynthetically induced chemical changes in the microenvironment are an important factor in overcoming the activation energy barrier of $CaCO_3$ precipitation in natural settings, even those that are already highly supersaturated with respect to $CaCO_3$ (Shiraishi *et al.*, 2008b). The organic carbon produced by the autotrophs is subsequently consumed by the heterotrophs as an energy source to make biomass. The aerobic heterotrophs use oxygen as their terminal electron acceptor (TEA) during the respiration of the organic carbon:

$$O_2 + CH_2O \rightarrow CO_2 + H_2O \tag{2.15}$$

In simple terms aerobic heterotrophy can be viewed as a reversal of the photosynthetic process with dissolution of calcium carbonate occurring (Baumgartner *et al*., 2006), so that:

$$CH_2O + CaCO_3 + O_2 \rightarrow 2HCO_3^- + Ca^{2+} \qquad (2.16)$$
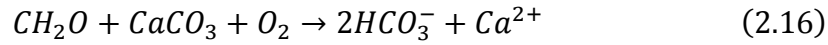
Anaerobic heterotrophs, mainly sulphate reducing bacteria (SRB), use a different TEA in the reduction of sulphate to sulphide:

$$SO_4^{2-} + 2(CH_2O) + OH^- \rightarrow HS^- + 2HCO_3^- + 2H_2O \qquad (2.17)$$
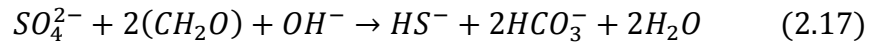
As with photosynthesis carbonate equilibrium needs re-establishing (Baumgartner *et al*., 2006) with consequential calcium carbonate precipitation as in equations (2.10 and 2.13). The overall equation for SRB being:

$$SO_4^{2-} + 2(CH_2O) + OH^- + Ca^{2+} \rightarrow CaCO_3 + CO_2 + 2H_2O + HS^- \qquad (2.18)$$

The reduction of sulphate to sulphide favours precipitation as it increases alkalinity, sulphate (sulphuric acid) is a much stronger acid than hydrogen sulphide (Baumgartner *et al*., 2006).

2.12   The role of cyanobacteria in carbonate precipitation

Cyanobacteria appear to play a significant role in photosynthetically induced calcification compared to other primary producers. In a study of a karst water creek in the mountains of central Germany, Shiraishi *et al*. (2008a) observed that the tufa stromatolites were colonised by a green coloured biofilm in the centre of the flow path but brownish biofilms were found in the marginal part of the flow path. The biofilms were examined by fluorescence in situ hybridization (FISH). The green biofilm was densely populated by filamentous cyanobacteria plus a number of heterotrophic bacteria and diatoms, whilst the brown biofilm was sparsely populated by cyanobacteria but contained a similar number of diatoms and heterotrophic bacteria as the green biofilm. Biofilm microprofiles of pH, O_2, Ca^{2+} and CO_3^{2-} obtained by Shiraishi *et al*. (2008a) all showed that the green biofilms had a higher

photosynthetic capacity and thus exerted more influence on the carbonate system at the tufa surface.

The extent to which cyanobacterial photosynthesis will induce precipitation depends on hydrodynamic (Merz-Preiβ and Riding, 1999 and Shiraishi *et al*., 2008a) and hydrochemical (Arp *et al*., 2001) factors. Cyanobacterial photosynthesis usually makes use of CO_2 but when its concentration is too low, HCO_3^- is used as an alternative with a consequential release of OH$^-$ ions (Merz-Preiβ and Riding, 1999), the resulting increase in alkalinity favours precipitation (Dupraz *et al*., 2004). In a freshwater setting two different types of cyanobacterial calcification have been identified, sheath encrustation and sheath impregnation (Merz-Preiβ and Riding, 1999 and Dupraz *et al*., 2004). Sheath impregnation has been shown to be associated with a low saturation index (SI) in slow flowing streams where reduced CO_2 levels force the use of HCO_3^- during photosynthesis (Merz-Preiβ and Riding, 1999). Sheath encrustation is associated with high SI and CO_2 levels in fast flowing waters (Merz-Preiβ and Riding, 1999).

Photosynthesis and other metabolic processes are influenced by a number of environmental factors including pH and temperature changes and hence have the potential to impact on photosynthetically induced calcification of cyanobacterial biofilms, however to date these influences have not been thoroughly investigated (Bissett *et al*., 2008).

2.13 Thermodynamics

2.13.1 Enthalpy

The internal energy (U) of a system is the sum of its potential and kinetic energies. If a system is heated its molecules will move faster and have a greater kinetic energy and if a system is compressed (i.e. work is done to the system), its potential energy will increase. The change in internal energy that results from the application of heat (q) and work (w) is expressed in differential form as:

$$dU = dq + dw \qquad\qquad (2.19)$$

Energy changes at a constant pressure are described by the term enthalpy (H), which can simply be defined as the heat absorbed or evolved from a system during a reaction. In its simplest form it can be written as:

$$H = U + PV \qquad\qquad (2.20)$$

The formation of chemical compounds results in an enthalpy change which is defined under standard conditions (T = 298.15 K, P = 101, 325 Pa (1 bar)) as (ΔH^0_f):

ΔH^0_f *is the enthalpy change when 1 mole of a compound is formed under standard conditions from its constituent elements in their standard states.* (Price, 1998). Standard enthalpies of formation can be calculated from equation (2.21) where v_i is the stoichiometric coefficient:

$$\Delta H^0_{298}(reaction) = \sum v_i\, \Delta H^0_{f,298}(products) - \sum v_i\, \Delta H^0_{f,298}(reactants) \qquad (2.21)$$

The ΔH^0_{298} value for the formation of calcium carbonate ($CaCO_3$) is -1206.9 kJ mol^{-1}, it is therefore a highly exothermic reaction.

2.13.2 Entropy

Entropy can be described loosely as a measure of randomness of disorder of a system (Price, 1998). A definition of entropy (S) is given through the *Boltzman equation:*

$$S = k_b ln\, \omega \qquad\qquad (2.22)$$

Where k_b is the Boltzman constant and ω is the number of ways in which the molecules of the system can be arranged. Therefore, the greater the number of ways the system is arranged, or less organised it is, the larger the entropy is. Entropy is related to the second law of thermodynamics which is well described by White (2002):

There is a natural direction in which reactions will tend to proceed. This direction is inevitably that of higher entropy of the system and its surroundings.

Entropy dictates the direction of spontaneous reactions; such reactions can only occur if they lead to an increase in entropy. Reactions that lead to a decrease in entropy cannot take place spontaneously. Determining the entropy change for a reaction makes it possible to predict its direction. Thermodynamically, the definition of entropy is based on equation (2.23):

$$dS = \frac{dq_{rev}}{T} \qquad (2.23)$$

Where q_{rev} is an amount of heat added in a reversible fashion. For measurable changes between an initial (*i*) and final (*f*) states equation (2.24) gives:

$$\Delta S = \int_{i}^{f} \frac{dq_{rev}}{T} \qquad (2.24)$$

As with enthalpy, the standard entropy of a reaction is determined from the difference in the standard entropies of the reactants and products:

$$\Delta S_{298}^0 (reaction) = \sum v_i \, \Delta S_{298}^0 (products) - \sum v_i \, \Delta S_{298}^0 (reactants) \qquad (2.25)$$

The impact of temperature on entropy at a constant pressure is determined by making use of the fact that the heat capacity at a constant pressure (c_p) can be expressed as $q_{rev} = c_p \, dT$ so:

$$\Delta S = S_{T_f} - S_{T_i} = \frac{dq_{rev}}{T} = \int_{T_i}^{T_f} \frac{c_p}{T} dT \qquad (2.26)$$

The standard molar entropy of calcite formation is 92.9 J K^{-1} mol^{-1}.

2.13.3 Gibbs free energy

Enthalpy and entropy can be combined into a single function which determines the viability of reactions, this is known as the *free energy* (*G*). It represents the energy that is freely available to do 'work' at a constant pressure and temperature. For any system the free energy is not directly measurable, instead it is calculated from the enthalpy and entropy values where:

$$G = H - TS \qquad (2.27)$$

The function $H - TS$ is known as the *Gibbs function*, or *Gibbs free energy*. As with entropy and enthalpy the change in Gibbs free energy (ΔG) is related to the Gibbs free energy of the initial and final states:

$$\Delta G = G_{final} - G_{initial} = \Delta H - T\Delta S \qquad (2.28)$$

For spontaneous processes occurring at a constant pressure and temperature the Gibbs free energy is always reduced:

$$(\Delta G)_{p,T} < 0 \qquad (2.29)$$

However, although a negative value for the Gibbs free energy means that a reaction can occur spontaneously, it does not mean it will actually happen, a catalyst may be required to activate the reaction. The Gibbs free energy of reactions is related to temperature changes by equation (2.30):

$$\left(\frac{d\Delta G}{dT}\right)_p = -\Delta S \qquad (2.30)$$

Therefore G decreases as temperature increases at a constant pressure.

2.14   Gibbs free energy and equilibrium

During a reaction process the Gibbs free energy will be constantly changing in proportion to the amount of reactants or products that exist but at some point it will reach a minimum. At this point the system is in equilibrium and the reaction will not proceed any further, therefore a system is at equilibrium when its minimum free energy is reached. A key feature to the concept of equilibrium is the law of mass action. For a reaction of the form:

$$\alpha A + \beta B \rightarrow \gamma C + \delta D \qquad (2.31)$$

The ratio of the reaction quotient (Q) is found from:

$$Q = \frac{(a_C)^\gamma (a_D)^\delta}{(a_A)^\alpha (a_B)^\beta} \qquad (2.32)$$

Where α is the activity or effective concentration of the species. When the reaction in (2.31) reaches equilibrium the quotient Q becomes an equilibrium constant (K_{eq}):

$$Q_{eq} = \frac{(a_C)^\gamma_{eq}(a_D)^\delta_{eq}}{(a_A)^\alpha_{eq}(a_B)^\beta_{eq}} = K_{eq} \qquad (2.33)$$

where α represents the effective concentration or activity of the species. The equilibrium constant is related to the Gibbs free energy through equation (2.34):

$$K_{eq} = exp\left(\frac{-\Delta G^0}{RT}\right)$$

(2.34)

2.15 Activity coefficients

Activity coefficients are a consequence of ionic interactions in a solution. These interactions cause variations in the free energy associated with the ions from what it would be if the interactions did not occur (Morse and Mackenzie, 1990). The activity (a_i) of a chemical species i, is related to but not necessarily equal to its concentration. On a molar scale the activity is defined by:

$$\alpha_i = \gamma_i c_i$$

(2.35)

Where c_i is the molar concentration and γ_i is the molar activity coefficient. At the limit of an infinitely dilute (ideal) solution the activity coefficient tends to a value of 1 as no ionic interactions occur so $\alpha_i = c_i$. The value of γ_i can be calculated from the ionic strength of the solution (I):

$$I = \frac{1}{2}\sum_i c_i z_i^2$$

(2.36)

(The observation that the ionic charge is expressed as z^2 shows that ions with a higher charge have a greater impact on ionic interactions in solution). Ionic strength is used to calculate the value of γ_i through the experimentally derived equations: *Debye-Hückel* and the *extended Debye-Hückel*. The determination of which equation to use depends on the ionic strength of the solution for $I \leq 0.1$ mol kg^{-1} the extended version (2.37) is most useful and this gives useful results for I values up to about 1 mol kg^{-1} (Misra, 2012).

$$log\,\gamma_i = \frac{-Az_i^2\sqrt{I}}{1 + å_i B\sqrt{I}}$$

(2.37)

Where A and B are characteristics of the solvent (at a specified P and T), $å_i$ is the hydrated ionic radius of the *ith* ion. When the ionic strength is ≤ 0.001 mol kg^{-1} the term $a_i \dot{B} \sqrt{I}$ approaches zero so the extended equation can be reduced to:

$$log\ \gamma_i = -Az_i^2 \sqrt{I} \qquad (2.38)$$

Freshwater normally has an ionic strength of ≤ 0.02 mol kg^{-1}, for seawater it is about 0.7 mol kg^{-1} so calculation of activity coefficients in these environments is best carried out using the extended Debye-Hückel equation (Appelo and Postma, 2005).

2.16   Solubility products

Solubility products are derived from the concept of the solubility of salts. A salt is a compound containing a cation (other than H$^+$) and an anion (other than OH$^-$ and O^{2-}). When acids (A) (source of cation) and bases (B) (source of anion) react a salt is formed (along with water) (Misra, 2012). Whether a salt precipitates out or remains in solution depends on its solubility. If a solid solute is placed in a solvent it will dissolve until the solution is saturated with respect to the solute, at this stage equilibrium has been achieved, so saturation is a state of equilibrium (Atkins and de Paula, 2006). The dissolution of a salt $B_p A_{n(s)}$ is described by:

$$B_p A_{n(s)} \rightarrow pB^+{}_{(aq)} + nA^-{}_{(aq)} \qquad (2.39)$$
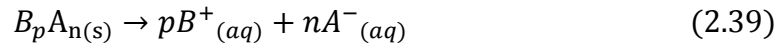
Because $\alpha_{BpAn(s)} = 1$ the equilibrium constant (K_{eq}) for equation (2.39) is simply a product of the activities of the ions raised to a power that is equal to the respective stoichiometric constants (Misra, 2012). The equilibrium constant for slightly soluble compounds in water is called the solubility product (K_{sp}) which represents the product of the activities:

$$K_{eq} = \frac{(a_{B^+})^p (a_{A^-})^n}{a_{B_p A_{n(s)}}} = \frac{(a_{B^+})^p (a_{A^-})^n}{1} = (a_{B^+})^p (a_{A^-})^n = K_{sp(B_p A_n)} \qquad (2.40)$$

Since $\alpha_i = \gamma_i c_i$ (2.35) substitution for α_i gives:

$$K_{sp(B_p A_n)} = (c_{B^+} \gamma_{B^+})^p (c_{A^-} \gamma_{A^-})^n \qquad (2.41)$$

The solubility product is a function of pressure and temperature, in most cases the value of K_{sp} (and hence solubility) for salts increases as temperature increases. However, for calcite this is not the case, solubility decreases with increasing

temperature. The saturation state (Ω) of a salt in aqueous solution is related to K_{sp} through equation (2.42):

$$\Omega = \left(\frac{IAP}{K_{sp}}\right) \tag{2.42}$$

where *IAP* is the ion activity product which represents the product of the activities of free ion species:

$$IAP = \prod_{i=m}^{n} \alpha_i = \alpha_m \, \alpha_{m+1} \, \alpha_{m+2} \, ... \, \alpha_{n-1} \, \alpha_n \tag{2.43}$$

Or, alternatively equation (2.42) can be use to define a saturation index (*SI*):

$$SI = log_{10}\left(\frac{IAP}{K_{sp}}\right) \tag{2.44}$$

An SI of zero indicates equilibrium, supersaturation exists at SI > 0 and undersaturation occurs when SI < 0. Precipitation of calcite has been observed at an SI of < 0.5 but is more rapid at an SI of 1 (Jacobson and Usdowski, 1975, Chen *et al.*, 2004).

2.17   Chemical kinetics and activation energy

Chemical reactions can occur in either a single step or via two or more steps. A single step reaction is known as an elementary reaction and multi step reactions as composite reactions. Each step in a reaction sequence requires energy to proceed, if insufficient energy is available then the reaction cannot take place. There is an energy barrier, which must be overcome, the energy required to achieve this is known as the *activation energy* (Figure 2.11), for calcite precipitation the activation energy has been experimentally determined to be 48 ± 4.3 kJ mol^{-1} (Inskeep and Bloom, 1985).
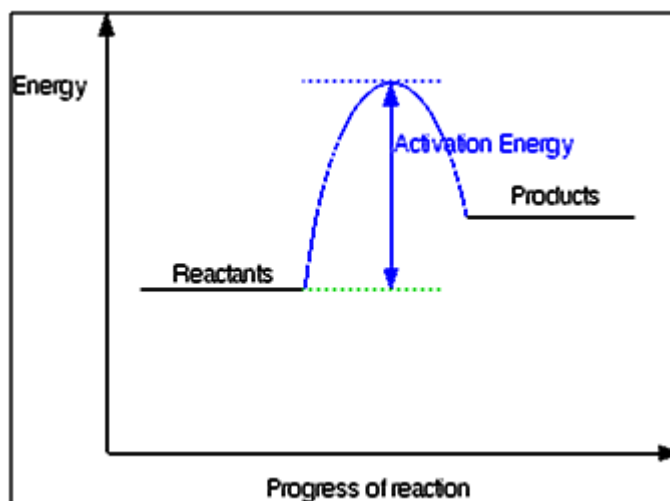
Figure 2.11 Schematic representation of the energy profile of an elementary chemical reaction

The rate (*J*) of a chemical reaction is reflected in the rate of change of the reactants and products as a function of time:

$$J = \frac{1}{v_i}\frac{d[i]}{dt} \tag{2.45}$$

where v_i is the coefficient of stoichiometry which is negative for reactants and positive for products, [*i*] is the concentration of the *ith* species. One of the factors that impacts on the reaction rate is the collision frequency between the reactants, which is directly proportional to the product of their concentrations:

$$collision\ rate = c[A][B] \tag{2.46}$$

where c is a proportionality constant. Not all collisions result in a reaction to products, if the kinetic energy of the collision is insufficient to overcome the activation energy barrier no reaction can occur so only some fraction (*f*) of collisions result in a reaction. Combining the proportionality constant from equation (2.46) with this fraction gives a theoretical rate constant $k_{theory} = cf$. In practice, experimental rate constants (*k*) are used, these are determined experimentally at fixed temperatures.

2.17.1 Effect of temperature on reaction rates – the Arrhenius equation

In addition to concentrations, reaction rates are influenced by catalysts and temperature, of which temperature is the most significant (Misra, 2012). The impact of temperature on the rate constant (k) is expressed by the Arrhenius equation:

$$k = Ae^{-E_a/RT}$$ (2.47)

where A is a frequency factor (s^{-1}) and E_a is the activation energy (J mol^{-1}) (see Figure 2.11), R the gas constant (J mol^{-1} kg^{-1}) and T the temperature (K). The form of the Arrhenius equation reveals what parameters control the rate constant. The term $exp(E_a/RT)$ indicates the fraction of collisions that have sufficient energy to overcome the activation energy barrier at temperature T. The value of k increases exponentially with increasing temperature but is reduced at higher activation energies.

2.17.2 Partition coefficients

A number of divalent cations are able to substitute for the position of Ca^{2+} in the calcite crystal structure. The degree to which this substitution occurs is generally expressed through a partition coefficient (K_d). The heterogeneous partition coefficient for the partitioning of Mg^{2+} between a carbonate mineral and the aqueous solution is given by the equation (Oomori *et al.*, 1987):

$$log \frac{\left(m_{Mg^{2+}}\right)_i}{\left(m_{Mg^{2+}}\right)_f} = \lambda_{Mg} \frac{(m_{Ca^{2+}})_i}{(m_{Ca^{2+}})_f}$$ (2.48)

Where m is the concentration of the subscripted species and i and f represent the initial and final solutions respectively. In the carbonate literature the partition coefficient is usually expressed in the general simple form:

$$K_d = \frac{\left(Tr/Ca_{CaCO_3}\right)}{(Tr/Ca)_{soln}}$$ (2.49)

Where Tr is the trace cation and K_d is the partition coefficient. The value of K_d is dependent on factors such as temperature, precipitation rate, crystal morphology and solution composition (Fairchild and Treble, 2009). It is worth noting however, that

equation (2.49) is based on the non thermodynamic relation of Henderson and Kracek (1927):

$$D = \frac{(c_i/c_j)_{solid}}{(c_i/c_j)_{soln}} \qquad (2.50)$$

Where c_i and c_j are the concentrations of the i and j components respectively and D is the partition coefficient. This is not a thermodynamic approach as the thermodynamic activities of the individual components have not been used (Morse and Mackenzie (1990). Using the activities of the components the partition coefficient (K) is given by:

$$K = \frac{(a_i/a_j)_{solid}}{(a_i/a_j)_{soln}} \qquad (2.51)$$

Where a_i and a_j are the thermodynamic activity coefficients and K the partition coefficient. Relating the two partition coefficients D and K together is achieved by equation (2.52) (Morse and Mackenzie, 1990):

$$D = K(\lambda_i/\lambda_j)(\gamma_i/\gamma_j) \qquad (2.52)$$

Where λ and γ are the solid and solution phase activity coefficients respectively. The values of D and K will only be equal if the ratio of activity coefficients $(\lambda_i/\lambda_j)(\gamma_i/\gamma_j)$ is at unity. The activity coefficient ratios of the solid and solution phases can be changed by factors such as compositional, temperature and pressure variations which will alter the relative relationship between D and K. This has the potential to cause differences to arise in partition and distribution coefficients which have been determined from different solutions (e.g. dilute solutions and seawater) (Morse and Mackenzie, 1990).

2.17.3   Effect of DBL on trace element ratios

If divalent trace element partitioning is described by the reaction (Wang and Xu, 2001)

$$M_H X + M^{z+} = MX + M_H^{z+} \qquad (2.53)$$
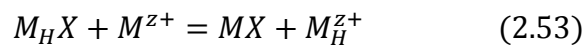
where M^{z+} and M_H^{z+} are the substituent and host ions respectively then the equilibrium partition coefficient (K_{eq}) of the trace cation between solid and solution is defined as:

$$K_{eq} = \left(\frac{X_{MX}}{X_{M_HX}}\right)\bigg/\left(\frac{m^{Z+}}{m_{M_H^{Z+}}}\right) \qquad (2.54)$$

where X_{MX} and X_{M_HX} are the mol fractions of the trace and host cations in the solid respectively, m^{Z+} and $m_{M_H^{Z+}}$ are the molalities of M^{Z+} and M_H^{Z+} in the solution. The boundary layer may alter the relationship of equation 2.54 as a function of precipitation rate. At higher rates of precipitation cation depletion may limit availability at the solid surface and create a boundary layer that has a different cation ratio to that of the bulk water (Wang and Xu, 2001). The influence of the DBL on $M^{2+}_{(aq)}$ partitioning between solution and calcite is determined from the mass balance equations (Wang and Xu, 2001):

$$R_p = \lambda(m^{\infty}{}_{Ca^{2+}} - m^0{}_{Ca^{2+}}) \qquad (2.55)$$

$$R_p K_{eq} = \frac{m^0_{M^{2+}}}{m^0_{Ca^{2+}}} = \lambda(m^{\infty}{}_{M^{2+}} - m^0{}_{Ca^{2+}}) \qquad (2.56)$$

where R_p is the precipitation rate (mol cm^{-2} s^{-1}), $m^0{}_i$ and $m^{\infty}{}_i$ are the concentrations of cation i at the solid surface and in the bulk solution respectively and λ is the rate constant for the mass exchange between the bulk solution and the DBL by diffusion. When equations 2.53 and 2.54 are solved for $m^0_{M^{2+}}$ and $m^0_{Ca^{2+}}$ they give:

$$\frac{m^0_{M^{2+}}}{m^0_{Ca^{2+}}} = \frac{m^{\infty}_{M^{2+}}}{m^{\infty}_{Ca^{2+}} + (K_{eq} - 1)\frac{R_p}{\lambda}} = \frac{m^{\infty}_{M^{2+}}}{m^{\infty}_{Ca^{2+}}}\left(\frac{1}{1 + (K_{eq} - 1)R'_p}\right) \qquad (2.57)$$

where $R'_p = R_p/\lambda m^{\infty}_{Ca^{2+}}$, a scaled calcite precipitation rate in the range of 0 to 1 according to equation 2.55 (Wang and Xu, 2001). Equation 2.57 can be simplified by dividing both sides by X_{MCO_3}/X_{MCaCO_3}, and using equation 2.55 to give:

$$K_{exp} = \frac{K_{eq}}{1 + (K_{eq} - 1)R'_P} \qquad (2.58)$$

where

$$K_{exp} = \left(\frac{X_{MCO_3}}{X_{CaCO_3}}\right)\bigg/\left(\frac{m^{\infty}_{M^{2+}}}{m^{\infty}_{Ca^{2+}}}\right) \qquad (2.59)$$

and K_{exp} is the empirical partition coefficient. The implications of equation 2.58 are that if the DBL was the main controlling influence on trace element incorporation in calcite then the value of K_{exp} would tend to 1 as precipitation rates increased (i.e. $R'_p \rightarrow 1$) (Wang and Xu, 2001) but as this observation has not been observed experimentally the depletion of ions in the DBL at faster precipitation rates may only have a partial control on trace element ratios in calcite and other minerals. It is possible however, that the chemoselectivity of anionic function groups within the biofilm matrix may accentuate the effect of DBL processes on trace element partitioning.

2.18 (Mg/Ca)$_{calcite}$ palaeothermometry

The magnesium ion, Mg^{2+} is one of a number of divalent cations which may substitute for Ca^{2+} in calcium carbonate minerals (Barker *et al*., 2005). The existence of a possible connection between the magnesium content of marine calcite and water temperature was first detected when a correlation was observed between latitude and magnesium content in marine skeletal calcites (Chave, 1954). The ratio of magnesium to calcium incorporated into the shells of marine organisms has been put forward as a method of independently assessing the temperature at which calcification took place (Rosenthal *et al*., 1997; Elderfield *et al*., 1996). It has notable advantages over other temperature proxies in that the oceanic residence times of Ca and Mg are of the order of 10^6 and 10^7 years allowing the reasonable assumption that Mg/Ca ratios in seawater are constant on a glacial-interglacial timescale (Barker *et al*., 2005). A number of carbonate deposits have been either utilised or considered as potential archives of palaeotemperature data from their (Mg/Ca)$_{calcite}$ ratios. Foraminiferal and coral carbonates have been the main focus of research; considerably fewer studies have been conducted on freshwater carbonates such as speleothems and tufas.

2.18.1 Foraminifera

Early experiments on the relationship between Mg/Ca ratios in foraminiferal tests and water temperature were inconclusive (Delaney *et al*., 1985). Subsequent culture studies on the species *G. sacculifer* revealed a link between calcification temperature and (Mg/Ca)$_{calcite}$ ratios where the mean (Mg/Ca)$_{calcite}$ ratio increased linearly from about 1.39 at 19.5°C to 3.28 at 29.5°C giving an increase of about 130%. However,

collated data from a number of studies on $(Mg/Ca)_{calcite}$ ratios versus water temperature in foraminiferal tests obtained from sediment traps, core tops and culture experiments revealed an exponential relationship was more appropriate than the linear one suggested by the data on *G. sacculifer* (Figure 2.12, Equation 2.60) (Nurnberg *et al.*, 1996):

$$(Mg/Ca)_{calcite} = 0.000284(10^{0.03547T(°C)}) \qquad (2.60)$$
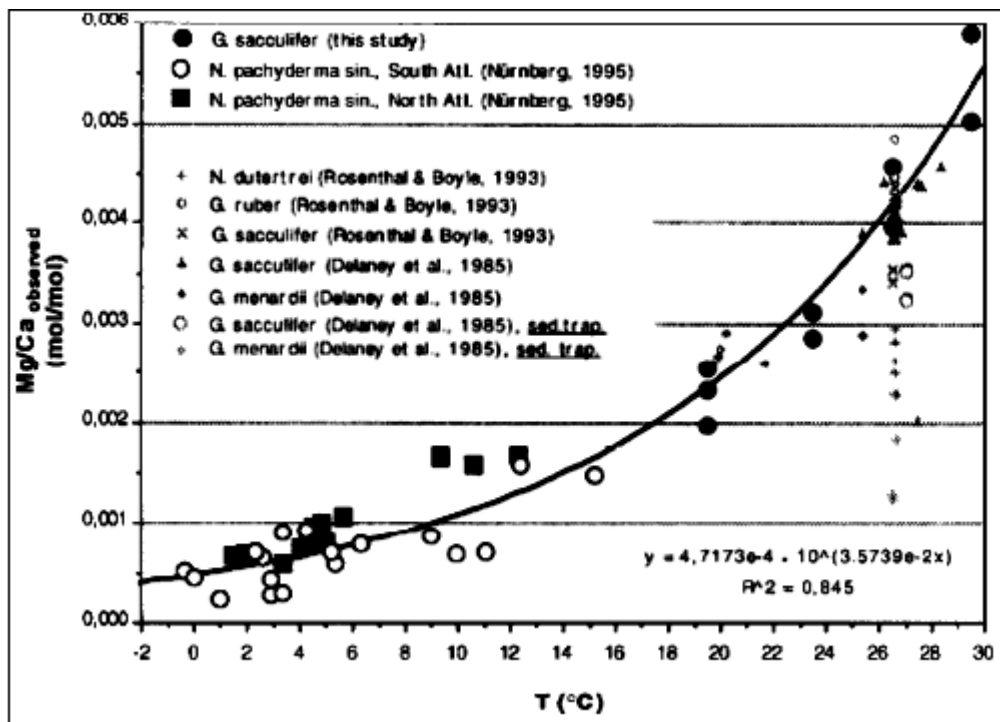
Figure 2.12 $(Mg/Ca)_{calcite}$ ratios against temperature from foraminiferal tests obtained from core tops, sediment traps and culture experiments (Nurnberg *et al.*, 1996).

Other studies have confirmed the exponential correlation between temperature and $(Mg/Ca)_{calcite}$ in foraminiferal tests (e.g. Rosenthal *et al.*,1997, Lea *et al.*, 1999, Anand *et al.*, 2003, Mckenna and Prell., 2004, Regenberg *et al.*, 2008, Groeneveld and Chiessi 2011). Generally the sensitivity of foraminiferal calcite Mg/Ca ratios to temperature has been found to be fairly consistent between single species culture experiments and sediment based multi species samples. Combined data from several single species calibrations shows a sensitivity of 9.7 ± 0.9 % per °C, (Rosenthal and Linsley, 2006), multispecies sediments have resulted in sensitivities of 9.5 ± 0.5 % (Rosenthal and Lohmann, 2002) and 9.0 ± 0.3 % per °C (Anand *et al.*, 2003).

45

Despite the successes of foraminiferal Mg/Ca palaeothermometry it has been observed that factors other than temperature can impact test $(Mg/Ca)_{calcite}$ such as salinity (Ferguson *et al*., 2008, Arbuszewski *et al*., 2010), dissolution effects such as the partial dissolution of high magnesium parts of the test in seawater that is undersaturated with respect to calcite (Dekens *et al*., 2002, Regenberg *et al*., 2008), test size and weight (Anand *et al*., 2003) and the concentration of CO_3^{2-} (at low ion values) (Russell *et al*., 2004, Elderfield *et al*., 2006, Rosenthal *et al*., 2006). A number of common conclusions arise from the published work on the $(Mg/Ca)_{calcite}$ palaeothermometer in foraminifera (see Nurnberg *et al*., 1996; Lear *et al*., 2002; Anand *et al*., 2003; Barker *et al*., 2005; Elderfield *et al*., 2006; Kisakurek *et al*., 2008):

i)   Although a single calibration equation may have some use, particularly for extinct species, calibration equations should be species specific. Mg/Ca ratios in benthic species avoid the complication of the uncertainties associated with calcification depth and dissolution effects.

ii) The calibration equation takes the general form $Mg/Ca = Be^{AT}$, where A and B are species dependant constants and T is the calcification temperature in °C.

iii) The sensitivity of the Mg/Ca ratio is around 9 ± 1 % per °C. (thermodynamics predicts 3% per °C) (Rosenthal and Linsley, 2006).

In relation to the second point above, the value of the pre exponential constant B has been found to differ significantly for both same and different species calibrations, therefore the accuracy of foraminiferal calcite Mg/Ca palaeothermometry is better when estimating relative changes in sea temperatures than absolute temperatures (Rosenthal and Linsley, 2006).

2.18.2   Corals

Initial studies on the use of Mg/Ca ratios in corals as palaeoclimate indicators suggested significant potential. For example, variations in the Mg/Ca ratio of coral skeletons from Ishigaki Island, Japan closely matched sea surface temperatures (SST) over an 8 year period, furthermore neither temporal nor geographic changes in

the Mg/Ca ratio of the local seawater as a result of river discharge had any significant influence on the coralline Mg/Ca ratio (Mitsuguchi *et al.*, 1996). This led to the conclusion that the Mg/Ca ratio in corals had the potential to provide a precise, fast and high resolution proxy for tropical SSTs. However, subsequent studies found that although seasonal variations in coralline $(Mg/Ca)_{calcite}$ ratios were evident, the correlation with annual SSTs was only moderate ($R^2 = 0.52$ Schrag, 1999, $R^2 = 0.66$ Fallon *et al.*, 1999 and $R^2 = 0.55$ Quinn and Sampson, 2002). It has been claimed that the incorporation of Mg into coral skeletons is predominantly controlled by biological or kinetic processes rather than factors such as SST and water chemistry (Allison and Finch, 2007).

Whilst several studies of coralline Mg/Ca values show clear uninterrupted annual cycles which are highly correlated with SSTs (e.g. Mitsuguchi *et al.*, 1996, 2003, Sinclair *et al.*, 1998, Fallon *et al.*, 1999, Wei *et al.*, 2000, Yu *et al.*, 2005), others do not (e.g. Fallon *et al.*, 2003, Allison and Finch, 2007, Mitsuguchi *et al.*, 2008). Despite the uncertainties a number of calibrations of the Mg/Ca ratio in coral skeletons for SSTs have been determined, but unlike foraminiferal calibrations which generally take an exponential form, coralline calibrations are linear (Reynaud *et al.*, 2007) and are described by the general equation:

$$(Mg/Ca)_{calcite} = bT + a \qquad (2.61)$$

where *T* is the temperature (°C) and *a* and *b* are constants. The value of these constants varies as demonstrated by the data in Table 2.2 which provides detail of calibrations from the literature.

Table 2.2 Calibration equation constants for different coral species (adapted from Reynaud *et al.*, 2007).

Reference	Coral species	*b*	*a*
Mitsuguchi *et al.* (1996)	*Porties sp.*	0.129	1.15
Fallon *et al.* (1999)	*Porties lobata*	0.088	1.38
Wei *et al.* (2000)	*Porties sp.*	0.113	1.60
Fallon *et al.* (2003)	*Porties sp.*	0.098	1.54
Yu *et al.* (2005)	*Porties lutea*	0.110	1.32
Reynaud *et al.* (2007)	*Acropora sp.*	0.138	0.90

The variations in the slopes and intercepts of the published Mg/Ca – SST relationships give rise to an implied average seasonal SST change varying between 6.5 and 12.5 °C, compared to the actual instrumental record of 10°C (Yu *et al*., 2005). The variations in the calibration constants of the coralline Mg/Ca palaeothermometer have been attributed to poorly understood biological processes termed the 'vital effect', which modify the thermodynamic relationship between SSTs and the trace element composition of coral skeletons (Reynaud *et al*., 2007). The vital effect has been described as the most important problem for coral trace element proxies (Shirai *et al*., 2005). At some locations the discrepancies between the SSTs inferred from Mg/Ca ratios and actual SSTs have been attributed to local variations of seawater Mg/Ca ratio as a result of nearby river discharge (Reynaud *et al*., 2007).

Determining the absolute magnitude of vital effects on the partitioning of trace elements between seawater and corals requires a comparison with thermodynamic partitioning between abiotic aragonite and seawater, and then to kinetic effects (Gagnon *et al*., 2007). However, this has proven problematic due to difficulties in attaining thermodynamic equilibrium in precipitation experiments (Gagnon *et al*., 2007). Coral growth rate has been cited by many as an influencing factor in coralline trace element ratios (e.g. de Villiers *et al*., 1994; de Villiers *et al*., 1995; Fallon *et al*., 1999; Schrag *et al*., 1999). A study on *Acropora sp.* found that a temperature change from 21 to 29 °C induced a 5.7 fold increase in the calcification rate and an increase in the Mg/Ca ratio of 30%, whilst an increase in light levels by a factor of 4 resulted in a 9% increase in the Mg/Ca ratio (Reynaud *et al*., 2007) Therefore the calcification rate is not simply a function of SST, but is also influenced by light intensities.

The structure of coral skeletons may also be a factor in reducing the reliability of Mg/Ca ratios in corals as a palaeothermometer. The branching coral *Acropora nobilis* skeleton has two distinct components to its skeleton, the framework skeleton and the infilling skeleton. The skeletal density increases with distance from the tip which is attributed to secondary aragonite precipitation in the pore spaces (the infilling skeleton) of the framework skeleton (Shirai *et al*., 2008). Microscale analyses revealed that the infilling skeleton had a lower Mg/Ca ratio than the

framework skeleton. The differing ratios of trace elements in the infilling and framework skeletons had a significant impact on the bulk ratio limiting its use as a palaeothermometer (Shirai *et al*., 2008).

2.18.3 Speleothems

The growth of speleothems can occur continuously for 10^3 to 10^5 years and they can be dated accurately by uranium series methods (Fairchild *et al*., 2006), making these calcareous deposits very appealing to palaeoclimatologists. The multiple proxies held within speleothem deposits have been used to reveal Pleistocene and Holocene palaeoenvironmental data on soil conditions, rainfall, temperature and cave pCO$_2$ (Fairchild and Treble, 2009). They are particularly useful in low to mid-latitude terrestrial settings where ice core records are unavailable (Baldini, 2010, Wong *et al*., 2011). However, the nature of the karstic system in which they are deposited makes unravelling the climate record they contain inherently more difficult than ice cores (Fairchild *et al*., 2006). Although trace element ratios such as Mg/Ca represent a significant proportion of speleothem proxies they have received less attention than the stable isotopes δ^{13}C and δ^{18}O due to complicating factors of the karstic system (Fairchild and Treble, 2009).

The main factors of the karstic system reported as potentially impacting on the reliability of speleothem Mg/Ca as a palaeotemperature proxy are variability in drip water composition and drip rate, changes in the depositional environment such as variations in water supply rate and degree of saturation and prior calcite precipitation (PCP) along the flow path (Gascoyne, 1983, Fairchild *et al*., 2006, Wong *et al*., 2011). Therefore, before any useful information can be obtained from fossil speleothems it is necessary to isolate the temperature induced variations from other sources of variation. Changes in drip rate chemistry could potentially be determined by observing the M^{2+}/Ca ratio of a second trace metal with a non temperature dependant distribution coefficient and which covaries with magnesium. However, isolating changes caused by variations in depositional conditions will be more difficult as they are likely to vary both spatially and temporally (Gascoyne, 1983).

Annual (Mg/Ca)$_{calcite}$ variations in Holocene speleothems have been shown to correlate with temperature, however longer term variations in the same sample were

not explainable by temperature records (Roberts *et al*., 1998). The mean annual temperature increase inferred in the longer term $(Mg/Ca)_{calcite}$ ratios has not been recorded during the Holocene. Therefore, these longer term variations may reflect changes in residence times which are controlled by variations in effective precipitation and/or hydrological mixing of waters in the epikarstic region above the cave exposed to two different source rocks, calcite and dolomite (Roberts *et al*., 1998).

An understanding of trace element variations in cave drip waters is crucial to speleothem Mg/Ca palaeothermometry and this has been the subject of several studies (e.g. Fairchild *et al*., 2000; Fairchild *et al*., 2006; Baldini *et al*., 2006). A number of hydrological factors can influence the trace element composition of the water in a karstic environment that eventually seeps into caves, such as the faster dissolution rate of calcite compared to dolomite, prior calcite precipitation along the flow path, selective leaching of trace elements (Fairchild *et al*., 2000), length of residence time of the water above the cave (Verheyden *et al*., 2000) and flow rates (Fairchild *et al*., 2006).

The role of prior calcite precipitation along the flowpath and its influence on the trace element composition of drip waters has been observed in a study based in an old limestone mine overlain by 15 m of poorly karstified Jurassic limestones in southwest England (Fairchild *et al*., 2006). The precipitation of $CaCO_3$ in the aquifer above the mine occurred when low pCO_2 cave air penetrated the aquifer allowing CO_2 to degas resulting in the solution becoming supersaturated with respect to calcite. Fairchild *et al*. (2006) related this prior precipitation to drip water trace element composition through a low (<<1) partition coefficient which will not result in significant amounts of the trace element being removed through prior calcite precipitation. Consequently there will be an increase in trace element ratios, such as Mg/Ca and Sr/Ca, in drip waters which have been subjected to prior calcite precipitation compared to drip waters where no prior precipitation has occurred. From this it can reasonably be inferred that spatially separated speleothems formed under the same temperature regime may present with different Mg/Ca ratios and provide conflicting palaeotemperature data (Fairchild *et al*., 2006).

Experiments conducted under karst analogue conditions produced a partition coefficient for Mg of approximately 0.0006 per °C (Huang and Fairchild, 2001), such a low value means any palaeotemperature signal will typically be masked by variations in drip water Mg/Ca (Fairchild and Treble, 2009). The difficulties in isolating the temperature induced component on speleothem $(Mg/Ca)_{calcite}$ has resulted in karstic research community moving its focus towards hydrologically induced variations in speleothem Mg/Ca ratios at the expense of temperature effects.

2.18.4 Tufas

The potential for tufa deposits as a palaeoclimate archive has been recognised in a number of studies on their stable isotope composition (Pazdur *et al*., 1988; Andrews *et al*., 1993; Andrews *et al*., 1997; Andrews *et al*., 2000; Matsuoka *et al*., 2001; Garnett *et al*., 2004; Brasier *et al*., 2010; Lojen *et al*., 2009). To date only two studies appear to have focused on utilising tufa Mg/Ca ratios as a palaeothermometer (Chafetz, 1991, Ihlenfeld *et al*., 2003), although other studies have discussed it (Garnett *et al*., 2004; Brasier *et al*., 2010; Lojen *et al*., 2009). The use of Mg/Ca ratios in tufa carbonate deposits as a palaeothermometer requires that the $(Mg/Ca)_{water}$ be constant, however in a fluvial setting prior precipitation upstream from a given sampling point will result in the $(Mg/Ca)_{water}$ increasing with distance downstream. Furthermore, the magnitude of the variation of stream water Mg/Ca values will differ from stream to stream (Ihlenfeld *et al*., 2003, Andrews and Brasier, 2005, Kawai *et al*., 2006).

Whether the variations in stream water Mg/Ca are of a magnitude to mask any potential temperature induced $(Mg/Ca)_{calcite}$ variations appears to be dependent on the characteristics of individual streams. The magnitude of the $(Mg/Ca)_{water}$ variations along the Gregory River in Queensland, Australia is relatively small ($\sim 0 - 5\%$) with higher values in the dry season due to longer residence times allowing increased dolomite dissolution compared to calcite (Ihlenfeld *et al*., 2003). With a seasonal temperature range of 10°C in the Gregory River it has been suggested that the relatively small $(Mg/Ca)_{water}$ variations would not significantly mask any temperature induced changes in $(Mg/Ca)_{calcite}$ values (Ihlenfeld *et al*., 2003). However, in contrast a five year study on the water chemistry of a tufa depositing stream in southwest Japan found significant variations in the $(Mg/Ca)_{water}$ ratio with values ranging from

0.015 to 0.030 leading to the conclusion that the $(Mg/Ca)_{water}$ ratio was too unstable and applying a $(Mg/Ca)_{calcite}$ palaeothermometer at this site would result in large perturbations (Kawai *et al*., 2006).

Despite the potential difficulties of calibrating an $(Mg/Ca)_{calcite}$ palaeothermometer for tufa carbonates there has been some evidence that it may be achievable. Incorporation of Mg^{2+} into tufas (Arbuckle stream, Oklahoma, U.S.A.) deposited in the summer was found to be higher than in winter (Chafetz *et al*., 1991). In the aforementioned Gregory River, a seasonal temperature change in stream water of ~ 10 °C appeared to be the dominating influence on Mg^{2+} incorporation into a 14 year (1985 – 1999) tufa deposit, however there were significant discrepancies in the record (Ihlenfeld *et al*., 2003). A further complicating factor in the generation of an accurate tufa $(Mg/Ca)_{calcite}$ palaeothermometer is the existence of benthic microbial biofilms which are ubiquitous in tufa precipitating streams. The observation that the EPS produced by the organisms within the biofilm are able to selectively chelate cations (Rogerson *et al*., 2008) from the bulk stream water has major implications for the trace element ratios in tufa precipitates. However, it has yet to be determined whether selectivity in favour of Ca^{2+} over Mg^{2+} will be able to override the thermodynamic control on Mg^{2+} partitioning in tufa carbonates.

2.19 Impact of salinity on $(Mg/Ca)_{calcite}$

The earliest studies (Chave, 1954 and Savin and Douglas, 1973) concluded that salinity variations had no impact on the calcite of foraminiferal tests, therefore palaeoenvironmental models had largely assumed that the incorporation of Mg^{2+} into calcite is largely insensitive to seawater salinity variations (Stephensen *et al*., 2011). This assumption was held despite some evidence that salinity was able to influence Mg^{2+} partitioning into calcite. Although not quantitatively described, salinity was found to cause an increase in $(Mg/Ca)_{calcite}$ in Red Sea cores, furthermore the Mg/Ca ratios were found to be more strongly correlated with salinity than temperature (Yusuf, 1980). More recent studies have shown $(Mg/Ca)_{calcite}$ increases by about 4 ± 3 % per ppm change in salinity (Nurnberg *et al*., 1996, Lea *et al*., 1999, Kisakurek *et al*., 2008, Duenas-Bohorquez *et al*., 2009, Dissard *et al*., 2010). A stronger correlation where $(Mg/Ca)_{calcite}$ increases by about 15 - 59 % per ppm change in

salinity was reported by Ferguson *et al*., (2008), they also reported that salinity had a greater influence on the (Mg/Ca)$_{calcite}$ of foraminiferal tests than temperature.

The observation that salinity can have a significant impact on the partitioning of magnesium into foraminiferal calcite requires that careful consideration be given to the palaeotemperature calibrations obtained from marine carbonates. Species specific calibration equations combining both temperature and salinity impacts would be useful step forward in increasing the reliability of the foraminiferal (Mg/Ca)$_{calcite}$ palaeothermometer. A study on a single species of planktonic foraminifera, *Globigerinoides ruber*, collected from the Gulf of Eilat, Israel and cultured at varying temperatures and salinities revealed that the sensitivity of (Mg/Ca)$_{calcite}$ to temperature was 8 ± 3 % per °C and to salinity was 5 ± 3 % per ppm A calibration equation combing these two influences was determined to be (Kisakurek *et al*., 2008):

$$Mg/Ca = \exp 0.06 \pm (0.02)\, S + 0.08(\pm 0.02)T - 2.8(\pm 1.0) \ (R^2 = 0.95) \qquad (2.62)$$

where S is salinity (ppm) and T temperature (°C). Despite the clear correlation shown between salinity and (Mg/Ca)$_{calcite}$, the mechanisms that drives this influence are not well understood (Ferguson *et al*., 2008, Duenas-Bohorquez *et al*., 2009). It has been suggested that complex biological processes and pathways may control the uptake of trace elements into foraminiferal calcite. Specifically, the level of salinity may influence the cellular Mg pumps and channels by changing the efficiency at which they extract Mg^{2+} from the seawater (Ferguson *et al*., 2008, Duenas-Bohorquez *et al*., 2009).

3 Literature derived methods

3.1 Introduction

This chapter describes the generic (i.e. non original) methods used in this work. Chapter 4 provides a detailed description of the experimental design and sample recovery methods that were developed specifically for this research; along with an analysis of the effectiveness of the methods.

3.2 EPS extraction methods

Physical methods for EPS extraction include centrifugation, sonication, heat treatment mixing and shaking (Nielsen and Jahn, 1999, Flemming *et al*., 2000). Chemical methods involve the addition of various chemicals to the sample which break down the differing linkages within the EPS matrix resulting in the release of EPS to the water (Nielsen and Jahn, 1999). Chemical protocols include Ethylenediamine tetraacetic acid (EDTA), glutaraldehyde, formaldehyde + NaOH (Comte *et al*., 2006) and H_2SO_4 (Barranguet *et al*., 2004). The use of a combination of both physical and chemical protocols is often used, with centrifugation being the most popular physical treatment prior to the application of a chemical protocol. The composition of the extracted EPS depends on the method used (Comte *et al*., 2006) and it was also noted by (Comte *et al*., 2006) that the extracted EPS may be contaminated by the extracting reagents and that the presence of this contamination can affect the cation chelation of the functional groups within the EPS.

Four methods of extraction were tested and are detailed in the following subsections. In all cases the biofilm was collected from the mesocosm colonising flume (see section 4.2.3), excess water was removed by filtration through 11 μm filter papers. The mass of filtered biofilm used in the extraction processes was 5 g ± 0.1 g for each 12 mL of ultrapure water (18 MΩ). All filter papers used in the filtration processes described below were wetted with ultrapure water to minimise loss of the EPS solution through absorption to the filter papers.

3.2.1 Immersion in ultrapure water

The biofilm was added to sterilin tubes each containing 12 mL of ultrapure (18 MΩ) water and shaken vigorously to ensure even mixing. The solution was left to sit for 24 hours and was shaken every hour (during normal working hours) then filtered through 11 μm filter papers followed by filtration through 0.2 μm filter papers into a sterilised (by pure ethanol) sterilin tube giving a sterile solution of EPS. This method is considered the most basic method of EPS extraction (Nielsen and Jahn, 1999).

3.2.2 Centrifugation

The biofilm was added to sterilin tubes each containing 12 mL of ultrapure (18 MΩ) water and shaken vigorously to ensure even mixing. The samples were shaken every 15 minutes for a period of 2 hours and then centrifuged at 3300 rpm for 15 minutes. The supernatant (containing the stripped EPS) was filtered, firstly through 11 μm filter papers into a sterilin tube and then through 0.2 μm filter papers into sterilised sterilin tubes giving a sterile solution containing the EPS.

3.2.3 Heat treatment

Oven proof 50 mL conical flasks were used to mix 24 mL of ultrapure (18 MΩ) water with 10 g of biofilm. The mixture was shaken vigorously to ensure even mixing and left to sit for 2 hours. It was then placed in a preheated oven at 130 °C for 2 hours (Barranguet et al., 2004). The solution was gently shaken every 20 minutes whilst in the oven. The solution was allowed to cool before being centrifuged at 3300 rpm for 15 minutes. The supernatant was filtered through 11 μm filter papers and then through 0.2 μm filter papers into sterilised sterilin tubes to give a sterile EPS solution.

3.2.4 Centrifugation plus sulphuric acid treatment

This method began by following the centrifugation method to the point of completion and setting aside the sterile EPS solution. The centrifuged biofilm pellets were recovered and placed in 10 mL volumetric flasks containing 8 mL of ultrapure 0.2M H_2SO_4, the mixture was shaken vigorously and placed in a preheated oven at 95 °C for 30 minutes (Barranguet *et al*., 2004) shaking gently every 5 minutes. The solution was allowed to cool before being centrifuged at 3300 rpm for 15 minutes. The supernatant was filtered through 11 μm filter papers followed by filtration

through 0.2 μm filter papers into sterilised sterilin tubes. This solution was then mixed with the reserved solution from the centrifugation stage of the process and shaken to homogenise.

3.2.5 Effectiveness of EPS extraction methods

To assess the effectiveness of each method of EPS extraction 12 mL samples from each extraction method were dehydrated on pre-weighed watch glasses over a Bunsen burner. The watch glass holding the dehydrated EPS molecules was re-weighed to determine the mass of EPS extracted. The process of extraction and dehydration was repeated three times for each method. The results from each process and the mean mass of EPS obtained from the different extraction protocols are detailed in Table 3.1.

Table 3.1 Mass of EPS extracted from 5 g of biofilm using different extraction protocols.

Extraction method	Mass of EPS (mg) Procedure 1	Mass of EPS (mg) Procedure 2	Mass of EPS (mg) Procedure 3	Mean mass of EPS (mg)
De – ionised water	1.7	1.4	1.5	1.5
Centrifugation	4.2	3.9	4.3	4.1
Heat	10.7	11.2	11.4	11.1
Centrifugation + H_2SO_4	11.3	10.9	11.7	11.3

The method chosen for all isolated EPS experiments described in this work was the heat method. Although the centrifugation combined with H_2SO_4 method had a slightly higher mean yield, it was considered that the introduction of sulphate ions to the experimental solution had the potential to both impact on the chelation dynamics and remove $Ca^{2+}_{(aq)}$ through the precipitation of $CaSO_4$.

3.3 Salinity variation Petri dish experiments

This experiment undertaken in association with Nuffield Project students but was overseen throughout by the author of this thesis. The methods used in the experiment were developed by the author who was intimately involved in their application throughout.

3.3.1 Solution preparation and EPS extraction

Experimental water was collected from a spring sourced by a Cretaceous chalk aquifer at Welton Beck, East Yorkshire (UK grid reference SE 965 275). It was analysed for its Ca^{2+} and Mg^{2+} concentrations by ICP – OES. Acetates of calcium $(Ca(C_2H_3O_2)_2$ and magnesium $(Mg(C_2H_3O_2)_2$ (Alfa Aesar, Massachusetts., USA) were added to the spring water to bring the concentrations of Mg^{2+} and Ca^{2+} to 51 ± 1.8 and 1544 ± 19.8 mg l^{-1} respectively giving a Mg/Ca molar ratio of 0.054 ± 0.002. The saturation state was determined using the aqueous geochemical modelling software PHREEQC. The saturation index for the experimental solution was 1.64 at 16 °C. The solution was divided between five sterilised conical flasks. One flask was retained as freshwater whilst NaCl was added to the other flasks in quantities to give saline solutions of 10, 20, 30 and 40 ppm. The method of EPS extraction was the 'heat' method described in subsection 3.2.3.

3.3.2 Precipitation environment

The experiment was conducted in 20 clear plastic Petri dishes each containing two frosted glass microscope slides. The dishes and slides were sterilised with pure ethanol. The dishes were prepared by adding 25 mL of the varying saline solutions to each one giving four dishes each with salinities of 10, 20, 30 and 40 ppm. Four dishes were retained as freshwater replicates. Two replicates of each salinity and freshwater treatments received 3 mL of extracted EPS solution leaving two replicates of each treatment without isolated EPS. Lids were placed on each dish and they were sealed by applying a thin coating of clear silicone gel. The dishes were then covered to exclude light and left under ambient laboratory conditions at 16 °C for 14 days.

3.3.3 Precipitate recovery and analysis

At the end of the experiment the lids were carefully removed and a sample of the dish solution was taken from each dish and immediately acidified by dilution with 5 % ultrapure HNO_3 for determination of Ca^{2+} and Mg^{2+} concentrations by ICP – OES. The slides were gently rinsed with UHQ water and returned to new Petri dishes and placed in an oven at 60 °C to dry. The washing of the slides was done to ensure no further precipitation could take place during the drying process. Ultrapure 10 % HNO_3 was gravimetrically added to each dried dish to dissolve the precipitates on the slides. Each dish was left for two hours and shaken gently every 20 minutes to aid

dissolution. Samples of solution were taken from each dish and immediately diluted gravimetrically with 5 % ultrapure HNO_3 prior to analysis by ICP – OES for Ca^{2+} and Mg^{2+} concentrations.

3.4 Varying EPS concentrations - Petri dish experiments

3.4.1 Solution preparation and EPS extraction

Experimental water was also collected from Welton Spring (as described in section 3.3.1). It was prepared and analysed for its Ca^{2+} and Mg^{2+} concentrations by ICP – OES. Acetates of calcium $(Ca(C_2H_3O_2)_2$ and magnesium $(Mg(C_2H_3O_2)_2$ (Alfa Aesar, Massachusetts, USA) were added to the spring water to bring the concentrations of Mg^{2+} and Ca^{2+} to 8.0 and 160.0 mg L^{-1} respectively giving a molar $(Mg/Ca)_{solution}$ ratio of 0.082. The saturation state was determined using the aqueous geochemical modelling software PHREEQC. The saturation index value for the experimental solution was 1.01 at 16 °C. The method of EPS extraction was the 'heat' method described in subsection 3.2.3.

3.4.2 Precipitation environment

The experiment was conducted in clear plastic Petri dishes each containing two frosted glass microscope slides. The dishes and slides were sterilised with pure ethanol. Four replicates of each treatment were prepared by adding 25 mL of the prepared acetate solution. Five different treatments were created by adding 1, 2, 3, 4, and 5 mL of EPS solution to the individual replicates. Four replicates were retained as controls with no added EPS solution. Lids were placed on each dish and they were sealed by applying a thin coating of clear silicone gel. The dishes were then covered to exclude light and left under ambient laboratory conditions at 16 °C for 27 days.

3.4.3 Precipitate recovery and analysis

This was undertaken using the same procedures as described in section 3.3.3.

3.5 Sampling of Holocene tufa for trace element ratios

3.5.1 Tufa sample origin

The sample used in this experiment came from an early Holocene encrusted reed tufa deposit in Caerwys, North Wales (see chapter 7 for more details). The sample was

part of an extensive deposit overlaying glacio-fluvial siliciclastic sands and gravels most probably originating from Triassic rocks of the Vale of Clwyd.

3.5.2 Drilling procedure and sample preparation

The tufa sample was firmly secured to a plastic mount and secured to the drilling platform by a vice to ensure no movement during the drilling process (Figure 3.1). Drilling was undertaken using an Elco variable speed dental drill with a 30 micron tungsten carbide burr. Five sampling lines were chosen and drilled individually (Figure 3.2). Samples of drilling dust were collected at 0.5 mm intervals along each line and carefully added to 2 mL aliquots. The sample was cleaned with compressed air between each sample collection to ensure no cross contamination occurred.
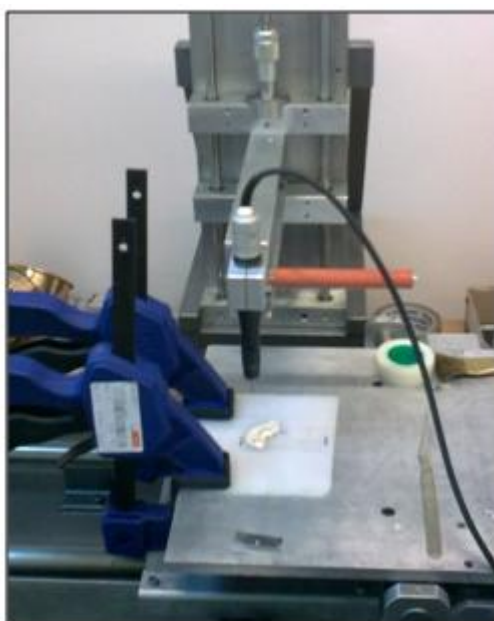
Figure 3.1 Set up of drilling apparatus.

Figure 3.2 Drilling lines across tufa sample

The tufa dust samples were digested in 200 µL of concentrated HNO_3 and subsequently diluted with 5 % HNO_3 prior to analysis for Ca^{2+}, Mg^{2+} and Sr^{2+} by ICP − OES to determine their Mg/Ca, Sr/Ca and Sr/Mg ratios.

3.6 Inductively coupled plasma optical emission spectroscopy

Making full use of the potential of Mg/Ca ratios in carbonate minerals as a palaeothermometer requires a technique which can quickly and precisely analyse small samples of varying compositions (de Villiers *et al*., 2002, Green *et al*., 2003, Shrag, 1999). Early work on Mg/Ca ratios of marine carbonates relied on the related technique of atomic absorption (AA) analysis (Elderfield *et al*., 1996), however this technique has been criticised by Green *et al*. (2003) as being time consuming, in that differing elements are determined sequentially and that it is not conducive to high precision ratio determinations. Other related techniques which have been utilised in the determination of trace element ratios in carbonate minerals are inductively coupled plasma mass spectrometry (ICP-MS) (Martin *et al*., 2002, Rosenthal *et al*., 2006) and thermal ionization mass spectrometry (TIMS) (Nurnberg *et al*., 1996, Beck *et al*., 1992), however these techniques are considerably more expensive and also less precise than inductively couple plasma optical emission spectrometry (ICP-OES) (de Villiers *et al*., 2002). The background to ICP − OES methods and the characteristics of the instrument used are detailed in the following subsections.

3.6.1 Atomic emission spectra

The photon model of light describes a beam of light of frequency (f) as consisting of a stream of individual particles called photons with each photon carrying an identical amount of energy (ε) which is related to the frequency by:

$$\varepsilon = hf \qquad (3.1)$$

where h is Planck's constant (6.6262×10^{-34} Js). This model of light is useful when considering atomic spectrometry as individual atoms can only emit or absorb an entire photon of light, not fractions of photons and different elements can be identified by the wavelengths (λ) of the light they emit. To ascertain the wavelengths of the light emitted by individual elements the light is passed through a diffraction grating which splits the light beam into its individual wavelengths where:

$$\lambda = \frac{sin\theta_n d}{n} \qquad (3.2)$$

where θ_n is the angle of diffraction, d is the grating spacing and n is the optical order. The existence of photons of specific energies being emitted from an atom results from changes in the positions of the electrons around the atomic nucleus. In simplistic terms electrons can be found at different distances from the nucleus depending on the energetic state of the atom, with each distance equating to a discrete energy level. The ground, or lowest energy, state of an atom is the most stable and occurs when the electron is at its closest to the nucleus, n = 1 in Figure (3.3).
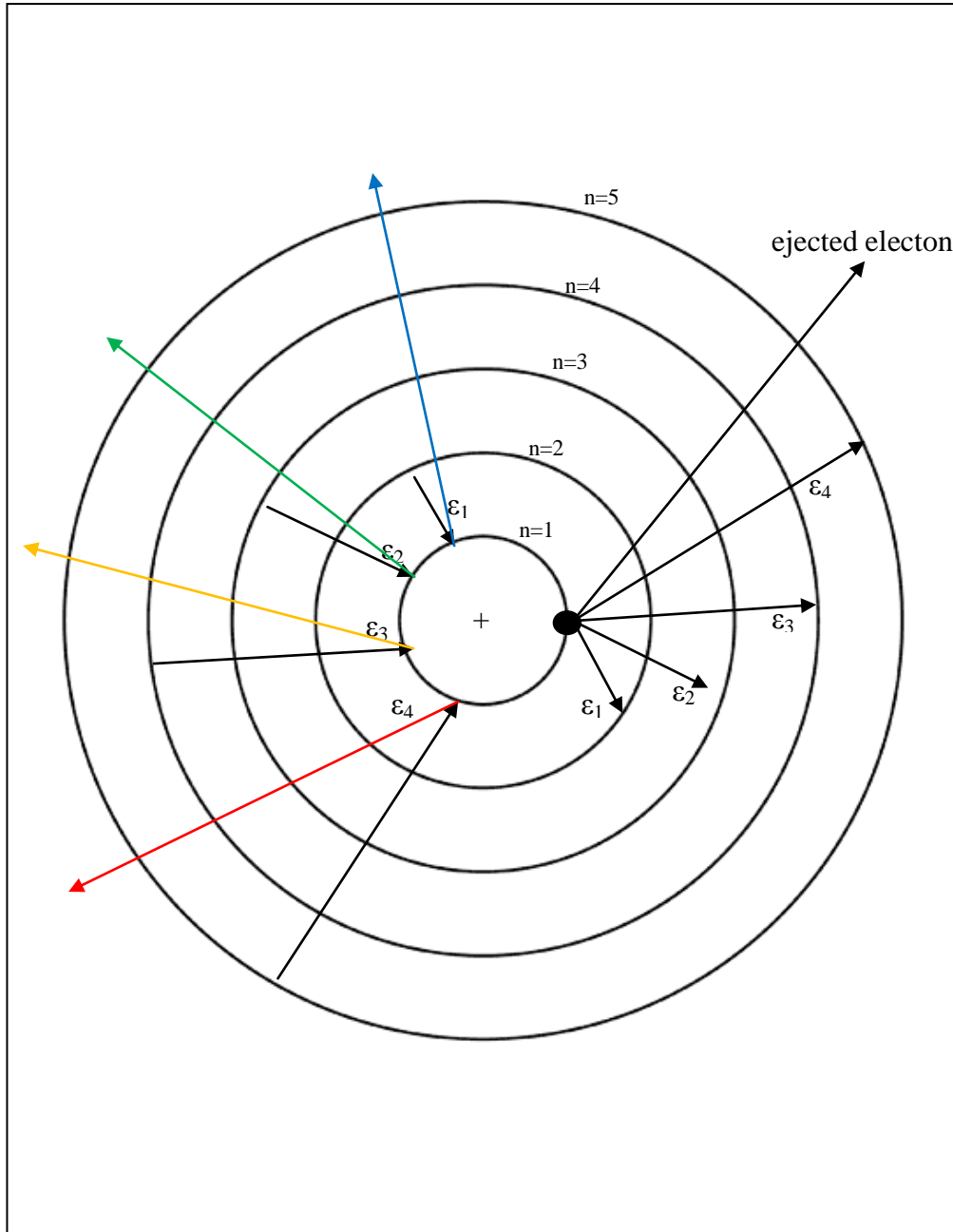
Figure 3.3 Schematic illustration of electron 'orbits' in a hydrogen atom. The values ε₁ – ε₅ represent the energy change of the atom when the electron jumps from one orbital to another. If sufficient energy is received the electron may jump straight from n = 1 to n = 3 or higher. If the energy received is above a certain amount, known as the ionization energy, the electron will be ejected from the atom completely resulting in the creation of a hydrogen ion and a free electron (represented by the 'ejected electron'. Coloured arrows represent the emission of a photon of light of ε=*hf*. The different values of ε represent photons of different wavelengths which can be detected and 'counted' by the ICP – OES instrument to determine the concentration of an element in the sample being analysed.

When an atom acquires energy the two most likely events are that the energy will result in an increase in the kinetic energy of the atom or that the atom will absorb energy and move from the ground state to an excited state (Boss and Fredeen, 2004). For an atom to be in an excited state an electron must have jumped from its ground

state orbital (n = 1) to a higher orbital e.g. n = 2, 3 ,4, 5 (see Figure 3.3). The amount of energy absorbed by the atom determines whether the electron jumps from n = 1 to n = 2, 3, 4, 5 or higher. However, the excited state is less stable for the atom and it will only remain in this state for about 10^{-8} s (Nolte, 2003) before decaying back to a lower orbital by losing energy, either through collision with another particle or through the emission of a photon (Boss and Fredeen, 2004).The frequency of the emitted photon is dependent on the energy difference ($\Delta\varepsilon$) between that of the initial orbital (ε_i, where the subscript i represents the initial level) and that of the subsequent orbital (ε_h where the subscript h represents the higher orbital). From equation (3.1) it follows that:

$$f = \frac{\varepsilon}{h} \qquad\qquad (3.3)$$

therefore, the transition of an electron from the lower to higher orbital will result in the emission of photons of frequency (f_{ph}):

$$f_{ph} = \frac{1}{h}(\varepsilon_h - \varepsilon_i) \qquad\qquad (3.4)$$

and since the wavelength (λ) of light is equal to its velocity divided by the frequency, then the wavelength of emitted photons (λ_{ph}) will be:

$$\lambda_{ph} = \frac{vh}{\varepsilon_h - \varepsilon_i} \qquad\qquad (3.5)$$

where v is the velocity of the photons.

Individual elements have a unique electron shell structure which gives rise to the different series of wavelengths possible as a result of electrons jumping from one energy level to another. These electron transitions are represented schematically by energy level diagrams, the simplest of which is for hydrogen having only one electron (Figure 3.4).
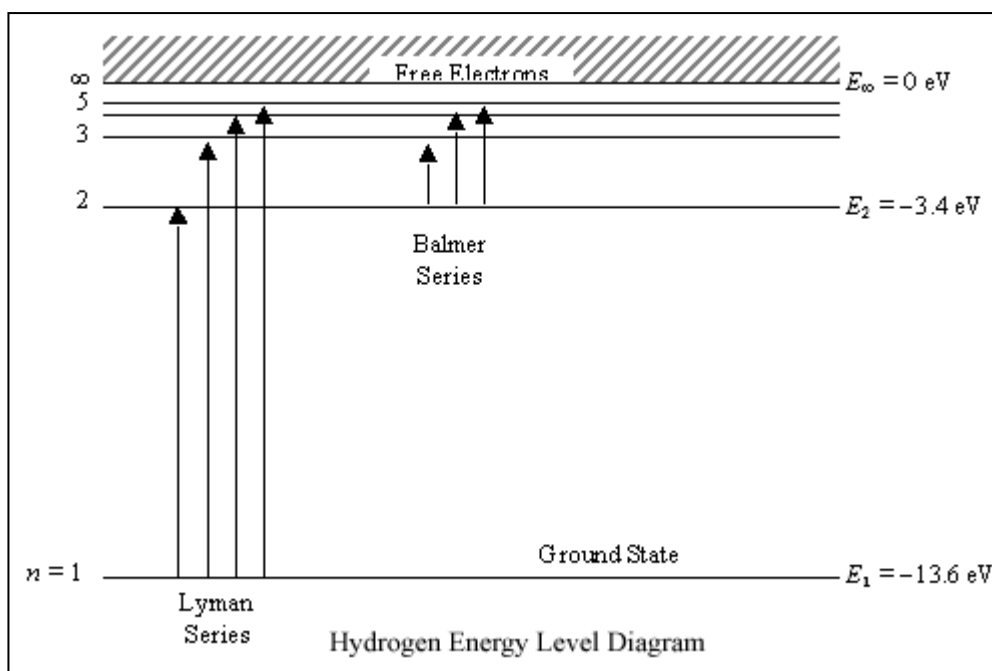
Figure 3.4 Energy level diagram for the hydrogen atom (Nolte, 2003)

The wavelengths most commonly used in atomic spectrometry are in the ultraviolet (190 – 380 nm) and partly in the visible (380 – 800 nm) range (Nolte, 2003). The fact that emission results from an excited state with electrons in higher orbitals gives rise to many 'starting points' from which an electron can fall back and consequently a vast number of emission wavelengths for each element (Nolte, 2003). This fact can be both a help and a hindrance, it is useful to have a choice of analytical lines to choose from for each element but the disadvantage is the possibility of spectral interference (Nolte, 2003).

3.6.2 General characteristics of ICP – OES

The analytical emission lines generated by an ICP – OES instrument are generated by subjecting the sample to temperatures which are sufficiently high to cause its dissociation into atoms and also, through collisional excitation, to cause significant ionisation of the dissociated atoms (Boss and Fredeen, 2004). The predominant gas used for plasma creation is argon due to the combination of its relatively low ionisation energy and low cost. The plasma is created by passing the argon gas through a torch where the application of radio frequency (RF) power to a coil results in RF electric and magnetic fields being generated. In addition, when the argon gas

passes through the torch a spark is applied causing a number of electrons to be removed from the argon atoms and then accelerated by the magnetic field. These high energy electrons collide with further argon atoms creating a chain reaction until the gas is broken down into hot plasma consisting of argon atoms, electrons and argon ions (Boss and Fredeen, 2004). The temperature of the plasma reaches about 10,000 K but is not uniform across the plasma (Nolte, 2003).

The process by which ionisation of a sample is achieved begins with the sample introduction. The sample is initially introduced into the instrument as a liquid and is subsequently converted into an aerosol by a nebuliser. The aerosol droplets are carried into the hot plasma with the mean dwell time of the sample in the plasma being in the order of a few milliseconds (Nolte, 2003). Once in the plasma the sample is firstly stripped from the solvent then vaporised, atomised and ionised. Excitation occurs in the atomised and ionised states and it is the resulting emission of light that is measured to obtain information about the sample. The light emitted by the atoms and ions of the sample is divided spectrally by the instrument's optics and measured by detectors. The presence of an element is usually determined by examining at least three spectral lines of that element. The general set up of an ICP – OES system is shown in Figure 3.5.

.
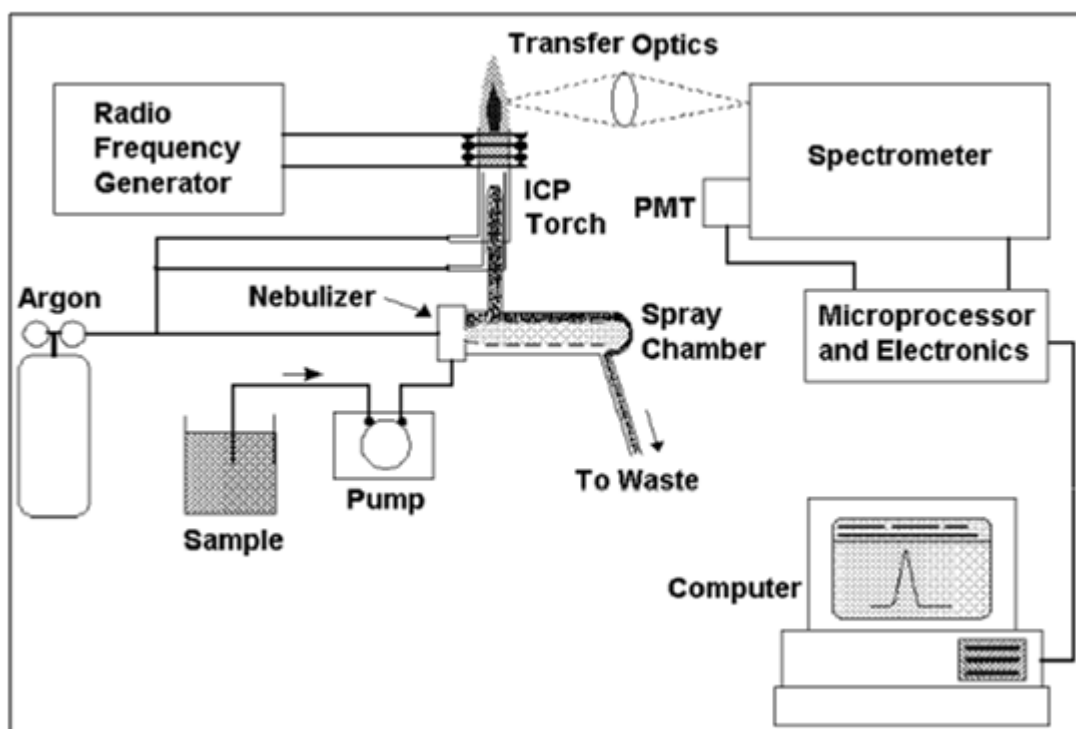
Figure 3.5 Schematic representation of ICP – OES instrumentation (Boss and Fredeen, 2004).

3.6.3 Sample analyses

The analyses were carried out on a Perkin Elmer Optima 5300DV ICP – OES instrument under the preset operating conditions shown in Table 3.1.

Table 3.2 Operating conditions of ICP – OES.

Parameter	Condition
Power	1.4 k W
Plasma gas flow	15 L min^{-1}
Nebuliser flow	0.95 L min^{-1}
Auxiliary gas flow	0.2 L min^{-1}

Each analytical line was measured three times for both the samples and blank calibration solutions (2% ultrapure HNO_3) and the mean of these measurements presented in the output data. The standard deviation (*s*) and relative standard deviation (RSD) was calculated by the internal software, the RSD is calculated by:

$$RSD = \frac{s}{x} \qquad (3.6)$$

Where *s* is the standard deviation and $\bar{x}$ the mean of the measurements, multiplying by 100% gives the RSD in percentage form. The precision of the instrument is

determined by the relative RSD of the measurements and should optimally be about 1% but not more than 3% (Nolte, 2003). The selection of the analytical lines used in the results was based on the Perkin Elmer recommendations for the Optima 5300 DV spectrometer, 393.366 nm for calcium and 280.271 nm for magnesium. Although only one analytical line was chosen as being representative of the sample measurements the fact that the RSD % of the other analytical lines for each element were very similar to the line chosen provides an enhanced trust in the accuracy of the analysis (Nolte, 2003).

3.6.4 Sample preparation. standards and calibration.

Calibration standards were prepared using 1000 ppm standard stock solutions (99.9% pure or greater, PrimAg, Xtra, Romil, Cambridge) of calcium and magnesium. Mixed standards of calcium and magnesium were prepared through dilution with 2% ultrapure HNO_3 to give calibration standards of 1, 2, 3, 4 and 5 ppm for calcium and 0.1, 0.2, 0.3, 0.4, and 0.5 ppm for magnesium. Samples for analysis were diluted with 5 % ultrapure HNO_3 to bring the expected concentrations to within or very near the linear calibration of the standards.

3.7 Scanning electron microscopy

This was undertaken using a Zeiss SMG EVO 60 instrument (Carl Zeiss SMT Ltd., Cambridge, UK) with an Oxford Instruments INCA energy 350 energy dispersive X-Ray spectrometer probe (Oxford Instruments, High Wycombe, UK). Samples for SEM were sited on frosted squares of microscope slide glass and conductively coated by gold spluttering.

3.8 Statistical analyses

Experimental data was analysed and presented through the scientific graphing and statistical analysis platform Sigma Plot 11.0 (Systat Software, California, USA). Correlation analyses between data parameters were conducted using the inbuilt regression wizard. Linear, power and exponential regressions were applied to the data sets in order to determine the correlation of best fit at the 95 % confidence level. The correlation giving the best R^2 value was selected for presentation in the thesis.

Data sets with outliers were analysed with and without the outliers and both correlations presented.

4 Basic experiment characterisation and supporting evidence.

4.1 Introduction

Obtaining palaeotemperature data from $(Mg/Ca)_{calcite}$ ratios is a commonly used approach for marine carbonates such as foraminiferal (Nurnberg *et al*., 1996; Anand *et al*., 2003; Barker *et al*., 2005; Elderfield *et al*., 2006; Kisakurek *et al*., 2008) and corals (Mitsuguchi *et al*., 1996, 2003; Sinclair *et al*., 1998; Fallon *et al*., 1999; Wei *et al*., 2000; Yu *et al*., 2005). Tufa carbonates are ambient temperature freshwater deposits which have been considered, but not thoroughly investigated, as potential archives of terrestrial palaeotemperature data through their Mg/Ca ratios (Garnett *et al*., 2004; Rogerson *et al*., 2008, Brasier *et al*., 2010, Lojen *et al*., 2009).

There is however, considerable uncertainty whether the presence of microbial biofilms in freshwater settings can alter the incorporation of minor ions, such as magnesium, into calcite. These biogenic affects may arise from microbial metabolic activity and / or the presence of extracellular polymeric substances (EPS). EPS has been shown to chelate divalent cations from the bulk water, and to strongly favour ions with low charge density. This influence could be transmitted to solid carbonate chemistry by altering the M^{2+} / Ca^{2+} ratios within the biofilm interstitial waters from which carbonates are precipitated and also by directly influencing the precipitation mechanism itself.

The precipitation of calcite in association with microbial communities has been investigated in a variety of ways. A number of studies have examined calcite precipitation in the presence of specifically selected and isolated microbial communities (Cacchio *et al*., 2003, Cacchio *et al*., 2004, Bosak and Newman, 2005, Baskar *et al*., 2006, Jimenez-Lopez *et al*, 2011, Rusznyak *et al*., 2012), in extracted EPS (Kawaguchi and Decho, 2002, Tourney and Ngwenya, 2009, Dittrich and Sibbler, 2010) and even in the presence of a full biofilm community (Rogerson *et al*., 2008, Pedley *et al*., 2009). Field studies on tufas and travertines have been conducted that examine the macro scale morphology (Emeis *et al*., 1987, Pedley *et al*., 1996,

Manzo *et al*., 2011), whilst other studies have focused on laminations in tufa deposits (Kano *et al*., 2003, Takashima and Kano, 2008, Kawai *et al*, 2009). To date very few studies have had any real focus on utilising tufa $(Mg/Ca)_{calcite}$ ratios as a palaeothermometer. Incorporation of Mg^{2+} into tufas deposited in the summer was found to be higher than in winter (Chafetz *et al*., 1991) and a seasonal temperature change in stream water of $\sim 10\ °C$ appeared to be the dominating influence on Mg^{2+} incorporation into a 14 year (1985 – 1999) tufa record from Queensland Australia (Ihlenfeld *et al*., 2003).

In order to achieve a realistic calibration of an $(Mg/Ca)_{calcite}$ palaeothermometer that is applicable to natural systems it is necessary to generate data from an in vitro system that mimics a natural system as closely as logistically possible. Isolated bacterial strains precipitating in laboratories are not consistent with a natural tufa stream system, but such studies are essential to gaining an understanding of the processes involved at the full scale. The recirculating mesocosm systems of Rogerson *et al*., (2008) go some way to achieving a more natural environment by utilising a full biofilm sourced from a tufa depositing stream. However, the recirculation of the experimental solution results in time-variant $(Mg/Ca)_{solution}$ and Ω values due to ongoing precipitation and chelation which will be a severe complication in determining a purely thermodynamic control on $(Mg/Ca)_{calcite}$.

This chapter describes the development of a novel experimental system which modifies the recirculating mesocosm approach of Rogerson et al., (2008). The goal of the design was to develop an experimental system in which it is feasible to derive an $(Mg/Ca)_{calcite}$ palaeotemperature calibration equation for freshwater calcite precipitated in the presence of microbial biofilms.

4.2 Flow-through microcosm experiment design

4.2.1 Introduction

The precipitation of calcite under experimental conditions of constant temperature and constant $(Mg/Ca)_{solution}$ required the design of a unique experimental flow-through microcosm system (Figure 4.1). This comprised a series of vessels in which a biofilm could be cultured whilst submerged in a water bath. The temperature of the

water bath was controlled by a Titan 150 in-line chiller unit (Aqua Medic, Bisendorf, Germany), The water in the bath was recirculated from an open sump system set below the main experimental chamber. Water was returned to the sump directly from the water bath by gravity. Experimental water was supplied to the microcosms via an SP1500 peristaltic dosing pump, (Aqua Medic, Bisendorf, Germany), with flow control taps ensuring that the flow of water was equal between the microcosms. Water flowed through the microcosms and drained via a sump to the waste water system. Light was supplied to the system via a single 'Thorn Lopak 250 W HPS-T' sodium lamp on a 7: 17 day: night cycle in a windowless, air conditioned laboratory and thus was strongly buffered from all external influences. A detailed description of the individual components of the system is given in the following subsections.
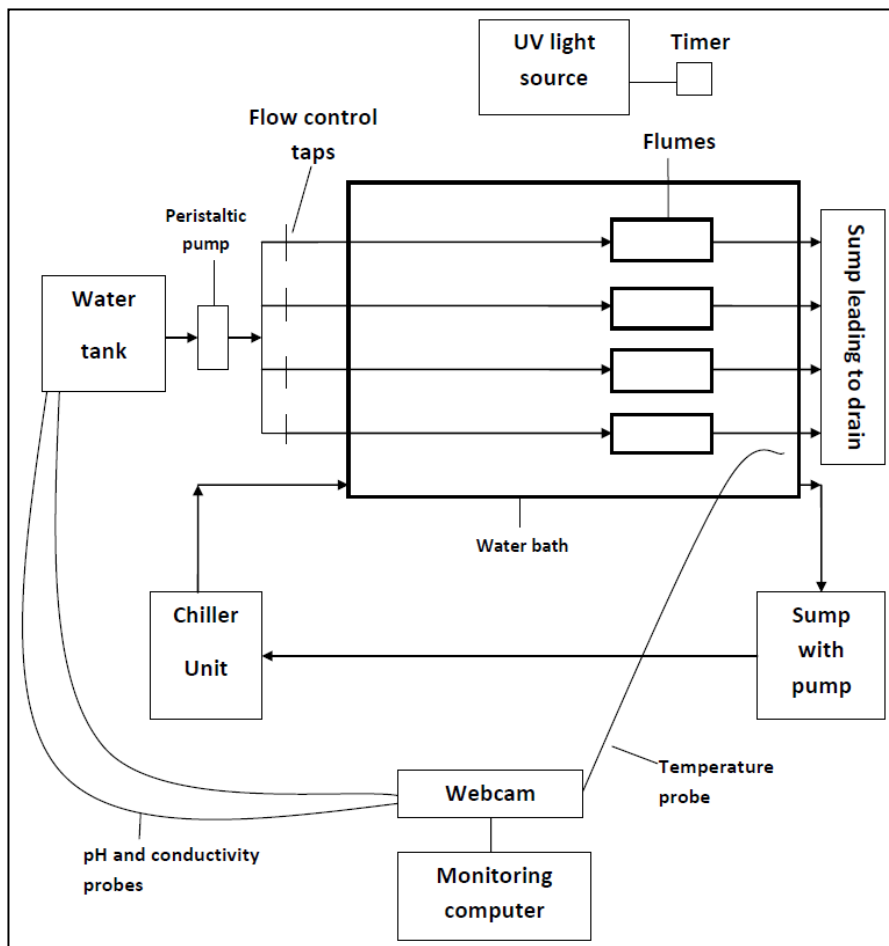
Figure 4.1 Schematic representation of the microcosm experiments. Arrows indicate direction of water flow.

4.2.2 Microcosm design

Experiments were performed with four replicates which were run within identical Perspex microcosms (flumes) with dimensions of 20 cm by 8 cm and a depth of 2.5 cm. Each flume had a Perspex lid which was secured to the flume with clear silicon gel, providing a water tight seal allowing the microcosms to be submerged in the water bath. Inflow and outflow ports with a diameter of 6 mm were built into the ends of each flume. Water collection and storage issues required that the flow rate to each flume be restricted. As a consequence it was necessary to restrict the flow to a channel about 7 mm wide and deep along the length of the flume. In the first experiments this was achieved by filling the microcosm with wax so that the inlets and outlets were submerged and then cutting a channel to the depth of the bottom of the openings (Figure 4.2).

Figure 4.2 Initial microcosm design.

Later experiments used redesigned microcosms again constructed in Perspex but with a built in 7 mm wide and deep flow channel available for water to flow through. The dimensions for flow were the same as the previous experiments (Figure 4.3).

Figure 4.3 Redesigned microcosm with built in flow channel

4.2.3 Source of biofilm and colonisation of microcosms

Biofilm was sourced from the River Lathkill, Derbyshire (UK grid reference SK 225 645). Colonisation was onto carbon fabric secured to house bricks which were submerged in an active tufa precipitating reach on the 3rd of April 2009 and recovered on the 5th of August 2009. To ensure a constant supply of a common biofilm the colonised carbon fabric was detached from the bricks and secured within a 1 metre long, 112 mm wide polycarbonate gutter within a mesocosm (Figure 4.4) previously used in earlier experiments (Rogerson *et al*., 2008, Pedley *et al*., 2009).
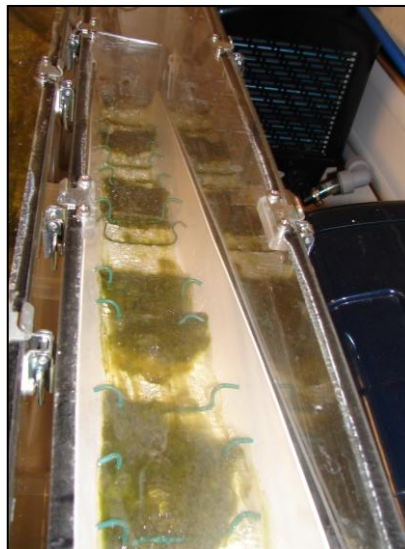
Figure 4.4 Biofilm colonising in mesocosm flume.

In its initial state the biofilm from the River Lathkill was unable to be used in the microcosm experiments, coming from a tufa precipitating environment meant it

would naturally contain calcite precipitates. This calcite would contaminate the results obtained from the precipitates obtained experimentally. The colonisation of calcite free biofilm was achieved by placing plastic mesh pads within the mesocosm in the gaps between the mats imported from the river Lathkill. Standard glass microscope slides cut to 5 mm wide strips and frosted with corundum glass frosting powder were secured to the mesh pads to be colonised for use in the microcosms. 30 L of deionised (15 MΩ) water was circulated between the colonising gutter and a sump via a Titan 150 in line chiller set at 12 °C. The colonising flume was illuminated by a single 'Thorn Lopak 250 W HPS-T' hydroponic lamp. This was initially set at 18 h on and 6 h off to mimic British summer time conditions. However, this level of exposure resulted in the deterioration of the biofilm. It was reset to a 7 hour on and 17 hour off cycle. Figure 4.5 show a schematic representation of the colonising flume system.
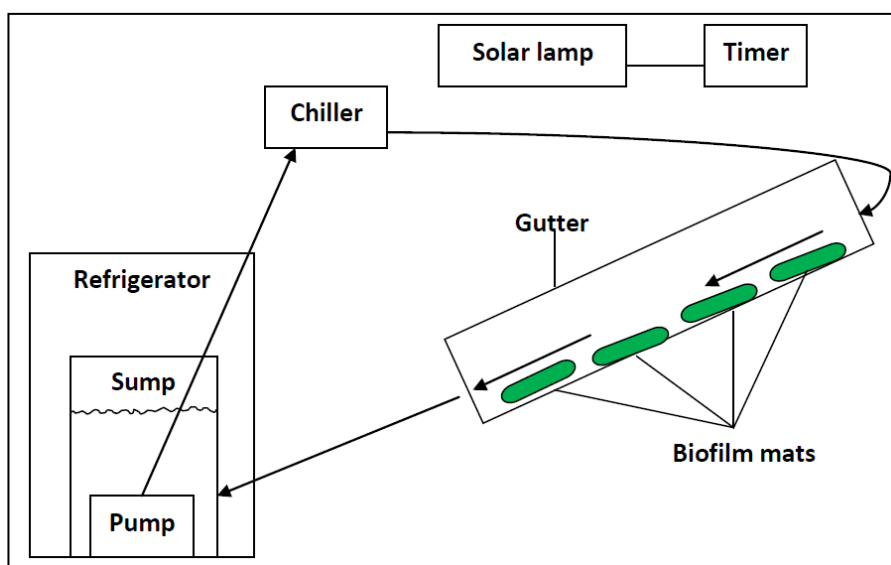
Figure 4.5 Schematic representation of the colonising flume system.

After 3 months of colonisation the new mesh pads were sufficiently colonised to allow the removal of the original colonised carbon fabric (containing calcite) from the mesocosm. The colonisation process was continued for a further 3 months to achieve a sustainable amount of biofilm for all future experiments. Prior to the first experiment a sample of the newly colonised biofilm was taken and prepared for examination by scanning electron microscopy (SEM). This examination revealed that the biofilm was free of calcite precipitates (Figure 4.6).
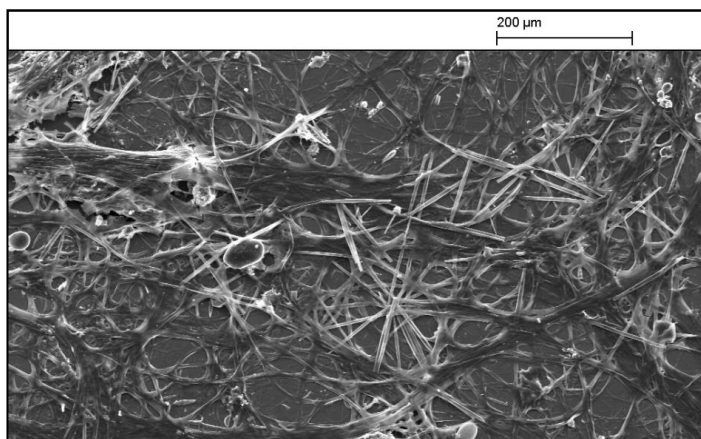
Figure 4.6 SEM image of calcite free biofilm from mesocosm.

4.2.4 Temperature control

The ambient laboratory air temperature was maintained between 16 and 20 °C by an 'Airforce Climate Control' air conditioning unit (10,000 BTU hr^{-1}; 2.9 kW cooling capacity, Airconwarehouse, Stockport, UK). This provided the experiments some buffering from changes in room temperatures due to seasonal changes. A constant experimental temperature was obtained by fully submerging the microcosms and connecting pipes in a metal water bath with the water temperature controlled by a Titan 150 mini cooler chiller unit (Aqua Medic, Bisendorf, Germany). This unit is controlled by a digital temperature controller adjustable in increments of 1°C ($\pm$ 0.5 °C). Water was re-circulated through the chiller unit via a submerged pump in the sump. The water bath was surrounded by sheets of thermal aluminium foil (thermal resistance 1.455 m^2 K W^{-1}) to provide additional thermal buffering and exclude incoming UV from the water bath. Only the microcosms were left exposed to the lighting unit to allow photosynthesis.

Sheets of thermal aluminium foil were placed over piping which was external to the water bath to prevent heating from the lighting unit. The chiller unit was able to provide temperature control at 12, 14, 16 and 18 °C. The unit was unable to maintain the water temperature at 20 °C so additional heating was provided by a thermostatically controlled Aqua One 100 W fully submersible aquarium heater (Aqua Pacific Ltd., Southampton, UK) placed in the sump. The temperature of the water bath was monitored at ten minute intervals via a thermometer probe (range -50 to 200 °C) (Thermometers Direct, Aldershot, UK) inserted next to the microcosms.

The digital output from the thermometer was recorded to a PC via a webcam system, as previously used for mesocosm experiments (Rogerson *et al*., 2008, Pedley *et al*., 2009, Rogerson *et al*., 2010).

4.2.5 Solution preparation

Initial water for the experiments was collected from a spring sourced by a Cretaceous chalk aquifer at Welton Beck, East Yorkshire (UK grid reference SE 965 275). Each experiment required about 1000 litres of spring water. This was collected twice weekly in 20 litre plastic jerry cans. A 1 mL sample was taken on each occasion and immediately acidified with 5% ultrapure HNO_3 for analysis of $Mg^{2+}_{(aq)}$ and $Ca^{2+}_{(aq)}$ concentrations by ICP – OES. The first water was collected on the 12th February 2010; it had $Mg^{2+}_{(aq)}$ and $Ca^{2+}_{(aq)}$ levels of 4.6 and 132.4 mg L^{-1} respectively. To ensure the water for all experiments had equal levels of $Mg^{2+}_{(aq)}$ and $Ca^{2+}_{(aq)}$ acetates of calcium $(Ca(C_2H_3O_2)_2$ and magnesium $(Mg(C_2H_3O_2)_2$ (Alfa Aesar, Massachusetts., USA) were added to the spring water to bring the concentrations of $Mg^{2+}_{(aq)}$ and $Ca^{2+}_{(aq)}$ to 8.0 and 160 mg L^{-1} respectively giving an $(Mg/Ca)_{solution}$ molar ratio of 0.082. This had the additional benefit of increasing the degree of saturation, which would promote calcite precipitation in the experiments. The saturation state was determined using the aqueous geochemical modelling software PHREEQC. Saturation index values for the experimental solutions were 0.95, 0.98, 1.01, 1.04 and 1.07 for the temperatures, 12, 14, 16, 18 and 20 °C respectively.

Depending on the initial $Mg^{2+}_{(aq)}$ and $Ca^{2+}_{(aq)}$ concentrations of the spring water the amounts of acetates added per 20 L was between 2 and 5 g for calcium and 0.6 and 0.8 g for magnesium. To ensure complete dissolution of the acetates 2 litres was removed from each jerry can and added to a conical flask which was then placed on a Stewart SB301 magnetic stirrer (Bibby Scientific Limited, Staffordshire, UK) at 600 rpm. The acetates were added in small amounts until all acetate for each 20 litres was fully dissolved. This water was returned to the jerry can which was shaken vigorously to homogenise. A 1 mL sample was taken on each occasion and immediately acidified with 5% HNO_3 for analysis of $Mg^{2+}_{(aq)}$ and $Ca^{2+}_{(aq)}$ concentrations by ICP – OES. The prepared solution was added to the experimental water tank.

4.2.6 Precipitate recovery

At the end of each experiment the glass slides containing the biofilm and experimental precipitates were removed from the microcosms and photographed. The biofilm covering of the glass slide was added to 20 mL sterilin tubes and centrifuged in a Centaur 2 non refrigerated bench top centrifuge (MSE, London, UK) at 3300 rpm for 20 minutes. The supernatant water was discarded and a small sample of the pellet was taken for SEM examination. Prior to dissolution of the calcite precipitates in the biofilm it was necessary to 'clean' the biofilm of Mg^{2+} and Ca^{2+} cations that had been chelated by the extracellular polymeric substances (EPS) of the biofilm complex. Ultrapure water (18 MΩ) was added to each sterilin tube containing the biofilm pellet. The tube was shaken vigorously to ensure full mixing of the biofilm with the water and left to stand for two hours. It was then centrifuged at 3500 rpm for 15 minutes. A sample was taken of the supernatant and immediately acidified with 5 % ultrapure HNO_3 for analysis of the $Mg^{2+}_{(aq)}$ and $Ca^{2+}_{(aq)}$ levels by ICP – OES. This process was repeated five or six times to ensure practically all chelated Mg^{2+} and Ca^{2+} cations were washed from the biofilm, after which the biofilm pellet was oven dried.

In order for the total mass of precipitates to be calculated for each biofilm, and hence precipitation rate, the dissolution of calcite precipitates held within the dried biofilm pellet was achieved by gravimetrically adding 10% ultrapure HNO_3 to the sample. The samples were sonicated for three minutes in an Ultra 8000 bench top ultrasonic cleaner (Ultrawave, Cardiff, UK) left to stand for two hours, shaken vigorously, sonicated again and centrifuged for 15 minutes at 3300 rpm. A sample of the supernatant was taken and immediately acidified with ultrapure 5 % HNO_3 for analysis of $Mg^{2+}_{(aq)}$ and $Ca^{2+}_{(aq)}$ levels and determination of the precipitate $(Mg/Ca)_{calcite}$ ratios. The pellet was re – dried and stored. After later consideration as to whether the use of 10 % HNO_3 would have resulted in the full dissolution of calcite within the biofilm it was decided to digest the dried biofilm in 2 mL of ultrapure concentrated HNO_3. The digested solution was prepared for ICP – OES by the addition of 5% ultrapure HNO_3.

The data output from the ICP – OES analyses was presented by the instrument in units of mg L^{-1}. To determine the precipitation rates the mass of calcium and

magnesium needed to be calculated from the ICP – OES output data. Firstly the L^{-1} unit was removed by the application of a conversion factor individually determined for each sample based on the millilitres of acid used to dissolve the individual precipitate samples. The resulting masses in milligrams was converted to mmols through the equation *number of mmols = mass (mg)/mass of 1 mole (g)* (Ca = 40.078 g, Mg = 24.305 g). The total mass of $CaCO_3$ was obtained by summing the molar masses of Ca and Mg together with the stoichiometric balanced number of moles of CO_3. The precipitation rate was calculated based on the surface area of the precipitating surface and the duration of each experimental run and presented in units of $\mu mol\ cm^{-2}\ hr^{-1}$.

4.3 Agitated flask experiments

The experiment was set up adjacent to the microcosm apparatus and was designed to make use of the same water bath temperature control. This was achieved by placing a further pump into the sump which pumped water to a plastic water bath that itself was connected to a second water bath by rubber hosing (Figure 4.7).
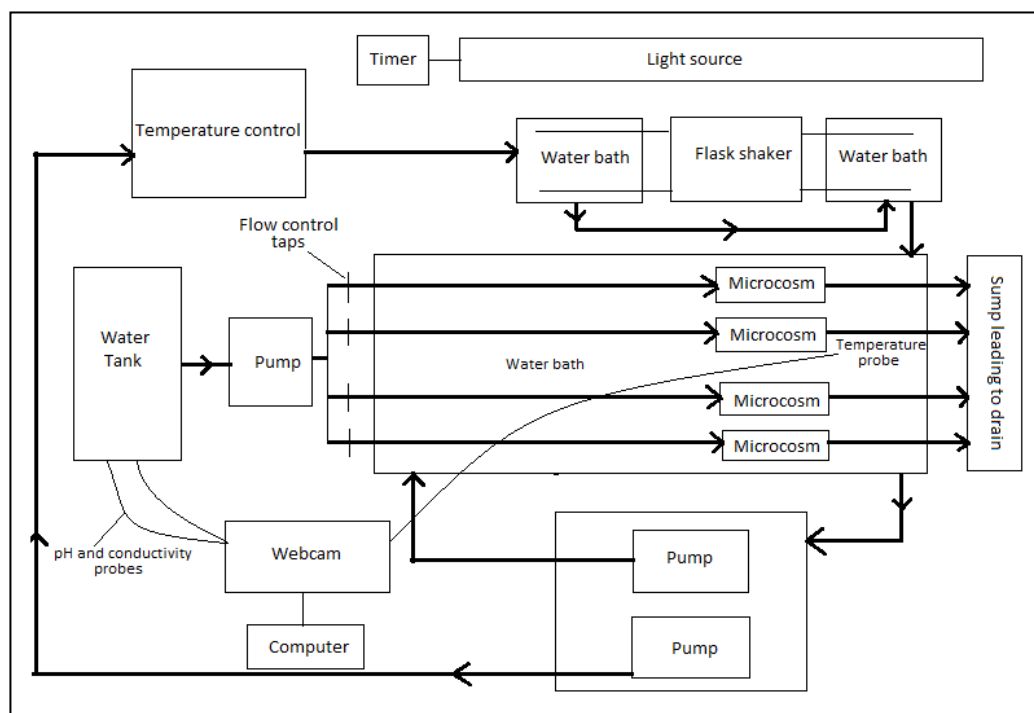
Figure 4.7 Schematic visualisation of the addition of the agitated flask experiment to the microcosm design. Arrows indicate direction of water flow.

Experiments were conducted at 12, 14, 16, 18 and 20 °C. Due to the later introduction of these flask experiments the 18 and 20 °C experiments were run concurrently with the microcosm experiments, the 12, 14 and 16 °C were run separately but using the same experimental set up. All flasks were sterilised with pure ethanol and given a wash of ultrapure 5 % HNO_3 and UHQ water (18 MΩ) prior to the experiment. The flask shaker was set to 100 oscillations per minute for all experiments.

4.3.1 Flask treatments

Eight 150 mL conical flasks were used with two replicates each of three different treatments and two controls. The treatments consisted of biofilm exposed to solar spectrum light, biofilm with light excluded and isolated EPS. The biofilm used was taken from the same colonising flume as the microcosm experiments. Each flask for the biofilm treatments received 3 g of biofilm and 50 mL of prepared solution (see section 4.3.2). The two flasks from which light was excluded were thoroughly wrapped in reflective thermal aluminium foil (thermal resistance 1.455 m^2 K W^{-1}) to exclude all light. For the controls and sterile EPS treatments two sterilised frosted microscope slides were placed in each flask to collect precipitates. The EPS used was extracted using the heat method described in chapter 3 section 3.2.3. The prepared solution for these flasks was sterilised by a UV steriliser and 50 mL of the prepared solution was added to each flask along with 3 mL of the sterile EPS solution. Foam bungs were used to prevent microbial invasion and reduce evaporative loss from the flasks whilst allowing gas exchange. The flasks were clamped to the shaker and further thermal aluminium foil (thermal resistance 1.455 m^2 K W^{-1}) was used to cover the section of the water tank containing the light excluded replicates.

4.3.2 Solution preparation

The solution was made to the same concentration of $Ca^{2+}_{(aq)}$ and $Mg^{2+}_{(aq)}$ as the microcosm experiments (160 mg L^{-1} and 8.0 mg L^{-1} for $Ca^{2+}_{(aq)}$ and $Mg^{2+}_{(aq)}$ respectively). These levels were achieved by adding the appropriate quantity of calcium and magnesium acetates to Welton spring water as described in subsection 4.2.4. The saturation state was determined using the aqueous geochemical modelling software PHREEQC. Saturation index values for the experimental solutions were the

same as for the microcosm experiments at 0.95, 0.98, 1.01, 1.04 and 1.07 for the temperatures, 12, 14, 16, 18 and 20 °C respectively.

4.3.3 Precipitate recovery

The precipitates were recovered from the biofilm in the same manner as that for the microcosm experiments detailed in subsection 4.2.5. For the control and EPS treatments the glass slides were removed from the flasks and placed in Petri dishes. Ultra pure 10% HNO_3 was added to each dish gravimetrically to dissolve the crystals. This was left for two hours and shaken every 20 minutes. To ascertain that all precipitates had dissolved from the slides they were examined under an optical microscope, this revealed that no precipitates remained on the slides. Samples of the dissolved calcite solutions for all treatments were taken and diluted by gravimetrically adding 5% ultrapure HNO_3 and analysed for $Ca^{2+}_{(aq)}$ and $Mg^{2+}_{(aq)}$ levels by ICP – OES.

4.4 Effectiveness of experimental methods

4.4.1 Temperature control

Throughout all microcosm and agitated flask experiments the water bath temperature was monitored on a 24/7 basis by means of a submerged probe linked to a digital display, this display was recorded every ten minutes by a webcam and stored on a dedicated computer. The mean temperature and 1σ values are shown in Table 4.1.

Table 4.1 Mean precipitation temperature

Experiment	Mean temperature achieved (°C)	1σ (°C)
Microcosm 1	12.2	± 0.2
Microcosm 2	14.3	± 0.2
Microcosm 3	16.3	± 0.2
Microcosm 4	18.3	± 0.2
Microcosm 5	20.6	± 0.5
Agitated flask 1	12.1	± 0.5
Agitated flask 2	14.3	± 0.2
Agitated flask 3	16.3	± 0.3
Agitated flask 4	18.3	± 0.2
Agitated flask 5	20.6	± 0.5

4.4.2 Concentration of $Ca^{2+}_{(aq)}$ and $Mg^{2+}_{(aq)}$ in precipitating solution

Each microcosm experiment required the water butt to be topped up two to three times a week throughout the experiment. Logistical reasons meant that the amounts of water added to the water butt varied on occasions. To ensure that the concentrations of $Ca^{2+}_{(aq)}$ and $Mg^{2+}_{(aq)}$ and hence $(Mg/Ca)_{solution}$ ratio were consistent for all experiments, samples of all additions to the water butt were analysed by ICP − OES. To account for the differences in the volumes of water added a weighted ($\bar{x}$), rather than arithmetical mean of the solutions was calculated by means of equation 4.1.

$$\bar{x} = \frac{\sum_{i=1}^{n} w_i x_i}{\sum_{i=1}^{n} w_i} \qquad (4.1)$$

The experimental method required the $Ca^{2+}_{(aq)}$ and $Mg^{2+}_{(aq)}$ levels to be 160.0 and 8.0 mg L^{-1} respectively, giving an Mg/Ca molar ratio of 0.082. The weighted means and 1σ values for the source water are shown in Table 4.2

Table 4.2 Mean $Ca^{2+}_{(aq)}$, $Mg^{2+}_{(aq)}$ and $(Mg/Ca)_{solution}$ values for precipitating solution.

Experiment (°C)	Ca^{2+} (mg L^{-1})	1σ (mg L^{-1})	Mg^{2+} (mg L^{-1})	1σ (mg L^{-1})	Mg/Ca (molar)	1σ
Microcosm 12	160.9	1.0	8.0	0.1	0.081	0.002
Microcosm 14	161.6	1.2	7.9	0.1	0.081	0.001
Microcosm 16	162.2	0.9	8.1	0.1	0.082	0.001
Microcosm 18	161.3	1.4	7.9	0.1	0.081	0.002
Microcosm 20	162.0	1.5	7.9	0.1	0.080	0.001

4.4.3 Cleansing of chelated Ca^{2+} and Mg^{2+} from biofilms

Figure 4.8 shows the results of the wash process to remove chelated Ca^{2+} and Mg^{2+} ions from the EPS molecules of the biofilm. Each successive wash resulted in lower levels of both Ca^{2+} and Mg^{2+} released from chelation.
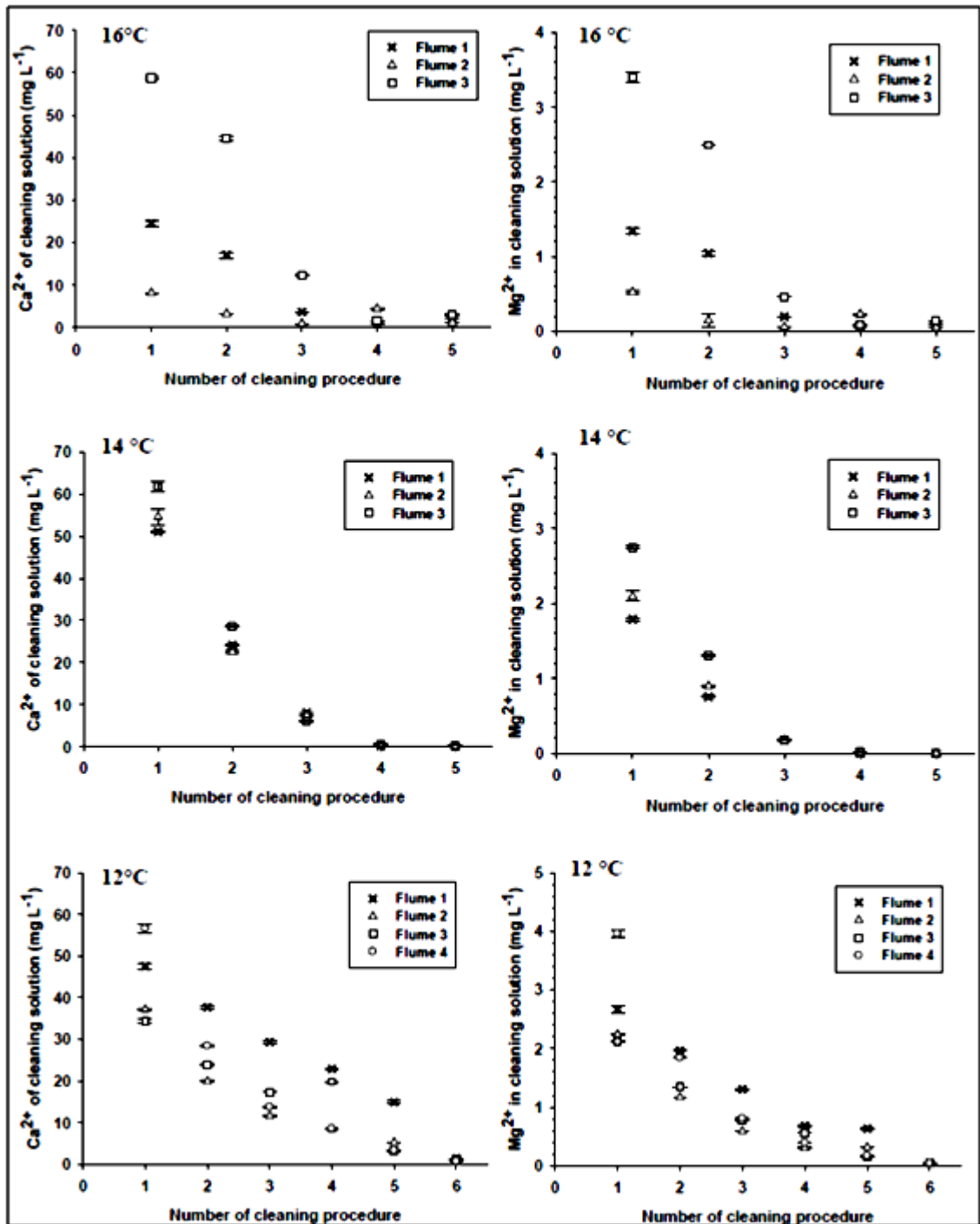
Figure 4.8 Removal of chelated cations from the biofilm by repeated 'washing' with 18 MΩ water.

The $(Mg/Ca)_{solution}$ ratios from the wash processes are shown in Figure 4.9. Although there are some exceptions (notably washes 5 and 6 of the 12 °C experiment), the overall trend is for the $(Mg/Ca)_{solution}$ ratio to decrease as the number of wash processes rises.
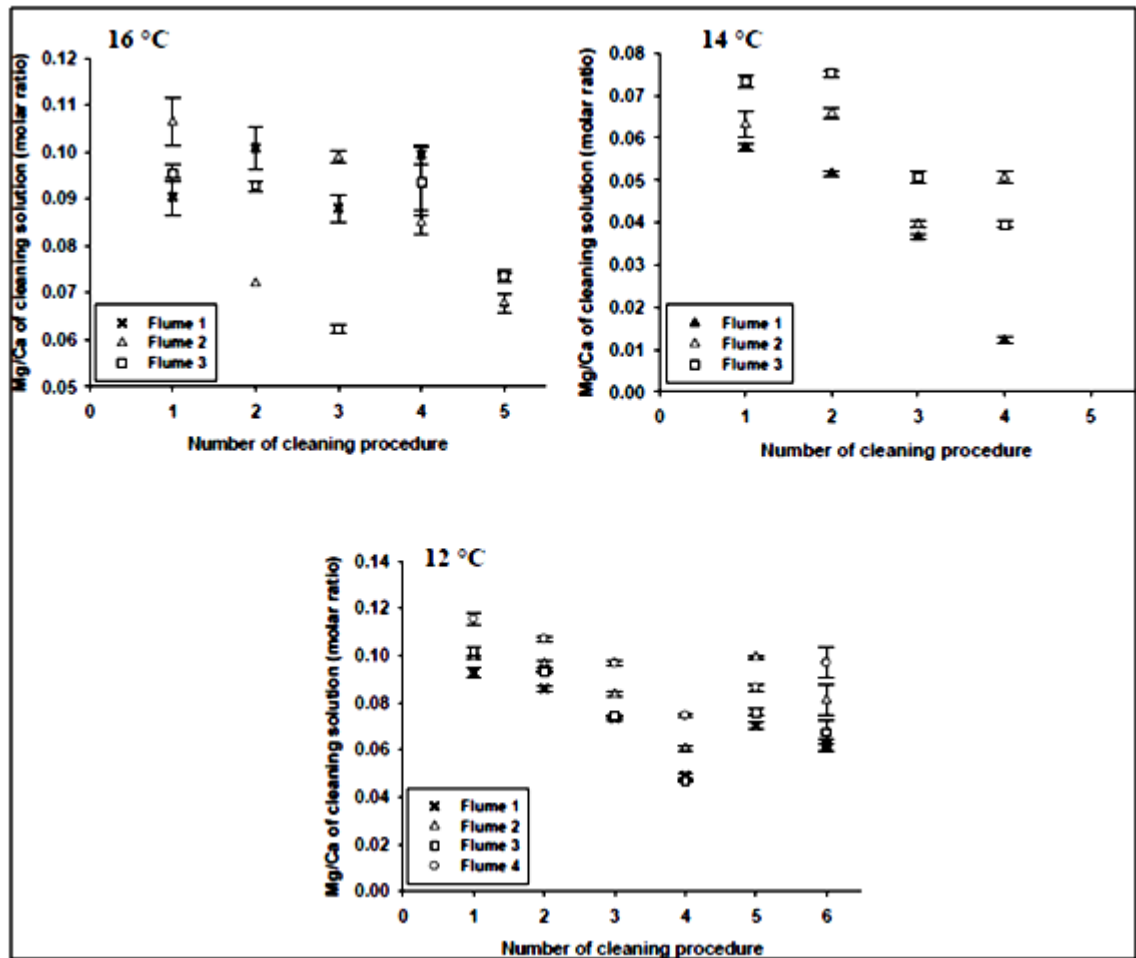
Figure 4.9 Mg/Ca ratios of wash solutions. No ratio is shown for wash 5 at 14 °C as the concentrations were below the limit of detection.

4.4.4 Dissolution of precipitated calcite

As described in section 4.3.3 the precipitated calcite within the biofilms was initially dissolved in 10 % ultrapure HNO_3. As a safe guard the stored biofilm pellets were digested in ultrapure concentrated HNO_3 to determine if total dissolution had taken place with the 10% acid solution. The mass of Ca^{2+} and Mg^{2+} released to solution from each biofilm for the initial 10 % HNO_3 was calculated and subsequently the mass of Ca^{2+} and Mg^{2+} released to solution from the digestion in concentrated acid was also calculated.

The results of these mass calculations are detailed in Table 4.3. Analysis of the digestion solutions revealed that using 10 % HNO_3 resulted in an average of 94.9 % of the precipitates being dissolved across the 18 samples of the microcosm experiments. The range of percentages was from 80 to 100, with only 3 of the 18

being below 90 %. A sample of calcite free biofilm from the source colonising flume was 'washed' to remove any traces of chelated Ca and Mg and also digested in concentrated HNO_3. The resulting solution had Mg^{2+} and Ca^{2+} levels below the limit of detection as analysed by ICP – OES. Therefore, it can safely be concluded that the additional Mg^{2+} and Ca^{2+} released from the biofilm by digestion in concentrated HNO_3 was derived from experimental precipitates rather than the constituents of the biofilm matrix itself.

Table 4.3 Percentage dissolution of precipitates using 10 % HNO_3 (LOD = Limit of detection).

Experimental temperature (°C)	Microcosm	Mass of precipitate from 10 % HNO_3 (mmol)	Mass of precipitate from concentrated HNO_3 (mmol)	Dissolution (%) using 10 % HNO_3
12	Flume 1	0.092	0.0026	97.3
12	Flume 2	0.028	0.0006	97.9
12	Flume 3	0.052	0.0008	98.5
12	Flume 4	0.024	0.0004	98.4
14	Flume 1	0.012	0.0004	96.8
14	Flume 2	0.172	0.0118	93.6
14	Flume 3	0.072	0.0036	95.2
16	Flume 1	0.01	0.0008	92.6
16	Flume 2	0.008	0.002	80.0
16	Flume 3	0.018	0.0038	82.6
18	Flume 1	0.138	0.0106	92.9
18	Flume 2	0.05	0.0056	89.9
18	Flume 3	0.178	0.0108	94.3
18	Flume 4	0.142	Below LOD	100
20	Flume 1	1.122	0.0056	99.5
20	Flume 2	0.836	0.0118	98.6
20	Flume 3	1.108	Below LOD	100
20	Flume 4	1.174	Below LOD	100

To obtain the most accurate $(Mg/Ca)_{calcite}$ ratio from the experimental precipitates the molar masses of calcite from both dissolution procedures were added together to give a total precipitation mass from which the precipitation rate could be calculated. The $(Mg/Ca)_{calcite}$ ratios obtained from the initial dissolution in 10 % HNO_3 and the ratios from the subsequent dissolution in concentrated HNO_3 are shown in Table 4.4 along with the percentage difference between the final ratio and the ratio that was obtained from the initial dissolution in 10 % HNO_3.

Table 4.4 (Mg/Ca)$_{calcite}$ ratios of dissolved precipitates.

Experimental temperature (°C)	Microcosm	Mg/Ca from 10% HNO$_3$ (mg L^{-1})	Mg/Ca from concentrated HNO$_3$ (mg L^{-1})	Final Mg/Ca	Difference in Mg/Ca (%) (molar ratio)
12	Flume 1	0.028	0.089	0.029	5.6
12	Flume 2	0.063	0.148	0.064	3.0
12	Flume 3	0.037	0.121	0.038	3.2
12	Flume 4	0.073	0.198	0.075	2.9
14	Flume 1	0.064	0.067	0.064	0.2
14	Flume 2	0.007	0.007	0.007	Nil
14	Flume 3	0.021	0.011	0.020	-2.4
16	Flume 1	0.041	0.081	0.044	6.1
16	Flume 2	0.031	0.041	0.033	5.7
16	Flume 3	0.036	0.071	0.042	14.5
18	Flume 1	0.019	0.020	0.019	0.5
18	Flume 2	0.041	0.045	0.041	0.9
18	Flume 3	0.012	0.012	0.012	-0.2
18	Flume 4	0.014	---	0.014	Nil
20	Flume 1	0.012	0.015	0.012	0.1
20	Flume 2	0.009	0.018	0.009	1.2
20	Flume 3	0.011	---	0.011	Nil
20	Flume 4	0.012	---	0.012	Nil

The mean difference between the two ratios was 2.6 %. Of all the microcosms, only flume 3 of the 16 °C experiment showed a significant difference at 14.5 %. The ratios obtained by summing the total precipitation from both dissolution procedures have been used in all the forthcoming results for the microcosm experiments.

4.5 Discussion

The microcosm design allowed the flow through of water with a constant flow rate and (Mg/Ca)$_{solution}$, this ensured that changes in (Mg/Ca)$_{calcite}$ and precipitation rate were able to be attributed solely to the influences of temperature, microbial metabolism and EPS or any combination thereof. The microcosm vessels were proven to be water tight prior to the commencement of each experiment therefore no contamination was possible from water in the water bath. The experimental design ensured that if leaks had developed during the experiment this would have become obvious due to the water level in the sump decreasing. This in fact occurred on the first experimental run resulting in the system having to be cleaned out and recommenced.

4.5.1 Temperature control

Temperature was well controlled with 1σ errors ranging from ± 0.2 – 0.5 °C. Previous studies on freshwater calcite precipitation at varying temperatures have not made reference to temperature errors (Cacchio *et al.*, 2003, Cacchio *et al.*, 2004, Baskar, *et al.*, 2006) but culture studies on cultured foraminiferal calcite have been reported with 1σ temperature errors of ± 0.5 °C (Nurnberg *et al.*, 1996, Kisakurek *et al.*, 2008). The errors in temperature reported in these experiments are therefore acceptable.

4.5.2 Mg/Ca of experimental solution

The target concentrations were 160 mg L^{-1} and 8 mg L^{-1} for Ca^{2+} and Mg^{2+} respectively. Analyses by ICP – OES showed that the mean levels achieved for all solutions combined were 161.6 ± 1.2 and 8.0 ± 0.1 mg L^{-1}. The range for values (see Table 4.2) was 160.9 to 162.0 mg L^{-1} for Ca^{2+} and 7.9 to 8.1 mg L^{-1} for Mg^{2+}. To determine the errors in the Mg/Ca ratios it was necessary to use propagation of error techniques. For the ratio $z = x/y$ where the error in x is Δx and the error in y is Δy the calculation of Δz is achieved by using equation 4.2.

$$\frac{\Delta z}{z} = \sqrt{\left(\frac{\Delta x}{x}\right)^2 + \left(\frac{\Delta y}{y}\right)^2} \tag{4.2}$$

Applying this to Mg/Ca ratios gives

$$\Delta\left(\frac{Mg}{Ca}\right) = \left(\frac{Mg}{Ca}\right)\sqrt{\left(\frac{\Delta Mg}{Mg}\right)^2 + \left(\frac{\Delta Ca}{Ca}\right)^2} \tag{4.3}$$

The mean percentage error in (Mg/Ca)$_{\text{solution}}$ was 1.7 %. This value shows that the method of adding measured amounts of calcium and magnesium acetates to a natural spring water results in concentration errors that are within acceptable limits.

4.5.3 Removal of chelated Ca^{2+} and Mg^{2+} prior to precipitate dissolution

The results of the wash process analysis (Figure 4.8) prove the effectiveness of this method. The fact that the chelated Ca^{2+} and Mg^{2+} ions have been removed ensures that any Ca^{2+} and Mg^{2+} released to solution through the dissolution process must be from calcite precipitates and were not from the release of chelated ions. The

observation in Figure 4.9 that the Mg/Ca of the cleaning solution increased as the number of wash processes grew strongly indicates that Mg^{2+} cations are preferentially released from chelation over Ca^{2+} during the wash process. This provides further support to the idea of chemoselectivity for ions with a lower charge density previously observed in mesocosm experiments (Rogerson *et al*., 2008).

4.5.4 Effectiveness of 10 % HNO$_3$ as a dissolution agent

Concentrated HNO_3 is extremely hazardous to health therefore a weaker 10 % solution was used as the standard dissolution agent. At the end of the experiments it was decided to digest the biofilm pellets in concentrated HNO_3 to assess the effectiveness of the 10 % solution and confirm that the trace element ratios derived from this were an accurate representation. The mean dissolution percentage from 10 % HNO_3 was 94.9 %. Calculations revealed that the use of concentrated HNO_3 resulted in a mean difference of 2.6 % between the final $(Mg/Ca)_{calcite}$ ratio and that initially generated from the 10 % dissolution. To determine how this impacted on the relationship between $(Mg/Ca)_{calcite}$ and precipitation rate, the ratios obtained from both were plotted as a function of precipitation rate (R) (Figure 4.10) and a statistical correlation carried out.
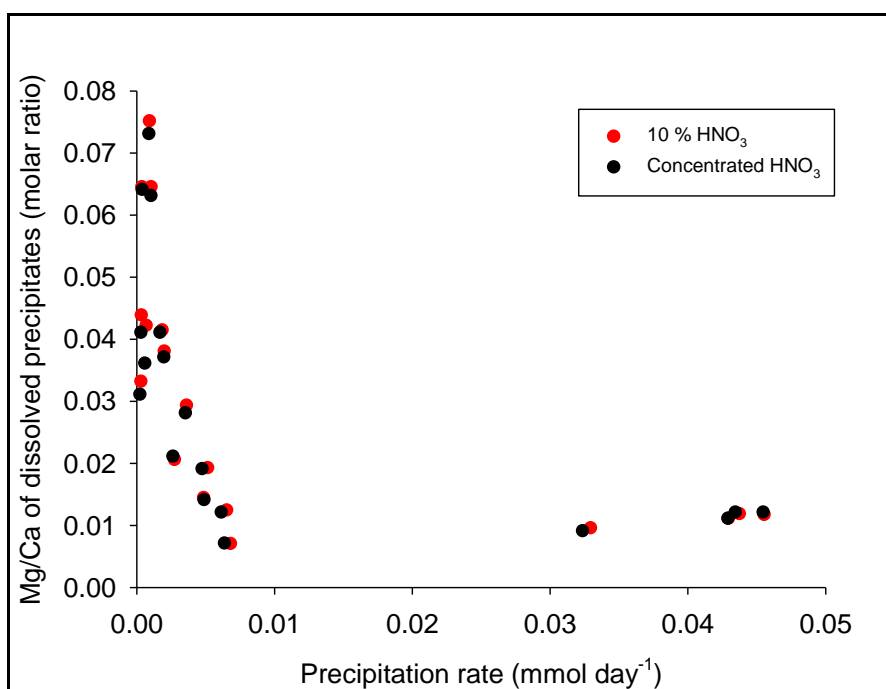
Figure 4.10 Comparison of the data from the 10 % and concentrated nitric acid dissolutions.

The correlation resulting from the 10 % dissolution was significant at the 95 % confidence level where $(Mg/Ca)_{calcite} = 0.005R^{-0.2995}$ ($R^2 = 0.52$, n = 18). This compares very well to the correlation generated by the concentrated nitric acid where $(Mg/Ca)_{calcite} = 0.004R^{-0.2992}$ ($R^2 = 0.53$, n = 18). Given the small percentage changes to the precipitation mass and $(Mg/Ca)_{calcite}$ ratios that were generated by the second dissolution process in concentrated acid and the extreme hazard associated with using this it is proposed that 10 % HNO_3 is sufficient for general exploratory purposes.

4.6 Conclusion

It is believed that this experimental design has allowed the first example of calcite precipitation in a full biofilm under constant temperature, flow rate and $(Mg/Ca)_{solution}$. By creating a flow through environment with a constant supply of ions and day/night cycles it has come reasonably close to mimicking a natural river system. For logistical reasons the flow rate was necessarily very slow and the substrate on which the biofilm was secured was uniformly flat. Neither of these conditions are representative of a natural tufa precipitating stream. However, by scaling up the microcosms to mesocosms (to match the size of the colonising flume) and adding an element of uneven topography to the flow channel, a natural system could be well approximated if an adequate supply of water can be maintained. The experimental methods used to control temperature, $(Mg/Ca)_{solution}$, and the dissolution processes have been proven to constrain the parameters within acceptable limits.

5 Influence of microbial biofilms on freshwater (Mg/Ca)$_{calcite}$

5.1 Abstract

The ratio of magnesium to calcium (Mg/Ca) in carbonate minerals in an abiotic setting is believed to be predominantly controlled by (Mg/Ca)$_{solution}$ and a temperature dependant partition coefficient. This temperature dependence suggests that both marine (e.g. foraminiferal calcite and corals) and freshwater (e.g. speleothems and tufas) carbonate deposits may be important archives of palaeotemperature data. However, there is considerable uncertainty regarding whether the presence of microbial biofilms in freshwater settings can alter the incorporation of minor ions into calcite. These biogenic affects may arise from microbial metabolic activity and / or the presence of extracellular polymeric substances (EPS). EPS have been shown to chelate divalent cations from the bulk water, and to strongly favour ions with low charge density. This influence could be transmitted to solid carbonate chemistry by altering the M^{2+} / Ca^{2+} ratios within the biofilm interstitial waters from which carbonates are precipitated and also by directly influencing the precipitation mechanism itself.

In this work a series of novel through-flow and agitated flask experiments where freshwater calcite was precipitated under controlled conditions are investigated. These experiments reveal there is no strong relationship between (Mg/Ca)$_{calcite}$ and temperature, which is inconsistent with the expected control from thermodynamic fractionation. However, there is a pronounced influence on (Mg/Ca)$_{calcite}$ from precipitation rate, so that rapidly forming precipitates develop with very low magnesium content. The control on (Mg/Ca)$_{calcite}$ arising from precipitation rate is found in the presence of biofilm regardless of whether the system was exposed to solar spectrum light, so photosynthetic influences are not important These experiments suggest that the chemoselectivity in favour of Ca^{2+} by EPS molecules is the dominant factor in (Mg/Ca)$_{calcite}$ ratios of freshwater calcite precipitated in the presence of microbial biofilms and not temperature.

5.2 Introduction

The potential of the $(Mg/Ca)_{calcite}$ palaeothermometer was first observed in the 1950's when a link between latitude and magnesium content was recognised in a study on the biogeochemistry of marine skeletal calcites (Chave, 1954). The use of $(Mg/Ca)_{calcite}$ ratios as a palaeothermometer has since become widespread in marine settings with many studies on benthic and planktonic foraminifera (Delaney *et al*., 1985, Nurnberg *et al*., 1996, Rosenthal *et al*., 1997, Anand *et al*., 2003, Elderfield *et al*., 2006, Kisakurek *et al*., 2008, Bousetta *et al*., 2011, Martinez-Boti *et al*., 2011) and to a lesser extent in corals (Mitsuguchi *et al*., 1996, Shirai *et al*., 2005, Reynaud *et al*., 2007). In freshwater settings early studies to determine the potential of speleothem Mg/Ca ratios as a palaeoenvironmental indicator were optimistic (Katz, 1973, Gascoyne, 1983). However, subsequent work has revealed that a number of factors such as the faster dissolution rate of calcite compared to dolomite, prior calcite precipitation along the flow path, selective leaching of trace elements, the length of residence time of the water above the cave and flow rates can influence the trace element composition of the water that eventually seeps into caves, thereby masking the temperature induced variations that may be found in speleothem calcite (Fairchild *et al*., 2000, Verheyden *et al*., 2000, Fairchild *et al*., 2006). As a consequence the research community has largely shifted its focus towards hydrologically induced variations in speleothem Mg/Ca ratios at the expense of temperature effects (Fairchild and Treble, 2009).

Mg/Ca palaeothermometry in tufa carbonates has received little attention in comparison to other carbonates. Its potential has been discussed by a number of authors (Garnett *et al*., 2004, Andrews and Brasier, 2005, Rogerson *et al*., 2008, Brasier *et al*., 2010, Lojen *et al*., 2009). However, only two studies have directly examined $(Mg/Ca)_{tufa}$ ratios as a function of temperature. Incorporation of Mg^{2+} into tufas deposited in the summer was found to be higher than in winter (Chafetz *et al*., 1991) and a seasonal temperature change in stream water of ~ 10 °C appeared to be the dominating influence on Mg^{2+} incorporation into a 14 year (1985 – 1989) tufa record from Queensland Australia (Ihlenfeld *et al*., 2003). Although these studies show support for the potential of tufa $(Mg/Ca)_{calcite}$ palaeothermometry they do not take into account the presence of microbial biofilms and the significant impact these

may have on trace element incorporation into tufa carbonates. The study by Ihlenfeld *et al*., (2003) revealed considerable discrepancies in the correlation between the tufa $(Mg/Ca)_{calcite}$ ratios and water temperature. These discrepancies may be due to the presence of a microbial biofilm with its associated microbial metabolism and/or the chemoselective chelation of cations from the river water.

This chapter describes the results of a series of experiments which examine the influence of microbial biofilms on Mg/Ca of freshwater calcite precipitated under temperature controlled conditions from water with a constant $(Mg/Ca)_{solution}$. The aim of these experimental runs was to determine whether the presence of a biofilm at the calcite precipitation site could override the thermodynamic control on Mg^{2+} partitioning in freshwater $CaCO_3$ deposits.

5.3 Methods

The generic methods used in the experiments described in this chapter are detailed in Chapter 3 sections 3.6 and 3.7. The characterisation of the experimental systems and the demonstration of the validity of the results are presented in Chapter 4. At the commencement of each experimental run two sealed Petri dishes containing the experimental solution and frosted microscope slides were placed in the water bath to act as controls. No biofilm was contained within these dishes. Additional control data were obtained by conducting flow through experiments at 12 and 14 °C in the absence of any biofilm within the microcosms.

5.4 Results

5.4.1 Microcosm flow through experiments

Figure 5.1 shows the $(Mg/Ca)_{calcite}$ ratios of the biofilm derived precipitates against the mean precipitation temperature. Apart from the 20 °C experiment there is considerable variation of $(Mg/Ca)_{calcite}$ ratios at a given temperature, at 14 °C there is nearly an order of magnitude range. There is a weak negative linear correlation between the parameters where $(Mg/Ca)_{calcite} = 0.1 - (0.00429T(°C))$ (significant at P < 0.05, $R^2 = 0.44$, n = 18) so that $(Mg/Ca)_{calcite}$ generally decreased as temperature increased. However, this correlation is in direct contrast to the anticipated

thermodynamic control where $(Mg/Ca)_{calcite}$ ratios increase exponentially with increasing temperature.
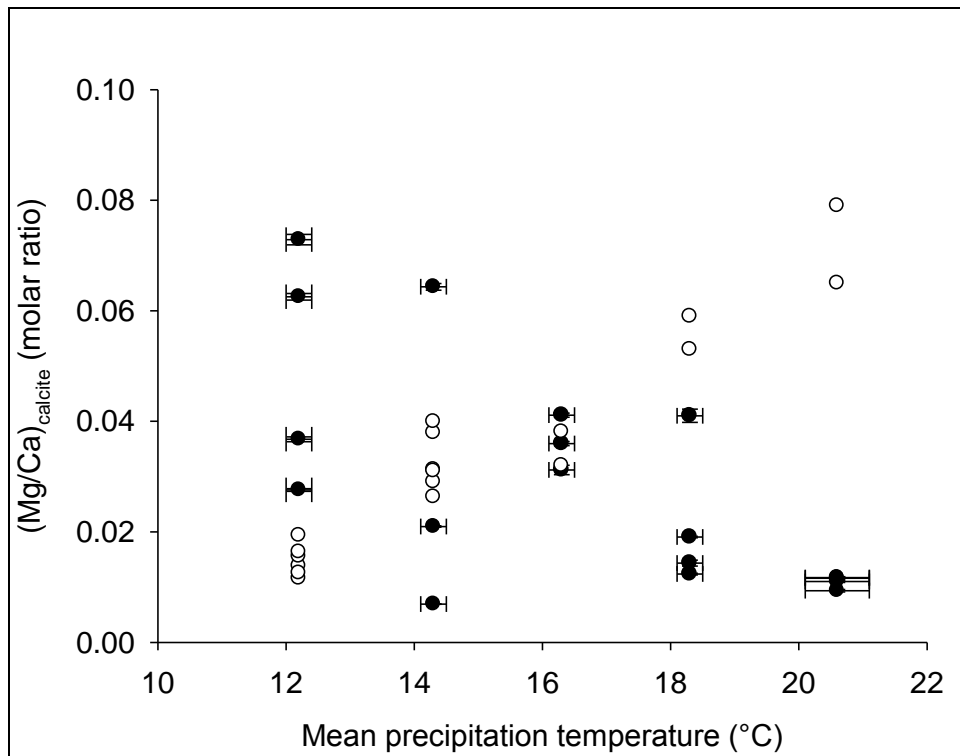
Figure 5.1 $(Mg/Ca)_{calcite}$ as a function of temperature (error bars represent 1σ). Data from control experiments are shown by the open circles.

The range of $(Mg/Ca)_{calcite}$ values for each temperature and the percentage variation is shown in Table 5.1.

Table 5.1 Range of Mg/Ca values at differing precipitation temperatures

Temperature (°C)	Minimum Mg/Ca (molar ratio)	Maximum Mg/Ca (molar ratio)	Percentage variation
12.2 ± 0.2	0.029	0.075	159
14.3 ± 0.2	0.0069	0.064	828
16.3 ± 0.2	0.033	0.044	33
18.3 ± 0.2	0.012	0.041	242
20.6 ± 0.5	0.0095	0.011	16

High rates of precipitation (R) were found only at higher temperatures (Figure 5.2). Indeed a general exponential ($R = \{5.4 \times 10^{-11}\}\exp^{0.96T}$) correlation between precipitation rates and temperature is observed (significant at $P < 0.05$, $R^2 = 0.86$, n = 18).
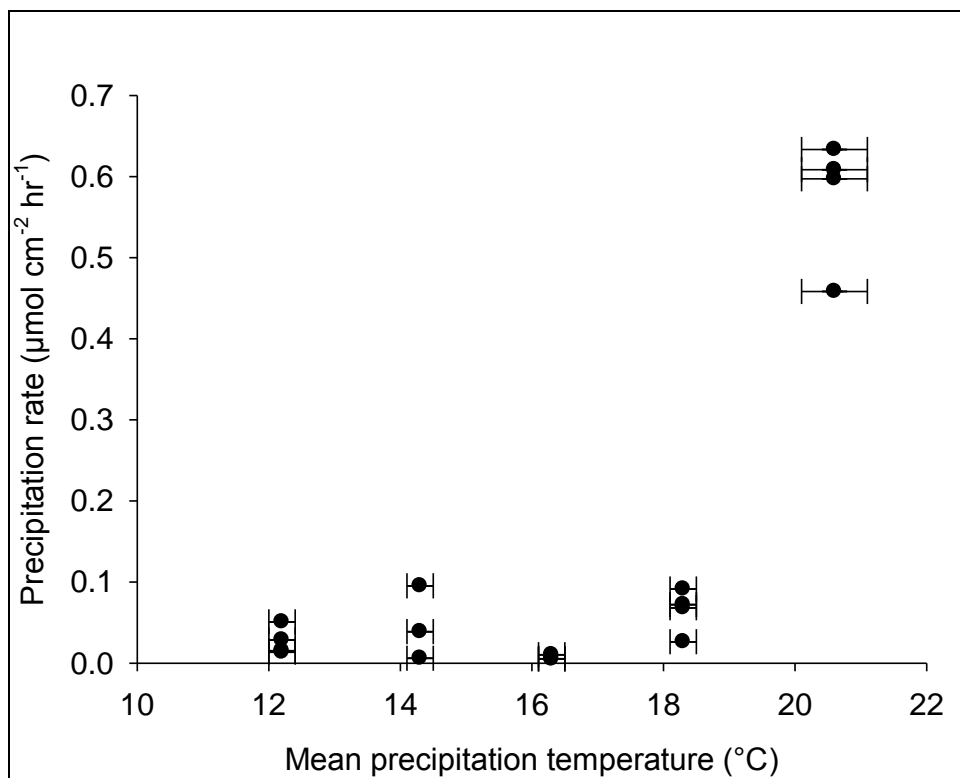
Figure 5.2 Calcite precipitation rate as a function of experimental temperature.

When $(Mg/Ca)_{calcite}$ ratios are plotted against the precipitation rate (Figure 5.3) a negative power correlation existed between the parameters where $(Mg/Ca)_{calcite}$ = $0.005R^{-0.2995}$. The relationship is significant at the 95 % confidence level (n = 18) with $R^2 = 0.52$.
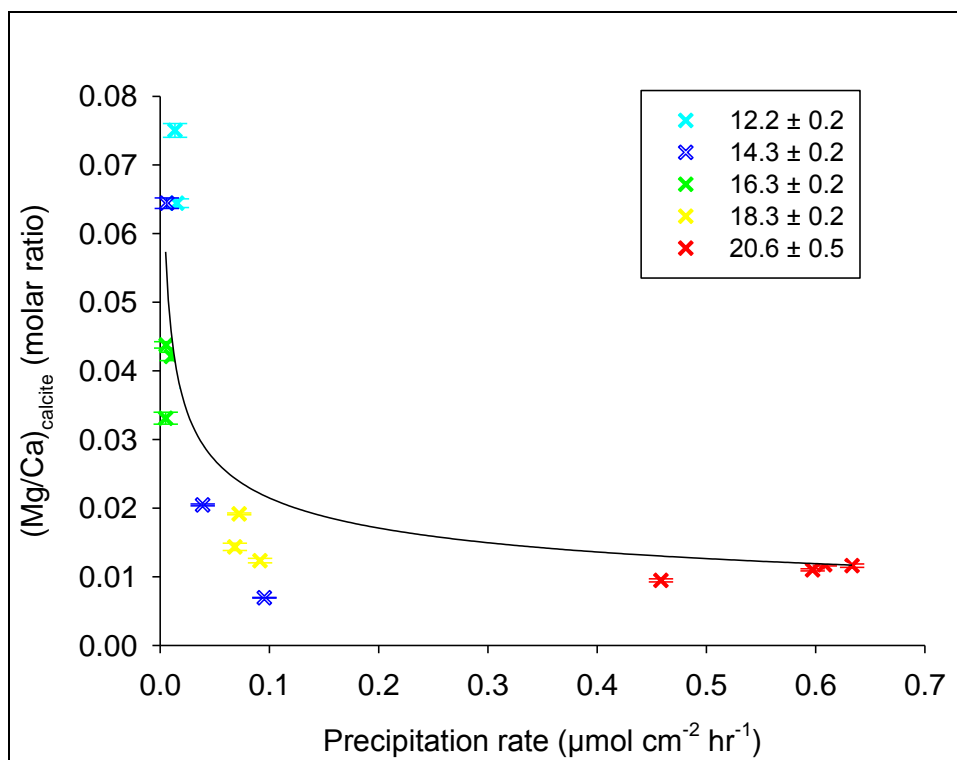
Figure 5.3 (Mg/Ca)$_{calcite}$ as a function of precipitation rate (Key = mean experimental temperature with 1σ errors).

At the conclusion of the microcosm experiments photographs were taken of each strip of biofilm and a sample was retained for SEM examination. Figures 5.4 – 5.8 show the gross appearance of the biofilm and its respective SEM image for a representative selection of biofilms.
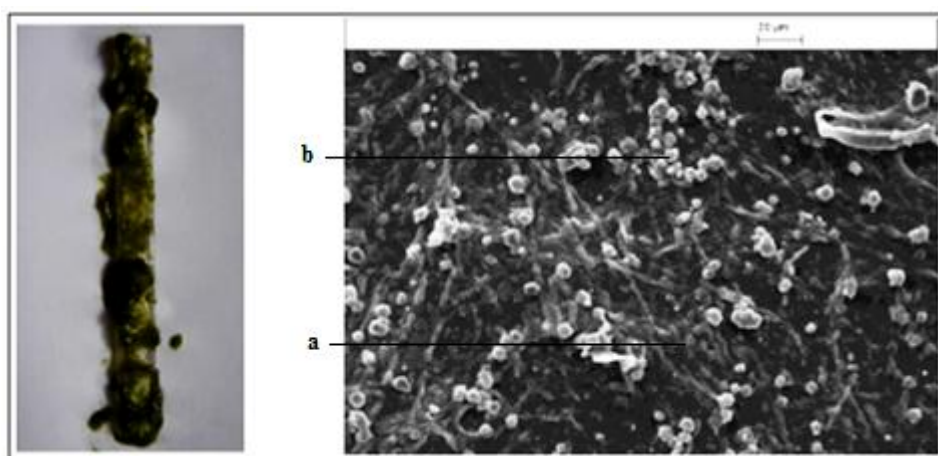
Figure 5.4 Biofilm photo and SEM image from microcosm 3 at 12 °C showing small crystals: (a) covered by a thin biofilm layer, (b) free from biofilm covering.
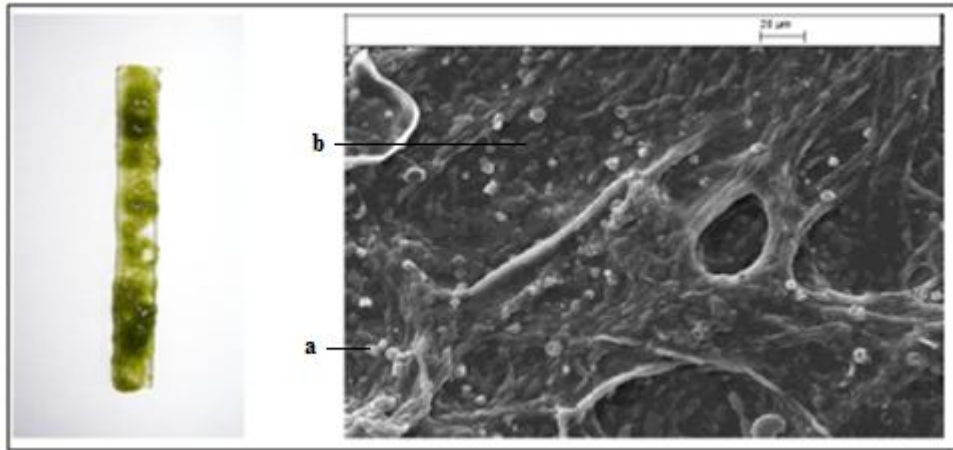
Figure 5.5 Biofilm photo and SEM image from microcosm 1 at 14 °C showing small crystals: (a) covered by a thin biofilm layer, (b) free from biofilm covering.
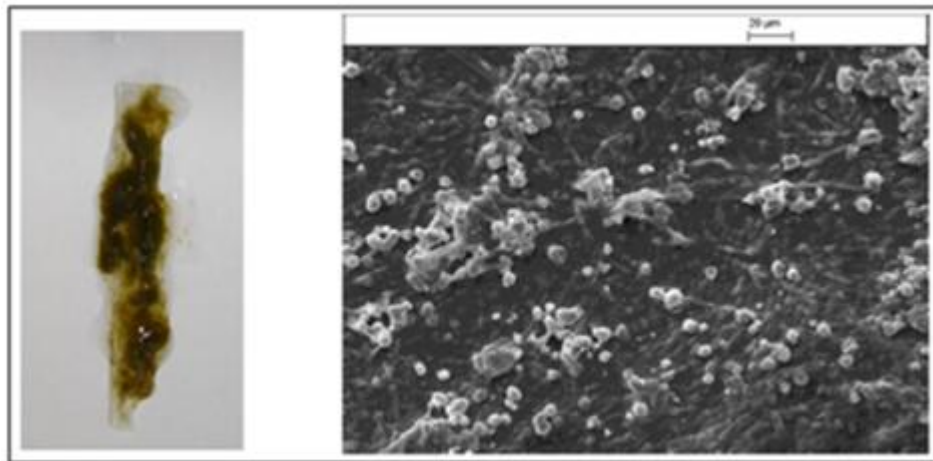
Figure 5.6 Biofilm photo and SEM image from microcosm 3 at 16 °C showing both single crystals and aggregates of crystals. Crystal size is larger than at 12 and 14 °C.
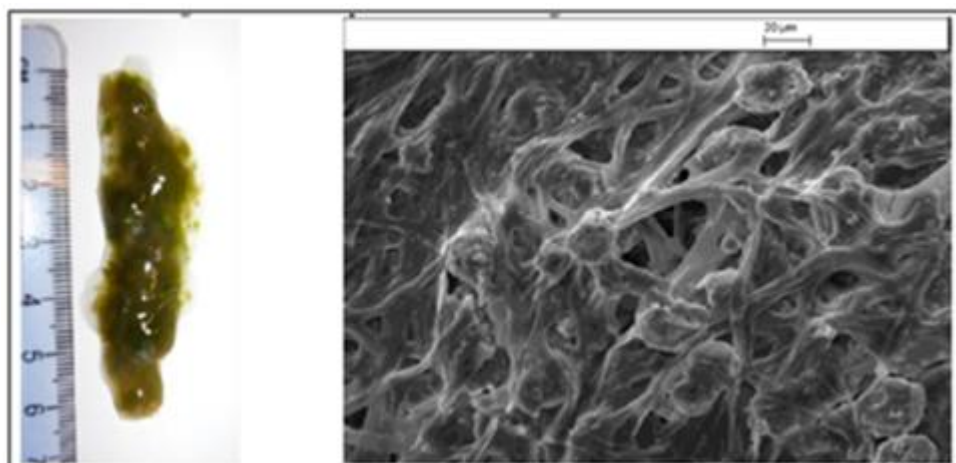
Figure 5.7 Biofilm photo and SEM image from microcosm 3 at 18 °C. Calcite crystals are very tightly associated with the biofilm and are larger than at 12, 14 and 16 °C.
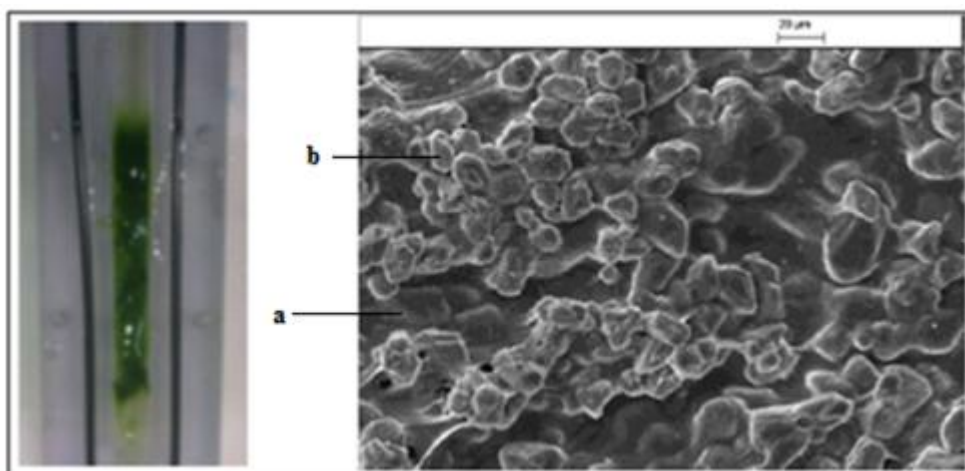
Figure 5.8 Biofilm photo and SEM image from microcosm 3 at 20 °C showing aggregates of crystals: (a) covered by a thin biofilm layer, (b) free from biofilm covering.

Calcite crystal sizes were seen to increase in size as temperature increased. The precipitates tended to be more aggregated and encapsulated within the biofilm/EPS matrix at the higher temperatures of 18 and 20 °C as (Figures 5.7 and 5.8) but generally existed as single crystals with some encapsulation. Many crystals were not encapsulated at lower temperatures. This encapsulation at higher temperatures is also seen in Figures 5.9 and 5.10.
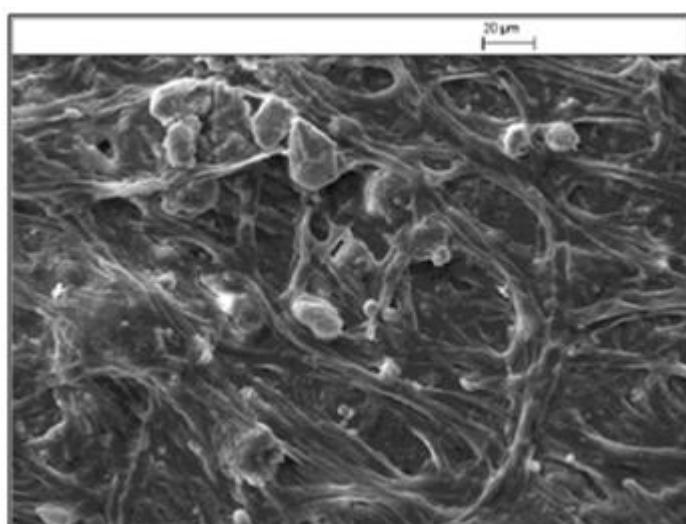
Figure 5.9 Calcite in close association with filamentous strands of biofilm/EPS matrix (microcosm 1 at 18 °C).
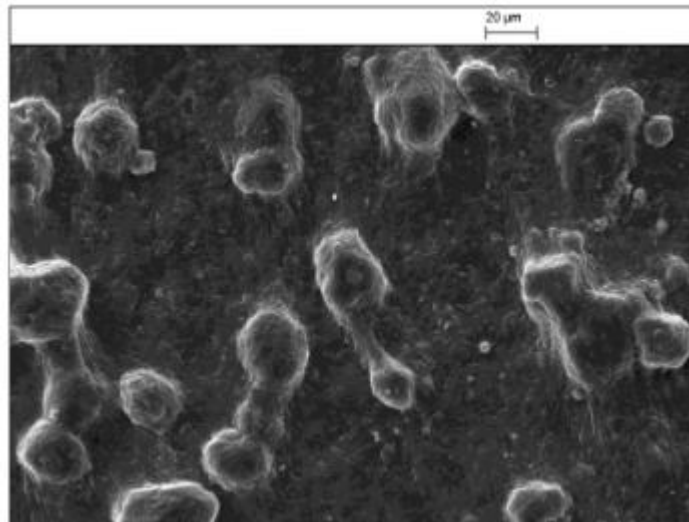
Figure 5.10 Calcite crystals covered in a thin continuous layer of biofilm/EPS matrix (microcosm 2 at 20 °C).

To confirm that the crystal like features in Figure 5.10 were $CaCO_3$ they were analysed by an energy dispersive X-Ray spectrometer probe (EDX). The EDX spectra (Figure 5.11) confirmed the presence of calcite. The 'Au' spikes represent the conductive gold spluttering applied to the sample.
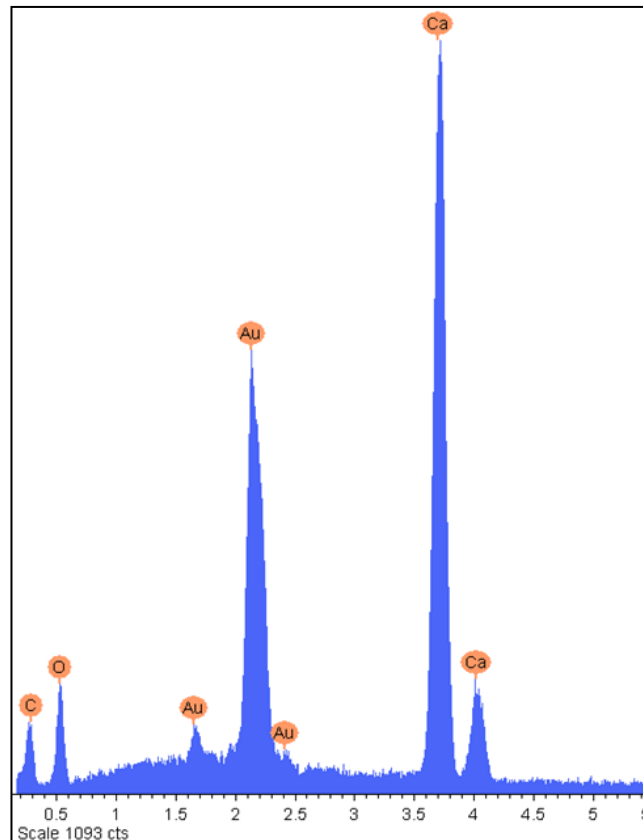
Figure 5.11 EDX spectra of precipitates from microcosm 2 at 20 °C.

5.4.2 Agitated flask experiments

The results of the biofilm exposed to light (BFL) and biofilm in the dark (BFD) are presented here and the EPS results in Chapter 6. Figures 5.12 and 5.13 show the $(Mg/Ca)_{calcite}$ ratios against the mean precipitation temperature with error bars representing 1 σ values for the BFL and BFD respectively.
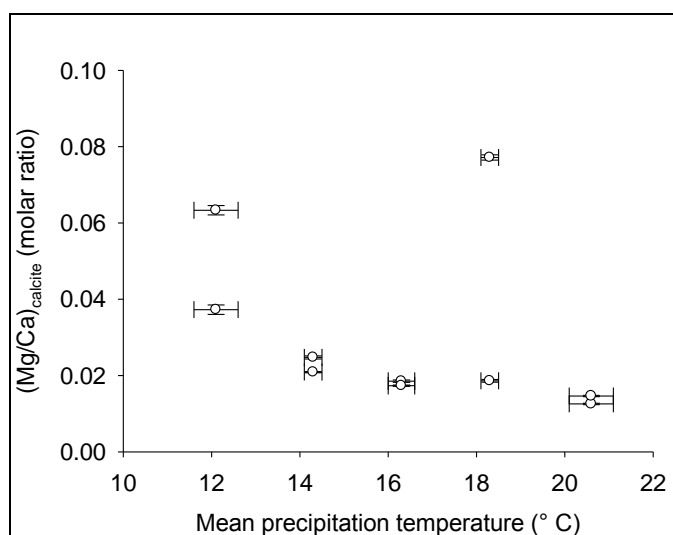
Figure 5.12 $(Mg/Ca)_{calcite}$ of flask precipitates as a function of temperature from biofilm exposed to light.
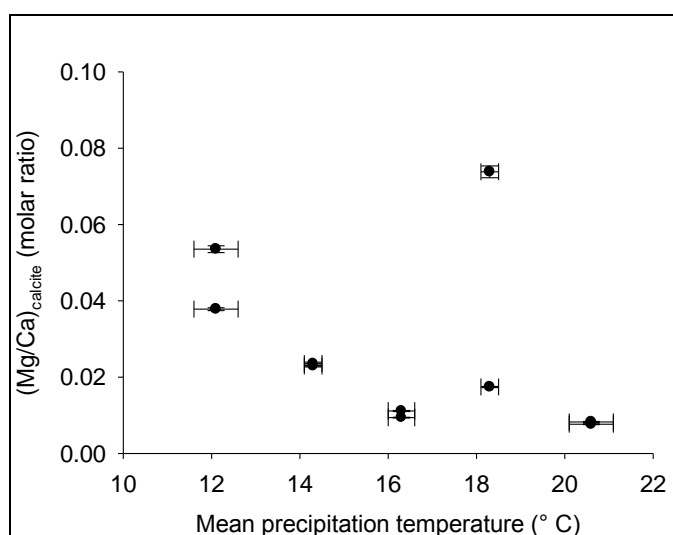
Figure 5.13 $(Mg/Ca)_{calcite}$ of precipitates as a function of temperature from biofilm excluded from light.

The data for both BFL and BFD follow an almost identical pattern. Two replicates have plots well off the general pattern; both are at 18 °C, one from the BFL and one from the BFD. The presence of the anomalous plot at 18 °C results in no significant correlation between temperature and $(Mg/Ca)_{calcite}$ for the BFL or BFD experiments

($R^2 = 0.13$, and $R^2 = 0.16$ respectively). The exclusion of the anomalous data points results in a significant relationship at the 95 % confidence level for both BFL and BFD experiments $(Mg/Ca)_{calcite} = 98.4T^{-3.06}$ ($R^2 = 0.76$, n = 9) and $(Mg/Ca)_{calcite} = 550.9T^{-3.78}$ ($R^2 = 0.88$, n = 9) respectively. Figure 5.14 shows both BFL and BFD data combined and highlights the very similar pattern of $(Mg/Ca)_{calcite}$ ratios seen in both the BFL and BFD precipitates. The combined data points, including the anomalous 18 °C plots, do not give a significant correlation. Removing the two anomalous points gives a significant relationship at the 95 % confidence level $(Mg/Ca)_{calcite} = 222.1T^{-3.40}$ ($R^2 = 0.80$, n = 18). Similarly to the microcosm experiments this is in direct contrast to the anticipated thermodynamic correlation.
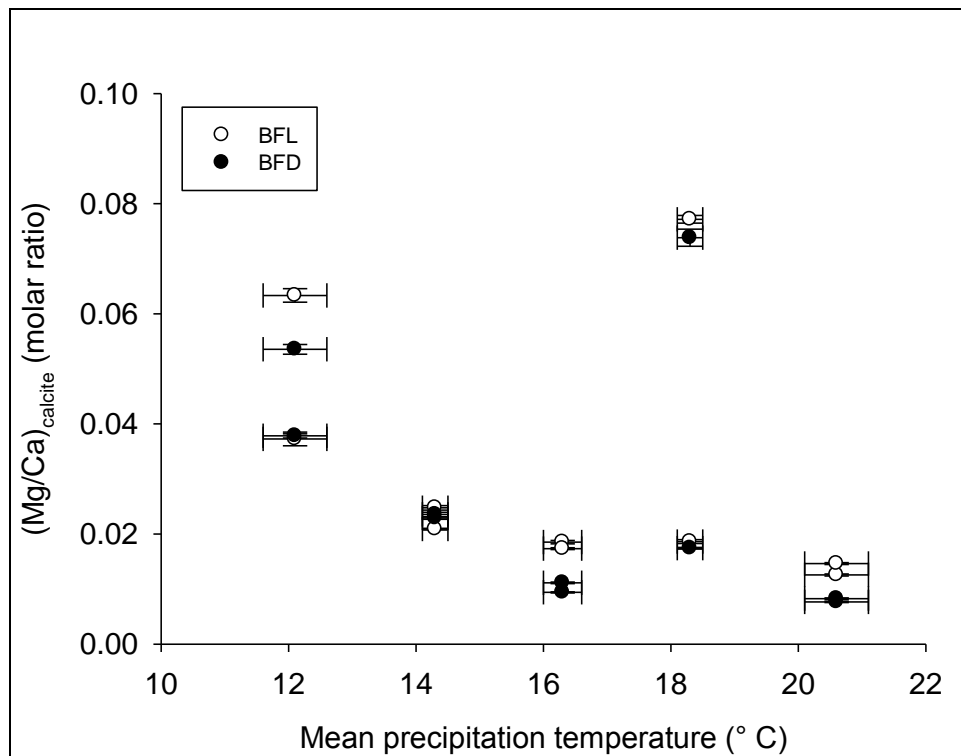
Figure 5.14 Combined plots of BFL and BFD (Mg/Ca)_{calcite} as a function of temperature.

The relationships between $(Mg/Ca)_{calcite}$ and precipitation rate for BFL and BFD precipitates are shown in Figures 5.15 and 5.16 respectively.
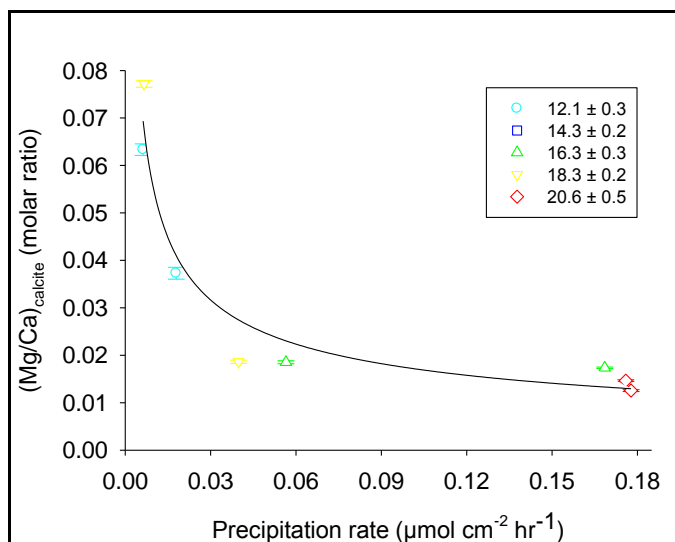
Figure 5.15 (Mg/Ca)$_{calcite}$ as a function of precipitation rate for BFL precipitates (key = mean experimental temperature with 1σ errors).
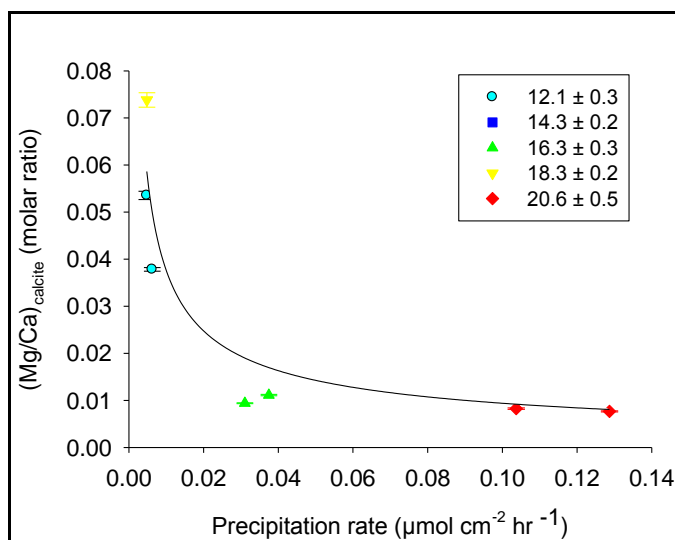
Figure 5.16 (Mg/Ca)$_{calcite}$ as a function of precipitation rate for BFD precipitates (key = mean experimental temperature with 1σ errors).

As with the microcosm data the relationship between the (Mg/Ca)$_{calcite}$ ratios and precipitation rate takes the form of a negative power regression. For the BFL (Mg/Ca)$_{calcite}$ = $0.003R^{0.4409}$ (R^2 = 0.89, n = 10), for BFD (Mg/Ca)$_{calcite}$ = $0.0009R^{-0.6023}$ (R^2 = 0.83, n = 10) and for both sets of data combined (Figure 5.17) (Mg/Ca)$_{calcite}$ = $0.002R^{-0.5056}$ (R^2 = 0.79, n = 20) all of which are significant at the 95 % confidence level.
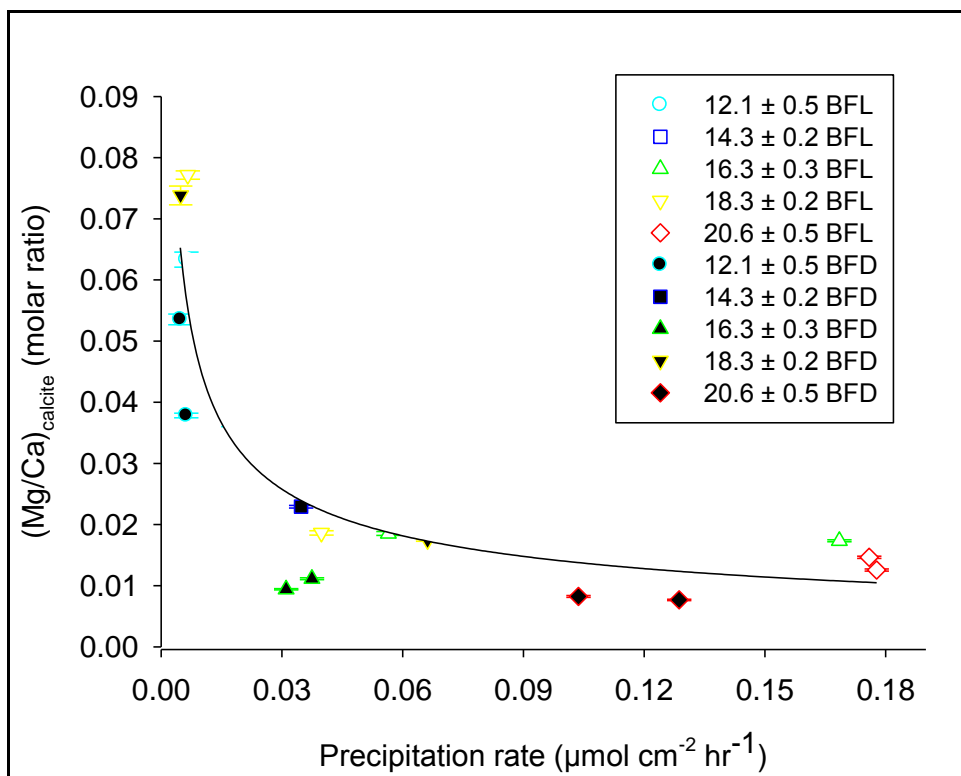
Figure 5.17 Combined plots of BFL and BFD for (Mg/Ca)$_{calcite}$ as a function of precipitation rate (key = mean experimental temperature with 1σ errors).

No significant correlation was found between precipitation rate and temperature for BFL precipitates (Figure 5.18). However for BFD a correlation significant at the 95 % confidence level was found (Figure 5.19) where R = -0.0241+ (0.00218T) (R^2 = 0.48, n = 10). The strength of the correlation for BFD precipitates is reduced by the apparently anomalous data point at 18 °C. Removing this data point gives a correlation of R = -0.0291 + (0.0259T) (R^2 = 0.74). For the BFL precipitates both data points at 18 °C do not follow the general trend of increasing rate at higher temperatures observed at the other temperatures. Excluding these points gives a correlation between precipitation rate and temperature for the BFL precipitates which is significant at the 95 % confidence level where R = -0.0461 + (0.00447T) (R^2 = 0.70).
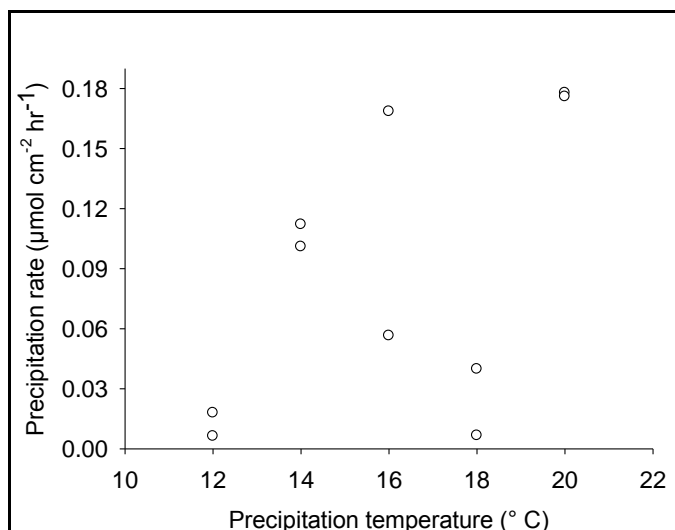
Figure 5.18 Precipitation rate as a function of temperature for precipitates from biofilm exposed to light.
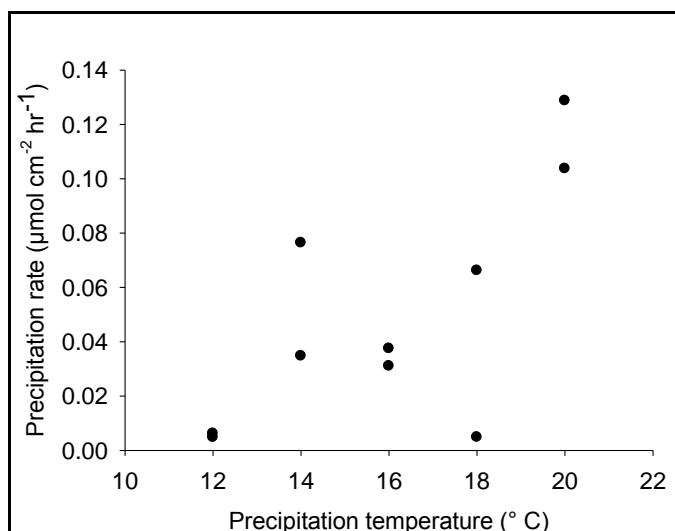
Figure 5.19 Precipitation rate as a function of temperature for precipitates from biofilm excluded from light.

Figure 5.20 combines the data for both sets of experiments. Combining the plots for BFL and BFD does not give a significant relationship. Exclusion of the two anomalous data points at 18 °C gives a weak but significant (at 95 % confidence level) correlation where $R = -0.141 + (0.0137T)$, ($R^2 = 0.48$, n = 18).
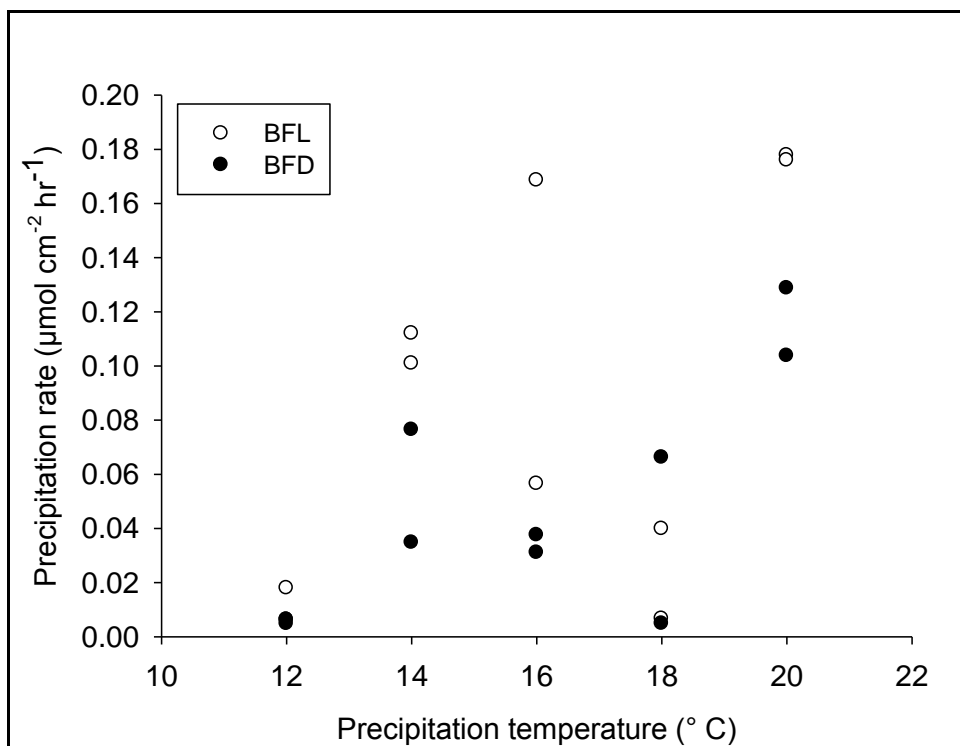
Figure 5.20 Combined plots of BFL and BFD for precipitation rate as a function of temperature.

Although there are a limited number of data points, generally it is seen that the precipitation rates at a given temperature are slightly higher for the BFL. Taking the mean precipitation rate for the 2 replicates at each temperature for BFL and BFD shows the rate was higher for BFL by a factor of 2.2 (12 °C), 1.9 (14 °C), 3.3 (16 °C) and 1.5 (20 °C). At 18 °C the rate was higher for BFD by a factor of 1.5.

Figures 5.21 and 5.22 show the gross visual appearance of the biofilms at the end of the 18 and 20 °C experiments respectively, (which are representative of all experimental temperatures). The biofilms exposed to light grew significantly in volume during the experiments and had generally developed a more strongly congealed texture than when initially added to the conical flasks. The biofilm from which light was excluded appeared to have shown no increase in volume and was in a less congealed state than when it was initially placed in the flasks.
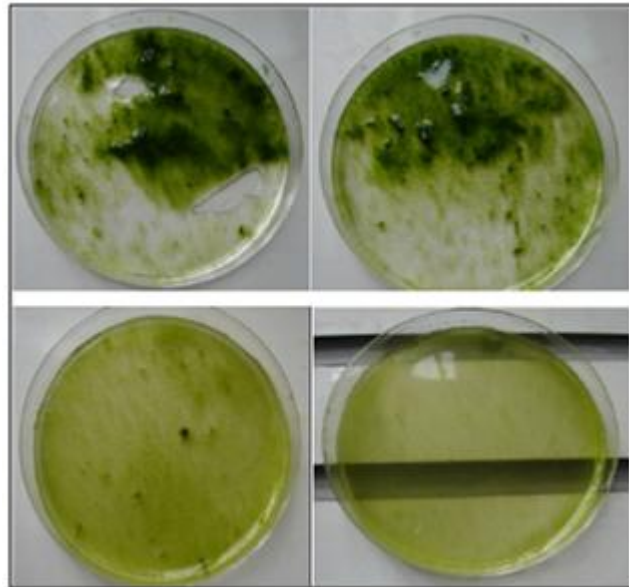
Figure 5.21 Condition of biofilm at end of 18 °C agitated flask experiment. Top dishes are BFL, bottom are BFD.

Figure 5.22 Condition of biofilms at end of 20 °C agitated flask experiment. BFD on the left and BFL on the right.

5.4.3 Combining the microcosm and agitated flask data

Figure 5.23 shows the combined data for $(Mg/Ca)_{calcite}$ ratios of all microcosm and agitated flask replicates against precipitation temperature. Apart from the 20 °C precipitates there is considerable variation of $(Mg/Ca)_{calcite}$ ratios at any given temperature indicating that temperature does not have a strong correlation with $(Mg/Ca)_{calcite}$ ratios derived from calcite precipitated within a biofilm under the given experimental conditions. Analysis shows a weak but significant (at 95 % confidence)

correlation where $(Mg/Ca)_{calcite} = 5.2T^{-1.8901}$ ($R^2 = 0.26$, n = 38). Excluding the two anomalous data points at 18 °C strengthens the correlation giving $(Mg/Ca)_{calcite} = 31.4T^{-2.6}$ ($R^2 = 0.52$, n = 36).

Figure 5.23 Combined plots of microcosm, BFL and BFD (Mg/Ca)$_{calcite}$ as a function of temperature.

Combining the data from the microcosm and agitated flask experiments for precipitation rate against temperature (Figure 5.24) reveals a significant relationship at the 95 % confidence level with $R = 0.0128T^{14.8016}$ ($R^2 = 0.58$, n = 38).

Figure 5.24 Combined plots of microcosm, BFL and BFD for precipitation rate as a function of temperature.

The impact of the precipitation environment on precipitation rates at a given temperature is highlighted in Figure 5.25 which shows the mean rate of precipitation for all replicates from the microcosm, BFL and BFD experiments. There is no consistency in which of the experimental conditions produced the greatest mean precipitation rates. When all temperatures are included there is a significant correlation (at the 95 % level) between precipitation rate and temperature where $R = 0.05646T^{14.3772}$ ($R^2 = 0.45$, n = 15). However, examination of Figure 5.25 suggests that this correlation may only be significant due to the presence of the 20 °C data. Exclusion of these data points shows that in the range of 12 - 18 °C there is no significant correlation (Figure 5.26).
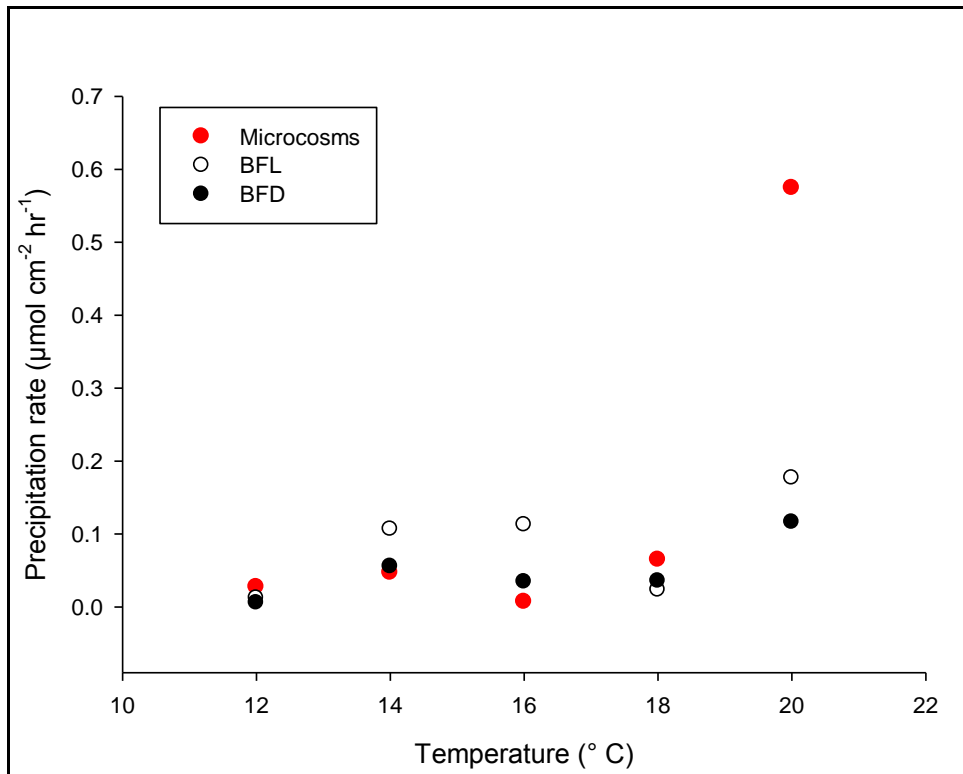
Figure 5.25 Mean precipitation rates of all replicates from the microcosm, BFL and BFD experiments as a function of temperature.
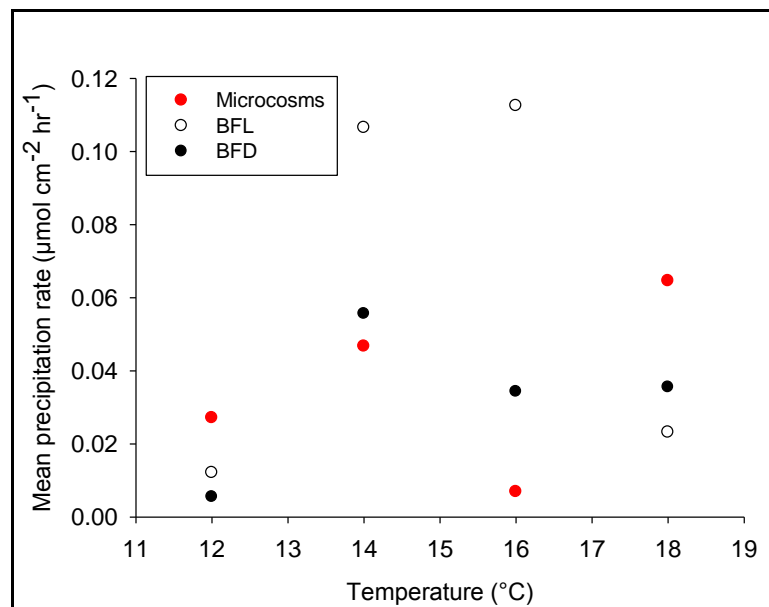
Figure 5.26 Mean precipitation rate as a function of temperature excluding the 20 °C data.

The mean precipitation rates across all experimental conditions are ranked from lowest to highest in Table 5.3.

Table 5.2 Mean precipitation rates from lowest to highest as related to experimental conditions

Experiment type	Temperature (°C)	Precipitation rate (μmol cm^{-2} hr^{-1})
BFD	12	0.006
Microcosm	16	0.007
BFL	12	0.012
BFL	18	0.023
Microcosm	12	0.027
BFD	16	0.034
BFD	18	0.036
Microcosm	14	0.047
BFD	14	0.056
Microcosm	18	0.065
BFL	14	0.107
BFL	16	0.113
BFD	20	0.116
BFL	20	0.177
Microcosm	20	0.574

When the data for (Mg/Ca)$_{calcite}$ versus precipitation rate are combined, the negative power relationship seen individually in the microcosm and flask experiments still persists (Figure 5.27). The relationship is significant at the 95 % confidence level with (Mg/Ca)$_{calcite}$ = 0.00831$R^{-0.4128}$ (R^2 = 0.67, n = 38).
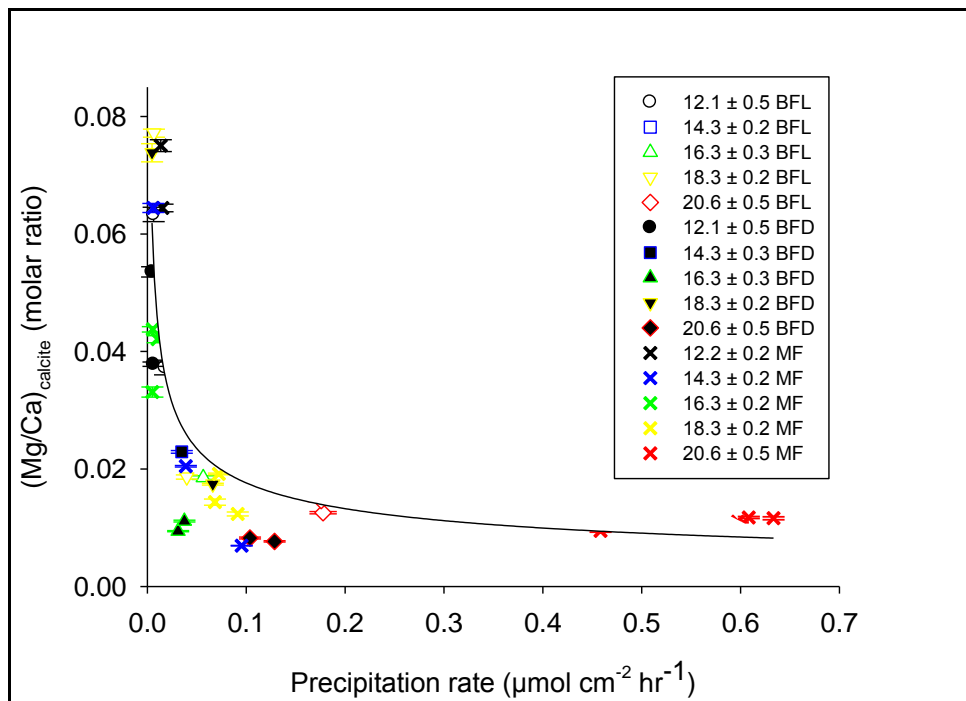
Figure 5.27 (Mg/Ca)$_{calcite}$ from the microcosm flumes (MF), BFL and BFD experiments as a function of precipitation rate.

5.5 Discussion

The discussion begins with a description of how the experimental $(Mg/Ca)_{calcite}$ values and precipitation rates compare to both thermodynamic expectations and to previous studies on other carbonate deposits. This is followed by an examination and discussion on the impact of precipitation rate on $(Mg/Ca)_{calcite}$. The possible mechanisms by which microbial biofilms are able to influence both precipitation rate and $(Mg/Ca)_{calcite}$ are then outlined and discussed.

5.5.1 Precipitation temperature and (Mg/Ca)$_{calcite}$

The experimental results reveal that the presence of a microbial biofilm is able to override the expected thermodynamic control on $(Mg/Ca)_{calcite}$ in a freshwater environment. The results suggest that the calibration of a tufa derived $(Mg/Ca)_{calcite}$ palaeothermometer may be impracticable. The finding that $(Mg/Ca)_{calcite}$ decreases with increasing temperature, albeit weakly (Figure 5.1), is in direct contrast to the expected thermodynamic response which indicates that $(Mg/Ca)_{calcite}$ will rise exponentially by about 3 % per °C within the temperature range of these experiments (Lea *et al*., 1999). It also contrasts previous studies on inorganic calcite which have confirmed the validity of the predicted 3 % rise of $(Mg/Ca)_{calcite}$ per °C (Katz, 1973, Mucci, 1987 and Oomori *et al*., 1987). Furthermore, the findings do not match with studies on foraminiferal calcite which have also confirmed that $(Mg/Ca)_{calcite}$ increases exponentially with increasing temperature (Nurnberg *et al*., 1996, Rosenthal *et al*., 1997, Elderfield *et al*., 2006, Bousetta *et al*., 2011, Martinez-Boti *et al*., 2011). However, not all studies on biogenic calcite have observed the exponential relationship, ostracode (Palacios-Fest and Dettman, 2001, Cronin *et al*., 2005), and coralline calcite (Mitsuguchi *et al*., 1996, Wei *et al*., 2000, Yu *et al*., 2005, Reynaud *et al*., 2007) show a linear correlation, although it does still generate increasing $(Mg/Ca)_{calcite}$ ratios with increasing temperature. Although foraminiferal calcite exhibits the expected exponential relationship, it does deviate from expectations in that $(Mg/Ca)_{calcite}$ ratios have generally been found to be 1 to 2 orders of magnitude lower than predicted for inorganic calcite (Barker *et al*., 2005).

The departures from expectations in these previous studies and the experimental results described here are a strong indication that biogenic influences can cause significant deviations from the expected thermodynamic relationship between

temperature and Mg^{2+} substitution in calcite. The results described here show wide variations in the $(Mg/Ca)_{calcite}$ at a specific temperature in the range of 12 – 18 °C but this variation is not seen at 20 °C, where there is a narrow range (0.0095 – 0.011). This observation suggests that there may be multiple factors influencing $(Mg/Ca)_{calcite}$. At temperatures < 20 °C the heterogeneous nature of the biofilm and its associated EPS may be the cause of the wide fluctuations in $(Mg/Ca)_{calcite}$, whilst at 20 °C temperature may be able to override the biogenic effects. The possible mechanisms behind this are discussed in section 5.5.4.

The agitated flask experiments generally present a tighter but still decreasing relationship between $(Mg/Ca)_{calcite}$ and temperature with the exception of two of the data points at 18 °C in both the BFL and BFD treatments (Figures 5.12 and 5.13). Including these outlying data points means there is no significant relationship but their exclusion results in R^2 = 0.76 and 0.88 (P < 0.05) for both BFL and BFD respectively. Examination of all the original ICP – OES outputs for that day do not reveal anything that may make these values obviously erroneous. It is suggested that these data points are valid and that their large deviation from the other points is due to the influence of the biofilm. The fact that the both the BFL and BFD treatments have these anomalous points eliminates the possibility that they resulted from the presence/absence of photosynthesis. Most likely, the portion of biofilm added to these two replicates had a significantly different microbial composition and the chelating ability of this biofilm was distinctly different from the 'representative' biofilm in all the other replicates. Furthermore, large areas of biofilm may consist mainly of EPS and actually be devoid of microbial cells (Wolfaardt et al., 1999). If microbial metabolism is the dominant factor in the breakdown of the expected theromodynamic control then precipitates from a biofilm sample with a greater ratio of EPS to living cells may have $(Mg/Ca)_{calcite}$ ratios closer to thermodynamically expected values. The reasoning behind these suggestions is contained in sections 5.5.4 and onwards which illustrate the potential for biofilms to cause wide deviations in $(Mg/Ca)_{calcite}$ values.

The argument that the $(Mg/Ca)_{calcite}$ values at 20 °C are more strongly controlled by temperature than the presence of the biofilm is strengthened when the results from the microcosm and agitated flask experiments are combined (Figure 5.23). The wide

scattering of data points at 12 – 18 °C is in stark contrast to the tight grouping seen at 20 °C. Interestingly, the apparently anomalous points at 18 °C discussed above do not seem so out of place when the data are combined.

5.5.2 Temperature and calcite precipitation rate

The data obtained from these experiments show an inconclusive relationship between precipitation rate and temperature in the presence of microbial biofilms. When all data points are included there is a weak but significant correlation whereby the rate increases with temperature. However, this correlation does not hold when the 20 °C data are excluded, in this case there is no correlation between the parameters (Figure 5.26). The lack of any correlation in the 12 – 18 °C range is contrary to expectations. At a given saturation state calcite precipitation should take place at a higher rate as temperature increases due to the fact that calcite solubility decreases with increasing temperature (Morse and Mackenzie, 1990). Higher temperatures also increase precipitation rates through the increased kinetic energy of the species, a higher number of collisions between ionic species at higher energies will increase the likelihood of precipitation reactions overcoming the activation energy barrier and going to completion. Increased calcification rates at higher temperatures have been observed in laboratory experiments involving precipitation in the presence of bacterial isolates (Cacchio *et al*., 2003, Cacchio *et al*., 2004, Baskar *et al*., 2006), however, no studies appear to have been conducted which examine precipitation rates as a function of temperature in the presence of a full microbial biofilm.

There was no consistent relationship between the mean precipitation rates at a given temperature (see Table 5.2) and the precipitation environment (e.g. the flow-through microcosms or the agitated flasks). Given that precipitation rates are related to the saturation state (Ω) through the equation $R = k(\Omega - 1)^n$ (Morse *et al*., 2007) then a higher saturation state should result in greater precipitation rates. At the commencement of the experiments the Ω values were the same for both microcosm and agitated flask experiments. In the microcosm experiments the saturation state remained the same throughout the duration of the experiment due to the constant concentration of ions in the experimental water flowing over the biofilm. In the

agitated flasks there was no replenishment of ions to the experimental solution so Ω values will have fallen over time as precipitation took place.

The flasks were agitated at a rate of 100 oscillations per minute, generating a mean water flow velocity over the precipitating calcite surface that will have been considerably greater than the 0.38 L hr^{-1} flow rate for each microcosm. As discussed in section 2.6 higher flow rates result in a thinner DBL which reduces solute transfer time to the precipitation site from the bulk water. A thinner DBL may have counteracted the falling saturation state in these replicates. The DBL should also exert some control over precipitation rates in response to temperature variations. The diffusion coefficient of ions diffusing across the DBL is temperature dependant (see Equation 2.7), for a given concentration gradient the ionic diffusion takes place at a higher rate as temperature increases. The faster supply of fresh ions at higher temperatures to the solid surface should result in greater precipitation rates. In the temperature range of 12 – 18 °C this was not observed, although there was a notable increase in rates at 20 °C for all experiments.

The overall absence of the expected relationship strongly suggests that the presence of the microbial biofilms had a substantial impact on precipitation rates. Furthermore, given the wide range of precipitation rates at a given temperature (Figures 5.25 and 5.26) it is believed that heterogeneity in biofilms (sections 5.5.4) impacts on precipitation rates.

5.5.3 (Mg/Ca)calcite and precipitation rate

The negative power relationship between (Mg/Ca)calcite and precipitation rate derived from the microcosm and agitated flask experiments is contradictory to theoretical expectations suggesting that the presence of the biofilm has strongly impacted on the correlation between the parameters. Partition coefficients (K) for both microcosm and agitated flask precipitates were calculated using the standard equation $K = (Mg/Ca)_{calcite}/(Mg/Ca)_{solution}$ and are presented as a function of precipitation rate in Figure 5.28 ($R^2 = 0.67$, P < 0.05, n = 38).
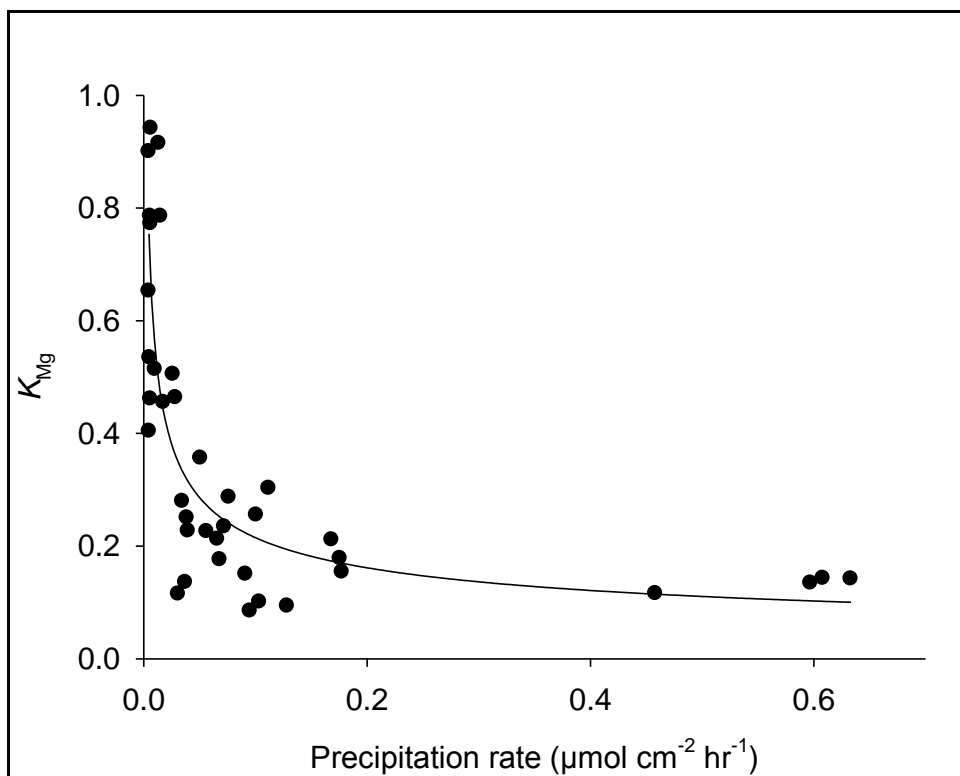
Figure 5.28 Distribution coefficients as a function of precipitation rate from the microcosm and agitated flask experiments combined.

Empirical distribution coefficients differ from theoretical coefficients which are determined from a system assumed to be at equilibrium. Experimental conditions can only approximate equilibrium, furthermore kinetic effects result in non uniform trace element partitioning in precipitates from actual experiments (Rimstidt *et al*., 1998). For the purposes of the following discussion empirical coefficients will be designated by (K_{exp}) and equilibrium coefficients by (K_{eq}). Table 5.4 shows the K_{exp} K_{eq} and ionic radii for selected divalent cations.

113

Table 5.3 Empirical and equilibrium distribution coefficients for selected divalent cations along with ionic radii. The ionic radii are in six-fold coordination from Shannon and Prewitt, 1969. For reference the ionic radii of Ca^{2+} is 1.00 (Table adapted from Rimstidt *et al.*, 1998).

Cation	Ionic radius	K_{exp}	K_{eq}
Ba^{2+}	1.36	0.020	1.95×10^{-2}
Cd^{2+}	0.95	188	6.92×10^{3}
Co^{2+}	0.65	10.9	4.68×10^{1}
Cu^{2+}	0.73	80.2	1.55×10^{3}
Fe^{2+}	0.61	27.7	2.40×10^{2}
Mg^{2+}	0.72	0.022	8.71×10^{-4}
Mn^{2+}	0.67	20.5	1.41×10^{2}
Pb^{2+}	1.18	17.2	2.63×10^{3}
Ra^{2+}	1.44	0.020	1.91×10^{-3}
Sr^{2+}	1.16	0.073	1.82×10^{-1}

Experimental evidence shows that a relationship exists between precipitation rates and K_{exp} which is dependent on the value of K_{eq} (Rimstidt *et al.*, 1998) where:

- for elements with a $K_{eq} < 1$ (e.g. Mg^{2+}) the value of K_{exp} is larger than K_{eq} and decreases towards K_{eq} as precipitation rates fall.

- for elements with $K_{eq} > 1$ the value of K_{exp} is smaller than K_{eq} and increases towards K_{eq} as precipitation rates fall.

These relationships have been observed experimentally (e.g. Lorens, 1981, Mucci 1987, Pingitore *et al.*, 1988, Tesoriero and Pankow, 1996). Accordingly, at faster precipitation rates the value of K_{exp} for Mg^{2+} into calcite should increase as precipitation rates rise (Figure 5.29). The K_{exp} values obtained in the experiments described here (Figure 5.28) are in complete contrast to the K_{exp} values obtained in experiments on inorganic calcite.
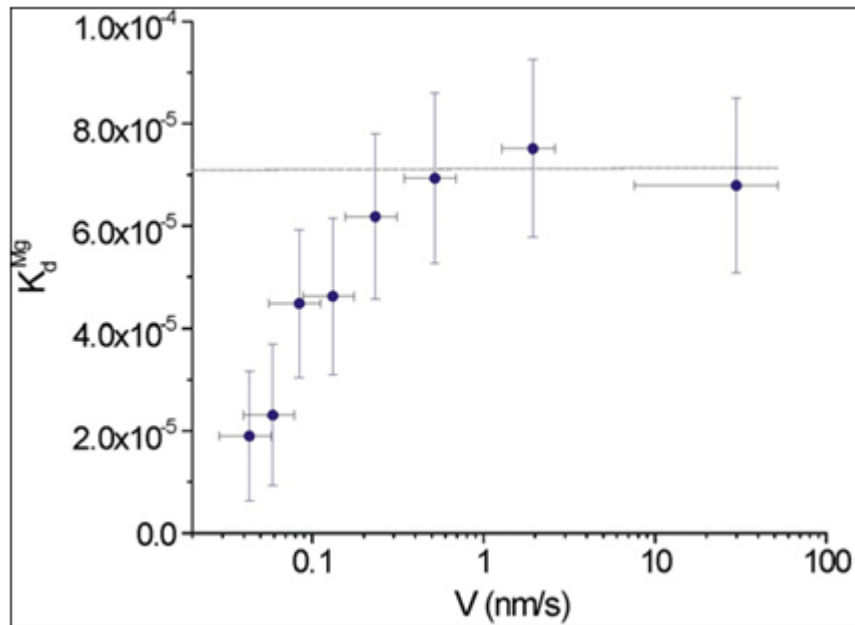
Figure 5.29 Distribution coefficient of Mg^{2+} in calcium carbonate as a function of growth rate (Gabitov *et al.*, 2008).

The variations in K_{exp} values with precipitation rate have been attributed to boundary layer effects (Rimstidt *et al.*, 1998). If for some reason (such as the presence of a biofilm) the trace element is being incorporated into the calcite faster than Ca^{2+} (K_{exp} >1) then the solution adjacent to the crystal face will have a lower M^{2+}/Ca^{2+} ratio than the bulk water. If Ca^{2+} is taken in faster ($K_{exp} < 1$) than M^{2+} , as has been the case in the described experiments, then the solution in the boundary layer adjacent to the crystal face will have a higher M^{2+}/Ca^{2+} ratio than the bulk water. Although the DBL is able to induce changes in the trace element ratios at the solid surface from those of the bulk water it has been demonstrated that the DBL only has a partial impact on trace element incorporation in calcite in response to precipitation rate changes (Wang and Xu, 2001). Therefore the complete contrast seen in the experimental results from expectations cannot adequately be explained by DBL processes. The most likely explanation must be the presence of the microbial biofilms. The potential mechanisms behind this are outlined in the following sections.

5.5.4 The potential of biofilms to influence calcite precipitation

The presence of the biofilm has shifted the (Mg/Ca)$_{calcite}$ ratios away from not only the thermodynamic expectations but also away from the type of relationships seen in other biogenic carbonates such as ostrocodes, foraminiferal and coral calcite.

Furthermore, at all temperatures apart from 20 °C there is considerable variation in $(Mg/Ca)_{calcite}$. In addition, apart from at 20 °C the expected increase in precipitation rates with increasing solution temperature was not observed. This indicates that trace element ratios and precipitation rate must be influenced by some aspect of the biofilm, namely microbial metabolic processes, structural components of the biofilm (EPS) or a combination of both.

The diversity of microorganisms held in a laboratory grown biofilm exposed to specific light and temperature conditions is strongly dependant on species specific growth rates and any species within the biofilm complex can only acclimatise to the imposed environment within their individual genetic limits (Defew *et al*., 2004). Temperature variations have been shown to have an impact on both biofilm microbial diversity and growth rates from photosynthesis and heterotrophic metabolism within the temperature range of the experiments described here (Blanchard *et al*., 1996, Watermann *et al*., 1999, Defew *et al*., 2004, Hancke and Glud, 2004, Salleh and McMinn, 2011). Given that the temperature range of tufa precipitating streams is similar to these laboratory experiments it is reasonable to infer that microbial mass and diversity in these streams will also be influenced by temperature and light conditions.

Figure 5.30 shows the relationship between a standardised maximum photosynthetic rate (P_{max}) and temperature for a benthic biofilm. Examination of the graph shows that P_{max} increases by about 3.5 % per °C, which for the experiments described means there is an approximate 30 % increase in P_{max} from the 12 to 20 °C treatments.
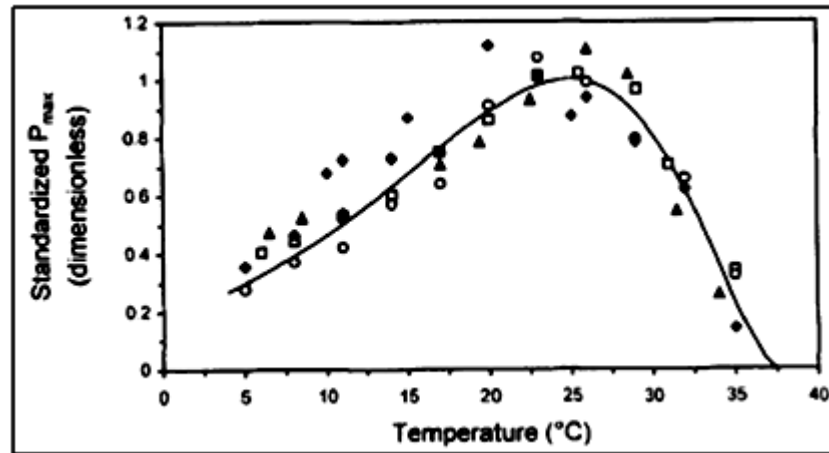
Figure 5.30 Standardised P$_{Max}$ values for a diatom benthic biofilm (Blanchard *et al.*, 1997).

P$_{max}$ values are species dependant, so the ability of any one species to outcompete and increase its percentage of the total biofilm composition will vary with temperature. In diatom/cyanobacterial biofilms such as those used in this work it has been observed that at 10 °C diatoms are the dominant organism but at 25 °C filamentous cyanobacteria dominate (Watermann *et al.*, 1999). Others have observed that at 10 °C changes in diatom species composition were minimal, whilst at 18 °C there was a significant change in the species composition and at these higher temperatures species diversity was at its lowest (Defew *et al.*, 2004). In light of these observations it is assumed that over the range of 12 – 20 °C of the described experiments considerable variation will have been induced in both genus and species variations during the course of each experimental run. This variation may also have differed between individual replicates at the same temperature depending on the health, number and diversity of species of the biofilm sample as it was separated from the bulk source.

The impact of photosynthesis on the biofilm mass and physical state is evident in Figures 5.21 and 5.22 which compare the end state of the biofilms from the agitated flask BFL and BFD experiments. Previous studies on biofilm growth in light and dark conditions have shown that biofilms grown in light have a greater thickness, species diversity, algal density and biomass than those grown in the dark (Romani and Sabater, 1999, Sekar *et al.*, 2002). The differences are not immediate; the first week of biofilm colonisation shows minimal differences between light and dark grown colonies (Romani and Sabater, 1999, Sekar *et al.*, 2002). Differences in

117

thickness stabilise after about 10 days but the difference in biomass continues to increase in light grown biofilms (Figure 5.31).
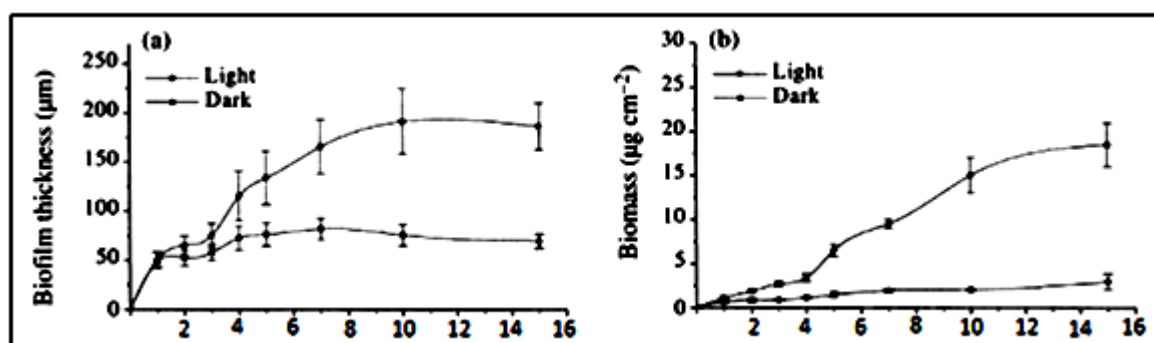
Figure 5.31 Biofilm thickness (a) and biomass (b) of biofilms grown under light and dark conditions for 15 days (Sekar *et al*., 2002).

Examination of Figure 5.31 (b) shows that the biomass was about 7 times greater in the BFL than BFD treatments after 15 days and that this divergence was still growing. Given that the average duration of the agitated flask experiments was around 26 days it is reasonable to speculate that the biomass in the BFL would have been in the range of $7 - 8$ times greater than that of the BFD. This speculation is supported by the examination of the biofilms in Figures 5.21 and 5.22. Across all temperatures the mean precipitation rate was greater for BFL, but only by a factor of about 1.75. Precipitation rates were therefore not likely to be directly proportional to biofilm mass.

The finding of Waterman *et al*., (1999) that cyanobacteria are the dominant organisms in biofilms at higher temperatures may explain the dramatic increase in precipitation rates at 20 °C seen in the microcosm experiments (Figure 5.2). It has been shown through biofilm microprofiles of pH, O_2, Ca^{2+} and CO_3^{2-} obtained (Shiraishi *et al*. (2008a) (see section 2.12) all showed that bright green cyanobacteria dominated biofilms had a higher photosynthetic capacity and thus exerted more influence on the carbonate system at the tufa surface. Comparison of the colour of the biofilm sample from the 20 °C microcosm experiment (Figure 5.8) with the colours of the biofilms at $12 - 18$ °C (Figures 5.4 – 5.7) show that the 20 °C biofilm is a much brighter green, suggesting it is dominated by cyanobacteria. The enhanced creation of an alkaline environment through the greater photosynthetic capacity of a cyanobacterial dominated biofilm at 20 °C in the experiments described here may

118

have enhanced precipitation rates significantly over those at the lower temperatures where cyanobacteria were not the dominant microorganism.

Changes in biofilm composition, mass and metabolic processes driven by photosynthetic rates appear to have significantly impacted on the expected increases in precipitation rate as a function of temperature in these experiments. Such changes may also have led to substantial changes in the amount, composition, physical state and chelating abilities of the EPS within each individual replicates biofilm and offers a possible explanation of the large range of $(Mg/Ca)_{calcite}$ seen at a given temperature.

5.5.5 Impact of EPS on $(Mg/Ca)_{calcite}$

The changing species composition which is likely to have occurred in the experimental biofilms may offer at least a partial explanation of the shifting of $(Mg/Ca)_{calcite}$ values from expectations. Variations in species diversity have been shown to have a large impact on the composition and amount of EPS produced (Di Pippo *et al*., 2009), this is important given its ability to chelate $Ca^{2+}_{(aq)}$ and $Mg^{2+}_{(aq)}$ from the bulk water of a calcite precipitating experimental solution or natural system. The chelating ability of EPS molecules depends on the availability of binding sites on negatively charged functional groups, which may be reduced by interactions between EPS molecules by causing them to become sterically inhibited or blocked (Dupraz *et al*., 2009). The nature of these interactions will vary alongside changes in biofilm composition. It has been suggested that the physical state of EPS also influences the binding abilities, whereby EPS in a gel state may bind more strongly with a particular cation than one in a loose slime state (Decho, 2000).

In addition to changes in binding abilities (i.e. the amount of a specific cation) there is a further potential influence on $(Mg/Ca)_{calcite}$ arising from EPS through chemoselectivity. The favouring for the chelation of $Ca^{2+}_{(aq)}$ over $Mg^{2+}_{(aq)}$ will ensure that water in the immediate microenvironment of the EPS will have a lower $(Mg/Ca)_{solution}$ than that of the bulk water and the water held within the biofilm matrix which is not in the immediate microenvironment of the EPS molecules. Although it has been shown that chelation exhibits an overall selectivity across a full biofilm based on charge density (Rogerson *et al*., 2008) it has also been demonstrated that some anionic groups differ in their chelation affinities for Ca^{2+} and

Mg^{2+} with some favouring calcium over magnesium and vice versa (Table 5.5) (Wang *et al*., 2009).

Table 5.5 Binding constants for multicarboxylic acids. The Binding constant *K* is for the generalised association reaction M+L ⇄ ML, with M representing the metal cation and L the ligand (adapted from Wang *et al*., 2009).

Carboxylic acid	Binding constant		
	$Log(K_{Ca}^{2+})$	$Log(K_{Mg}^{2+})$	$Log(K_{Ca}^{2+})$ /$Log(K_{Mg}^{2+})$
Oxydiacetic acid	3.38	1.8	- 1.58
D tartaric acid	1.8	1.36	- 0.44
Citric acid	3.5	3.37	- 0.13
Glutamic acid	1.43	1.9	0.47
Malonic acid	1.51	2.11	0.6
Aspartic acid	1.6	2.43	0.83

The relationship between differing functional groups and $(Mg/Ca)_{calcite}$ has been confirmed experimentally (Wang *et al*., 2009). Figure 5.32 shows how the presence of differing carboxylated functional groups influences Mg^{2+} uptake into calcite compared to when no biomolecules were present.
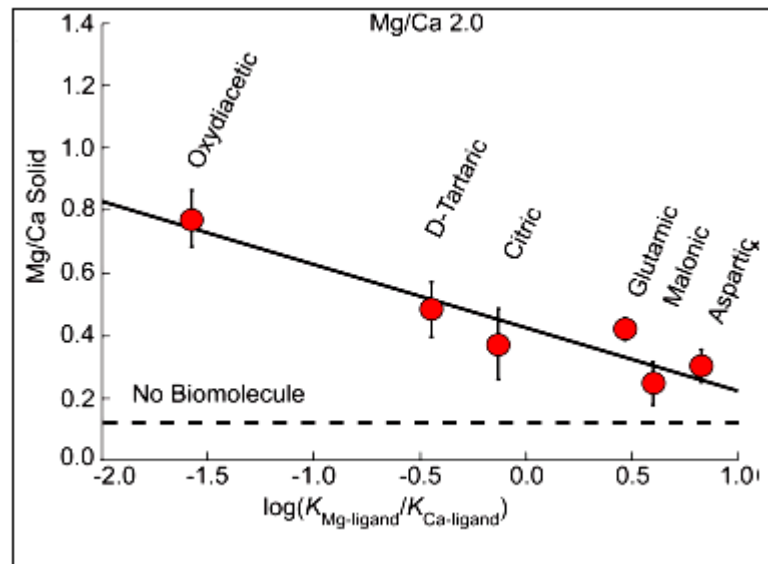
Figure 5.32 Influence of different carboxylated functional groups on $(Mg/Ca)_{calcite}$ (Wang *et al*., 2009).

Although the data in Figure 5.32 only relate to carboxylic acids, other anionic groups may exhibit similar behaviours further complicating the partitioning of Mg^{2+} into calcite. Biofilms from freshwater environments have been shown to contain a

number of different functional groups (Dupraz et $al.$, 2009) each of which may influence the Mg/Ca ratio of calcite precipitated in their presence to different degrees (Figure 5.32). The wide variations in $(Mg/Ca)_{calcite}$ ratios seen in the precipitates generated within the biofilms of the microcosm experiments are likely to be a consequence of heterogeneity in the composition of the functional groups within the biofilm matrix.

Chemoselectivity by EPS may also directly influence $(Mg/Ca)_{calcite}$ through the incorporation of the actual metal-ligand complex into the precipitating solid. When calcite precipitates within biofilms it does so in close proximity to numerous 'strands' of EPS, it is thus possible that as precipitation continues 'strands' of EPS and their chelated ions may become entrapped within the precipitating solid. If these strands of EPS have selectively chelated Ca^{2+} over Mg^{2+} then when the precipitates are dissolved there will be an overrepresentation of calcium in the solution resulting in lower apparent $(Mg/Ca)_{calcite}$ ratios.

5.5.6 Potential impact of water channels in biofilm matrix

The existence of open cell-free water channels that penetrate all areas of a biofilm (Costerton, 1995) will permit the flow of bulk water through the internal matrix of the biofilm. This will make additional $Ca^{2+}_{(aq)}$, $Mg^{2+}_{(aq)}$ and $CO_3^{2-}_{(aq)}$ ions available for precipitation within these flow channels and potentially increase precipitation rates. However, as the bulk water of the system will have become enriched in Mg^{2+} due to the chelating activities of the EPS, then the water in the flow channels must also have a higher $(Mg/Ca)_{solution}$ than that of the water in close proximity to the EPS which is not flowing within these channels. Figure 5.33 is a schematic representation of these bulk water flow channels within the biofilm matrix. Although not shown in the diagram there will be regions within the biofilm matrix where precipitated calcite may serve as a termination point for some flow channels due to the constricting effects on the channels by the growing calcite in the surrounding regions of the biofilm matrix. Any further precipitation caused by the arrival of higher $(Mg/Ca)_{solution}$ at these calcite blockages should result in an increase in the $(Mg/Ca)_{calcite}$ at that location and a faster precipitation rate due to the increased supply of available ions.
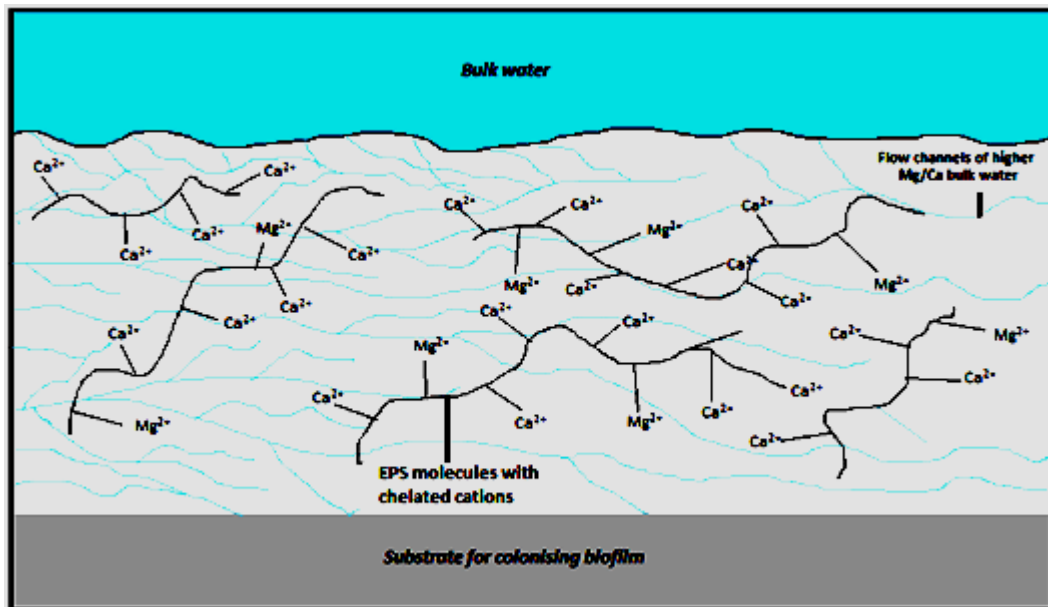
Figure 5.33 Flow channels permeate the biofilm matrix bringing in bulk water relatively enriched with Mg^{2+} cations. Where these channels meet a precipitation site the supply of additional ions may result in an increased precipitation rate. (Other ions such as CO_3^{2-} have been omitted for clarity).

The fact that the $(Mg/Ca)_{calcite}$ of the experimental precipitates decreased with increasing calcification rate indicates that the amount of higher $(Mg/Ca)_{calcite}$ generated through the presence of open water channels is not the dominating factor in determining bulk $(Mg/Ca)_{calcite}$ values from the dissolved precipitates. This may be due to the possibility that the activation energy for precipitation within these channels is higher than regions of the biofilm where low $(Mg/Ca)_{calcite}$ is being generated resulting in water channel precipitates making up a small fraction of the total calcite mass.

5.5.7 Unidentate and bidentate cation bonding to EPS

Cations may form either unidentate or bidentate bonds with anionic functional groups on the EPS molecules. Bidentate bonds form when both positive charges on the $Ca^{2+}_{(aq)}$ are linked to anionic groups, forming bidentate bridges between EPS molecules (Geesey and Yang, 1989). Such an arrangement would be an inhibiting factor to calcite precipitation as free Ca^{2+} ions have been removed from solution reducing the saturation index with respect to calcite (Kawaguchi and Decho, 2002). However, if only one of the positive charges on a $Ca^{2+}_{(aq)}$ cation is complexed with an anion (unidentate bonding) it leaves the other positive charge free to bind with a

122

CO_3^{2-} ion and initiate $CaCO_3$ precipitation by providing a nucleation site for further precipitation (Shiraishi *et al.*, 2008b, Decho, 2010). Figure 5.34 provides a schematic illustration of unidentate/bidentate bonding and how nucleation sites may develop on the free positive charge of a unidentate bonded Ca^{2+}.
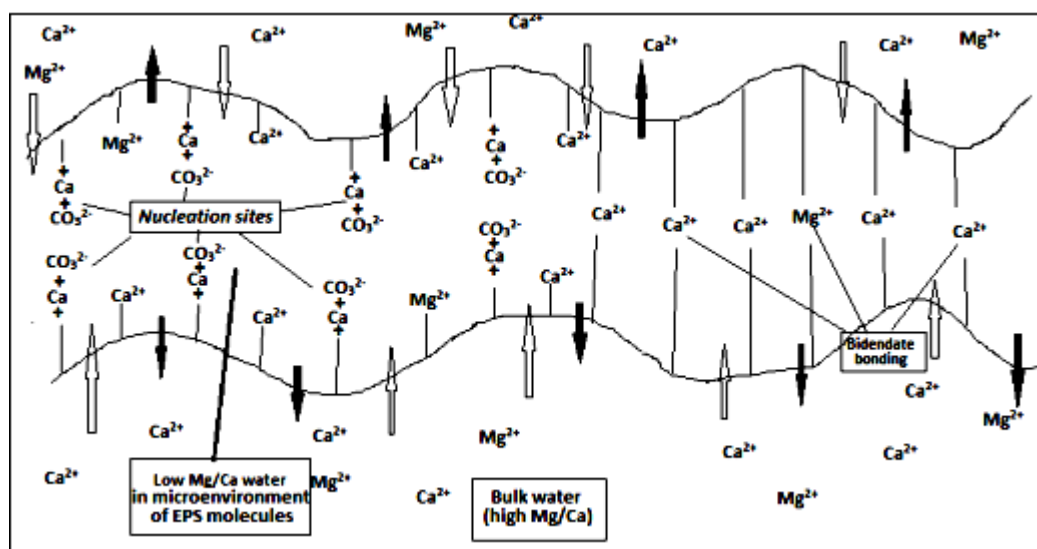
Figure 5.34 Schematic representation of unidentate and bidentate bonding of cations on anionic groups of EPS molecules. Nucleation sites are created on unidentate bonded Ca^{2+}. The large arrows represent the continuous diffusion of ionic species into and out of the microenvironment of the EPS molecules.

The chelation of ions is not a permanent state, ions will constantly move between chelation and solution. The ratio of ions in the solution in the immediate vicinity of the chelation sites will generally be determined by the binding preferences of the EPS. As Ca^{2+} is selectively favoured over Mg^{2+} by the EPS molecules then the $(Mg/Ca)_{solution}$ in this environment will be reduced relative to the bulk water. Therefore, if calcite precipitation is initiated on a unidentate bonded Ca^{2+} then the diffusive boundary layer at the nucleation site surface will be enriched with calcium ions relative to magnesium. Any precipitates forming in the immediate environment of the EPS will therefore have a $(Mg/Ca)_{calcite}$ lower than would be expected given the bulk water $(Mg/Ca)_{solution}$.

The generation of low $(Mg/Ca)_{calcite}$ within the EPS matrix will be accelerated due to the low Mg^{2+} concentrations in this microenvironment. It has been demonstrated that calcite precipitation rates are reduced in the presence of Mg^{2+} (Morse and Mackenzie, 1990, Paquette *et al.*, 1996, Zhang and Dawe, 2000) and that this

reduction is approximately proportional to the $(Mg/Ca)_{solution}$ (Morse and Mackenzie, 1990, Zhang and Dawe, 2000). Therefore the lower $(Mg/Ca)_{solution}$ in the immediate microenvironment of the EPS molecules created by the chemoselectivity for Ca^{2+} will result in a faster precipitation rate in these regions of the biofilm compared to other areas where the $(Mg/Ca)_{solution}$ is greater. This effect will become cumulative at higher precipitation rates, driving down the mean $(Mg/Ca)_{calcite}$ obtained from the biofilm as a whole.

5.6 Conclusion

A novel experimental design has allowed the precipitation of calcite in a flow through system from a solution of constant Mg/Ca ratio at varying temperatures in the presence of a natural biofilm sourced from a tufa precipitating system. They were supported by a further set of experiments in agitated flasks. Analysis of Mg/Ca ratios from calcite precipitated in the presence of biofilms at a temperature range of $12 - 20$ °C has revealed that the expected thermodynamic control on the partitioning of magnesium into calcite is overridden in these precipitates. With the exception of the 20 °C replicates for both sets of experiments there was significant variation in the $(Mg/Ca)_{calcite}$ ratios of replicates at the same temperature. This pattern held true for both the flow through microcosm and agitated flask precipitates.

A significant relationship was found between $(Mg/Ca)_{calcite}$ ratios and precipitation rate. This was found to be true for both the microcosm and agitated flask experiments. Furthermore, no difference was observed in this relationship between the biofilm exposed to photosynthetically active radiation and the biofilm which was excluded from this radiation. This would suggest that photosynthetic driven metabolic reactions and their by products are not the driving force behind the observed $(Mg/Ca)_{calcite}$ ratios.

Within the temperature range of these experiments it has been shown that the species composition of a biofilm may alter significantly. This will impact on the quantities and physical states of EPS which dominate within any one replicate. Large variations were observed in calcification rates and $(Mg/Ca)_{calcite}$ at the same temperature. It is suggested that temperature induced changes in species composition was the dominant factor in this due to the changes in EPS across the biofilm. The fact that

EPS will preferentially chelate Ca^{2+} over Mg^{2+} will result in the microenvironment around the EPS molecules being enriched in calcium over magnesium. Although bidentate bonding may be a precipitation inhibitor, Ca^{2+} ions bonded in a unidentate manner may provide nucleation sites for $CaCO_3$ precipitation by utilising their spare positive charge to bind with a CO_3^{2-} ion, effectively acting as a template for further precipitation.

Precipitation at these nucleation sites will be from a solution that has a low Mg/Ca ratio and given that Ca^{2+} will be more readily available than Mg^{2+} the Mg/Ca ratio of precipitates will become increasingly reduced at faster calcification rates. This mechanism explains the observed Mg/Ca ratios in the experimental precipitates. Although several calibrations of the Mg/Ca palaeothermometer have been constructed for foraminiferal and coralline calcite the findings here strongly suggest that the calibration of a palaeothermometer is not possible for tufa carbonates precipitated in the presence of microbial biofilms. The results presented here suggest that it is the characteristics of the EPS rather than microbial metabolism that are the major cause of the deviation from thermodynamic expectations. The following chapter will describe a set of calcite precipitation experiments in the presence of sterile EPS molecules.

6 Influence of isolated EPS molecules on (Mg/Ca)$_{calcite}$

6.1 Abstract

Microbial biofilms are believed to influence calcite morphology, precipitation rate and trace element ratios. It is uncertain though whether this is due to their metabolic processes or the presence of extracellular polymeric substances (EPS). These substances have been shown to chelate cations such as calcium and magnesium from solution in a chemoselective manner thus influencing both the saturation state and trace element composition of the bulk water. The presence of other positive ions such as Na^+ may impact on the chelation dynamics of cations such as Ca^{2+} and Mg^{2+} with a consequential impact on the trace element ratios of precipitated calcite. The experiments described here show that in the temperature range of $12 - 18$ °C (Mg/Ca)$_{calcite}$ values obtained from precipitates generated in the presence of isolated EPS are correlated with temperature in a manner which agrees with both thermodynamic expectations and previous studies on foraminiferal calcite. This is in contrast to the data obtained from living biofilms.

Salinity variations resulted in (Mg/Ca)$_{calcite}$ increasing by about 3 % per ppm increase in salinity in samples that contained EPS which is in line with previous studies on foraminiferal calcite. However, no correlation existed when EPS was absent from the solution. Experiments where EPS concentrations were varied showed that (Mg/Ca)$_{calcite}$ increased linearly in freshwater solutions with increasing EPS levels whilst precipitation rates decreased linearly with increasing EPS levels. This latter fact is attributed to blocking of active nucleation sites on the solid surface through the adsorption of EPS molecules to the growing crystal. These studies have shown that isolated EPS can have a significant impact on both calcite trace element ratios and precipitation rates. The results suggest that it is the metabolic processes of biofilms that cause the breakdown of the thermodynamic control on (Mg/Ca)$_{calcite}$ in freshwater carbonates and not the presence of EPS and that the presence of increasing concentrations of organic molecules such as EPS is generally inhibitive to calcite precipitation.

6.2 Introduction

This chapter describes the results of three different experiments which were conducted using EPS molecules in isolation from the cells that created them.. The first experiments described were conducted in agitated conical flasks at a temperature range of 12 – 20 °C, the other experiments described were conducted in static Petri dishes under an ambient laboratory temperature of 16 °C and introduced salinity variations and EPS concentration variations.

The precipitation of calcite in karstic streams generally occurs in the presence of microbial biofilms. It is well accepted that microorganisms have some influence on calcite precipitation through varying mechanisms such as metabolic processes (Merz-Preiβ and Riding, 1999, Bissett *et al*., 2008, Shiraishi *et al*, 2010) and acting as nucleation sites to enhance precipitation rates (Bosak and Newman, 2003). The specific role of EPS in calcite precipitation is becoming more recognised, and given that EPS generally accounts for between 50 and 90% of the total organic matter of a biofilm (Wingender *et al*., 1999) an understanding of its role is a crucial step in the quest to discovering the full role of biofilms in calcite precipitation. Of particular importance for tufa $(Mg/Ca)_{calcite}$ palaeothermometry is the ability of EPS to chelate cations in a chemoselective manner. This behaviour has been confirmed in biofilm colonised experimental flumes analogous to tufa precipitating streams (Rogerson *et al*., 2008) and suggests that the presence of EPS may significantly impact on trace element ratios of calcite precipitated in the immediate microenvironment of the EPS. This influence cannot exist however, unless precipitation actually occurs within the microenvironment of the EPS.

Although it has been reported that the chelation of Ca^{2+} ions to EPS is initially an inhibiting factor in carbonate mineral precipitation in seawater, *in vitro* experiments have shown this may not be the case in a freshwater setting (Rogerson *et al*., 2008 and Pedley *et al*., 2009). It has been suggested that the presence of anionic functional groups on EPS molecules may also help initiate calcite precipitation through the unidentate bonding of Ca^{2+} to the anionic groups (Decho, 2010). Furthermore, the binding of Ca^{2+} to EPS molecules can reduce the activation energy barrier which

usually limits spontaneous precipitation (Dittrich and Sibbler, 2010) indicating that the presence of EPS may result in greater precipitation rates.

The ability of isolated EPS molecules to precipitate calcite in the absence of the microbial processes of the associated organisms has been observed experimentally (Kawaguchi and Decho, 2002, Ercole *et al*., 2007, Tourney and Ngwenya, 2009, Dittrich and Sibler 2010). However, no studies to date appear to have examined whether cation chelation by EPS molecules actually causes deviations in trace element ratios from thermodynamic expectations. The experiments described here provide a first insight into the direct impact of isolated EPS on both precipitation rate and trace element ratios in calcite precipitated in a freshwater environment.

In addition to the freshwater experiments an investigation was carried out that examined the impact of EPS on calcite precipitation rate and trace element ratios in waters of varying salinities. In a freshwater setting there will be little competition between Ca^{2+} ions and other positive ions for chelation sites, therefore the number of potential nucleation sites on EPS molecules should be greater than in sea water. Consequently, increasing salinities would be expected to result in a decreasing calcite precipitation rate. The presence of $Na^+_{(aq)}$ (and other positive ions) in saline precipitating solutions has the potential to impact on $(Mg/Ca)_{calcite}$ values by interfering with the chelation dynamics of Ca^{2+} and Mg^{2+} by occupying binding sites otherwise available to Ca^{2+} and Mg^{2+}.

Although there appear to be no studies that have investigated the influence of salinity variations in the presence of biofilms or isolated EPS, several studies have examined it in foraminiferal calcite. The earliest studies (Chave, 1954 and Savin and Douglas, 1973) concluded that salinity variations had no impact on the calcite of foraminiferal tests. More recent studies have shown $(Mg/Ca)_{calcite}$ increases by about 4 ± 3 % per ppm (Nurnberg *et al*., 1996, Lea *et al*., 1999, Kisakurek *et al*., 2008, Duenas-Bohorquez *et al*., 2009, Dissard *et al*., 2010). A stronger correlation where $(Mg/Ca)_{calcite}$ increases by about 15 - 59 % per PSU was reported by Ferguson *et al*., (2008), they also observed that salinity had a greater influence on the $(Mg/Ca)_{calcite}$ of

foraminiferal tests than temperature. To determine whether this influence is driven solely by salinity variations or by the response of the organic molecules to these variations experiments were conducted where calcite is precipitated both the presence and absence of EPS molecules at varying salinities.

The overall combined aims of the experimental runs described in this chapter are:

- To determine whether the absence of the expected thermodynamic control on Mg^{2+} partitioning in the experiments detailed in chapter 5 was caused by microbial metabolism or whether it was simply the presence of EPS.
- To ascertain the impact of varying EPS levels on $(Mg/Ca)_{calcite}$ and precipitation rate.
- To examine the influence of salinity variations on $(Mg/Ca)_{calcite}$ and precipitation rate both in the presence and absence of EPS.

6.3 Methods

The generic methods such as EPS extraction and ICP-OES analyses of the samples are described in full in chapter 3. The methodology behind the agitated experiments is detailed in chapter 4.

6.4 Results

6.4.1 Agitated flasks

The data in this section is derived from the calcite precipitated in the presence of isolated EPS molecules in agitated conical flasks. Figure 6.1 shows the $(Mg/Ca)_{calcite}$ ratios plotted against the precipitation temperature. (Error bars on all graphs represent 1σ values.) Apart from the 20 °C data, $(Mg/Ca)_{calcite}$ increases as temperature increases. At 20 °C the $(Mg/Ca)_{calcite}$ is lower for both replicates than for all other experimental temperatures. There is no significant relationship at the 95 % confidence level when all data points are included, however, exclusion of the 20 °C data provides a significant exponential relationship where $(Mg/Ca)_{calcite} = 0.003exp^{0.31(T\,°C)}$ ($R^2 = 0.85$, $P < 0.05$, $n = 8$).
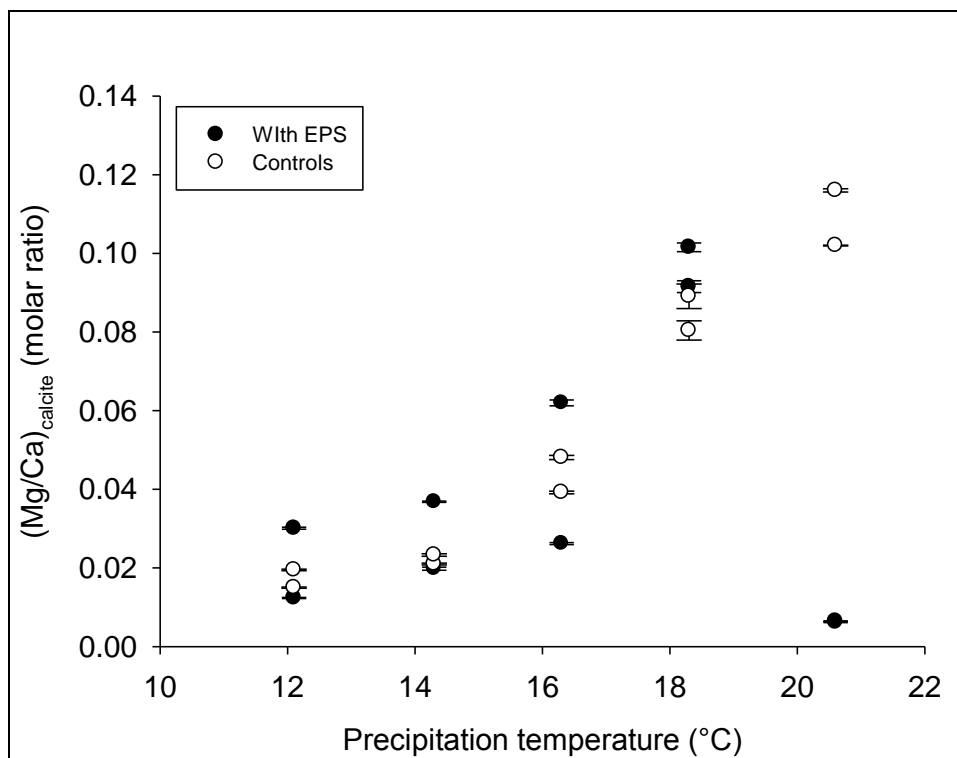
Figure 6.1 (Mg/Ca)_{calcite} as a function of temperature for calcite precipitated in the presence of isolated EPS.

The dependence of precipitation rate (R) on temperature is shown in Figure 6.2. There is no significant relationship when all data points are included but examination of the plots shows that, with the exception of the 20 °C data there is a decreasing precipitation rate as temperature increases. Excluding the 20 °C data Figure 6.2 reveals a significant linear relationship for the data in the temperature range of 12 – 18 °C where $R = 0.0060 – (0.00028*T(°C))$, ($R^2 = 0.67$, $P < 0.05$, n = 8).
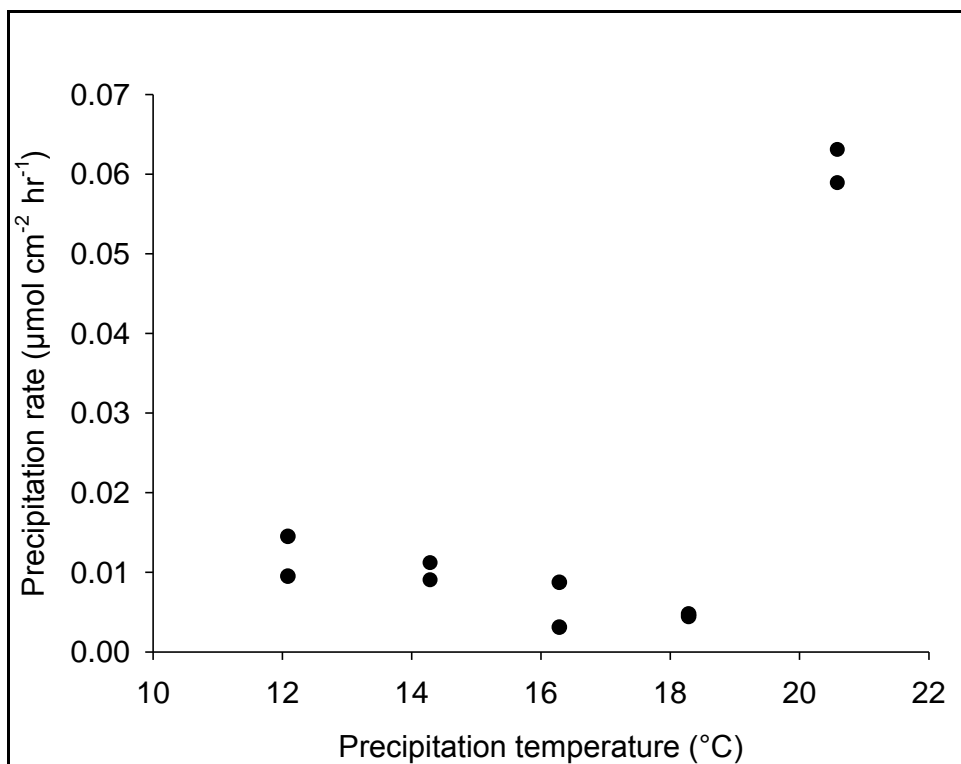
Figure 6.2 Precipitation rate against temperature for calcite precipitated in the presence of isolated EPS.

Figure 6.3 shows $(Mg/Ca)_{calcite}$ ratios plotted against the precipitation rate. As with the data shown in Figures 6.1 and 6.2 the plots at 20 °C are distinctly clear from the others however, in this case they do follow the relationship observed with the plots at 12 – 18 °C. There is a significant relationship where $(Mg/Ca)_{calcite} = 0.0002T(°C)^{-0.8285}$ ($R^2 = 0.68$, $P < 0.05$, $n = 10$).
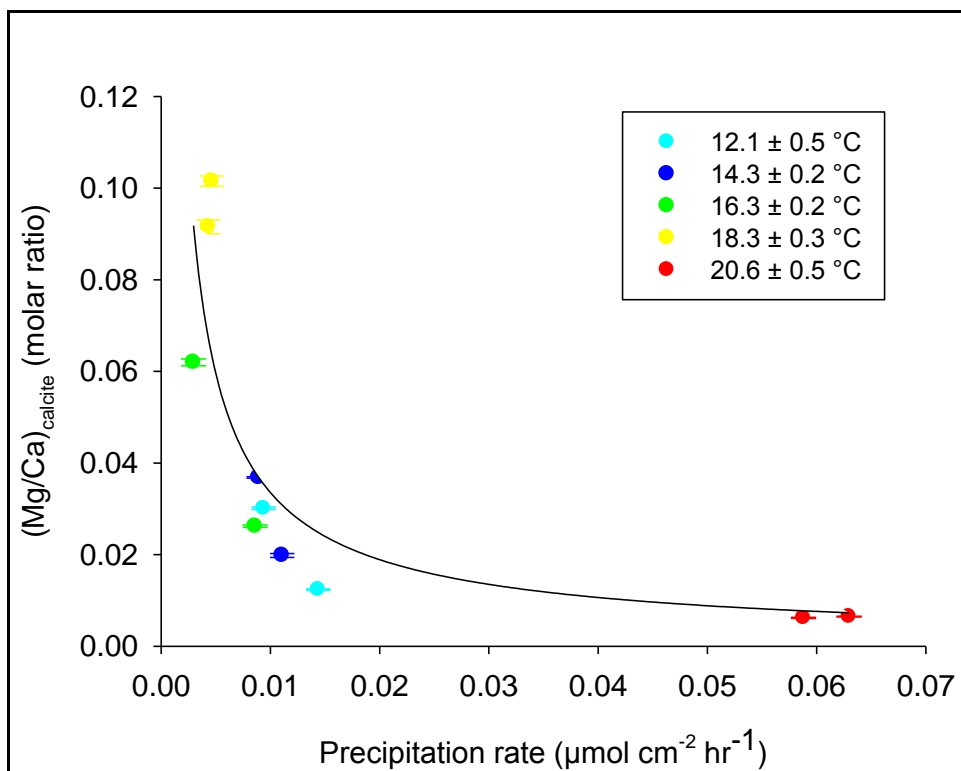
Figure 6.3 (Mg/Ca)$_{calcite}$ as a function of precipitation rate for calcite precipitated in the presence of isolated EPS (key = mean experimental temperature with 1σ values).

The nature of the relationship observed in Figure 6.3 is the same as that observed for the precipitates generated in the presence of a living biofilm (Figure 5.27).

6.4.2 Calcite precipitation with and without EPS at varying salinities

This section describes the results obtained by precipitating calcite at varying salinity levels from 0 to 40 ppm both in the presence and absence of isolated EPS. Figure 6.4 shows the (Mg/Ca)$_{calcite}$ against precipitation rate for precipitates in the absence of EPS. There is no correlation at the 95 % confidence level between precipitation rate and (Mg/Ca)$_{calcite}$ at varying salinity levels. The replicates with zero salinity plot well away from those with varying salinity levels. Apart from one plot at 30 ppm the data are well grouped.
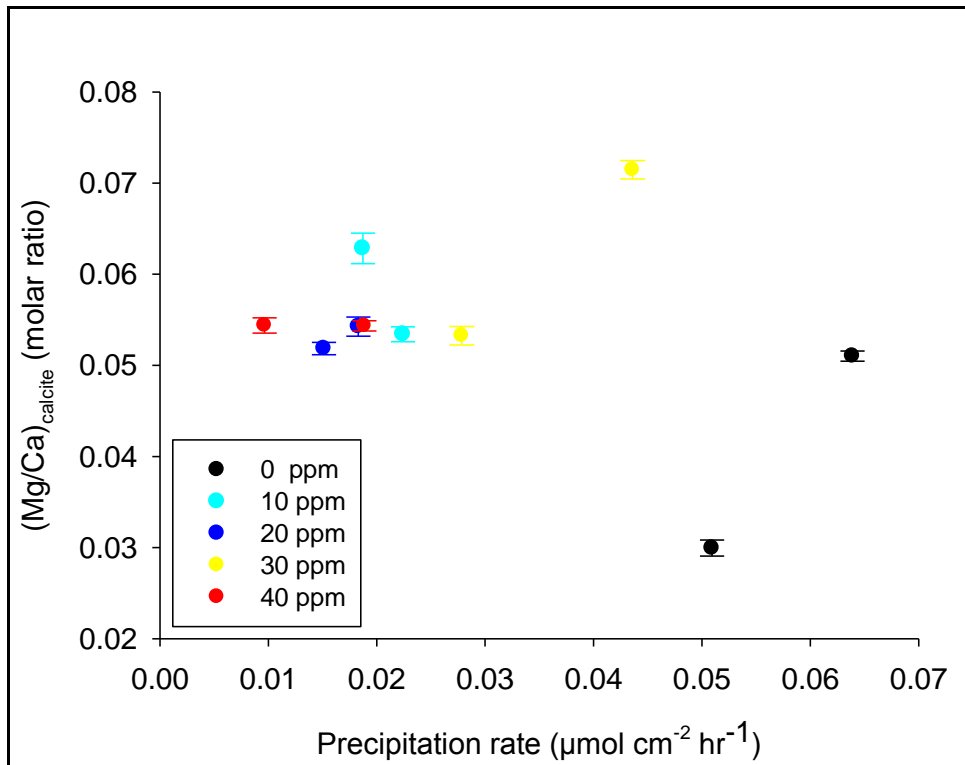
Figure 6.4 (Mg/Ca)$_{calcite}$ as a function of precipitation rate at varying salinities with no EPS in the solution (key = salinity level).

However, when EPS molecules are added to the precipitating solution there is a significant correlation between (Mg/Ca)$_{calcite}$ and precipitation rate (Figure 6.5) where (Mg/Ca)$_{calcite}$ = $0.008(R)^{-0.5141}$ (R^2 = 0.77, P < 0.05, n = 10).
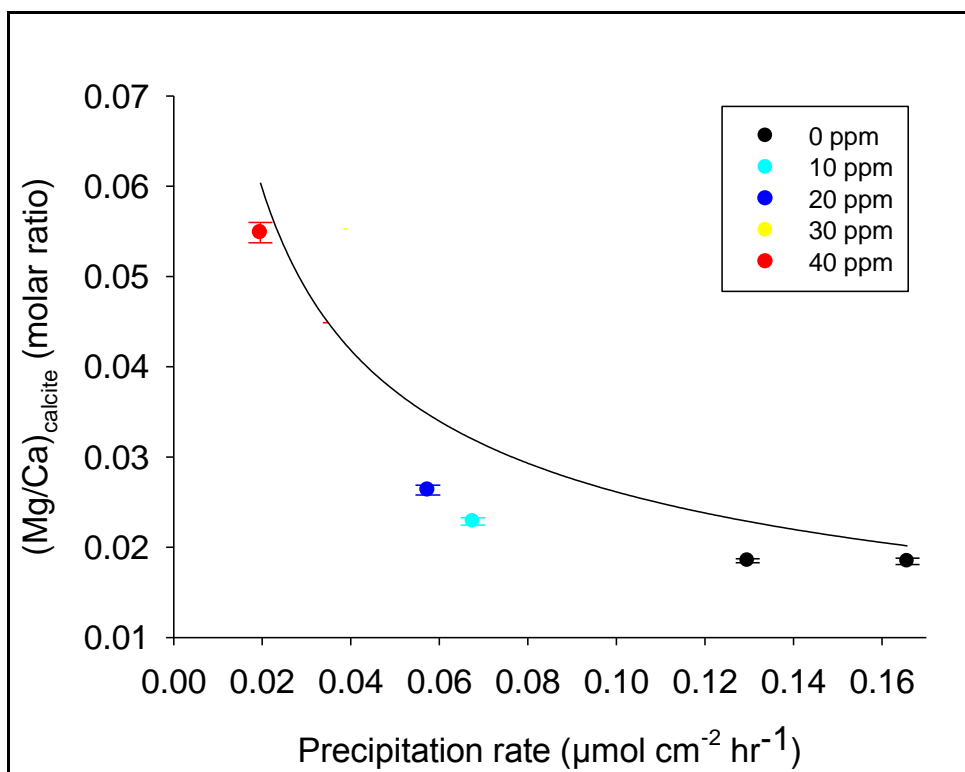
Figure 6.5 (Mg/Ca)$_{calcite}$ as a function of precipitation rate at varying salinities with EPS in the solution (key = salinity level).

Plots of $(Mg/Ca)_{calcite}$ as a function of salinity levels both with and without EPS are shown in Figures 6.6 and 6.7 respectively.
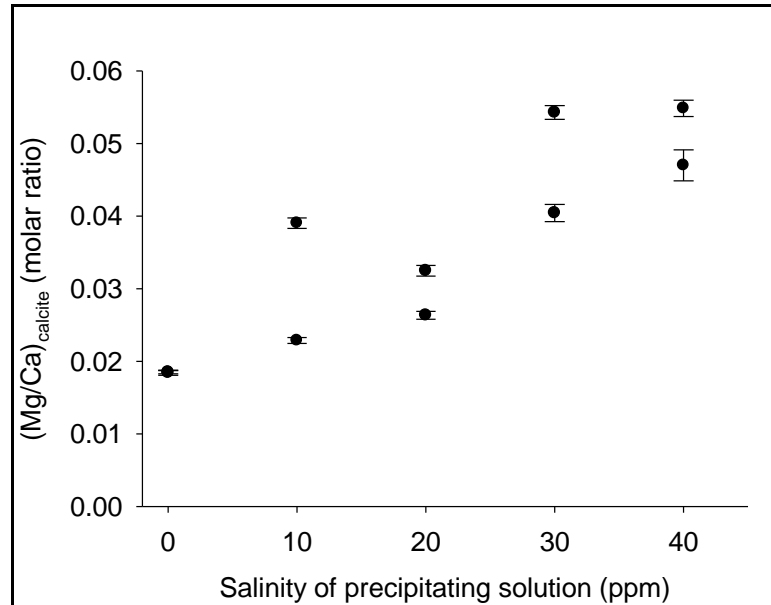
Figure 6.6 $(Mg/Ca)_{calcite}$ as a function of salinity with EPS in the solution.
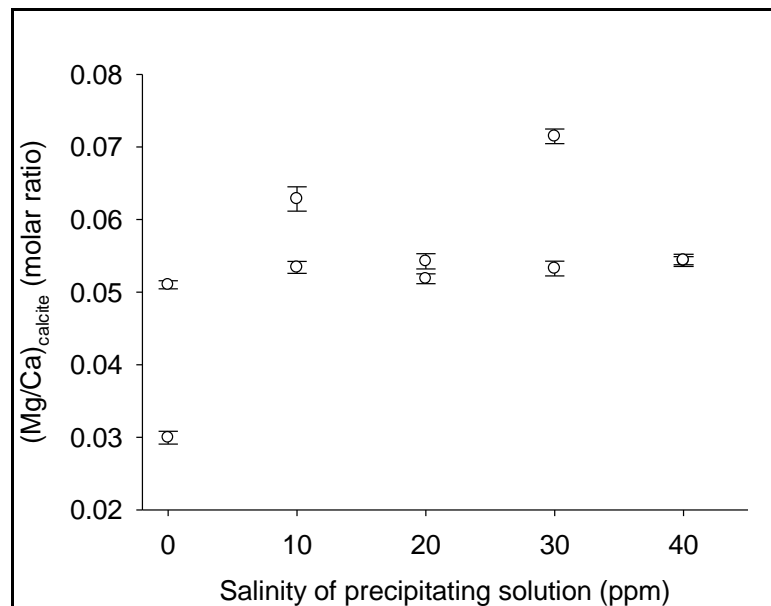
Figure 6.7 $(Mg/Ca)_{calcite}$ as a function of salinity without EPS in the solution.

In the absence of EPS there is no significant correlation between salinity and $(Mg/Ca)_{calcite}$ (P = 0.18). When isolated EPS is present in the precipitating solution there is a strong linear correlation where $(Mg/Ca)_{calcite} = 0.0192 + (0.000813(S))$, where S = salinity (ppm) ($R^2 = 0.78$, P < 0.05, n = 10).

When precipitation rate (R) was examined as a function of salinity there was a significant linear correlation in the replicates with EPS added to the precipitating solution where $R = 0.0263 - (0.00541(S)$, $R^2 = 0.67$, $P < 0.05$, n = 10 (Figure 6.8). In the absence of EPS there was no correlation at the 95 % confidence level (P = 0.069) (Figure 6.9).
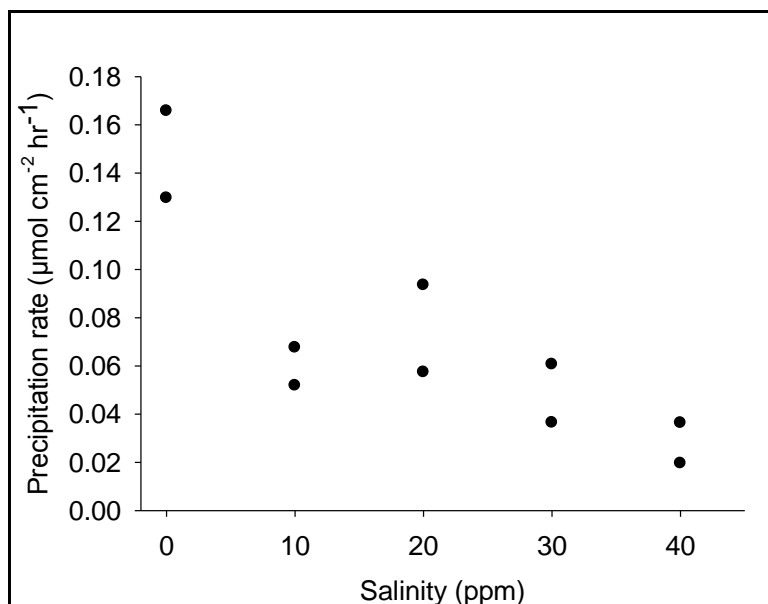
Figure 6.8 Precipitation rate against salinity in the presence of isolated EPS molecules.
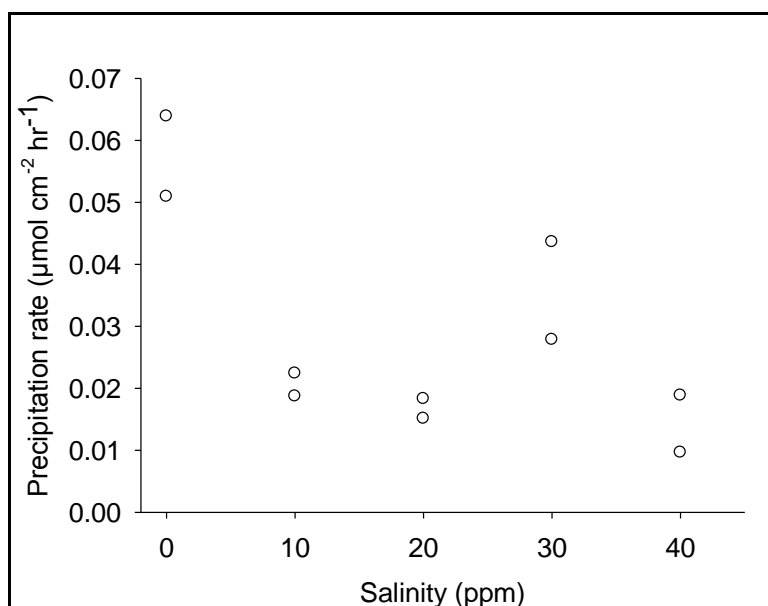
Figure 6.9 Precipitation rate against salinity in the absence of isolated EPS molecules.

Although there is no statistical correlation for the data without EPS it is still evident that the presence of any amount of salinity in the experimental range of 10 – 40 ppm resulted in a lower precipitation rate than the freshwater replicates. Figure 6.10

135

combines the data from Figures 6.8 and 6.9. Precipitation rates are generally higher in the replicates with EPS, particularly in the freshwater replicates. The mean precipitation rate for freshwater replicates with and without EPS is 0.15 and 0.057 $\mu mol\ cm^{-2}\ hr^{-1}$ respectively. The mean precipitation rate for all replicates in the salinity range 10 – 40 ppm with and without EPS is 0.053 and 0.022 $\mu mol\ cm^{-2}\ hr^{-1}$ respectively. Combining all fresh and saline replicates with and without EPS gave mean precipitation rates of 0.072 and 0.029 $\mu mol\ cm^{-2}\ hr^{-1}$ respectively.
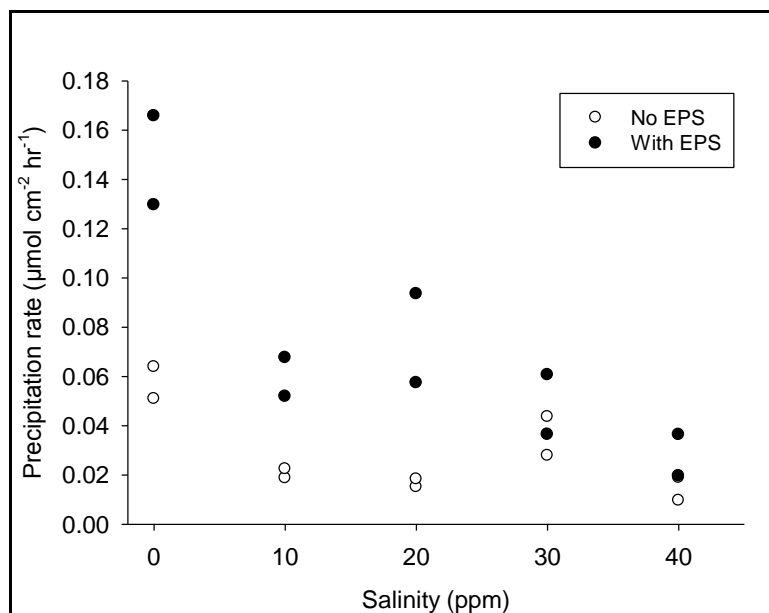
Figure 6.10 Combined plots of precipitation as a function of precipitation rate for calcite precipitated in the presence and absence of isolated EPS molecules.

6.4.3 Calcite precipitation under varying EPS levels

The impact of varying amounts of EPS in the precipitating solution on $(Mg/Ca)_{calcite}$ ratios is shown in Figure 6.11. There is a significant linear correlation ($R^2 = 0.53$, P < 0.05, n = 23) where $(Mg/Ca)_{calcite}$ increases with increasing levels of EPS in the precipitating solution. Analysis of precipitation rate as a function of EPS concentration also reveals a significant linear relationship ($R^2 = 0.64$, P < 0.05, n = 23) where the rate decreases with increasing levels of EPS in the precipitating solution (Figure 6.12).
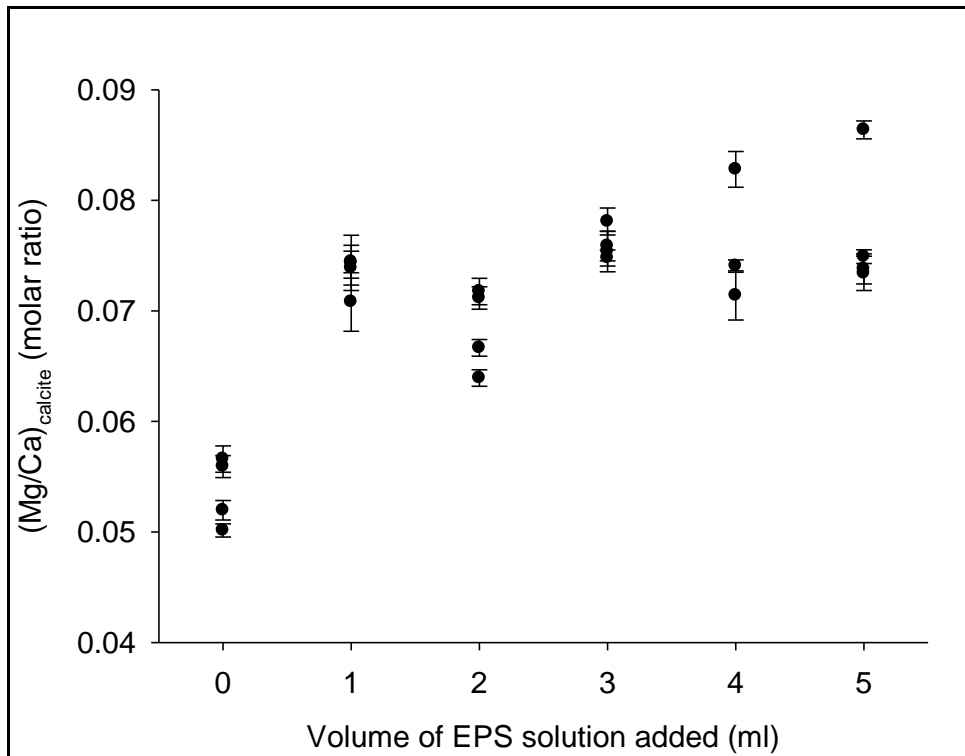
Figure 6.11 (Mg/Ca)$_{calcite}$ as a function of the quantity of isolated EPS molecules in the precipitating solution.
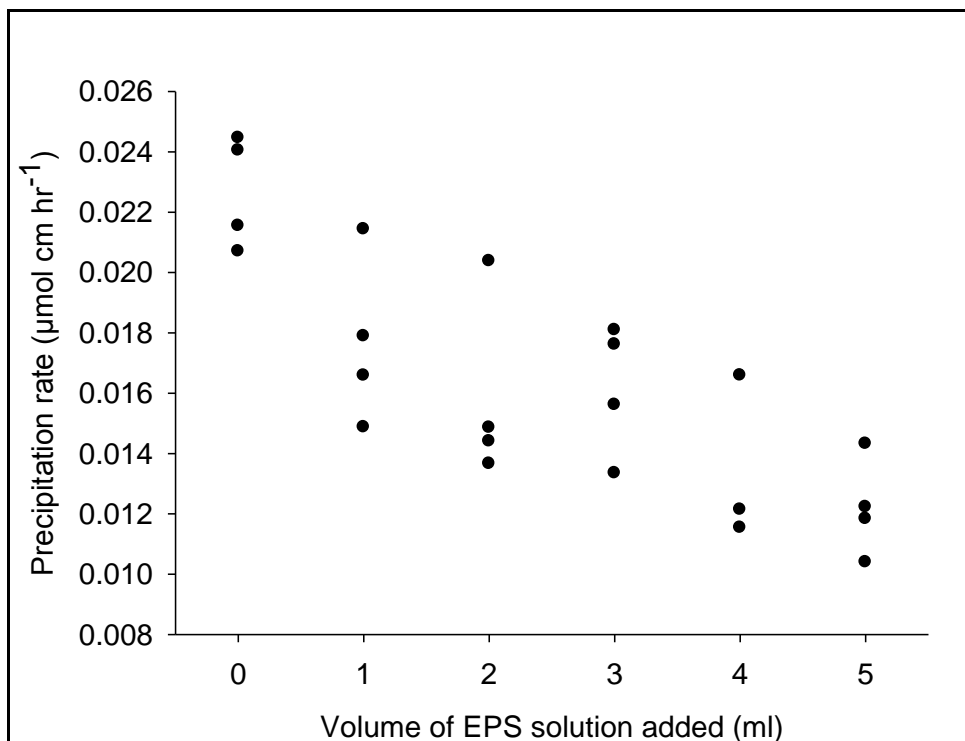
Figure 6.12 Precipitation rate as a function of the quantity of isolated EPS molecules in the precipitating solution.

The relationship between precipitation rate and (Mg/Ca)$_{calcite}$ is shown in Figure 6.13. The negative power relationship observed in the precipitates from the microcosm, agitated flask biofilms and isolated EPS (of a constant concentration) is not seen

when the EPS level is varied in the precipitating solution. Although no significant relationship was found between precipitation rate and $(Mg/Ca)_{calcite}$ at the 95 % confidence level, there was a notable separation of the data with EPS and the precipitates from the replicates with no added EPS.
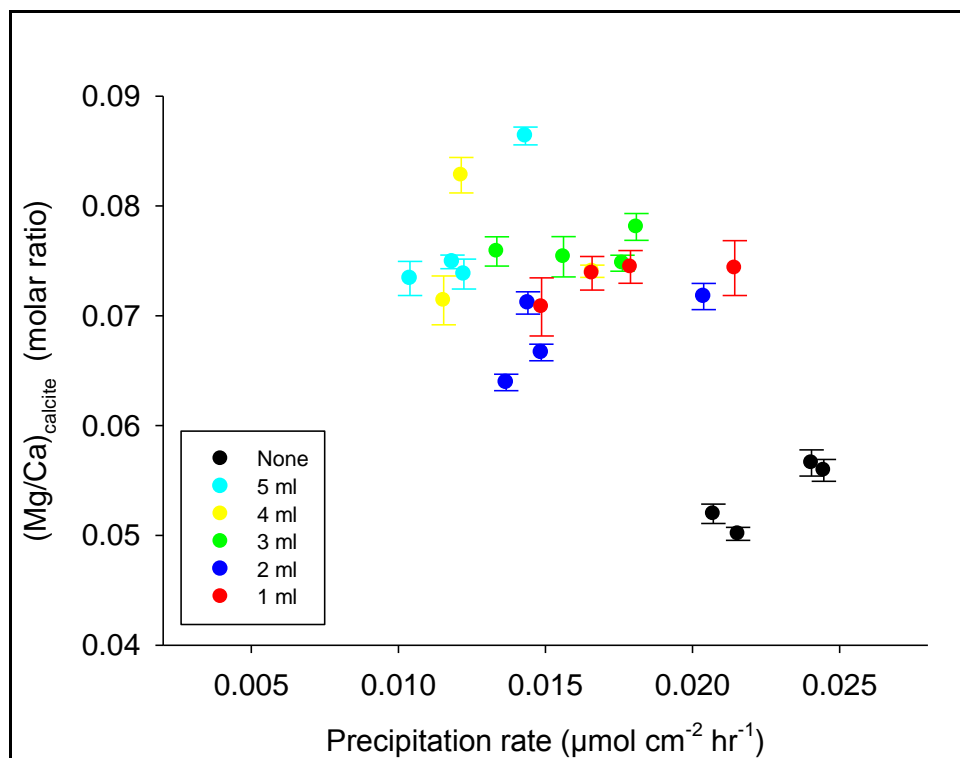
Figure 6.13 $(Mg/Ca)_{calcite}$ against precipitation rate for precipitates generated under varying levels of isolated EPS molecules in the solution.

6.5 Discussion

6.5.1 Temperature and $(Mg/Ca)_{calcite}$: agitated flasks

Although there was no significant correlation between temperature and $(Mg/Ca)_{calcite}$ precipitated in a solution containing isolated EPS molecules, there did appear to be two distinct behaviours. In the temperature range of 12 – 18 °C there was a significant correlation (R^2 = 0.85, P < 0.05) where $(Mg/Ca)_{calcite}$ increased exponentially, whilst at 20 °C $(Mg/Ca)_{calcite}$ values had decreased to less than those seen at 12 °C. For the data in the temperature range of 12 – 18 °C the relationship is described by equation 6.1

$$(Mg/Ca)_{calcite} = 0.003(\pm 0.004)exp^{0.31(\pm 0.066)(T°C)} \qquad (6.1)$$

The form of this relationship matches the general thermodynamic expectation and is similar to the correlations observed in investigations on foraminiferal $(Mg/Ca)_{calcite}$, although the pre exponential constant in the foraminiferal calcite is over an order of magnitude greater (Table 6.1).

Table 6.1 Summary of calibration constants for single and mixed species planktonic foraminifera (adapted from Barker *et al*, 2005)

Species	Pre exponential	Exponential	Reference
N. pachyderma	0.088	0.46	Nurnberg *et al*., 1995
G.succulifer	0.09	0.37	Dekens *et al*., 2002
G.succulifer	0.089 (± 0.008)	0.39 (± 0.06)	Nurnberg *et al*., 1996
G.succulifer	0.090	0.35 (± 0.001)	Anand *et al*., 2003
G. bulloides	0.102 (± 0.008)	0.53 (± 0.17)	Lea *et al*., 1999
G. bulloides	0.107 (± 0.003)	0.47 (± 0.03)	Mashiota *et al*., 1999
G. ruber	0.089 (± 0.007)	0.30 (± 0.06)	Lea *et al*., 2000
G. ruber	0.09	0.38	Dekens *et al*., 2002
G. ruber	0.102 (± 0.01)	0.34 (± 0.08)	Anand *et al*, 2003
Mixed	0.10	0.52	Elderfield and Gannsen, 2000
Mixed	0.09 (± 0.003)	0.38 (± 0.02)	Anand *et al*, 2003

Comparison of the $(Mg/Ca)_{calcite}$ as a function of temperature between the biofilm experiments in chapter 5 and the isolated EPS data (Figure 6.14) shows that at 12 to 18 °C the $(Mg/Ca)_{calcite}$ of the biofilm precipitates has no significant correlation with temperature (P = 0.16) in contrast to the significant exponential correlation seen in the isolated EPS precipitates.
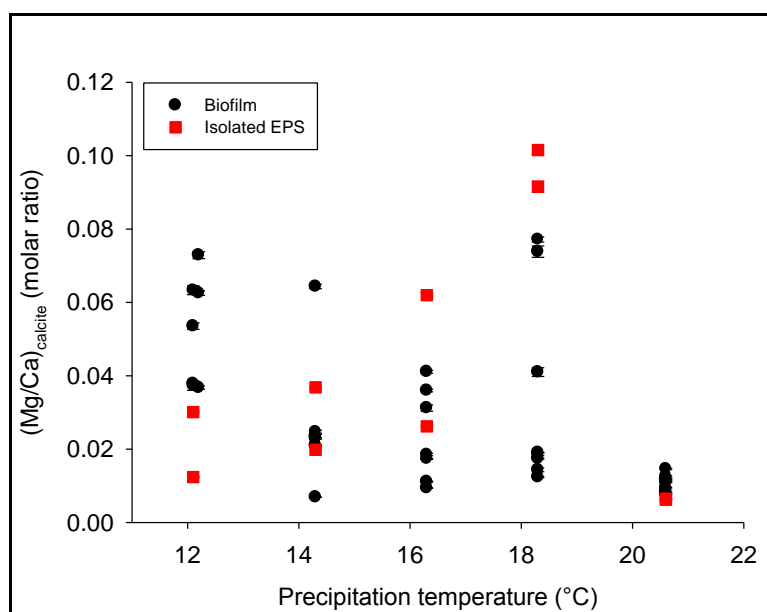
Figure 6.14 Comparison of biofilm and isolated EPS data for $(Mg/Ca)_{calcite}$ as a function of precipitation temperature.

This provides clear evidence that it is microbial metabolic processes are the dominant factor in overriding the thermodynamic control on Mg^{2+} incorporation into calcite and not simply the presence of EPS molecules. The deviation of the 20 °C data from the relationship expressed in Equation 6.1 suggests that there is either a stronger secondary control on the $(Mg/Ca)_{calcite}$ at this temperature or that the data is errant. Given that the data at 20 °C from the EPS experiments matches that from the biofilm experiments it is unlikely that the data are errant. All data at 20 °C are well constrained regardless of the experimental conditions which is in complete contrast to the data at 12 – 18 °C. Therefore, somewhere between 18 and 20 °C there is likely to be a threshold whereby $(Mg/Ca)_{calcite}$ in biofilm and isolated EPS experiments is tightly controlled by some dominant factor such as precipitation rate.

In the temperature range of 12 – 18 °C the expected thermodynamic relationship between $(Mg/Ca)_{calcite}$ and precipitation temperature exists in calcite precipitated in the presence of isolated EPS molecules. In the same temperature range this relationship is not observed in calcite precipitated in the presence of a living biofilm. It is therefore concluded that it is the metabolic activities of the organisms within the biofilm that mask the expected thermodynamic correlation between $(Mg/Ca)_{calcite}$ and precipitation temperature, not the presence of the EPS.

6.5.2 Influence of EPS on precipitation rate

In the agitated flask experiments the presence of the EPS has generated a small linear decrease in precipitation rate for temperatures in the range of 12 – 18 °C which is in contrast to the expected increase in rates at higher temperatures. These findings indicate that in this temperature range the presence of isolated EPS molecules inhibits the expected temperature control on precipitation rates. The inhibition of precipitation by EPS molecules has been reported in marine environments (Reid *et al*., 2000, Kawaguchi and Decho, 2002) however, in freshwater settings analogous to the experiments described here it has been suggested that EPS acts as an enhancer of calcite precipitation (Rogerson *et al*., 2008). At 20 °C the slight falling trend is sharply reversed so that there is about a 13 fold increase, indicating that at 20 °C the possible inhibiting effects of the EPS molecules are overridden by temperature driven increases in the kinetic energy of the ionic species. The sharp nature of the

deviation at 20 °C from the data at 12 – 18 °C matches that seen in the relationship between $(Mg/Ca)_{calcite}$ and temperature, further strengthening the suggestion that between 18 and 20 °C there is a threshold whereby temperature becomes the dominant control on calcite precipitation in the presence of EPS. Examination of the current literature reveals nothing to suggest a breakdown of the EPS molecules at this temperature.

In the experiments where EPS levels varied between replicates, precipitation rates decreased linearly as EPS levels increased. This was unexpected given that EPS molecules have been suggested as acting as nucleation templates whereby the activation energy barrier to precipitation is decreased (Dittrich and Sibbler, 2010). Some constituents of EPS molecules such as aspartic, glutamic and uronic acids have been shown to be inhibitors of calcite precipitation (Kawaguchi and Decho, 2002, Gautret and Trichet, 2005). The ability of EPS to chelate divalent cations from solution has led it to being described as a Ca^{2+} buffer whose capacity needs to be fully utilised before calcite nucleation can commence (Arp *et al.*, 1999) therefore at higher levels of EPS, precipitation rates would be reduced. However, the process of nucleation on unidentate bound Ca^{2+} suggests that nucleation can take place prior to the buffering capacity of the EPS being exhausted, but it may be that the precipitation rate generated through the nucleation sites created by unidentate Ca^{2+} binding is slow until the supply of fresh $Ca^{2+}_{(aq)}$ ions exceeds the buffering capacity.

Until all binding sites are occupied there will be competition between chelation and nucleation sites for $Ca^{2+}_{(aq)}$ ions which will reduce calcification rates. When all binding sites are occupied the remaining $Ca^{2+}_{(aq)}$ ions are free to begin calcification at nucleation sites. The loss of $Ca^{2+}_{(aq)}$ to chelation will cause a reduction in the saturation state with respect to calcite and therefore be expected to reduce precipitation rates (Hoch *et al.*, 2000), this effect should be accentuated at greater concentrations of EPS. However, the complexing of Ca^{2+} ions to carboxyl groups has been shown to have a minimal impact on precipitation kinetics (Inskeep and Bloom, 1986, Hoch *et al.*, 2000).

The presence of organic molecules in a precipitating solution has been recognised for some time as being inhibitive to calcite precipitation through their adsorption to the growing crystal and consequent blocking of nucleation sites (Chave, 1970). The extent to which precipitation rates are reduced appears to be dependent on the nature of the organic molecules present. Factors such as molecular size, hydrophobicity and functionality have been related to the inhibition of calcite precipitation (Hoch *et al*., 2000). Functional groups with higher molecular weights have been found to be stronger inhibitors of calcite precipitation than those with lower molecular weights (Lin *et al*., 2005). The variation in precipitation rates caused by different organic molecules is shown in Figure 6.15 where SRFA and PFA are fulvic acid anionic functional groups and WLHPOA a hydrophobic organic acid. The relative reduction rates in (d-f) are represented by the ratio (R_i/R_o) where R_o is the precipitation rate in the absence of organics and R_i the rate in the presence of organics (Lin *et al*., 2005). The pattern of decreasing precipitation rate with increasing functional groups in Figure 6.15 is very similar to that seen in the experiments described here where EPS concentrations in the precipitating solution were varied between replicates (Figure 6.12).
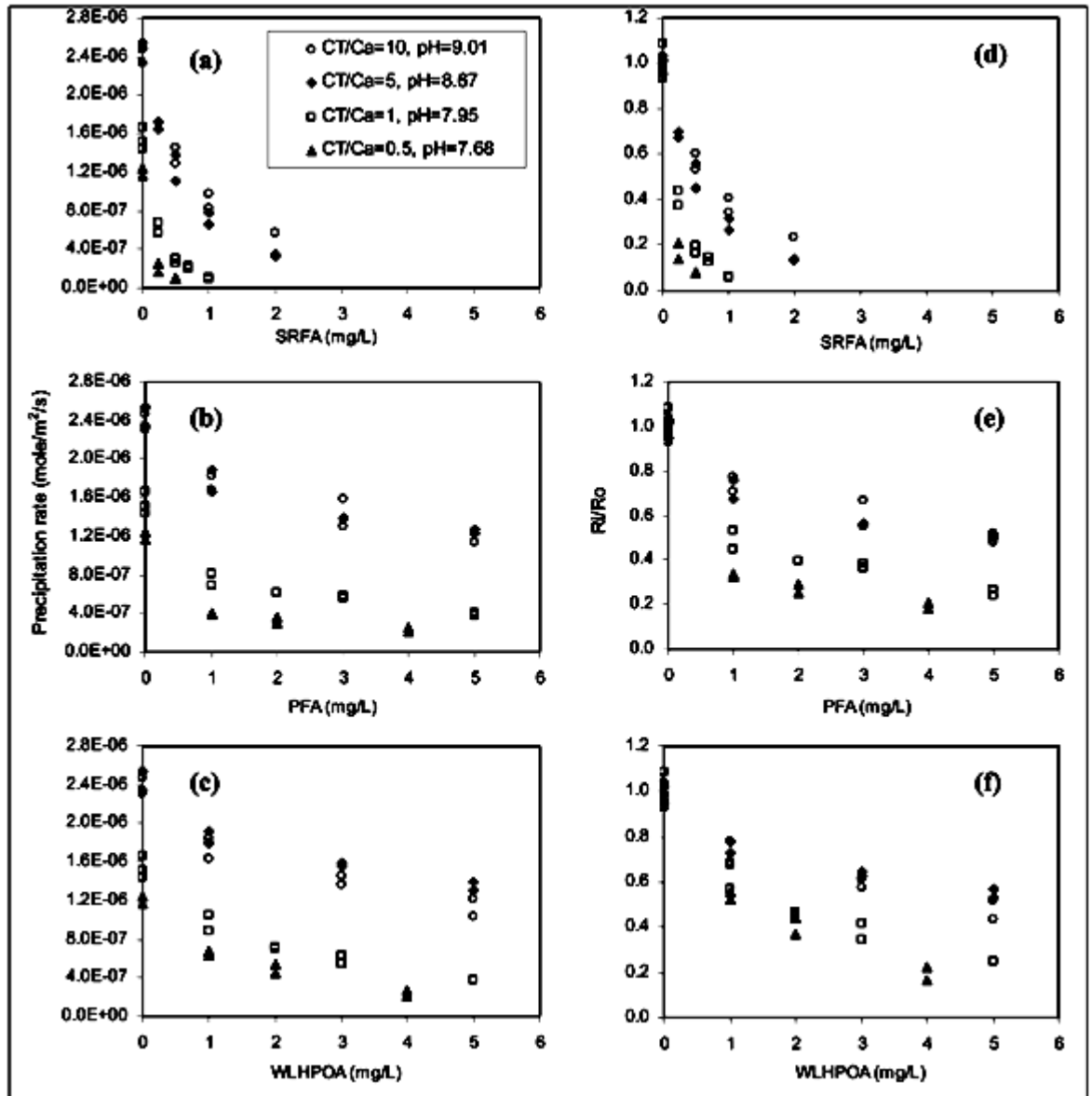
Figure 6.15 Inhibition of calcite precipitation as a function of natural organic matter at varying pH and inorganic carbon to calcium ratios (CT/Ca): (a) SFRA, (b) POFA, (c) WLHPOA, (d-f) are the relative rate reductions (Lin *et al*, 2005).

The adsorption of organic ligands onto various mineral surfaces, including calcite, has been suggested to follow Langmuir adsorption theory (Lebron and Suarez, 1996, Lin *et al*., 2005). Relating the adsorption of functional groups of natural organic matter (NOM) to the crystal surface and its inhibiting effect on precipitation rates is described by equation 6.2 (Lin *et al*., 2005):

$$> S^- + NOM => S^- \; K_{cond} = K_{cond} \frac{[> S^- - NOM]}{[> S^-][NOM]} \qquad (6.2)$$

where $> S^-$ represents the available active crystal growth sites on the crystal surface, $> S^- - NOM$ are the sites at which NOM is adsorbed and K_{cond} is a conditional equilibrium constant. In the presence of NOM the concentration of available active crystal growth sites ($[> S^-]_T$) is represented through (Lin *et al.*, 2005):

$$> S^- = \frac{[> S^-]_T}{1 + K_{cond}[NOM]} \qquad (6.3)$$

If the precipitation rate is proportional to the number of active sites available on the calcite surface then the precipitation rates in the absence (R_o) and presence (R_i) of NOM are proportional to $[> S^-]_T$ and $> S^-$ respectively so:

$$R_o \propto [> S^-]_T \qquad (6.4)$$

$$R_i \propto > S^- = \frac{[> S^-]_T}{1 + K_{cond}[NOM]} \qquad (6.5)$$

Therefore the normalised change in the precipitation rate of calcite as a function of varying concentrations of functional groups is expressed by (Lin *et al.*, 2005):

$$\frac{R_o - R_i}{R_i} = K_{cond}[NOM] \qquad (6.6)$$

The linear slope derived from the experiments described here where EPS concentrations were varied (Figure 6.12) which represents falling precipitation rates with increasing amounts of EPS in the solution supports a Langmuir adsorption model of functional group adsorption onto the growing crystal surface and inhibiting precipitation by blocking active precipitation sites (Lin *et al.*, 2005). This offers a plausible explanation for the falling precipitation rates seen when EPS concentrations in the precipitating solution increased.

The variations seen in the precipitation rates at a given level of EPS in the precipitating solution (Figure 6.12) may be explained by differences in the abundances of different functional groups within the EPS of individual replicates as

the individual characteristics of functional groups can affect their inhibitory ability (Lin *et al*., 2005). Thermodynamic data has shown that the Gibbs free energy of adsorption differs between functional groups (Lin *et al*., 2005), therefore the degree to which functional groups will adsorb to the crystal surface and block active nucleation sites will be determined by the relative amounts of individual functional groups and their values of Gibbs free energy of adsorption.

6.5.3 Effect of salinity on calcite precipitation rate

The observation that salinity variations in the replicates without EPS had no correlation with precipitation rate agrees with previous studies that show the kinetics of calcite precipitation has little or no correlation with salinity levels (Kazmierczak *et al*., 1982, Walter, 1986, Zhong and Mucci, 1989). Although there was no correlation in the salinity range of $10 - 40$ ppm the mean precipitation rate across this salinity range was about 2.6 fold lower than that of the freshwater replicates. This is attributed to the higher ionic strengths of the solutions at greater salinities. The presence of multiple other ions reduces the probability of collisions between Ca^{2+} and CO_3^{2-} ions and hence the formation of $CaCO_3$ complexes on which precipitation can further take place.

When EPS was present the precipitation rate was significantly correlated with salinity levels, falling linearly as salinity increased. In the salinity range of $10 - 40$ ppm the mean rate was lower than for the freshwater replicates by a factor of about 2.9 which is similar to the factor of 2.6 observed when EPS was absent. Although increasing salinity reduced precipitation rates in the EPS replicates, the rates were still generally higher than when EPS was absent (Figure 6.10). The mean precipitation rate of all replicates was about 2.5 times greater when EPS was present. This suggests that the presence of EPS increased the precipitation rate through the mechanism whereby unidentate bonding of Ca^{2+} provides nucleation sites for calcite precipitation. This is contrary to expectations as EPS has been reported as an inhibiting factor in marine environments (Reid *et al*., 2000). Furthermore, it is contradictory to the argument in section 6.5.2 that the adsorption of functional groups onto the surface of calcite crystals inhibits precipitation. Possible explanations to this apparent paradox are that the presence of salinity reduces the

ability of organic molecules to adsorb to the crystal surface or that at lower concentrations of EPS the precipitation enhancement generated through the provision of nucleation sites outweighs the inhibitory effects of the adsorption of EPS molecules onto nucleation sites.

6.5.4 Effect of varying EPS concentration on $(Mg/Ca)_{calcite}$

The value of $(Mg/Ca)_{calcite}$ increased with increasing EPS in the precipitating solution in a linear fashion (Figure 6.11). Increasing amounts of EPS would be expected to present a greater number of binding sites on negatively charged functional groups. The chemoselectivity for Ca^{2+} is believed to be responsible for creating an environment where precipitates have $(Mg/Ca)_{calcite}$ values lower than expected for a given $(Mg/Ca)_{solution}$ (bulk water) at faster precipitation rates. The observation in these results that $(Mg/Ca)_{calcite}$ was raised with increasing EPS amounts is contradictory to expectations based on the above principle. However, a mechanism explaining these results can be invoked by the fact that precipitates generated in a solution containing EPS can be divided into two categories, those that are precipitated on nucleation sites in the microenvironment of the EPS molecules and those that are precipitated from the bulk water way from this microenvironment.

The chemoselective chelation of $Ca^{2+}_{(aq)}$ from the precipitating solution will raise the bulk water Mg/Ca ratio and reduce it in the microenvironment of the EPS molecules where precipitation is taking place on unidentate bound Ca^{2+} ions.. Accordingly, precipitates generated from the bulk water solution will have a higher $(Mg/Ca)_{calcite}$ than those precipitated in the microenvironment of the EPS molecules. This effect will be accentuated in solutions with a higher EPS concentration due to the greater number of anionic functional groups which are selectively removing Ca^{2+} ions. Therefore, if the mass of precipitates from the bulk solution was greater than that from the microenvironment of the EPS then the mean $(Mg/Ca)_{calcite}$ of the combined precipitates would increase at higher EPS levels, a direct consequence of the greater chelation of Ca^{2+} from the bulk solution at higher EPS concentrations. Given the discussion in section 6.5.2 where precipitation is inhibited by adsorption of organic molecules onto crystal surfaces it is logical to conclude that in solutions with greater amounts of EPS, the ratio of precipitates from the microenvironment of the EPS to

precipitates from the bulk water will decrease and therefore drive up the mean $(Mg/Ca)_{calcite}$.

6.5.5 Effect of salinity variations on $(Mg/Ca)_{calcite}$

The finding that $(Mg/Ca)_{calcite}$ increased by about 3 % per ppm increase in salinity in the replicates containing isolated EPS molecules fits well with previous studies. Culture studies on foraminiferal calcite have shown $(Mg/Ca)_{calcite}$ increases by about 4 ± 3 % per PSU (Nurnberg et al., 1996, Lea et al., 1999, Kisakurek et al., 2008, Duenas-Bohorquez et al., 2009, Dissard et al., 2010). However, the results from the replicates without EPS do not show this correlation. It is difficult to compare these results with previous studies as there appear to be no studies to date which have examined the effect of salinity variations on the $(Mg/Ca)_{calicte}$ of inorganic precipitates. The fact that this relationship was not observed in the calcite from the solution without EPS suggests that presence of organic molecules such as EPS or the biological processes of organisms are required before salinity changes can influence $(Mg/Ca)_{calcite}$. Although the mechanism by which this takes place may be different in foraminiferal calcite the following discussion outlines a possible mechanism by which EPS molecules and salinity variations may combine to influence $(Mg/Ca)_{calcite}$.

As previously discussed, Ca^{2+} is preferentially chelated to the negatively charged functional groups on EPS molecules over Mg^{2+} and this preference creates an environment whereby low $(Mg/Ca)_{calcite}$ is precipitated. As sodium is present in solution as a positive ion (Na^+) it will also be able to be chelated by negatively charged functional groups on EPS molecules, taking up binding sites that would otherwise have been available to Ca^{2+} cations. A reduction in chelated Ca^{2+} will result in fewer microenvironments where low $(Mg/Ca)_{calcite}$ can be precipitated consequently raising the mean bulk $(Mg/Ca)_{calcite}$ of precipitates. This effect would be expected to increase at higher salinity levels as more Na^+ ions will be available to bind to the negative groups on the EPS. It is therefore proposed that the increasing $(Mg/Ca)_{calcite}$ values observed at higher salinities are a consequence of Na^+ ions reducing the number of binding sites for Ca^{2+} and hence the number of nucleation sites for precipitation of low $(Mg/Ca)_{calcite}$.

6.5.6 (Mg/Ca)$_{calcite}$ and precipitation rate

Similarly to the biofilm data from both the microcosm and agitated flask data, the isolated EPS data from the agitated flasks revealed a significant negative power correlation between precipitation rate and (Mg/Ca)$_{calcite}$. The relationship found in the isolated EPS data closely matches that obtained from the biofilm precipitates (Figure 6.16).
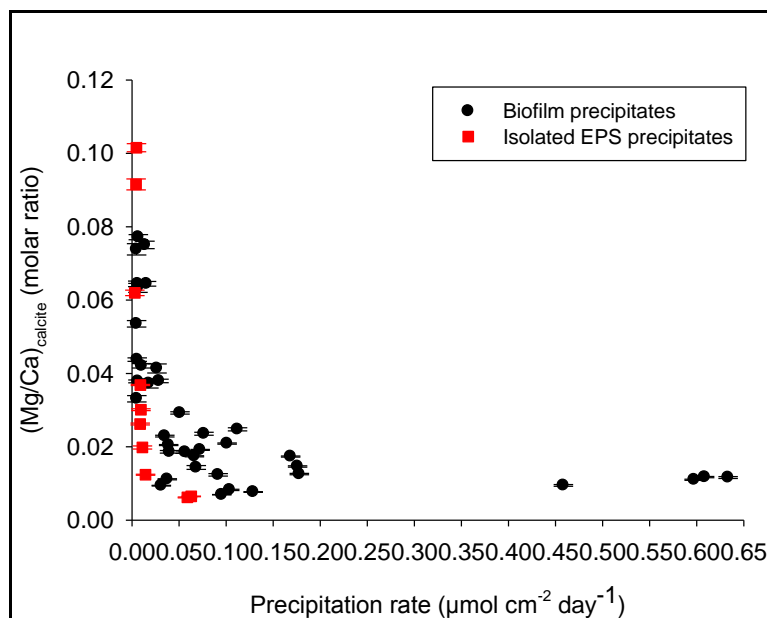
Figure 6.16 Comparison (Mg/Ca)$_{calcite}$ as a function of precipitation rate of data from living biofilms and isolated EPS molecules.

The continued existence of this relationship in the absence of living organisms strongly suggests that it is the EPS molecules that exert the dominant control on (Mg/Ca)$_{calcite}$ rather than the organisms of the living biofilm. The adsorption of cations to EPS molecules has been shown to be a metabolism – independent process (Perez-Huerta *et al*., 2008). As described in chapter 5 section 5.5.7 it is believed that calcite nucleation sites are created through the unidentate bonding of $Ca^{2+}_{(aq)}$ to negatively charged functional groups on EPS molecules and that chemoselectivity for Ca^{2+} over Mg^{2+} creates a microenvironment around these nucleation sites that favours the development of precipitates with a lower (Mg/Ca)$_{calcite}$ than expected from a given bulk water (Mg/Ca)$_{solution}$.

The results from the salinity experiment reinforce the agitated flask data by again showing that the presence of EPS molecules is needed to generate the negative power

correlation between $(Mg/Ca)_{calcite}$ and precipitation rate. In the replicates without isolated EPS molecules there was no correlation between these parameters (Figure 6.4). The addition of isolated EPS to the precipitating solution resulted in a significant negative power relationship (Figure 6.5) which is similar to that observed for the biofilm and isolated EPS precipitates of the microcosm and agitated flask experiments. The observation that this relationship remained in solutions of varying salinity suggests that the chemoselective preferences of cation chelation to EPS molecules is not significantly influenced by salinity variations.

6.5.7 $(Mg/Ca)_{calcite}$ and precipitation rate under varying EPS levels

The data from salinity and agitated flask experiments for isolated EPS precipitates revealed the same negative power correlation between $(Mg/Ca)_{calcite}$ and precipitation rate that was seen in the biofilm experiments. In those EPS experiments a constant amount of isolated EPS solution was added to each replicate. However, when EPS levels were varied there appeared to be no significant correlation at the 95 % confidence level between $(Mg/Ca)_{calcite}$ and precipitation rate (Figure 6.13). Examination of Figure 6.13 shows that the data for the replicates with EPS appear to be randomly plotted at the scale shown but are distinct from the EPS free control replicates. The EPS in any concentration has caused the $(Mg/Ca)_{calcite}$ to deviate from the control values.

Although in isolation the data did not produce a significant correlation when combined with the data from the salinity experiment a significant relationship was observed   between $(Mg/Ca)_{calcite}$ and precipitation rate where $(Mg/Ca)_{calcite} = 0.0049(R)^{-0.4691}$ ($R^2 = 0.85$, P < 0.05, n = 29). Figure 6.17 shows how the data from the replicates with varying EPS levels compares to the data from the salinity and agitated flask replicates.

Figure 6.17 Comparison (Mg/Ca)$_{calcite}$ as a function of precipitation rate of data from different isolated EPS experiments.

There are two distinct series of plots, one for the agitated flask data and the other for the combined data from the varying EPS and salinity experiments. A possible explanation for this is that both the varying EPS and salinity experiments were conducted in static Petri dishes, whilst the flask data was subjected to agitation at 100 oscillations per minute. The flow velocities over the precipitating surfaces induced by the agitation will have generated a thinner DBL than that in the static Petri dishes. The observed shift of the data for the agitated flask results may reflect a DBL process.

In combination the results from the agitated flasks, salinity and varying EPS concentration experiments support an assertion that isolated EPS molecules have a significant control on (Mg/Ca)$_{cslcite}$ values as a function of precipitation rate and that this control still exists in waters of varying salinities. The revelation that the negative power correlation still exists between (Mg/Ca)$_{calcite}$ and precipitation rate in the absence of microbial metabolic processes confirms the observation of Perez-Huerta *et al*., (2008) that cation chelation is a metabolism-independent process.

6.6 Synthesis and Conclusion

In this chapter a set of three differing experiments have examined the impact of isolated EPS molecules on calcite precipitation rates and (Mg/Ca)$_{calcite}$. The results

from the agitated flask experiment revealed an exponential increase in $(Mg/Ca)_{calcite}$ as a function of temperature in the range of 12 - 18 °C. The exponential constant of 0.31 matched well with those found in calibration equations for foraminiferal calcite, although the pre-exponential constant was generally about an order of magnitude lower. The absence of this correlation between $(Mg/Ca)_{calcite}$ and temperature in the precipitates generated in the presence of living biofilms strongly suggests that it is the microbial metabolic processes that are responsible for the breakdown of the expected thermodynamic control on $(Mg/Ca)_{calcite}$ and not simply the presence of EPS molecules. The observation that the data at 20 °C did not fit into this correlation indicated a separate and stronger control on $(Mg/Ca)_{calcite}$ than temperature. Comparison of the agitated flask EPS data with that from the biofilms in both the microcosms and agitated flasks showed that at 20 °C $(Mg/Ca)_{calcite}$ values were very well constrained but were highly variable at all other experimental temperatures.

The relationship between temperature and precipitation rate in the agitated flasks was generally contrary to expectations. In the temperature range of 12 – 18 °C there was a slight linear decrease in rate as a function of temperature. At 20 °C the mean rate was significantly (about 7.6 fold) higher than the mean rate at 12 – 18 °C. This observation, combined with the fact that precipitation rates were higher at 20 °C for the biofilm precipitates of chapter 5 offers a possible explanation for the finding that at 20 °C the $(Mg/Ca)_{calcite}$ values are tightly constrained compared to the ratios at 12 – 18 °C. Therefore, at 20 °C precipitation rate appears to be the dominant factor in determining $(Mg/Ca)_{calcite}$ ratios and not temperature. Precipitation rates in the presence of isolated EPS were well constrained at all temperatures, in contrast to the data from the biofilm experiments where, apart from at 12 °C, precipitation rates varied widely. It is proposed that in the temperature range of 14 – 20 °C the varying metabolic processes of the biofilm organisms are able to influence precipitation rates and mask the expected temperature control. At 12 °C it is likely that the lower metabolic rates were insufficient to impact on precipitation rates.

Precipitation rates were found to decrease linearly with increasing amounts of EPS present. Although the presence of nucleation sites generated through chelation of calcium ions is believed to aid precipitation in the microenvironment of the EPS molecules, the removal of calcium from the bulk water through chelation reduces the

saturation state with respect to calcite which may have some inhibitory impact on precipitation rates, however, this impact has been shown to be minimal (Inskeep and Bloom, 1986, Hoch *et al*., 2000). It is believed that the major mechanisms behind the falling precipitation rates in solutions with higher EPS levels is the blocking of active nucleation sites by the adsorption of these organic molecules onto the growing crystal surface.

In the presence of EPS the variations in salinity resulted in $(Mg/Ca)_{calcite}$ ratios increasing by about a 3 % per ppm rise in salinity which is in agreement with the correlation found in studies on foraminiferal calcite. This relationship was absent in the replicates without EPS suggesting that the presence of organic molecules is necessary for salinity variations to impact significantly on $(Mg/Ca)_{calcite}$. Given that salinity levels in places like the Mediterranean Sea can vary by about 4 ppm care must be taken when interpreting calibrations of foraminiferal calcite Mg/Ca values from such regions. Precipitation rates at differing salinities were correlated in the replicates that contained EPS but were not when EPS was absent. The increasing presence of positively charged sodium ions at higher salinities is the most likely explanation for the falling precipitation rates in the EPS replicates through their occupation of negatively charged binding sites, thus limiting the number of calcite nucleation sites on the EPS molecules.

When EPS amounts were varied in the precipitating solution $(Mg/Ca)_{calcite}$ values increased with increasing levels of EPS contrary to what was expected. A possible explanation is that at higher levels of EPS more free $Ca^{2+}_{(aq)}$ cations are removed from the bulk solution through chelation resulting in a higher bulk water $(Mg/Ca)_{solution}$. If the mass of precipitates generated from this bulk water is greater than the low $(Mg/Ca)_{calcite}$ precipitated from the microenvironment of the EPS molecules then the mean $(Mg/Ca)_{calcite}$ of all the precipitates will increase as EPS levels increase. This observation may explain why there was no significant correlation between $(Mg/Ca)_{calcite}$ and temperature in the biofilm samples. The constant modification in both the state and quantity of EPS by metabolic processes will necessarily cause variations in the chelating capacity and the bulk water $(Mg/Ca)_{solution}$.

7 Trace elements in a Holocene tufa: Implications for tufa (Mg/Ca)$_{calcite}$ palaeothermometry

7.1 Abstract

Trace elements in tufa carbonates are considered a potential source of high resolution data due to their annual laminations. However, the metabolic processes and secretory products of microbial biofilms on the precipitating surface of the deposit may mask the thermodynamic control on trace element incorporation into tufa calcites. This study examined a Holocene tufa sample from Caerwys, North Wales to determine whether its trace element ratios have the potential to provide palaeotemperature data by testing, 1) whether coherent curves can be generated from multiple transects through a single sequence of laminated layers and 2) to what extent the elemental information held in this fossil sequence can be interpreted quantitatively. Sample material was obtained by drilling at 0.5 mm intervals along five concentrically spaced transects across a laminated carbonate deposit that formed on the subaqueous parts of a reed. The recovered dust was digested in concentrated nitric acid and analysed by ICP – OES for the trace element ratios Mg/Ca and Sr/Ca. Colour analysis software was used to record the changes in colour of the laminations, which are conventionally interpreted as representing annual cycles, to determine any correlation between the laminations and trace element ratios.

There was no significant correlation between the colour of the laminations and the trace element ratios, although this may be due to the limited resolution of the sampling. There was however a general trend whereby the colour brightness increased from the inner to outer edges of the sample which was in direct contrast to the trend of trace element ratios decreasing across the transect. Trace elements profiles did not reveal a coherent pattern of behaviour across the concentrically spaced transects. Variations in (Mg/Ca)$_{calcite}$ ratios of $31 - 210$ % in calcite deposited at the same instant in time while being spatially separated by only a few millimetres provides further support to the assertions in chapters 5 and 6 that the (Mg/Ca)$_{calcite}$ rations held in fossilised tufas are not a reliable archive of palaeotemperature data.

7.2 Introduction

Laminations within tufas are believed to represent seasonal patterns of deposition, millimetre sized laminae have been considered to be annual growth rings (Chafetz and Folk, 1984) analogous to those seen in trees, speleothems and reef corals (Kano *et al*., 2003). These annual laminations are thought to reflect seasonal changes in water chemistry, the hydrology of the depositional environment (Matsuoka *et al*., 2001) and changing precipitation rates (Kano *et al*., 2003, Liu *et al*., 2006). Annual deposition rates in tufas have been described in the range of millimetres to centimetres (Matsuoka *et al*., 2001, Ihelenfeld *et al*., 2003, Liu *et al*., 2006) giving them considerable potential as archives of palaeoclimate data.

Laminae in tufa samples are generally seen as alternate dark and light coloured bands with the dark layers consisting of porous material and the lighter layers being of a denser micritic texture (Figure 7.1) (Kano *et al*., 2003). The dense lighter layers appear to be summer and early autumn deposits whilst the darker porous layers represent winter and spring deposits (Matsuoka *et al*., 2001, Kano *et al*., 2003).
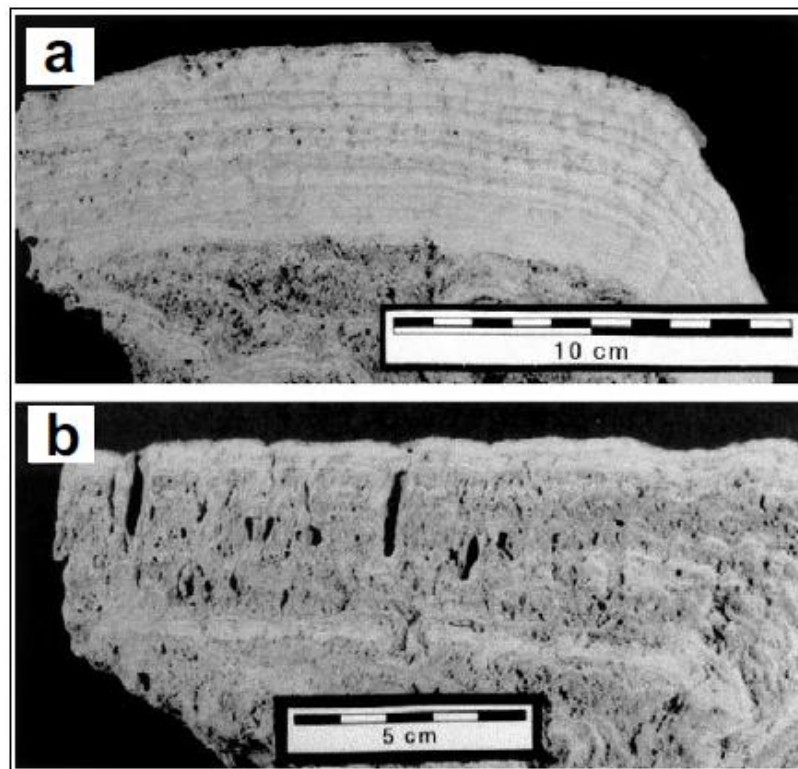
Figure 7.1 Tufa deposits from South West Japan: (a) laminated tufa showing alternating light and dark coloured bands, (b) tufa inhabited by moss (Kano *et al*., 2003).

In addition to the factors described above that drive the formation of laminae it has been suggested that seasonal changes in biofilm communities also generate laminations in tufa deposits (Arp *et al*., 2001). The porous layers of winter-spring deposits have been attributed to diatoms being the dominant organism in the biofilm whilst the denser summer-autumn deposits are indicative of a biofilm community dominated by cyanobacteria (Arp *et al*., 2001). However, seasonal variations in the composition of microbial communities does not always account for the presence of laminae in tufas. The biofilm community at a present day tufa site in South Western Japan is dominated throughout the year by cyanobacteria, yet the deposits still exhibit the same porous/dense lamination pattern associated with seasonal changes (Kawai *et al*., 2009).

Laminated tufa deposits have been put forward as potential archives of high resolution Quaternary terrestrial palaeoclimate data (Matsuoka *et al*., 2001, Ihlenfeld *et al*., 2003). Stable isotopes have generally received the majority of attention (e.g. Chafetz *et al*., 1991, Andrews *et al*., 1993, 1997, 2000, Matsuoka *et al*., 2001, Ihlenfeld *et al*., 2003, Garnett *et al*., 2004). In contrast trace elements have received little attention which is surprising given the vast coverage they have received in marine carbonates and to a lesser extent in speleothems. Studies on stable isotopes of specific tufas have confirmed the potential of laminated tufas as archives of terrestrial palaeoclimate data, $\delta^{13}C$ and $\delta^{18}O$ values of a laminated tufa sample from South West Japan were both observed to be higher in winter and lower in summer and were well correlated to each other (R = 0.88) (Matsuoka *et al*., 2001). Co-variation between $\delta^{13}C$ and $\delta^{18}O$ in Spanish Holocene tufas has been suggested as being intrinsically linked to climatic conditions such as aridity (Andrews *et al*., 2000).

The possibility of using trace elements for palaeoclimate reconstructions was first highlighted when it was observed that the concentrations of Sr, Mn and Mg were greater in summer than winter precipitates from a tufa precipitating stream in Oklahoma, U.S.A. (Chafetz *et al*., 1991). Additionally an ~ 10°C seasonal temperature change in the waters of the Gregory River, Queensland, Australia was

suggested as the dominant control on $(Mg/Ca)_{calcite}$ on local tufa precipitates. Although seasonal variations in $(Mg/Ca)_{calcite}$ ratios have been proposed as a useful addition to the stable isotope data (Ihlenfeld *et al*., 2003) its potential for long term tufa records has been questioned with the suggestion that any long term variations in the Mg content of temperate zone tufas is mainly attributable to changes in the Mg content of the source water (Garnett *et al*., 2004).

The use of $(Sr/Ca)_{calcite}$ as a palaeoclimate proxy is common in marine carbonates (e.g. Elderfield *et al*., 1996, Mitsuguchi *et al*., 2001, Marshall and McCulloch 2002, Alibert *et al*., 2003, Rosenthal and Linsley, 2006). However, some studies have shown that $(Sr/Ca)_{calcite}$ values increase by only about $0.4 - 1$ % per °C (Lea *et al*, 1999, Russell *et al*., 2004) leading to suggestions that temperature only plays a minor role in $(Sr/Ca)_{calcite}$ variations in foraminiferal calcite (Dissard *et al*., 2010). The incorporation of Sr into calcite depends on other factors in addition to temperature such as the presence of other cations and precipitation rate (Zhang and Dawe, 2000, Huang and Fairchild 2001, Terakado and Taniguchi, 2006). In particular, precipitation rate has a strong positive correlation with Sr incorporation (Tesoriero and Pankov, 1996, Gabitov and Watson, 2006, Nehrke *et al*., 2007) (Figure 7.2).
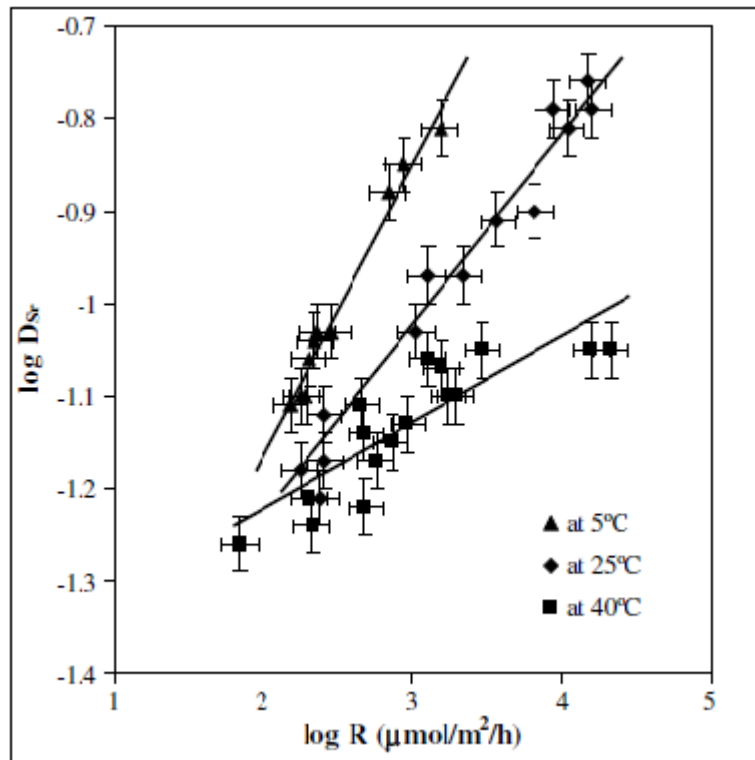
Figure 7.2 Distribution coefficient of Sr^{2+} into calcite as a function of precipitation rate at different temperatures (Tang *et al.*, 2008).

It has been suggested that the influence of temperature on Sr partitioning is an indirect one, whereby it is the increased precipitation rate caused by higher temperatures that results in the variations in Sr partitioning as a function of temperature (Roberts *et al.*, 1998). A strong co-variation between carbonate trace element ratios such as (Mg/Ca) and (Sr/Ca) suggests a single controlling mechanism (Cruz *et al.*, 2007) whereas little or no correlation indicates that Sr and Mg are incorporated in response to different or multiple controlling mechanisms (Dissard *et al.*, 2010).

The tufas of Caerwys, in the Wheeler Valley of North Wales (Figure 7.3) represent an extensive deposit comprised of oncoid and micrite facies and organic build ups including twig, leaf, moss, liverwort and cyanobacterial tufa (Pedley, 1987). The deposits overlie glacio-fluvial siliciclastic sands and gravels but were fed from a spring originating from a Carboniferous Limestone scarp. Although a number of studies have examined various aspects of these deposits, e.g. their molluscan fauna (McMillan, 1947), the biostratigraphy (Preece *et al*, 1982), palaeoecology of

associated gastropods (McMillan and Zeissler, 1986), no studies appear to have been conducted on trace element ratios in these deposits.
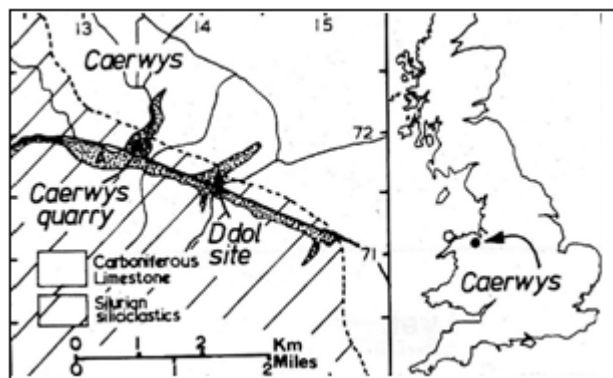
Figure 7.3 Location of Caerwys tufa deposit in North Wales (Pedley, 1987).

The aim of the work described in this chapter was to analyse the incorporation of the Mg^{2+} and Sr^{2+} into a sample of the Caerwys tufa deposit to determine whether the $(Mg/Ca)_{calcite}$ and $(Sr/Ca)_{calcite}$ ratios offered any further insight into the potential of trace element ratios in fossil tufas to act as a palaeotemperature proxy. Additionally, the aim was to apply the weak, but significant ($P < 0.05$) correlation between temperature and $(Mg/Ca)_{calcite}$ obtained from the microcosm experiments (see Figure 5.1) to these ratios to determine the extent of temperature variation implied from this correlation.

7.3 Methods

The sampling methods utilised in this study are detailed in chapter 3, section 3.5.2. Analyses of trace elements was conducted by ICP – OES as detailed in Chapter 3, section 3.6 and colour banding analysis was carried out using the 'Mirone' software package. Mirone is an open source code written in MATLAB[S] 6.5 and is frequently used by the scientific community (Luis, 2007).

7.4 Results

The results described below are from the drilling of 5 lines in a Holocene tufa sample (Figure 7.4).
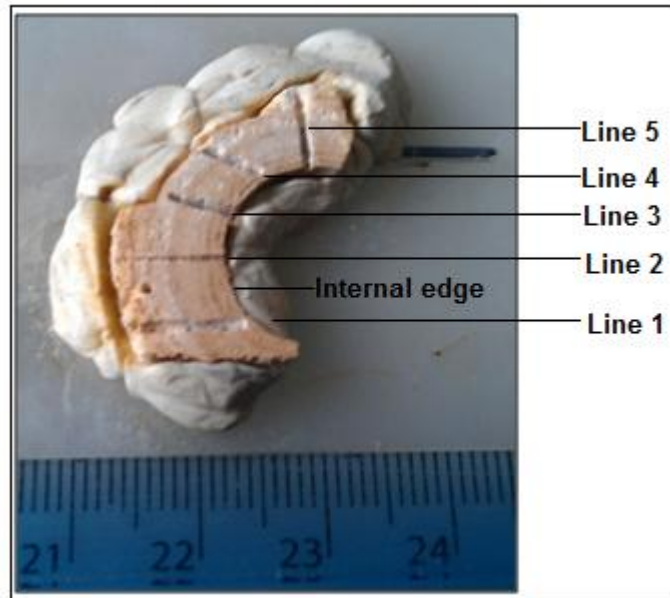
Figure 7.4 Sample of Caerwys tufa used in this study showing the location of the drilling lines.

The $(Mg/Ca)_{calcite}$ ratios obtained from the drilling lines 1 – 5 are shown in Figure 7.5. A mechanical breakdown of the ICP – OES led to the loss of some sample results.
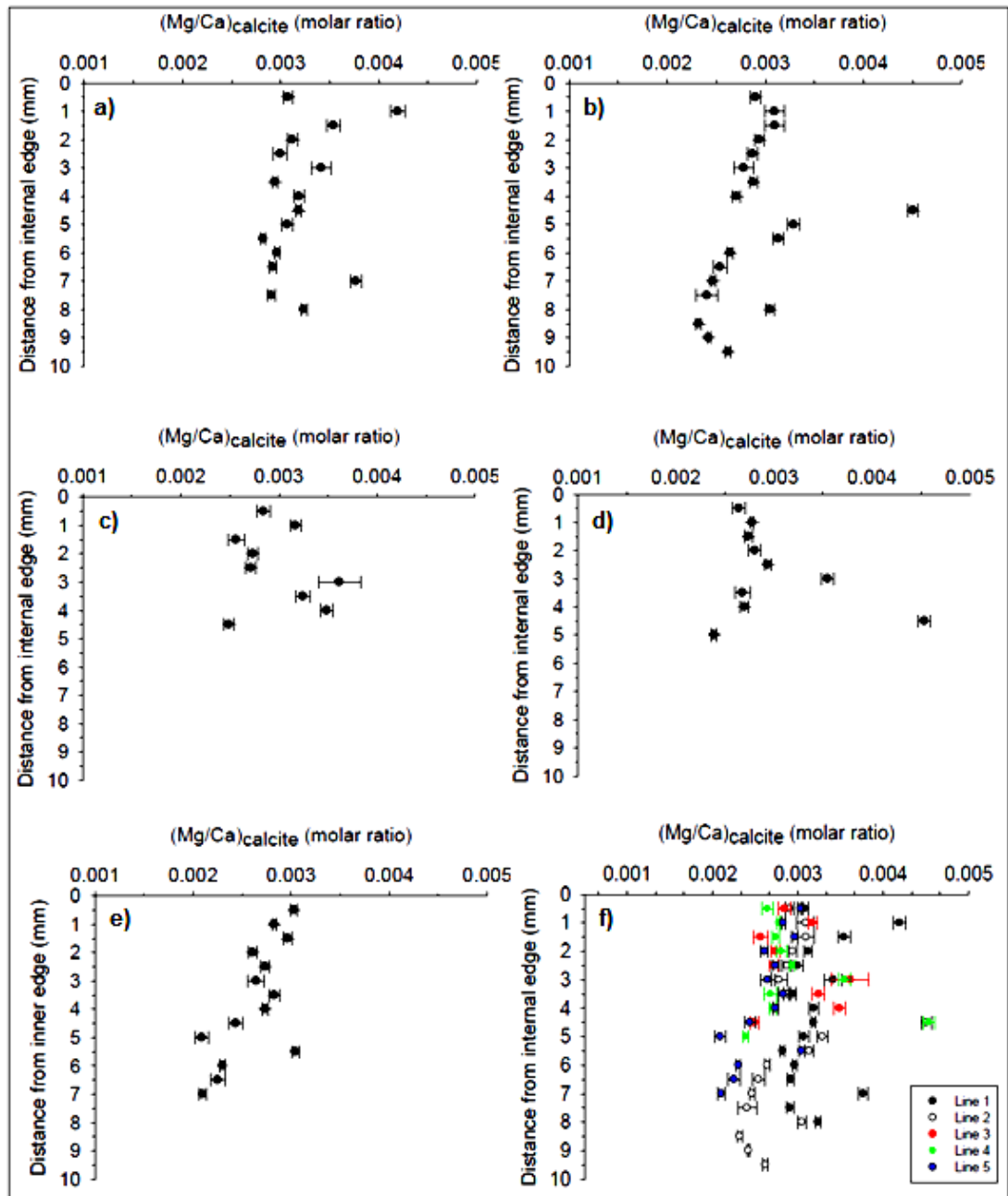
Figure 7.5 (Mg/Ca)calcite vs. distance from internal edge of sample: (a – e) represent lines 1 – 5 respectively, (f) is all lines combined.

No statistically significant correlation exists between (Mg/Ca)calcite and distance from the internal edge of the sample in lines 1 to 4. However, there is a significant ($P < 0.05$) linear correlation ($R^2 = 0.50$) between these parameters in line 5 (Figure 7.5 (e)). In figure 7.5 the profiles (a) and (b) suggest a mirror image 'S' shape to the profile and this appears to be at least partially upheld in the combined plots of (f). The significant correlation seen in line 5 is not observed when all lines are combined (Figure 7.5 (f)).

The plots of all lines combined show considerable variation in (Mg/Ca)$_{calcite}$ ratios for any given distance from the internal edge. Table 7.1 shows the percentage variation in (Mg/Ca)$_{calcite}$ ratios for distances of 0.5 to 7.0 mm from the internal edge.

Table 7.1 Variations in (Mg/Ca)$_{calcite}$ at given distances from the internal edge

Distance from internal edge (mm)	Maximum (Mg/Ca)$_{calcite}$ ratio	Minimum(Mg/Ca)$_{calcite}$ ratio	Percentage difference
0.5	0.0031	0.0026	43
1	0.0042	0.0028	142
1.5	0.0035	0.0026	97
2	0.0031	0.0026	51
2.5	0.0030	0.0027	28
3	0.0036	0.0026	97
3.5	0.0032	0.0027	57
4	0.0035	0.0027	79
4.5	0.0045	0.0024	210
5	0.0033	0.0021	120
5.5	0.0031	0.0028	31
6	0.0030	0.0023	66
6.5	0.0029	0.0023	67
7	0.0038	0.0021	167

Plots of (100*Sr/Ca)$_{calcite}$ as a function of distance from the internal edge are shown in Figure 7.6. The mirror 'S' shape to the profiles of lines 1 and 2 for (Mg/Ca)$_{calcite}$ is absent for strontium partitioning. Visual inspection of the graphs indicates a general linear correlation between (100*Sr/Ca)$_{calcite}$ and distance from the internal edge of the sample. Statistical analyses shows that this correlation is statistically significant at the 95 % confidence level in line 1 (R^2 = 0.44, n = 15), line 2 (R^2 = 0.28, n = 19) and line 5 (R^2 = 0.31, n = 14). Combining all lines gives a weak but significant (P < 0.05) correlation between (100*Sr/Ca)$_{calcite}$ and distance from the internal edge (R^2 = 0.26, n = 67).
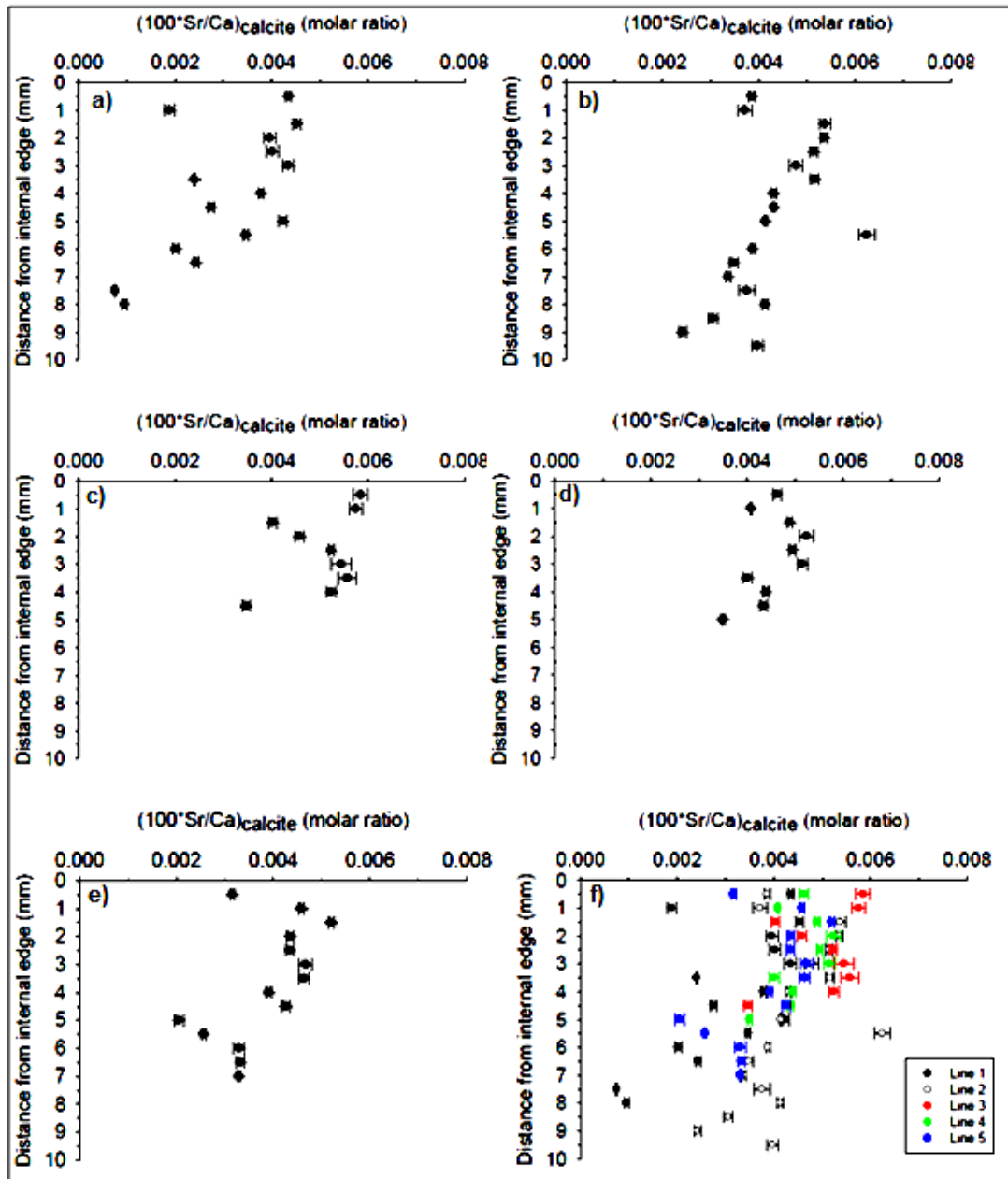
Figure 7.6 (100*/Ca)$_{calcite}$ vs. distance from internal edge of sample: (a – e) represent lines 1 – 5 respectively, (f) is all lines combined.

Figure 7.7 shows the values of (Sr/Mg)$_{calcite}$ against distance from the internal edge. Similarly to the (100*Sr/Ca)$_{calcite}$ ratios in Figure 7.6 there is a visual impression of a linear correlation between (Sr/Mg)$_{calcite}$ and distance from the internal edge of the tufa sample. Statistical analyses reveal that the correlation between these parameters is significant at the 95 % confidence level in line 1 ($R^2 = 0.33$, n = 15) and line 3 ($R^2 = 0.53$, n = 9). Combining all 5 lines results in a weak ($R^2 = 0.14$, n = 67) but significant correlation (P < 0.05).

162
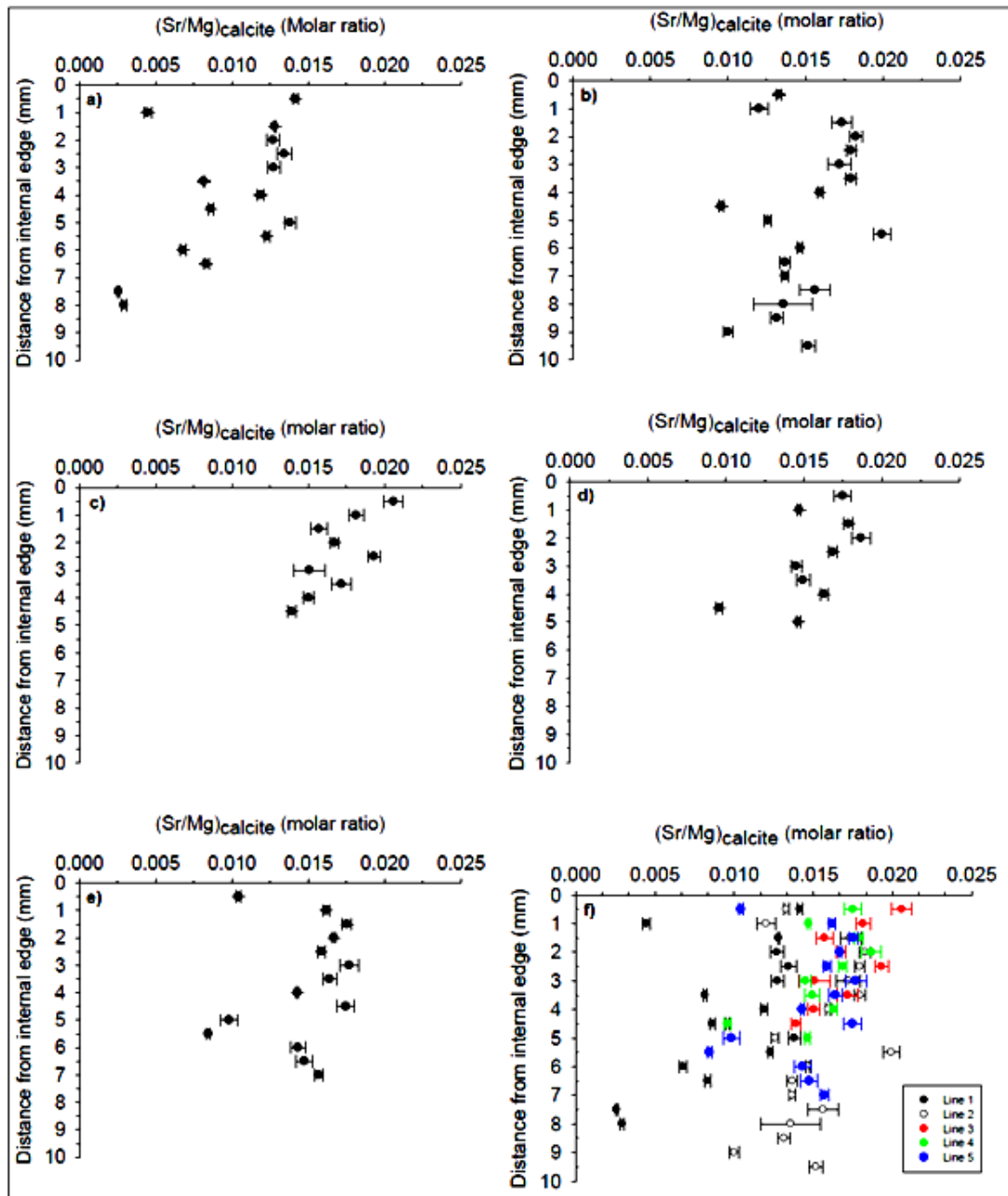
Figure 7.7 (Sr/Mg)calcite vs. distance from internal edge of sample: (a – e) represent lines 1 – 5 respectively, (f) is all lines combined.

Examination of the drilled lines by the Mirone software was undertaken after converting the images to greyscale (RGB was not supported). The output of the extracted profile had no units for the colour variations across the profile, therefore these variations are labelled as 'arbitrary brightness' in the following profiles with the numbers on the axis representing the original numbers of the output. Figure 7.8 shows the extracted profile for line 1 along with the graphs of the trace element ratios for the same line. The red dots on the extracted profiles in Figures 7.8 (d) – 7.12 (d)

represent the 0.5 mm spaced sampling points and are equivalent to the sampling points used for the trace element analyses.
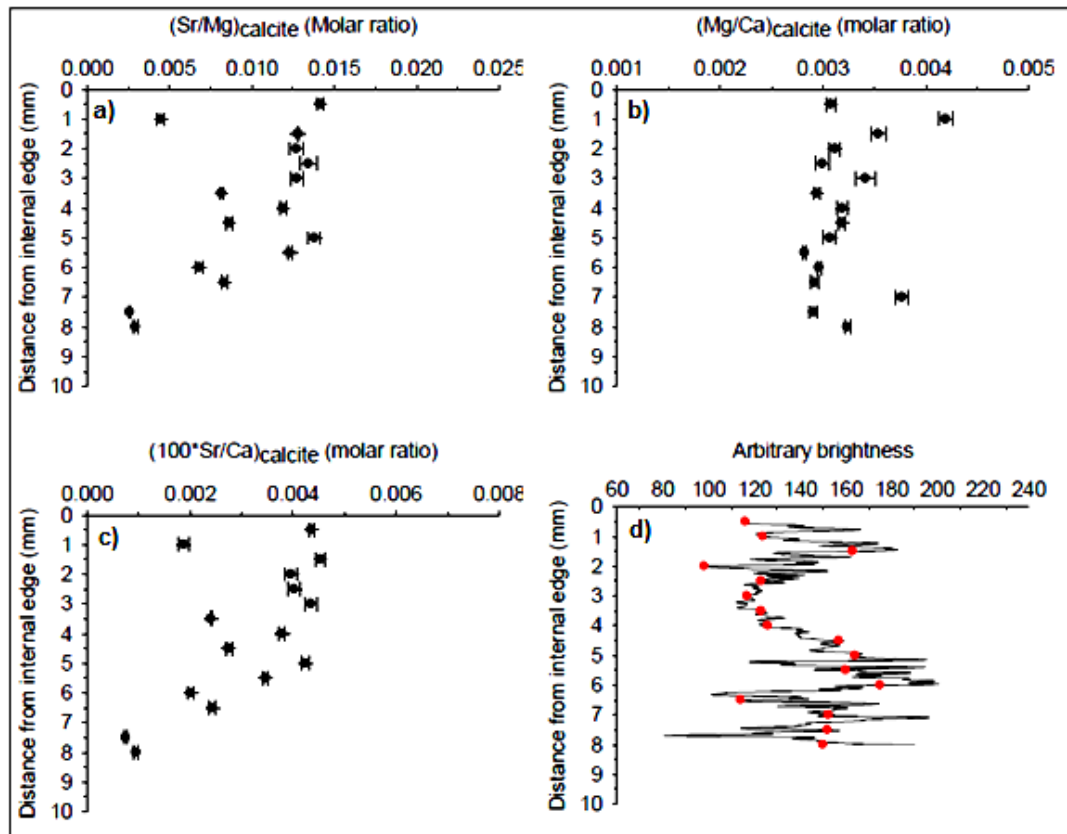
Figure 7.8 Profiles for line 2: (a – c) trace element ratios vs. distance from internal edge, (d) profile of 'brightness' of the laminae vs. distance from the internal edge.

There is no significant relationship between the brightness of the laminae and the trace element ratios. Figures 7.9 – 7.12 show the same profiles for lines 2, 3, 4 and 5, similarly to line 1 there is no significant correlation between trace element values and brightness of the laminae. However, visual inspection of the graphs indicates that there is a general relationship whereby trace element ratios decrease as brightness increases, this is particularly obvious for line 5 (Figure 7.12).
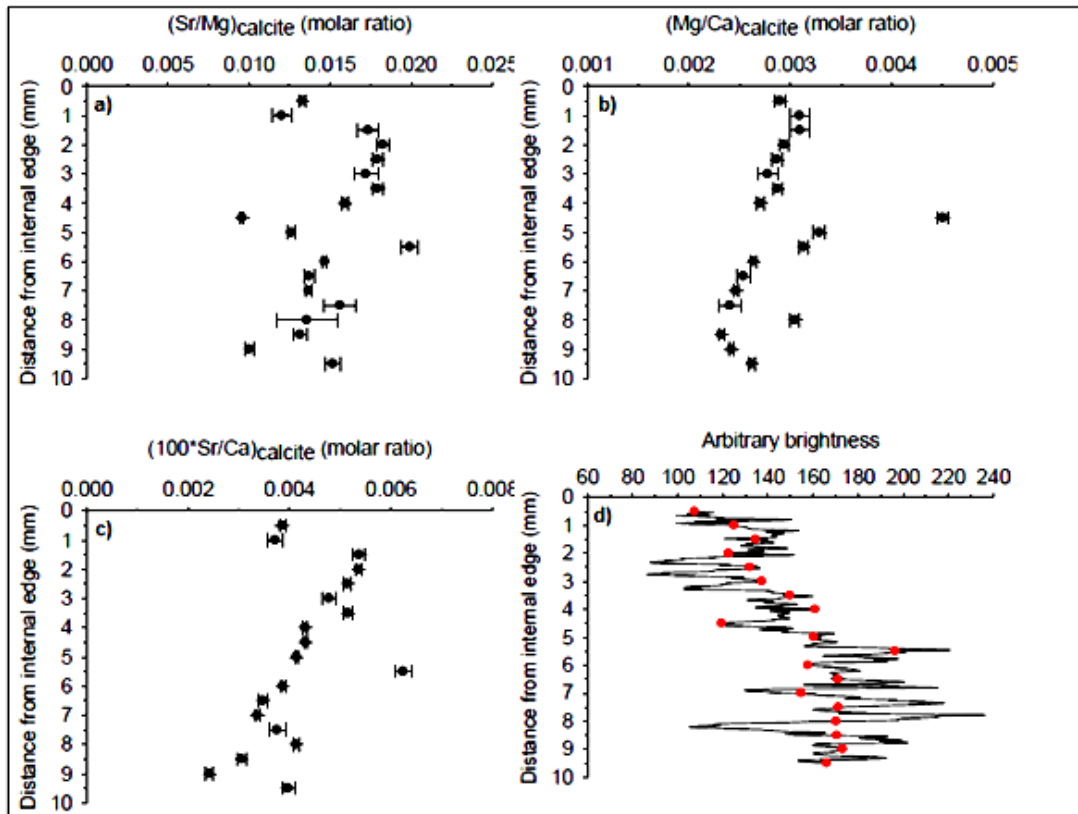
Figure 7.9 Profiles for line 2: (a – c) trace element ratios vs. distance from internal edge, (d) profile of 'brightness' of the laminae vs. distance from the internal edge.
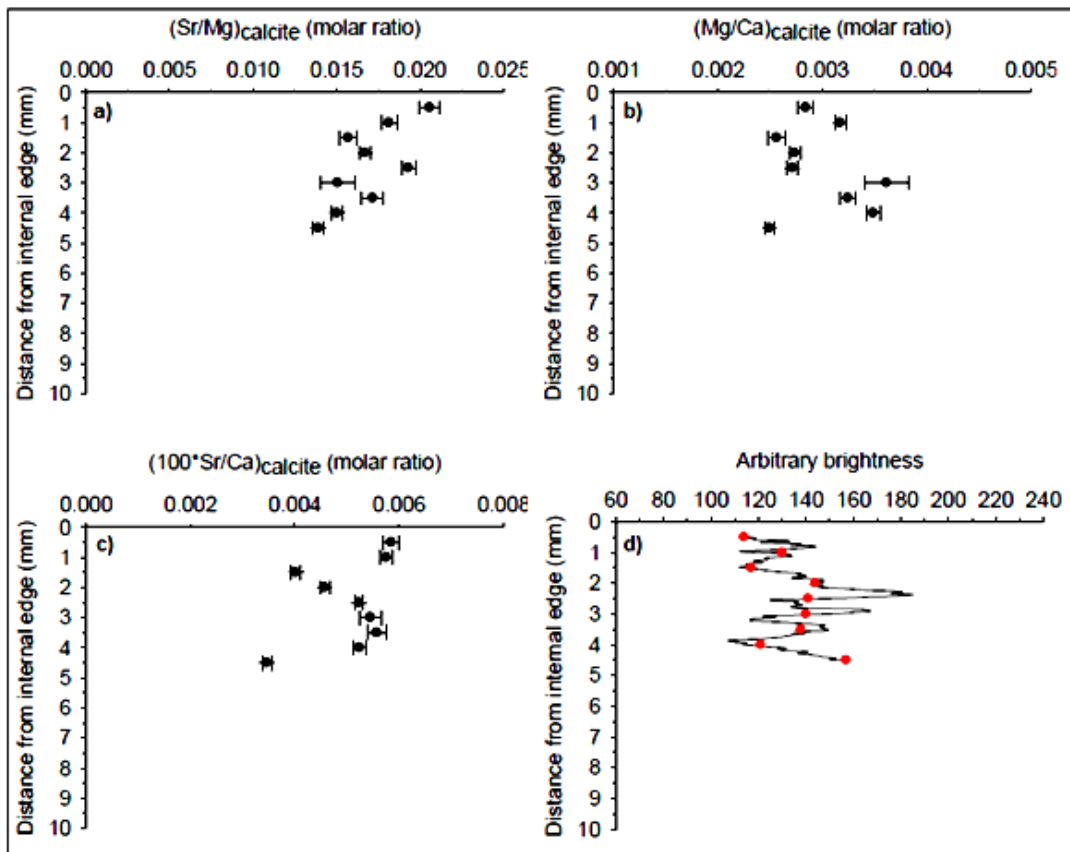
Figure 7.10 Profiles for line 3: (a – c) trace element ratios vs. distance from internal edge, (d) profile of 'brightness' of the laminae vs. distance from the internal edge.

165
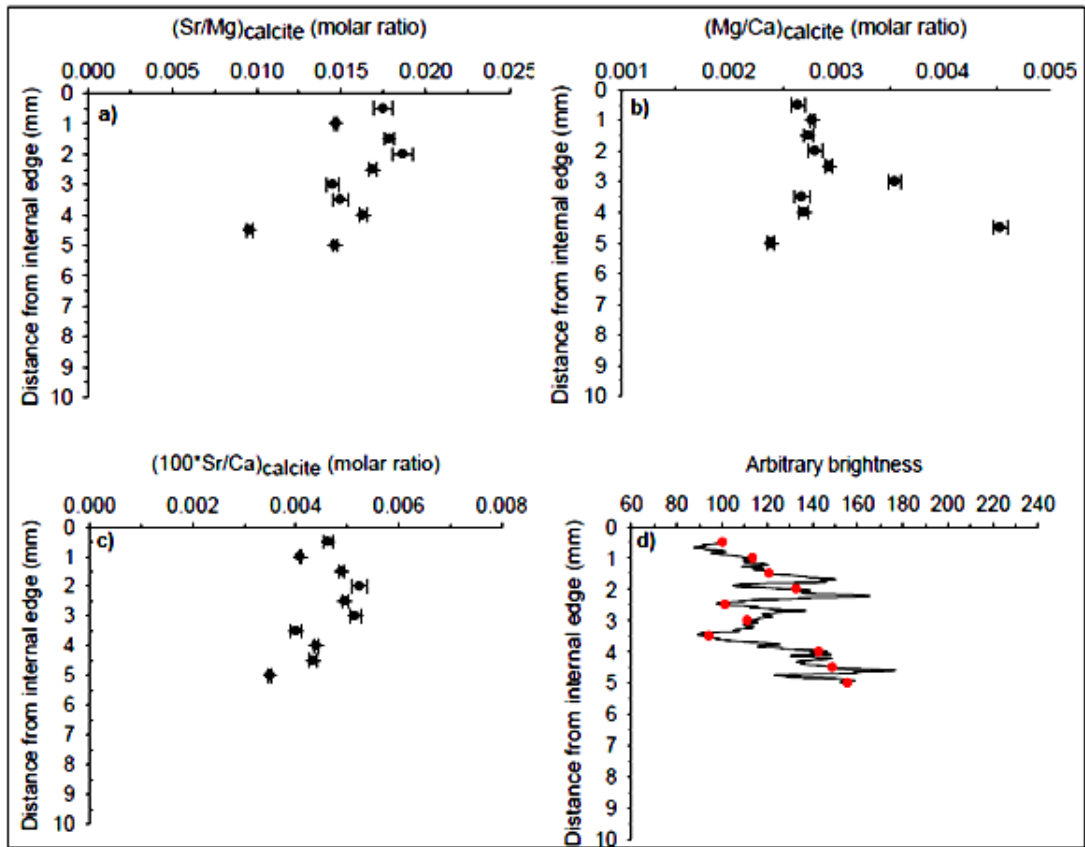
Figure 7.11 Profiles for line 4: (a – c) trace element ratios vs. distance from internal edge, (d) profile of 'brightness' of the laminae vs. distance from the internal edge.
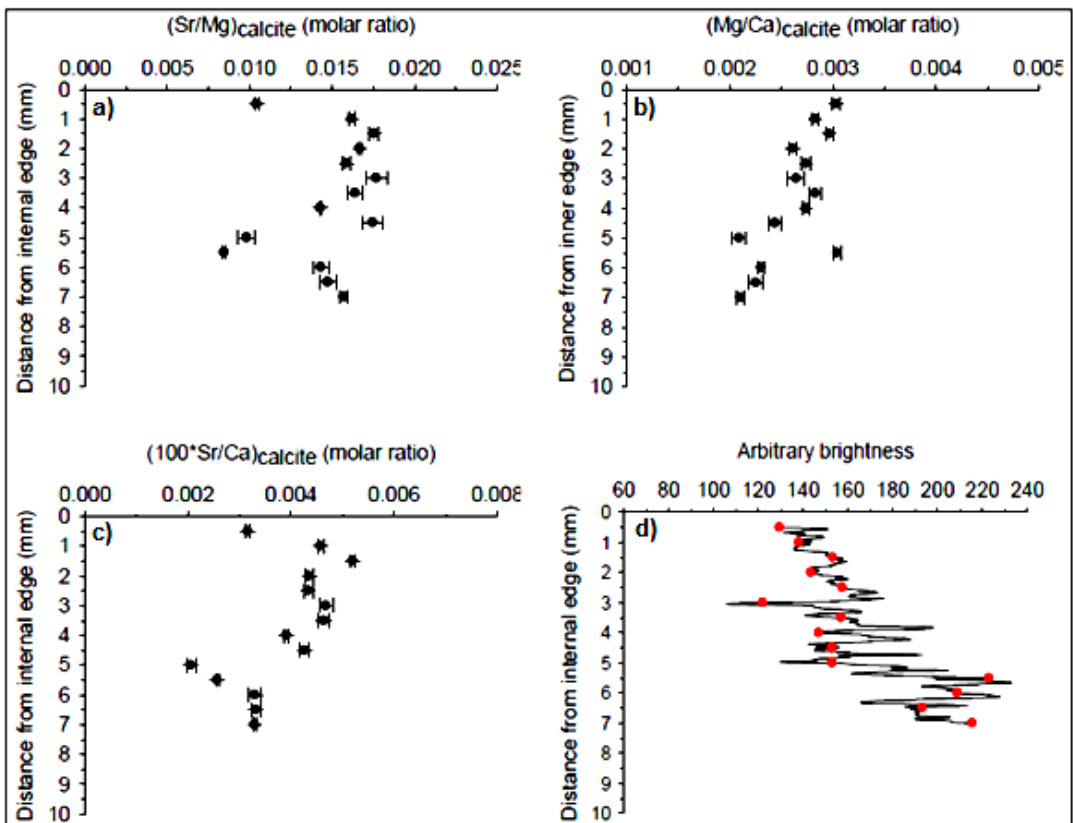
Figure 7.12 Profiles for line 4: (a – c) trace element ratios vs. distance from internal edge, (d) profile of 'brightness' of the laminae vs. distance from the internal edge.

Plots of the brightness value obtained for each drilling point along the line (i.e. the value of the red dots in Figures 7.8 – 7.12) against the trace element ratios (Mg/Ca)$_{calcite}$, (Sr/Ca)$_{calcite}$ and (Sr/Mg)$_{calcite}$ of the equivalent point are shown in Figures 7.13 to 7.17 for lines 1 – 5 respectively.
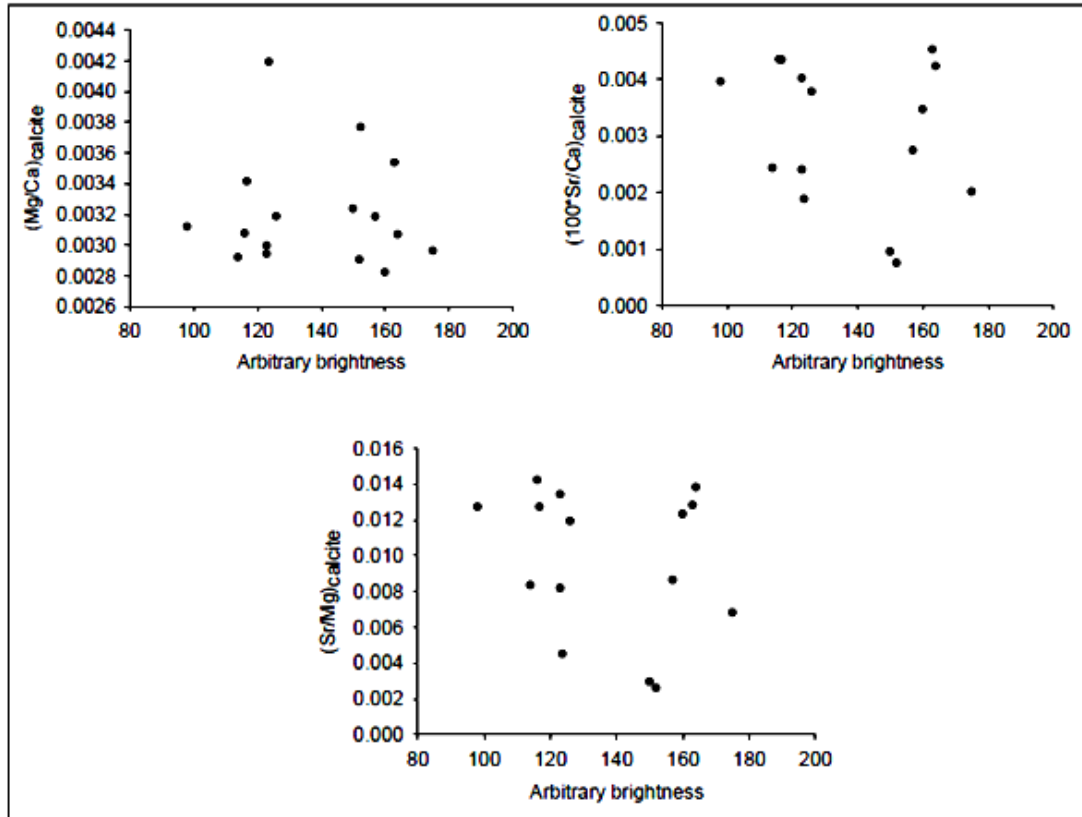
Figure 7.13 Trace element ratios from line 1 vs. lamination colour brightness.
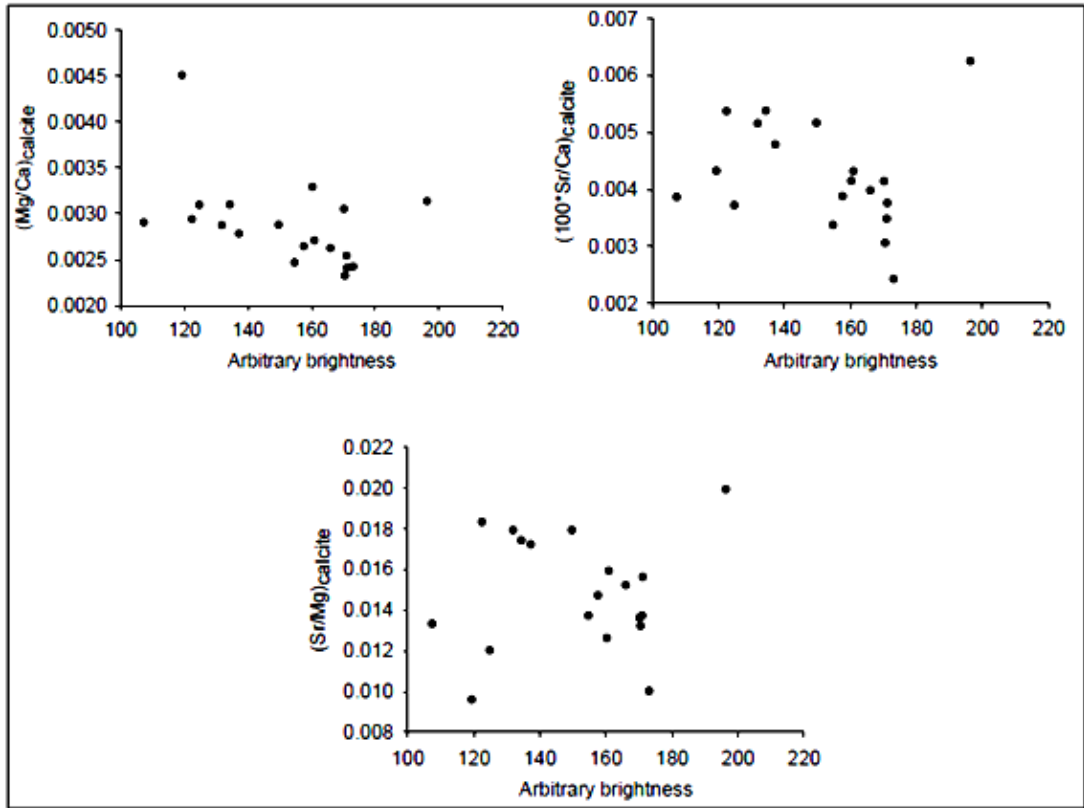
Figure 7.14 Trace element ratios from line 2 vs. lamination colour brightness.
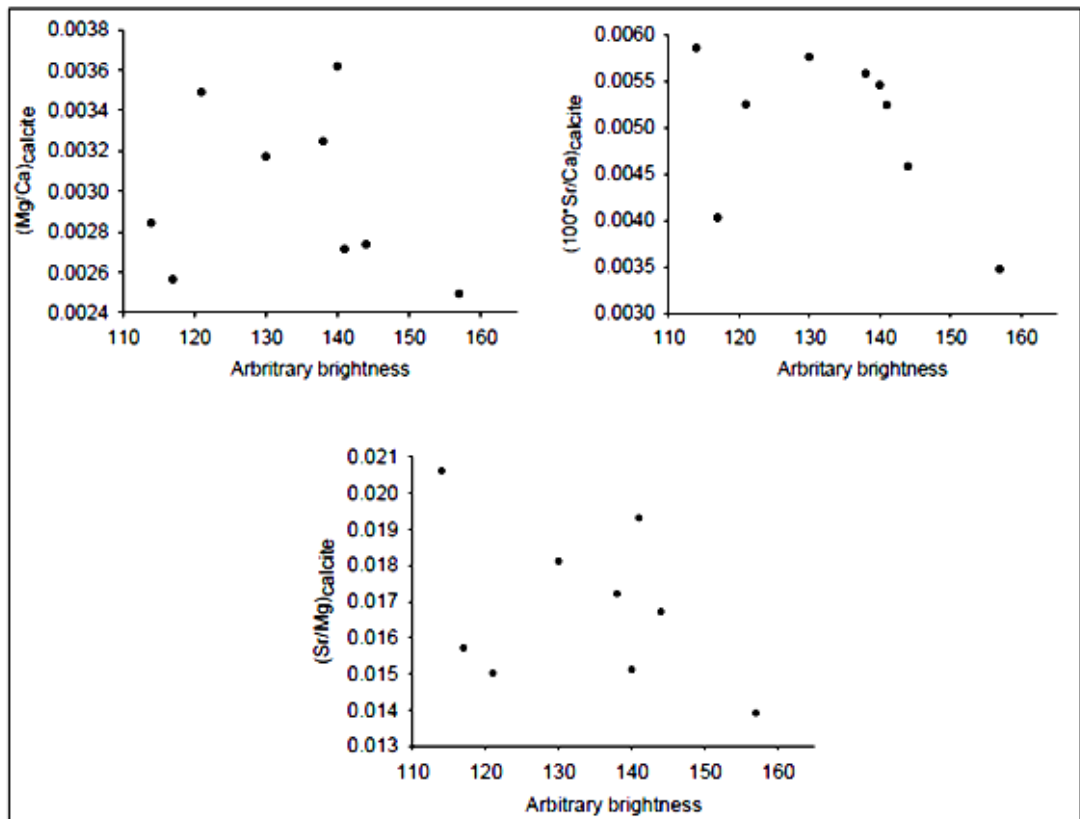
Figure 7.15 Trace element ratios from line 3 vs. lamination colour brightness.
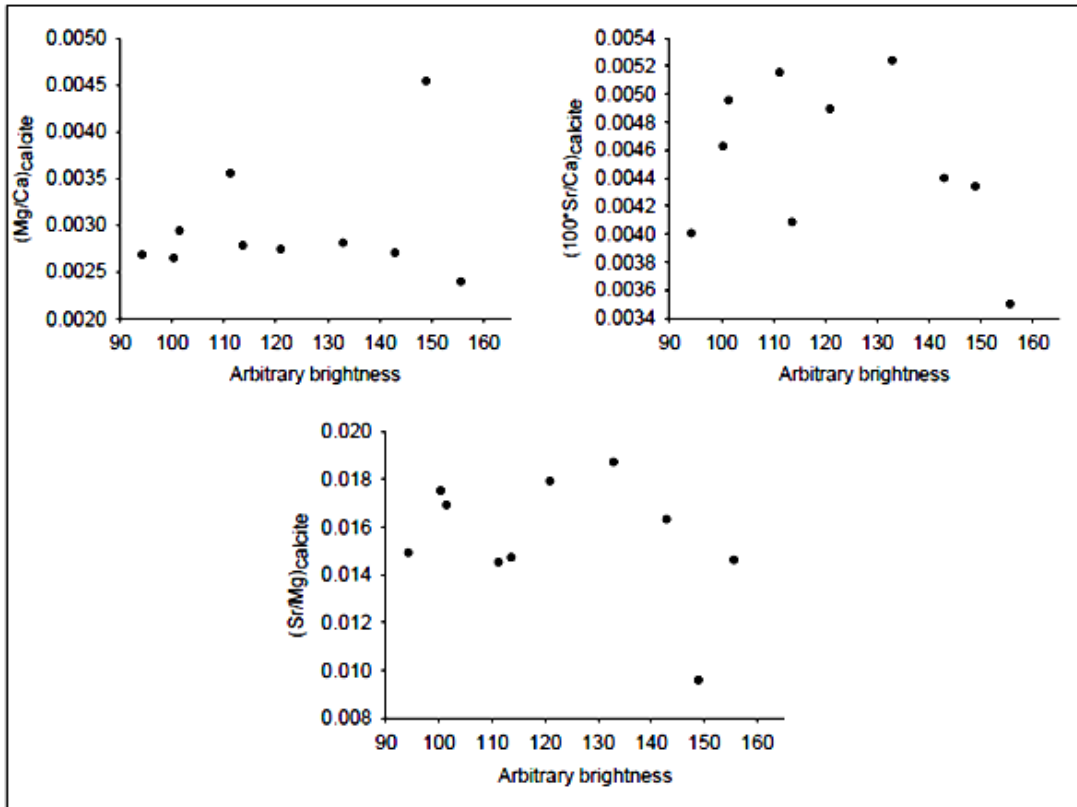
Figure 7.16 Trace element ratios from line 4 vs. lamination colour brightness.
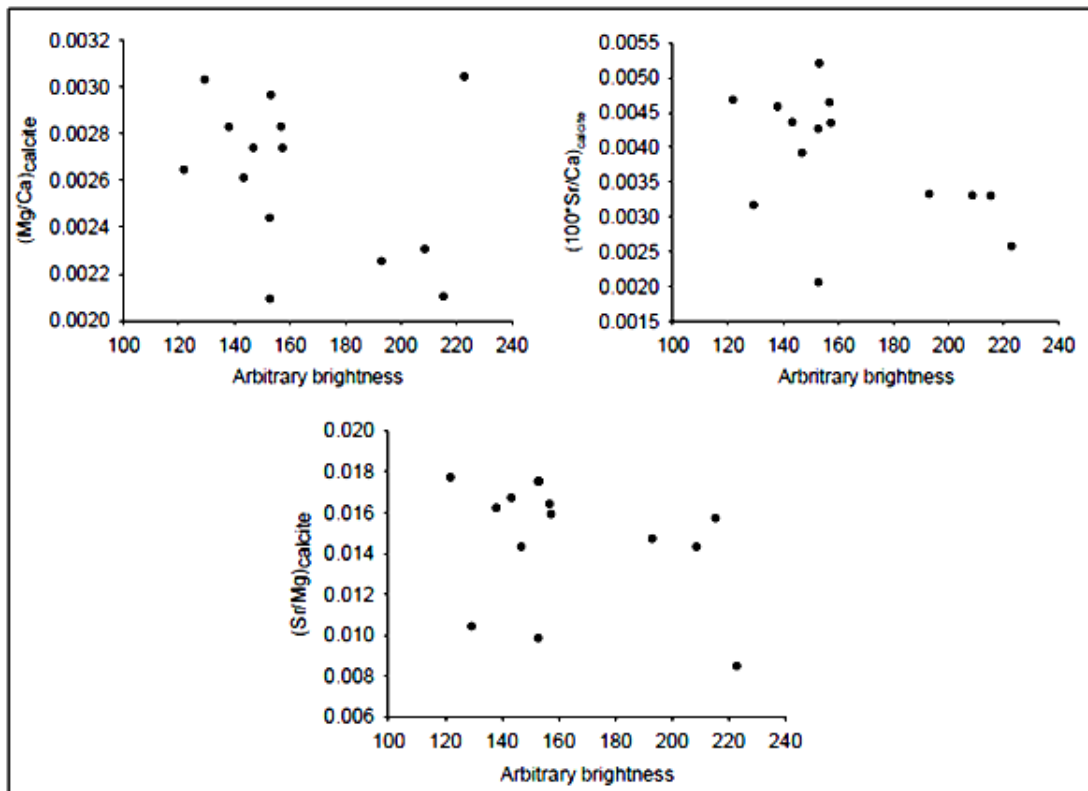
Figure 7.17 Trace element ratios from line 5 vs. lamination colour brightness.

There is no significant relationship between the parameters for any of the data plots contained within Figures 7.13 - 7.17.

7.5 Discussion

7.5.1 (Mg/Ca)$_{calcite}$ ratios

The (Mg/Ca)$_{calcite}$ profiles obtained from the Caerwys tufa show no overall consistent correlation with distance from the internal edge of the sample. The studies detailed in chapters 5 and 6 have highlighted the extent to which factors such as precipitation rate, temperature and in particular the presence of microorganisms and their associated extracellular substances can cause significant variations in the (Mg/Ca)$_{calcite}$ ratios of freshwater tufa calcite. There is however a statistically significant linear relationship between (Mg/Ca)$_{calcite}$ and the distance from the internal edge in the material recovered from the drilling of line 5. The value of (Mg/Ca)$_{calcite}$ reduces as the sampling point moves away from the inner edge, given that the sample represents tufa that has grown around a reed, the internal edge represents the oldest part of the deposit, so (Mg/Ca)$_{calcite}$ ratios decreased as the deposit grew over time. The (Mg/Ca)$_{calcite}$ ratio of the sampling point closest to the inner edge of this sampling line was 44 % higher than that at sampling point furthest from the internal edge.

Thermodynamics predicts that (Mg/Ca)$_{calcite}$ ratios will increase by about 3 % per °C, although in biogenic calcites such as foraminiferal deposits the sensitivity of the Mg/Ca ratio is around 9 ± 1 % per °C (Rosenthal and Linsley, 2006). However, the experiments described in chapter 5 reveal that these relationships do not hold for calcite precipitated in a fluvial system in the presence of a biofilm. As biofilms are ubiquitous in fluvial environments it is reasonable to assume that the tufa deposit in this study was precipitated in the presence of a biofilm of some degree of establishment. Applying the weak but significant correlation obtained in the microcosm experiments of chapter 5 to the 44 % change in (Mg/Ca)$_{calcite}$ across line 5 gives a temperature change of about 1 °C. However, it is not possible to attribute this correlation to part of a seasonal temperature change. The distance between the two end sampling points is 6.5 mm, given that tufas have been reported to have annual growth rates in the range of millimetres to centimetres (Matsuoka *et al.*, 2001,

Ihlenfeld *et al*., 2003, Liu *et al*., 2006) then the section of deposit examined could represent months growth or it may represent 6 – 7 years of growth. The correlation observed in line 5 pattern was not present in lines 1 to 4, in fact in line 1 the $(Mg/Ca)_{calcite}$ ratio was higher at the outer edge than the inner edge suggesting that the temperature had moved in the opposite direction to that implied by the ratios in line 5.

All points around the sample at a given distance from the internal edge must have been deposited at the same time and therefore at the same temperature. If thermodynamic controls were solely responsible for the $(Mg/Ca)_{calcite}$ ratios of the deposit then it would be expected that the $(Mg/Ca)_{calcite}$ ratios would be the same at a given distance from the internal edge at any point around the sample. Analyses of the $(Mg/Ca)_{calcite}$ ratios in this Caerwys tufa sample showed that for any given distance from the internal edge the ratios varied by about 31 – 210 %. The results of the microcosm experiments described in chapter 5 show a weak but statistically significant ($P < 0.05$) correlation between $(Mg/Ca)_{calcite}$ and precipitation temperature where $(Mg/Ca)_{calcite}$ ratios decreased as temperature increased (Figure 5.1). Applying the calibration equation obtained from this correlation to the maximum and minimum ratios at a given distance for the internal edge gives the temperature change inferred by the differences in the two ratios. Table 7.2 shows the inferred temperature changes from these calculations. In addition, it shows the inferred temperature changes using the relationship derived for foraminiferal calcite (about a 9 % change in $(Mg/Ca)_{calcite}$ per °C temperature change) and also for the expected thermodynamic control (about a 3 % change in $(Mg/Ca)_{calcite}$ per °C temperature change).

Table 7.2 Inferred temperature change from difference between maximum and minimum (Mg/Ca)$_{calcite}$ ratios from different correlation equations

	Correlation		
Distance from internal edge (mm)	Microcosm equation Inferred temperature change (°C)	Foraminferal calcite Inferred temperature change (°C)	Thermodynamic Inferred temperature change (°C)
0.5	1.0	5	14
1	3.3	16	47
1.5	2.3	11	32
2	1.2	6	17
2.5	0.7	3	9
3	2.3	11	32
3.5	1.3	6	19
4	1.8	9	26
4.5	4.9	23	70
5	2.8	13	40
5.5	0.7	3	10
6	1.5	7	22
6.5	1.6	7	22
7	3.9	19	56

The inferred temperature changes obtained using the accepted thermodynamic control on Mg^{2+} partitioning quite clearly show that the thermodynamics is not the dominant control on (Mg/Ca)$_{calcite}$ ratios across the tufa sample. The inferred temperature changes are considerably smaller when the calibration equation obtained from the microcosm experiments is used. However, it still infers temperature variations of up to about 5 °C which in reality cannot have existed as the precipitation at any given distance from the internal edge will have taken place at the same temperature around the whole circumference of the deposit.

The finding that (Mg/Ca)$_{calcite}$ ratios in this Holocene tufa sample vary significantly on a millimetre spatial scale and consequently infer temperature changes that cannot have existed strongly indicates that obtaining (Mg/Ca)$_{calcite}$ palaeotemperature data from fossil tufas is not viable. The findings of Chafetz, (1991) and Ihlenfeld *et al*., (2003) that tufa (Mg/Ca)$_{calcite}$ ratios appeared to be thermodynamically controlled may represent fortuitous sampling. The data in Table 7.2 show two occasions when the inferred temperature change was only 0.7 °C, therefore, the fortuitous sampling of a fossil tufa could possibly produce results which suggest a thermodynamic correlation exists when in fact it does not.

7.6 (100*Sr/Ca)$_{calcite}$ ratios

The observation that there is a significant correlation between (100*Sr/Ca)$_{calcite}$ and distance from the internal edge of the sample in lines 1, 2, 5 and in all lines combined is interesting as the nature of the correlation is similar to that observed in line 5 for (Mg/Ca)$_{calcite}$ ratios. Although this correlation is absent in lines 3 and 4 this may be due to the lack of sampling points from these lines due to the outer edge being missing in this section of the sample. The range of (100*Sr/Ca)$_{calcite}$ ratios across sampling lines 1, 2 and 5 showed a decrease from the highest to lowest values of 505, 158 and 154 % respectively. Reported values for the percentage change in (Sr/Ca)$_{calcite}$ values induced by temperature variations are in the range of only about 0.4 – 1 % per °C (Lea *et al*, 1999, Russell *et al*., 2004). The large percentage variations seen in the (Sr/Ca)$_{calcite}$ values of this tufa sample cannot therefore be attributable solely to temperature variations. Precipitation rate is one of the major factors controlling Sr^{2+} incorporation and has a strong positive correlation with Sr incorporation (Tesoriero and Pankov, 1996, Gabitov and Watson, 2006, Nehrke *et al*., 2007) (Figure 7.18).
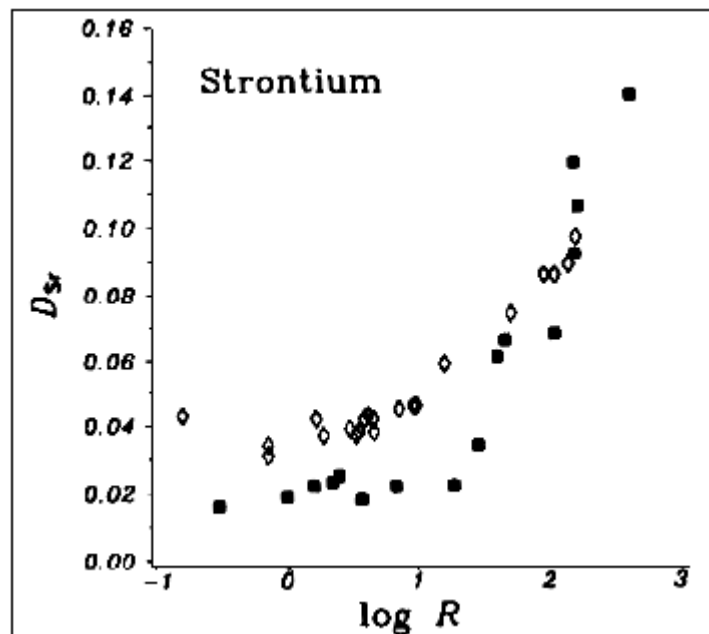
Figure 7.18 Partition coefficients of Sr^{2+} in to calcite as a function of precipitation rate (Tesoriero and Pankow, 1996).

The increasing value of the partition coefficient (D_{Sr}) in Figure 7.18 with increasing precipitation rate will result in greater (Sr/Ca)$_{calcite}$ ratios at faster precipitation rates. The decreasing trend in (Sr/Ca)$_{calcite}$ values in drilling lines 1, 2 and 5 (and the weak

correlation in all lines combined) suggests (according to Figure 7.18) that the precipitation rate of the Caerwys tufa sample was reducing over time. This may not be the case however, line 5 also showed a statistically significant decrease in $(Mg/Ca)_{calcite}$ ratios as the sample grew. The results of the experiments in chapters 5 and 6 clearly demonstrate that $(Mg/Ca)_{calcite}$ values decrease with increasing precipitation rates due to the presence of microbial biofilms and their associated EPS molecules. On the assumption that the correlation derived in the experiments of chapters 5 and 6 is true then precipitation rates were increasing with time in the sample examined. Therefore, Sr/Ca ratios should have been increasing as the deposit grew, however in this sample the Sr/Ca ratios were falling as the deposit grew. It is suggested that this reversed relationship is due to the presence of a microbial biofilm at the precipitating surface impacting on Sr incorporation through the same mechanisms described in chapter 5 for Mg incorporation into calcite.

7.7 $(Sr/Mg)_{calcite}$ ratios

The presence of a weak but significant correlation between $(Sr/Mg)_{calcite}$ ratios and the distance from the internal edge of the sample may a consequence of the presence of a microbial biofilm on the surface of the precipitating tufa. As discussed in chapter 2, section 2.10 anionic functional groups within the EPS matrix of a biofilm remove cations from the bulk water solution through the process of chelation. It has been shown experimentally that the chelation of cations is a chemoselective process with selectivity being in favour of larger ions with smaller charge densities (z_i^2/r_i), so chelation preferences will follow the order $Ba^{2+} > Sr^{2+} > Ca^{2+} > Mg^{2+}$ (Rogerson *et al*., 2008). Therefore Sr^{2+} will be preferentially chelated over Mg^{2+} within the biofilm matrix at the surface of the precipitating tufa. The tufa sample in this study was growing around a reed, therefore as it grows outward its circumference will increase giving a greater surface area for biofilm colonisation. A larger biofilm mat will present a greater number of chelation sites resulting in the water in the immediate microenvironment of the EPS molecules becoming increasingly depleted in Sr^{2+} with respect to Mg^{2+}. The greater depletion of Sr^{2+} over Mg^{2+} through chemoselective chelation will have caused Sr/Ca ratios in the solution from which the precipitates are generated to decrease to a greater extent than Mg/Ca ratios. Consequently, precipitates generated in this environment will become increasingly

depleted in Sr over Mg, offering a possible explanation to the falling Sr/Ca ratios as the deposit grew.

7.8 Laminations and trace element ratios

The profiles of the colour banding analyses of lines $1 - 5$ (Figures $7.8 - 7.12$) indicate that the 'brightness' of the laminations generally decreased with distance from the internal edge. In contrast to this is the observation that the trace element ratios shown in the same Figures generally decrease with distance from the internal edge of the sample. This suggests that there may be a significant correlation between the trace element ratios and the colour of the laminations. However, when the individual points are plotted against the trace element ratios (Figures $7.13 - 7.17$) there is no significant relationship between the trace element ratios $(Mg/Ca)_{calcite}$, $(Sr/Ca)_{calcite}$ and $(Sr/Mg)_{calcite}$ and the laminations of the tufa sample.

Figure 7.1 (a) shows a clear distinction between the dense and porous layers of the tufa deposit, comparing the Caerwys tufa sample examined in this study (Figure 7.4) with Figure 7.1 (a) indicates that the Caerwys sample is representative of the denser material in Figure 7.1 (a). Examination of the actual hand specimen also suggests that it is solely composed of the denser deposits; the porous material is absent indicating it may represent a summer - autumn deposit meaning that the deposit was laid down under a small temperature range. However, without knowing the actual deposition rate for this tufa it remains speculative that this sample represents part of a single summer – autumn deposit. Visual inspection under a hand lens reveals that there are a number of submillimetric laminations within this tufa sample, some of which are visible in Figure 7.4. Due to the size of the drill bit used in drilling of this sample there will inevitable have been some drilling samples that consisted of material from two or more submillimetric laminations. As such the trace element ratios in some cases can only be considered as homogenised material from these submillimetric laminations.

7.9   Conclusion

This study has examined $(Mg/Ca)_{calcite}$ and $(Sr/Ca)_{calcite}$ ratios in a laminated Holocene tufa deposit from Caerwys, North Wales. The sample represented about

half of a circular deposit which had encrusted the subaqueous part of a reed. Material from the sample was obtained through the drilling of five concentrically spaced lines in 0.5 mm steps using a modified dentist's drill. With the exception of line 5 there was no significant correlation between $(Mg/Ca)_{calcite}$ and the distance from the internal edge. Large variations (31 - 210 %) were seen in $(Mg/Ca)_{calcite}$ ratios of precipitated material deposited at a given distance from the internal edge. Due to the circular nature of the sample, precipitates deposited at a given distance from the internal edge must have been laid down at the same instant in time and consequently under the same ambient temperatures. The temperature changes inferred by the variations in $(Mg/Ca)_{calcite}$ cannot have existed in reality. It is therefore likely that the variations observe are due to the presence of a microbial biofilm on the tufa surface. This suggestion is supported by the results of the microcosm experiments described in chapter 5 which show considerable variations in $(Mg/Ca)_{calcite}$ in the temperature range of 12 – 18 °C.

$(Sr/Ca)_{calcite}$ was found to be correlated with distance from the internal edge in lines 1, 2, 5 and when all lines were combined, although the correlation was weak. The nature of the relationship between these parameters was the same as that observed in line 5 for $(Mg/Ca)_{calcite}$. However, the percentage changes across the lines 1, 2 and 5 of 505, 158 and 154 % respectively cannot be attributed to temperature changes. Previous studies have shown that the sensitivity of $(Sr/Ca)_{calcite}$ to temperature changes is only about 0.4 – 1 % per °C. Similarly to the variations seen in $(Mg/Ca)_{calcite}$ in this sample the Sr/Ca trace element ratios appear to have been influenced by the presence of microbial biofilms. The absence of coherent trace element ratios from the Holocene tufa sample analysed in this study strongly suggests that microbial biofilms were present on the precipitating surface of this tufa. The results add further weight to the conclusions from the experiments conducted for this thesis that $(Mg/Ca)_{calcite}$ ratios in fossil tufas are not a source of high resolution palaeotemperature data.

8 Conclusion and future work

A series of experiments have investigated whether $(Mg/Ca)_{calcite}$ ratios in ambient temperature freshwater carbonate deposits can be used as a palaeotemperature proxy. The $(Mg/Ca)_{calcite}$ proxy in marine carbonates is a significant tool in reconstructing palaeoclimate but this success has not been matched by freshwater carbonates. The metabolic processes of microbial biofilms and their associated extracellular polymeric substances have been suggested as a complicating factor in deriving a palaeotemperature calibration equation for tufa $(Mg/Ca)_{calcite}$. A novel experimental design allowed the precipitation of freshwater calcite in a microcosm environment under multiple ambient temperatures in the presence of a biofilm from a solution with a constant Mg/Ca ratio. The results of these experiments provide strong evidence that the expected thermodynamic control in Mg^{2+} incorporation into tufa carbonates is overridden by the presence of the biofilm and that the heterogeneous and ever changing nature of biofilms can lead to large scale variations in $(Mg/Ca)_{calcite}$ ratios at any given temperature.

In the temperature range of 12 - 18 °C the $(Mg/Ca)_{calcite}$ ratios varied by as much as about an order of magnitude at a given temperature, however at 20 °C the ratios were very well constrained suggesting that somewhere between 18 and 20 °C there is a threshold whereby $(Mg/Ca)_{calcite}$ precipitated in the presence of a biofilm is controlled by a dominant factor that can override the influence of a heterogeneous biofilm composition. Further support for the existence of this threshold comes from the precipitation rates over the same temperature range. In the range 12 - 18 °C increasing temperature had no significant impact on precipitation rate, mean rates were approximately the same for 12, 14 and 18 °C, at 16 °C the rate was lower. The expected impact of increasing temperature was only seen at 20 °C, with the mean rate being between 8 and 21 times that of the 12, 14 and 18 °C rates and about 81 times greater than the rate at 16 °C. The results show that the presence of a biofilm has a significant impact on both $(Mg/Ca)_{calcite}$ ratios and precipitation rate in the temperature range of 12 – 18 °C but at 20 °C temperature appears to be the dominant control.

In the microcosm experiments there was a weak but significant linear correlation between $(Mg/Ca)_{calcite}$ and temperature where $(Mg/Ca)_{calcite}$ ratios fell with increasing temperature. This is in direct contrast to the anticipated exponential increase in $(Mg/Ca)_{calcite}$ ratios with increasing temperature under a thermodynamic control. A negative power correlation was observed between precipitation rates and $(Mg/Ca)_{calcite}$ ratios, again this was in contrast to previous studies which show that Mg partitioning into calcite increases at faster precipitation rates.

The explanation for these contrasting behaviours appears to be the chemoselective chelation of Ca^{2+} over Mg^{2+} by anionic functional groups within the EPS matrix which creates at region of low $(Mg/Ca)_{solution}$ from which precipitation takes place. This effect is accentuated at faster precipitation rates and by the trapping of ligand – Ca^{2+} complexes within the growing crystal. It was unclear however whether the low $(Mg/Ca)_{calcite}$ generated at faster precipitation rates in the presence of biofilm required the presence of the actual living organisms or was it simply the existence of the chemoselective anionic functional groups of the EPS molecules.

An answer to this question was obtained through a series of experiments conducted in agitated conical flasks at the same temperatures as the microcosm experiments. In these experiments no biofilm was added to the precipitating solution. Instead, EPS molecules which had been isolated from the biofilm were added. These experiments provided some interesting results. The weak but significant negative linear correlation between $(Mg/Ca)_{calcite}$ and temperature seen in the biofilm experiments was not found. Instead two distinct behaviours were noted. In the temperature range of $12 – 18\ °C$ the expected thermodynamic control on Mg^{2+} incorporation into calcite was found with $(Mg/Ca)_{calcite}$ increasing exponentially with increasing temperature. The exponential constant of the observed relationship matched well with those derived from a number of studies on marine carbonates. Similarly to the results from the microcosm experiments the $(Mg/Ca)_{calcite}$ ratios at $20\ °C$ were distinctly separate from those seen at the other temperatures, instead of following the exponential increase they had fallen to values lower than at $12\ °C$. Examination of the precipitation rate again showed that at $20\ °C$ the rates were significantly higher, being about $5 – 12$ times higher than the rates at $12 – 18\ °C$.

Again, there appears to be a threshold between 18 and 20 °C whereby trace element partitioning is dominantly controlled by a factor which differs from that controlling it at 12 – 18 °C. In light of the fact that at 12 – 18 °C the $(Mg/Ca)_{calcite}$ values were following the relationship expected from thermodynamic control it is unlikely that the sudden change in behaviour seen at 20 °C is a direct consequence of the temperature change from 18 to 20 °C. It is proposed that this change in behaviour of Mg^{2+} partitioning into calcite in the presence of isolated EPS molecules is instead indirectly linked to the change in temperature from 18 to 20 °C through the influence on precipitation rate. Similarly to the precipitates generated in the presence of living biofilms, there is a significant negative power correlation whereby $(MgCa)_{calcite}$ ratios are reduced at higher precipitation rates. Again, this is attributed to the chemoselective chelation of Ca^{2+} over Mg^{2+} by anionic functional groups within the EPS matrix and the trapping of ligand – Ca^{2+} complexes within the growing crystal.

The exponential correlation between $(Mg/Ca)_{calcite}$ and temperature at 12 – 18 °C observed in the isolated EPS precipitates was not found in the precipitates generated in the presence of the living biofilm. This strongly suggests that it is microbial metabolism that leads to this relationship being absent in the biofilm precipitates and not the simple presence of the EPS molecules. The EPS molecules do however appear to be the driving force behind the fact that $(Mg/Ca)_{calcite}$ ratios decrease with increasing precipitation rates. This behaviour was observed in the precipitates from both the living biofilm and the isolated EPS molecules and is in direct contrast to studies on inorganic calcite which show that $(Mg/Ca)_{calcite}$ ratios increase when precipitation rates are raised.

Petri dish experiments were conducted to assess the impact of varying salinities on $(Mg/Ca)_{calcite}$ ratios in both the presence and absence of isolated EPS molecules. Additionally a further set of Petri dish experiments were conducted to examine the effect of different concentrations of isolated EPS molecules on $(Mg/Ca)_{calcite}$ ratios. There is an increasing acceptance that variations seen in the $(Mg/Ca)_{calcite}$ ratios of marine carbonates are not solely attributable to temperature variations, but may also reflect salinity variations. Salinity variations have been shown to cause about a 4 ± 3 % increase in $(Mg/Ca)_{calcite}$ per ppm change in salinity in marine biogenic carbonates. The results of this study add strength to this relationship as $(Mg/Ca)_{calcite}$ ratios

179

increased by about 3 % per ppm change in salinity in the precipitates generated in the presence of isolated EPS molecules. However, there was no correlation between these parameters in the precipitates generated in the absence of EPS molecules which suggests that the presence of organic molecules is needed for salinity variations to have a significant impact on $(Mg/Ca)_{calcite}$ ratios.

The salinity variation experiments provided further evidence that the chemoselective chelation of Ca^{2+} over Mg^{2+} by anionic functional groups within the EPS matrix is the main mechanism driving down $(Mg/Ca)_{calcite}$ ratios with increasing precipitation rates. The same negative power correlation between $(Mg/Ca)_{calcite}$ and precipitation rate that was seen in the biofilm and agitated flask isolated EPS experiments was also found in this experiment in the precipitates from the replicates containing isolated EPS molecules. The precipitates from the replicates without EPS showed no such correlation.

The experiments involving differing levels of EPS molecules in the precipitating solution revealed that precipitation rates were reduced as EPS levels increased. Although the presence of EPS has been suggested to be an inhibiting factor in calcite precipitation rates in marine stromatolites it has also been suggest that in the low ionic conditions of a freshwater environment the presence of EPS molecules would actually enhance precipitation rates. Various competing influences on precipitation rate can be attributed to EPS molecules. The provision of nucleation sites on EPS molecules combined with the reduction in the activation energy at these heterogeneous nucleation can act to facilitate precipitation rates. Conversely, the presence of organic molecules such as EPS can act as an inhibiting factor in calcite precipitation rates through their adsorption to the growing crystal and consequent blocking of nucleation sites. The similar pattern of decreasing precipitation rates at increasing EPS levels found in this study to studies involving increased levels of specific functional groups provides further support to the assertion that increasing levels of organic material adsorbing onto the crystal surface is an inhibitory mechanism in calcite precipitation.

There was no statistically significant correlation between $(Mg/Ca)_{calcite}$ and precipitation rate in the precipitates generated from solutions with varying

concentrations of EPS. This finding is in contrast to the negative power relationship seen in all other experiments when either isolated EPS or a living biofilm was present. However, when the data from this experiment was added to that from the salinity experiment they were found to fit well and strengthened the correlation. The lack of a correlation in the data in isolation is attributed the small range of precipitation rates over which the precipitates were generated (see Figure 6.17).

A laminated Holocene tufa sample from Caerwys, North Wales was examined to ascertain whether its $(Mg/Ca)_{calcite}$ and $(Sr/Ca)_{calcite}$ ratios contained any potential palaeoenvironmental data. The sample studied was a semi-circle of a deposit that had encrusted the subaqueous stem of a reed. The results from this sampling provided no consistent statistically significant correlations between the trace element ratios and the distance from the internal edge of the deposit nor with the colours of the laminations. There was however, a general trend for trace element ratios to decrease with increasing distance from the internal edge. Given the circular nature of the deposit this means that the trace element ratios were decreasing as the deposit grew. The clear association between precipitation rate and low $(Mg/Ca)_{calcite}$ in the presence of biofilms suggests that the precipitation rate was increasing as the deposit grew and that there was a biofilm covering the precipitating surface.

$(Mg/Ca)_{calcite}$ ratios in the Caerwys tufa varied between 31 and 210 % in precipitates deposited at the same time and spatially separated by less than 1 cm. If thermodynamics was the controlling factor on these large scale variations in Mg partitioning it would require temperature differences in the stream water around the circumference of the deposit at any given time to be between 9 and 70 °C. In reality the temperature had to have been equal around the circumference of the deposit. The variations seen in $(Mg/Ca)_{calcite}$ of the Caerwys tufa sample are likely to be a consequence of the presence of a biofilm on the tufa surface and again adds further support to the assertion that $(Mg/Ca)_{calcite}$ ratios held in fossil tufas are not a reliable source of high resolution palaeotemperature data.

8.1 Main conclusions

The main conclusions reached in this thesis are:

1/   The absence of the expected thermodynamic control on the partitioning of Mg^{2+} into calcite precipitated in the presence of a microbial biofilm is a consequence of the metabolic processes of the organisms and not simply the presence of extracellular polymeric substances.

2/   The decreasing $(Mg/Ca)_{calcite}$ ratios seen at higher precipitation rates are due to the presence of extracellular polymeric substances and their ability to selectively chelate Ca^{2+} over Mg^{2+}. The presence of living organisms and their metabolic processes is not required for this mechanism to exist.

3/   Results from the salinity experiment confirm the results of previous studies which show that $(Mg/Ca)_{calcite}$ ratios increase by about 3 % per ppm increase in salinity. The results also suggest that organic molecules need to be present in the precipitating solution for this relationship to exist.

4/   The results of the experiments described in this thesis, combined with the examination of a Holocene tufa sample, indicate that $(Mg/Ca)_{calcite}$ ratios in fossil tufas cannot be considered a reliable source of palaeotemperature data.

8.2 Future work

The experiments conducted have provided a first insight into the role of microbial biofilms on Mg/Ca ratios in freshwater ambient temperature carbonate deposits and suggest that further work could be carried out to further the investigation.

8.2.1 Expansion of the microcosm experiments

The microcosm experiments were kept necessarily on a small scale due to space limitations for both the housing of the water bath and the tank containing the experimental solution. Furthermore, the duration of each experiment was limited due

to time constraints. The precipitates generated in this study were at the microscopic scale. It is unclear whether the relationships derived from them will hold up at the macroscopic scale. An alternative approach to assessing the potential of tufas $(Mg/Ca)_{calcite}$ would be to conduct experiments in a larger flume similar to that used to colonise the calcite free biofilm for this study. Although this would probably mean that the system would operate as a recirculating one (as used by Rogerson *et al*., 2008 and Pedley *et al*., 2009) the use of programmable dosing pumps to supply Ca^{2+} and Mg^{2+} cations to replace that lost to precipitates and chelation could ensure a reasonably constant $(Mg/Ca)_{solution}$, which could be monitored via frequent sampling and continuous conductivity monitoring. The increased and variable flow rates generated by the uneven topography of the larger scale biofilm and precipitates would more closely mimic a mature natural system. Temperature control could be maintained through the use of in line chiller units. The generation of large scale deposits would allow spot sampling within different regions of the biofilm to assess its impact on $(Mg/Ca)_{calcite}$ ratios. If the presence of the biofilm was overriding the thermodynamic control, as indicated in this work, then the $(Mg/Ca)_{calcite}$ ratios would be expected to vary widely and would not follow thermodynamic expectations.

8.2.2 Bioremediation of contaminated waters

The heavy metal chelating capacities of microbial EPS molecules has frequently been utilised to remove contaminating cations such as Pb, Hg, Ni and Cd from aqueous environments (Bhaskar and Bhosle, 2006). Previous studies have shown that EPS isolated from single species chelates metals in s selective fashion. EPS isolated from *Marinobacter.* sp. was able to chelate 182 nmol of Cu^{2+} but only 13 nmol of Pb^{2+} mg^{-1} of EPS (Bhaskar and Bhosle, 2006). A number of factors have been recognised as influencing the maximum binding abilities of EPS such as pH, light intensity, biofilm density and the tolerance of individual species to heavy metals (Roeselers *et al*., 2008).

The ability of a biofilm to grow and thrive in a laboratory environment which mimics natural conditions by the use of hydroponic lamps opens up the possibility of assessing the chelation potential of biofilms for cationic contaminants in natural waters under a variety of different pH and light intensities. Utilising a flume similar

to that used to colonise the calcite free biofilm for this study will allow the dosing of the experimental waters with differing contaminants to known concentrations. By repeating the experiments with biofilms containing different compositions of organisms it may be possible to determine which consortium of microorganism is best adapted to removing specific contaminants from the water. Adding a number of different contaminants at the same time will allow selectivity preferences for specific biofilms to be determined and provide information on which specific consortium of microorganisms would be best suited to waters with a given profile of contaminants.

8.2.3 Restoration of stone monuments and buildings

The potential use of microorganisms in the restoration and preservation of historic limestone buildings and monuments is increasingly being recognised (e.g. Cacchio *et al*., 2003, Webster and May, 2006, Jroundi *et al*., 2012). However, the extent to which different microorganism promote calcite precipitation varies, furthermore, although some microorganisms are effective as agents of calcite precipitation, the precipitates generated are not necessarily suitable for consolidation of damaged stone works (Jroundi *et al*., 2012). The proven long term survival of microbial biofilms in laboratory flumes, (e.g. this work and Rogerson *et al*., 2008, Pedley *et al*., 2009) provides a unique opportunity to test the consolidation potential of calcite precipitated from biofilms of differing compositions. Samples of damaged stone representative of specific monuments or buildings could be placed within the flume in the presence of differing compositions of microorganisms in a solution saturated with respect to calcite. Over time calcite would become deposited onto the damaged stone. The recovered stone samples can be analysed to determine which group of microorganisms provided the best calcite deposits for consolidation of the sample. This knowledge would be highly beneficial to the restoration community and help preserve historic buildings and monuments for future generations.

Appendix

The appendix contains tables of data used in the generation of the graphs in this thesis. The data presented have been processed from the original ICP − OES output by the application of relevant dilution factors, experiment duration, volume of acid used to dissolve the precipitates. Errors in the $(Mg/Ca)_{calcite}$ ratios were determined using standard propagation of error techniques as detailed in chapter 4, section 4.5.2. All errors are stated as 1 standard deviation (1σ).

Data for calcite precipitated from the flow-through microcosm experiments

Temperature (°C)	Temperature 1σ (°C)	Precipitation rate (μmol cm^{-1} hr^{-1})	$(Mg/Ca)_{calcite}$ (molar ratio)	$(Mg/Ca)_{calcite}$ 1σ
12.2	0.2	0.0509	0.0292	0.0003
12.2	0.2	0.0153	0.0644	0.0006
12.2	0.2	0.0286	0.0380	0.0005
12.2	0.2	0.0136	0.0750	0.0010
14.3	0.2	0.0060	0.0644	0.0008
14.3	0.2	0.0953	0.0069	0.0001
14.3	0.2	0.0389	0.0205	0.0001
16.3	0.2	0.0054	0.0438	0.0005
16.3	0.2	0.0051	0.0331	0.0009
16.3	0.2	0.0103	0.0421	0.0006
18.3	0.2	0.0723	0.0192	0.0001
18.3	0.2	0.0264	0.0414	0.0012
18.3	0.2	0.0915	0.0123	0.0003
18.3	0.2	0.0683	0.0144	0.0005
20.6	0.5	0.6083	0.0117	0.0002
20.6	0.5	0.4583	0.0095	0.0002
20.6	0.5	0.5972	0.0110	0.0002
20.6	0.5	0.6333	0.0116	0.0003

Agitated flask data for calcite precipitates generated in the presence of biofilm exposed to light

Temperature (°C)	Temperature 1σ (°C)	Precipitation rate (μmol cm^{-1} hr^{-1})	(Mg/Ca)$_{calcite}$ (molar ratio)	(Mg/Ca)$_{calcite}$ 1σ
12.1	0.5	0.0179	0.0373	0.0013
12.1	0.5	0.0063	0.0633	0.0012
14.3	0.2	0.1120	0.0248	0.0004
14.3	0.2	0.1009	0.0209	0.0002
16.3	0.2	0.0565	0.0185	0.0003
16.3	0.2	0.1685	0.0173	0.0002
18.3	0.2	0.0398	0.0186	0.0004
18.3	0.2	0.0066	0.0772	0.0007
20.6	0.5	0.1778	0.0126	0.0002
20.6	0.5	0.1759	0.0146	0.0002

Agitated flask data for calcite precipitates generated in presence of biofilm excluded from light.

Temperature (°C)	Temperature 1σ (°C)	Precipitation rate (μmol cm^{-1} hr^{-1})	(Mg/Ca)$_{calcite}$ (molar ratio)	(Mg/Ca)$_{calcite}$ 1σ
12.1	0.5	0.0062	0.0378	0.0004
12.1	0.5	0.0048	0.0535	0.0009
14.3	0.2	0.0764	0.0235	0.0004
14.3	0.2	0.0348	0.0229	0.0002
16.3	0.2	0.0310	0.0094	0.0001
16.3	0.2	0.0375	0.0111	0.0001
18.3	0.2	0.0662	0.0174	0.0002
18.3	0.2	0.0048	0.0738	0.0015
20.6	0.5	0.1287	0.0077	0.0001
20.6	0.5	0.1037	0.0082	0.0002

Agitated flask data for calcite precipitates generated in the presence of isolated EPS

Temperature (°C)	Temperature 1σ (°C)	Precipitation rate (μmol cm^{-1} hr^{-1})	(Mg/Ca)$_{calcite}$ (molar ratio)	(Mg/Ca)$_{calcite}$ 1σ
12.1	0.5	0.0144	0.0124	0.0001
12.1	0.5	0.0094	0.0301	0.0003
14.3	0.2	0.0089	0.0368	0.0002
14.3	0.2	0.0111	0.0198	0.0004
16.3	0.2	0.0086	0.0262	0.0003
16.3	0.2	0.0030	0.0620	0.0007
18.3	0.2	0.0043	0.0915	0.0015
18.3	0.2	0.0046	0.1015	0.0011
20.6	0.5	0.0630	0.0065	0.0001
20.6	0.5	0.0588	0.0062	0.0001

Data for calcite precipitated under varying levels of EPS in the precipitating

Vol of EPS solution added (mL)	Precipitation rate (μmol cm^{-1} hr^{-1})	(Mg/Ca)$_{calcite}$ (molar ratio)	(Mg/Ca)$_{calcite}$ 1σ
0	0.0245	0.0559	0.0010
0	0.0207	0.0520	0.0009
0	0.0215	0.0501	0.0006
0	0.0240	0.0566	0.0012
5	0.0143	0.0864	0.0008
5	0.0118	0.0749	0.0006
5	0.0122	0.0738	0.0014
5	0.0104	0.0734	0.0016
4	0.0115	0.0714	0.0022
4	0.0166	0.0741	0.0006
4	0.0121	0.0828	0.0016
3	0.0181	0.0781	0.0012
3	0.0176	0.0748	0.0007
3	0.0156	0.0754	0.0018
3	0.0133	0.0759	0.0013
2	0.0149	0.0667	0.0008
2	0.0137	0.0639	0.0007
2	0.0204	0.0718	0.0012
2	0.0144	0.0712	0.0010
1	0.0179	0.0744	0.0015
1	0.0166	0.0739	0.0015
1	0.0149	0.0708	0.0026
1	0.0214	0.0743	0.0025

Data for calcite precipitated under varying salinities in the absence of EPS.

Salinity (ppm)	Precipitation rate (μmol cm^{-1} hr^{-1})	(Mg/Ca)$_{calcite}$ (molar ratio)	(Mg/Ca)$_{calcite}$ 1σ
0	0.0509	0.0299	0.0009
0	0.0639	0.0510	0.0006
10	0.0187	0.0628	0.0017
10	0.0224	0.0534	0.0008
20	0.0151	0.0518	0.0007
20	0.0183	0.0542	0.0011
30	0.0436	0.0715	0.0010
30	0.0278	0.0532	0.0010
40	0.0189	0.0543	0.0006
40	0.0097	0.0544	0.0008

Data for calcite precipitated under varying salinities in the presence of EPS.

Salinity (ppm)	Precipitation rate (μmol cm^{-1} hr^{-1})	(Mg/Ca)$_{calcite}$ (molar ratio)	(Mg/Ca)$_{calcite}$ 1σ
0	0.1657	0.0184	0.0004
0	0.1296	0.0185	0.0002
10	0.0519	0.0390	0.0007
10	0.0676	0.0229	0.0004
20	0.0935	0.0325	0.0007
20	0.0574	0.0263	0.0005
30	0.0606	0.0404	0.0012
30	0.0365	0.0543	0.0009
40	0.0196	0.0549	0.0011
40	0.0363	0.0470	0.0021

Data from line 1 of tufa drilling. Ratios represent trace element ratios of the tufa calcite.

Distance from edge (mm)	(Mg/Ca)	(Mg/Ca) 1σ	(100*Sr/Ca)	(100*Sr/Ca) 1σ	(Sr/Mg)	(Sr/Mg) 1σ	Arbitrary brightness
0.5	0.0031	4.5E-05	0.0044	5.2E-05	0.0142	1.6E-04	116
1.0	0.0042	7.1E-05	0.0019	1.0E-04	0.0045	2.4E-04	124
1.5	0.0035	7.1E-05	0.0045	9.1E-05	0.0128	7.5E-05	163
2.0	0.0031	5.3E-05	0.0040	1.2E-04	0.0127	4.2E-04	98
2.5	0.0030	6.5E-05	0.0040	1.2E-04	0.0134	4.9E-04	123
3.0	0.0034	9.9E-05	0.0043	1.2E-04	0.0127	4.1E-04	117
3.5	0.0029	2.8E-05	0.0024	1.4E-05	0.0082	8.0E-05	123
4.0	0.0032	5.7E-05	0.0038	5.2E-05	0.0119	2.0E-04	126
4.5	0.0032	2.6E-05	0.0027	6.0E-05	0.0086	1.8E-04	157
5.0	0.0031	5.9E-05	0.0042	8.1E-05	0.0138	3.7E-04	164
5.5	0.0028	2.2E-05	0.0035	4.5E-05	0.0123	1.6E-04	160
6.0	0.0030	2.5E-05	0.0020	6.3E-05	0.0068	2.2E-04	175
6.5	0.0029	3.7E-05	0.0024	5.5E-05	0.0083	1.8E-04	114
7.0	0.0038	5.5E-05					152
7.5	0.0029	4.2E-05	0.0007	2.0E-05	0.0026	6.8E-05	152
8.0	0.0032	3.2E-05	0.0009	4.9E-05	0.0029	1.5E-04	150

Data from line 2 of tufa drilling. Ratios represent trace elements of the tufa calcite.

Distance from edge (mm)	(Mg/Ca)	(Mg/Ca) 1σ	(100*Sr/Ca)	(100*Sr/Ca) 1σ	(Sr/Mg)	(Sr/Mg) 1σ	Arbitrary brightness
0.5	0.0029	5.0E-05	0.0039	5.6E-05	0.0133	1.6E-04	108
1.0	0.0031	1.0E-04	0.0037	1.5E-04	0.0120	5.8E-04	125
1.5	0.0031	1.0E-04	0.0054	1.2E-04	0.0174	6.7E-04	135
2.0	0.0029	4.7E-05	0.0054	7.3E-05	0.0183	3.8E-04	123
2.5	0.0029	5.2E-05	0.0051	8.2E-05	0.0179	3.1E-04	132
3.0	0.0028	9.6E-05	0.0048	1.4E-04	0.0172	7.4E-04	137
3.5	0.0029	4.2E-05	0.0052	8.1E-05	0.0179	3.5E-04	150
4.0	0.0027	4.2E-05	0.0043	4.9E-05	0.0159	1.8E-04	161
4.5	0.0045	5.5E-05	0.0043	3.2E-05	0.0096	1.1E-04	120
5.0	0.0033	6.1E-05	0.0041	3.3E-05	0.0126	2.3E-04	160
5.5	0.0031	5.1E-05	0.0062	1.7E-04	0.0199	5.3E-04	196
6.0	0.0026	3.3E-05	0.0039	4.0E-05	0.0147	1.5E-04	158
6.5	0.0025	7.3E-05	0.0035	8.0E-05	0.0137	3.2E-04	171
7.0	0.0025	2.6E-05	0.0034	5.4E-05	0.0137	2.2E-04	155
7.5	0.0024	1.1E-04	0.0038	1.6E-04	0.0156	9.8E-04	171
8.0	0.0030	4.3E-05	0.0041	6.3E-05	0.0136	1.9E-03	170
8.5	0.0023	3.0E-05	0.0031	9.0E-05	0.0132	3.9E-04	171
9.0	0.0024	1.7E-05	0.0024	7.0E-05	0.0100	3.0E-04	173
9.5	0.0026	3.0E-05	0.0040	1.2E-04	0.0152	4.4E-04	166

Data from line 3 of tufa drilling. Ratios represent trace elements of the tufa calcite.

Distance from edge (mm)	(Mg/Ca)	(Mg/Ca) 1σ	(100*Sr/Ca)	(100*Sr/Ca) 1σ	(Sr/Mg)	(Sr/Mg) 1σ	Arbitrary brightness
0.5	0.0028	7.0E-05	0.0058	1.4E-04	0.0206	6.2E-04	114
1.0	0.0032	5.3E-05	0.0058	1.3E-04	0.0181	4.8E-04	130
1.5	0.0026	8.4E-05	0.0040	8.3E-05	0.0157	5.4E-04	117
2.0	0.0027	5.3E-05	0.0046	9.4E-05	0.0167	3.1E-04	144
2.5	0.0027	5.3E-05	0.0052	7.1E-05	0.0193	4.2E-04	141
3.0	0.0036	2.1E-04	0.0055	2.0E-04	0.0151	1.0E-03	140
3.5	0.0032	7.3E-05	0.0056	1.8E-04	0.0172	6.6E-04	138
4.0	0.0035	6.5E-05	0.0052	1.1E-04	0.0150	3.4E-04	121
4.5	0.0025	4.8E-05	0.0035	8.4E-05	0.0139	3.0E-04	157

Data from line 4 of tufa drilling. Ratios represent trace elements of the tufa calcite.

Distance from edge (mm)	(Mg/Ca)	(Mg/Ca) 1σ	(100*Sr/Ca)	(100*Sr/Ca) 1σ	(Sr/Mg)	(Sr/Mg) 1σ	Arbitrary brightness
0.5	0.0026	6.7E-05	0.0046	8.7E-05	0.0175	5.5E-04	100
1.0	0.0028	1.6E-05	0.0041	2.1E-05	0.0147	8.8E-05	114
1.5	0.0027	4.2E-05	0.0049	4.7E-05	0.0179	2.9E-04	121
2.0	0.0028	6.3E-05	0.0052	1.4E-04	0.0187	6.2E-04	133
2.5	0.0029	3.1E-05	0.0050	6.4E-05	0.0169	2.7E-04	102
3.0	0.0035	6.4E-05	0.0052	1.1E-04	0.0145	3.5E-04	111
3.5	0.0027	7.7E-05	0.0040	9.8E-05	0.0149	4.5E-04	94
4.0	0.0027	4.2E-05	0.0044	5.4E-05	0.0163	2.3E-04	143
4.5	0.0045	6.2E-05	0.0043	6.9E-05	0.0096	1.8E-04	149
5.0	0.0024	2.7E-05	0.0035	3.6E-05	0.0146	1.4E-04	156

Data from line 5 of tufa drilling. Ratios represent trace elements of the tufa calcite.

Distance from edge (mm)	(Mg/Ca)	(Mg/Ca) 1σ	(100*Sr/Ca)	(100*Sr/Ca) 1σ	(Sr/Mg)	(Sr/Mg) 1σ	Arbitrary brightness
0.5	0.003	3.30E-05	0.003	3.30E-05	0.0104	1.50E-04	130
1.0	0.0028	2.50E-05	0.0028	2.50E-05	0.0162	1.90E-04	138
1.5	0.003	3.90E-05	0.003	3.90E-05	0.0175	3.00E-04	153
2.0	0.0026	4.00E-05	0.0026	4.00E-05	0.0167	1.20E-04	144
2.5	0.0027	4.30E-05	0.0027	4.30E-05	0.0159	2.30E-04	158
3.0	0.0026	8.40E-05	0.0026	8.40E-05	0.0177	6.40E-04	122
3.5	0.0028	5.70E-05	0.0028	5.70E-05	0.0164	4.40E-04	157
4.0	0.0027	3.30E-05	0.0027	3.30E-05	0.0143	7.20E-05	147
4.5	0.0024	6.60E-05	0.0024	6.60E-05	0.0175	5.80E-04	153
5.0	0.0021	6.60E-05	0.0021	6.60E-05	0.0098	5.20E-04	153
5.5	0.003	3.50E-05	0.003	3.50E-05	0.0085	1.10E-04	223
6.0	0.0023	2.60E-05	0.0023	2.60E-05	0.0143	5.00E-04	209
6.5	0.0023	7.10E-05	0.0023	7.10E-05	0.0147	5.30E-04	193
7.0	0.0021	4.00E-05	0.0021	4.00E-05	0.0157	2.60E-04	216

References

Alibert, C., Kinsley, L., Fallon, S.J., McCulloch, M., Berkelmans, R., McAllister, F. (2003) Sources of trace element variability in Great Barrier Reef corals affected by the Burdekin flood plumes. *Geochemica. Cosmochimica. Acta*, **67**, 231–246.

Allison, N. and Finch, A.A. (2007) High temporal resolution Mg/Ca and Ba/Ca records in modern Porites lobata corals. *Geochemistry, Geophysics, Geosystems,* **8**, 5.

Alonso-Zarza, A.M. (2003) Palaeoenvironmental significance of palustrine carbonates and calcretes in the geological record. *Earth-Science Reviews,* **60**, 261–298

Anand, P., Elderfield, H., Conte, M.H. (2003) Calibration of Mg/Ca thermometry in planktonic foraminifera from sediment trap time series. *Paleoceanography,* **18 (2)**, 1050.

Andres, M.S. and Reid, R.P. (2006) Growth morphologies of modern marine stromatolites: A case study from Highborne Cay, Bahamas. *Sedimentary Geology,* **185**, 319–328.

Andrews, J.E. (2005) Seasonal records of climatic change in annually laminated tufas: short review and future prospects. *Journal of Quaternary Science,* **20(5)** 411–421

Andrews J. E., Riding R., and Dennis P. F. (1993) Stable isotopic compositions of recent freshwater cyanobacterial carbonates from the British Isles: Local and regional environmental controls. *Sedimentology,* **40**, 303–314.

Andrews, J.E., Riding, R. and Dennis, P.F. (1997) The stable isotope record of environmental and climatic signals in modern terrestrial microbial carbonates from Europe. *Palaeogeography, Palaeoclimatology, Palaeoecology,* **129**, 171 – 189.

Andrews J. E., Pedley M., and Dennis P. F. (2000) Palaeoenvironmental records in Holocene Spanish tufas: A stable isotope approach in search of reliable climatic archives. *Sedimentology,* **47**, 961–978.

Andrews, J.E. and Brasier, A.T. (2005) Seasonal records of climatic change in annually laminated tufas: short review and future prospects. *Journal of Quaternary Science,* **20**, 5, 411–421.

Appelo, C.A.J. and Postma, D. (2005) *Geochemistry groundwater and pollution.* A.A. Balkema Publishers, London.

Arbuszewski J., deMenocal P., Kaplan A., Farmer E.C. (2010) On the fidelity of shell-derived $\delta^{18}O_{seawater}$ estimates. *Earth and Planetary Science Letters*, **300,** 185–196.

Arp, G., Thiel, V., Reimer, A., Michaelis, W., and Reitner, J., (1999) Biofilm exopolymers control microbialite formation at thermal springs discharging into the alkaline Pyramid Lake, Nevada, USA. *Sedimentary Geology*, **126**, 159–176.

Arp, G., Wedemeyer, N., Reitner, J., (2001) Fluvial tufa formation in a hard-water creek (Deinschwanger Bach, Franconian Alb, Germany). *Facies,* **44**, 1 –22.

Atkins, P. and de Paula, J. (2006) *Atkins' physical chemistry.* Oxford, Oxford University Press.

Baldini, J.U.L., McDermott, F., Fairchild, I.J., (2006) Spatial variability in cave drip water hydrochemistry: implications for stalagmite paleoclimate records. *Chemical Geology,* **235**, 290–304.

Baldini, J.U.L. (2010) Cave atmosphere controls on stalagmite growth rate and palaeoclimate records. In: H.M. Pedley and M. Rogerson (Editors), *Speleothems and Tufas: Unravelling Physical and Biological controls*. Geological Society Special Publication. Geological Society of London, London, **336**, pp. 283-294

Barker, S., Cachob, I., Benwayc, H. and Tachikawad, K. (2005) Planktonic foraminiferal Mg/Ca as a proxy for past oceanic temperatures: a methodological overview and data compilation for the Last Glacial Maximum. *Quaternary Science Reviews*, **24**, 821–834.

Barranguet C., van Beusekom, S.A.M., Veuger, B., Neu, T.R., Manders, E.M.M., Sinke, J.J., Admiraal, W. (2004) ─Studying undisturbed autotrophic biofilms: still a technical challenge. *Aquatic Microbial Ecology*, **34**, 1-9

Baskar, S., Baskar, R., Mauclaire, L. and McKenzie, J.A. (2006) Microbially induced calcite precipitation in culture experiments: Possible origin for stalactites in Sahastradhara caves, Dehradun, India. *Current Science,* **90**, 1, 58 ─ 64.

Baumgartner LK, Reid, RP, Dupraz C, Decho AW, Buckley DH, Spear JR, Przekop, KM, Visscher PT. (2006) Sulfate reducing bacteria in microbial mats: changing paradigms, new discoveries. *Sedimentary Geology*, **185**, 131–145.

Beck, J. W., Edwards, R. L., Ito, E., Taylor, F. W., Récy, J., Rougerie, F., Joannot, P. and Henin, C. (1992) Sea-surface temperature from coral skeletal strontium/calcium ratios. *Science* **257**, 644–647.

Beer, T. (1996) *Environmental Oceanography*. CRC Press, Florida.

Bhaskar PV, Bhosle NB (2006) Bacterial extracellular polymeric substance (EPS): a carrier of heavy metals in the marine food chain. *Environment Inernational*, **32**, 191–198.

Bissett, A., Reimer, A., de Beer, D., Shiraishi, F. and Arp, G., (2008) Metabolic microenvironmental control by photosynthetic biofilms under changing macroenvironmental temperature and pH conditions. *Applied Environmental Microbiol*ogy, **74(20),** 6306-6312.

Blanchard, G.F, Guarini, J.M, Richard, P., Gros, P., Mornet, F. (1996) Quantifying the short-term temperature effect on lightsaturated photosynthesis on intertidal microphytobenthos. *Marine Ecology Progress Series,* **134**, 309–313.

Blanchard, G.F., Guarini, J.M, Gros, P., Richard, P. (1997) Seasonal effect on the relationship between the photosynthetic capacity of intertidal microphytobenthos and temperature. *Journal of Phycology,* **33**, 723–728.

Boch, R., Spotl, C., Reitner, J. and Krammers, J. (2005) A late glacial travertine deposit in eastern Tyrol Austria. *Austrian Journal of Earth Sciences,* **98**, 78 ─ 91.

Boquet, E., Boronat, A. and Ramos-Cormenza, A. (1973) Production of calcite (calcium carbonate) crystals by soil bacteria is a general phenomenon. *Nature*, **246**, 527–529.

Bosak, T., and Newman, D.K., (2003) Microbial nucleation of calcium carbonate in the Precambrian. *Geology*, **31,** 577-580.

Bosak, T., and Newman, D.K., (2005) Microbial kinetic controls on calcite morphology in supersaturated solutions. *Journal of Sedimentary Research*, **75**, 190–199.

Bosnich, B. (2012) Science, climate, carbon and tax [Online]. Available from: http://joannenova.com.au/2011/11/the-chemistry-of-ocean-ph-and-acidification/ [Accessed 5th June 2012].

Boss, C. B., Fredeen, K. J. (2004) *Concepts, Instrumentation and Techniques in Inductively Coupled Plasma Optical Emission Spectrometry.* Perkin Elmer, USA.

Boussetta, S., Bassinot, F., Sabbatini, A., Caillon, N., Nouet, J., Kallel, N., Rebaubier, H., Klinkhammer, G., Labeyrie, L. (2011) Diagenetic Mg-rich calcite in Mediterranean sediments: Quantification and impact on foraminiferal Mg/Ca thermometry. *Marine Geology*, **280 (1–4),** 195–204.

Bradding, M.G., Jass, J. and Lappin-Scott, H.M. (1995) Dynamics of bacterial biofilm formation. In: *Microbial biofilms.* Edited by Hilary Lappin-Scott, and J. William Costerton. Cambridge University Press, Cambridge, UK, pages 46 – 63.

Brady, P.V. and House, W.A. (1995) Surface-controlled dissolution and growth of minerals. in: *Physics and Chemistry of Mineral Surfaces*. Edited by P.V. Brady. Boca Raton, New York CRC Press, pages 225–306.

Braissant, O., Decho, A.W., Dupraz, C., Glunk, C., Przekop, K.M. and Visscher, P.T. (2007) Exopolymeric substances of sulfate-reducing bacteria: interactions with calcium at alkaline pH and implication for formation of carbonate minerals. *Geobiology,* **5**, 401–411.

Brand, A., Dinkel, C and Wehrli, B. (2009) Influence of the diffusive boundary layer on solute dynamics in the sediments of a seiche-driven lake: A model study. *Journal of Geophysical Research,* **114**, G01010.

Brasier, A.T., Andrews, J.E., Marca-Bell, A.D. and Dennis, P.F. (2010) Depositional continuity of seasonally laminated tufas: Implications for $\delta^{18}O$ based palaeotemperatures. *Global and Planetary Change,* **71**, 160-167.

Brasier, M.D. (1980) *Microfossils*. George Allen & Unwin, London.

Buhmann D. and Dreybrodt W. (1985a) The kinetics of calcite dissolution and precipitation in geologically relevant situations of karst areas: 1. Open system. *Chemical Geology,* **48**, 189-1211.

Buhmann D. and Dreybrodt W. (1985b) The kinetics of calcite dissolution and precipitation in geologically relevant situations of karst areas: 2. Closed system. *Chemical Geology,* **53**, 109-124.

Burne, R.V., Moore, L.S. (1987) Zircons from Syros, - Microbialites: Organosedimentary deposits of benthic microbial communities. *Palaios*, **2**, 241 – 254.

Burroughs, W.J. (2001) *Climate change: A multi disciplinary approach.* Cambridge University Press, Cambridge.

Cacchio P, Ercole C, Cappuccio G, Lepidi A. (2003) Calcium carbonate precipitation by bacterial strains isolated from limestone cave and from a loamy soil. *Geomicrobiology Journal,* **20**, 85–98.

Cacchio P., Contento R., Ercole C., Cappuccio G., Martinez M. P. and Lepidi A. (2004) Involvement of microorganisms in the formation of carbonate speleothems in the Cervo Cave (L'Aquila—Italy). *Geomicrobiology Journal,* **21**, 497–509.

Chanson, H. and Toombes, L. (2003) Strong Interactions between Free-Surface Aeration and Turbulence in an Open Channel Flow. *Experimental Thermal and Fluid Science*, **27**, 5, 525-535.

Chafetz, H.S. and Folk, R.L., (1984) Travertines - depositional morphology and the bacterially constructed constituents. *Journal of Sedimentary Petrology*, **54(1),** 289-316.

Chafetz, H., Rush, P.F. and Utech, N.M. (1991) Microenvironmental controls on mineralogy and habit of CaCO precipitates: an example from an active travertine system. *Sedimentology,* **38**, 107-126.

Chafetz, H.S., Buczynski, C. (1992) Bacterially induced lithification of microbial mats. *Palaios,* **7**, 277–293.

Chave, K.E. (1954) Aspects of the biogeochemistry of magnesium: Calcareous marine organisms. *Journal of Geology*, **62**. 266–283.

Chave K. and Seuss E. (1970) Calcium carbonate supersaturation in seawater: Effects of dissolved organic matter. *Limnology and Oceanography* **15,** 633–637.

Chen J. A., Zhang D. D., Wang S. J., Xiao T. F. and Huang R. G. (2004) Factors controlling tufa deposition in natural waters at waterfall sites. *Sedimentary Geology,* **166**, 353–366.

Clark, J. (2000) *Calculations in AS/A level chemistry.* Longman, Harlow, Essex.

Comte, S., Guibaud, G., Baudu, M. (2006) Relations between extraction protocols for activated sludge extracellular polymeric substances (EPS) and complexation properties of Pb and Cd with EPS Part II. Consequences of EPS extraction methods on Pb^{2+} and Cd^{2+} complexation. *Enzyme and Microbial Technology,* **38**, 246-252.

Costerton, J.W. (1995) Overview of microbial biofilms. *Journal of Industrial Microbiology,* **15**, 137-140.

Cronin, T.M. (1999) *Principles of paleoclimatology.* Cambridge University Press, Cambridge.

Cruz, F. W., Jr., S. J. Burns, M. Jercinovic, I. Karmann, W. D. Sharp, and M. Vuille (2007) Evidence of rainfall variations in southern Brazil from trace element ratios

(Mg/Ca and Sr/Ca) in a late Pleistocene stalagmite. *Geochimica Cosmochimica Acta*, **71**, 2250– 2263.

Decho, AW. (2000) Microbial biofilms in intertidal systems: an overview. *Continental Shelf Research,* **20**, 1257–1273.

Decho, A.W., Visscherb, P.T. and Reid, R.P. (2005) Production and cycling of natural microbial exopolymers (EPS) within a marine stromatolite. *Palaeogeography, Palaeoclimatology, Palaeoecology,* **219**, 71– 86.

Decho, A.W. (2010) Overview of biopolymer-induced mineralization: What goes on in biofilms? *Ecological Engineering,* **36(2)**, 137-144.

Defew, E. C., Perkins, R. G., Paterson, D. M. (2004) The influence of light and temperature interactions on a natural estuarine microphytobenthic assemblage. *Biofilms,* **1**, 21–30.

Dekens, P., Lea, D., Pak, D., Spero, H., 2002. Core top calibration of Mg/Ca in tropical foraminifera: refining paleotemperature estimation. *Geochemistry Geophysics Geosystems,* **3(4),** 1023.

Delaney, M.L., Be, A.W.H. and Boyle, E.A. (1985) Li, Sr, Mg and Na in foraminiferal calcite shells from laboratory culture, sediment traps, and sediment cores. *Geochimica Cosmochimica Acta,* **49**, 1327-1341.

de Nooijer J., Toyofuku T., Kitazato H. (2009) Foraminifera promote calcification by elevating their intracellular pH. *Proceedings of National Academy of Sciences U.S.A.,* **106,** 15374–15378.

de Villiers, S., Shen, G.T., Nelson, B.K. (1994) The Sr/Ca-temperature relationship in coralline aragonite: influence of variability in (Sr/Ca)seawater and skeletal growth parameters. *Geochimica Cosmochimica Acta*, **58**, 197–208.

de Villiers, S., Nelson, B.K., Chivas, A.R. (1995) Biological controls on coral Sr/Ca and $\delta^{18}O$ reconstructions of sea surface temperatures. *Science,* **269**, 1247–1249.

de Villiers, S., Greaves, M, Elderfield, H. (2002) An intensity ratio calibration method for the accurate determination of Mg/Ca and Sr/Ca of marine carbonates by ICP-AES. *Geochemistry, Geophysics, Geosystems,* **3**, 10.1029/2001GC000169.

Di Pippo, F.; Bohn, A.; Congestri, R.; De Philippis, R.; Albertano, P. Capsular polysaccharides of cultured phototrophic biofilms. *Biofouling,* **25**, 495-504.

Dissard, D., Nehrke, G., Reichart, G.J., Bijma, J. (2010) The impact of salinity on the Mg/Ca and Sr/Ca ratio in the benthic foraminifera Ammonia tepida: Results from culture experiments. *Geochimica Cosmochimica Acta,* **74**, 928-940.

Dittrich, M. and Sibler, S. (2010) Calcium carbonate precipitation by cyanobacterial polysaccharides. In: H.M. Pedley and M. Rogerson (Editors), *Speleothems and Tufas: Unravelling Physical and Biological controls*. Geological Society Special Publication. Geological Society of London, London, **336**, pp. 65-81.

Dreybrodt W., and Buhmann D. (1991) A mass transfer model for dissolution and precipitation of calcite from solutions in turbulent motion. *Chemical Geology,* **90**, 107–122.

Dreybrodt, W., Buhmann, D., Michaelis, J. & Usdowski, E. (1992) Geochemically controlled calcite precipitation by CO_2 outgassing: Field measurements of precipitation rates in comparison to theoretical predictions. *Chemical Geology*, **97**, 285–294.

Dreybrodt W., Lauckner J., Zaihua Liu, Svensson U., and Buhmann D. (1996) The kinetics of the reaction $CO_2 + H_2O \rightarrow H^+ + HCO_3^-$ as one of the rate limiting steps for the dissolution of calcite in the system $H_2O\text{-}CO_2\text{-}CaCO_3$. *Geochimica Cosmochimica Acta,* **60**, 3375-3381.

Dreybrodt, W., Eisenlohr, L., Madry, B., & Ringer, S. (1997) Precipitation kinetics of calcite in the system $CaCO_3\text{-}H_2O\text{-}CO_2$: the conversion to CO_2 by the slow process $H^+ + HCO_3 \rightarrow CO_2 + H_2O$ as a rate limiting step. *Geochimica et Cosmochimica Acta*, **61**, 3897-3904.

Druffel E. R. M. (1997) Geochemistry of corals: proxies of past ocean chemistry, ocean circulation, and climate. *Proceedings of Nationa. Academy of Sciences USA,* **94**, 8354–8361.

Dueñas-Bohórquez, A., da Rocha, E. S., Kuroyanagi, A., Bijma, J., Reichart, G.J. (2009) Effect of salinity and seawater calcite saturation state on Mg and Sr incorporation in cultured planktonic foraminifera. *Marine Micropaleontology,* **73(3–4),** 178–189.

Dupraz, C., Visscher, P.T., Baumgartner, L.K. and Reid, R.P. (2004) Microbe–mineral interactions: early carbonate precipitation in a hypersaline lake (Eleuthera Island, Bahamas). *Sedimentology,* **51**, 745–765.

Dupraz C. and Visscher P. T. (2005) Microbial lithification in marine stromatolites and hypersaline mats. *Trends in Microbioliology,* **13**, 429–438.

Dupraz, C., Reid, P.R., Braissant, O., Decho, A.W. Norman, S.R. and Visscher, P.T. (2009). Processes of carbonate precipitation in modern microbial mats. *Earth Science Reviews,* **96(3)** 141-162.

Drysdale, R.N., Taylor, M.P. and Ihlenfeld, C. (2002) Factors controlling the chemical evolution of travertine-depositing rivers of the Barkly karst, northern Australia. *Hydrological Processes,* **16**, 2941–2962.

Elderfield, H., Bertram, C.J. and Erez, J. (1996) Biomineralization model for the incorporation of trace elements into foraminiferal calcium carbonate, *Earth and Planetary Science Letters,* **142**, 409–423.

Elderfield, H., Yu, J., Anand, P., Kiefer, T., Nyland, B. (2006) Calibrations for benthic foraminiferal Mg/Ca palaeothermometry and the carbonate ion hypothesis. *Earth and Planetary Science Letters,* **250**, 633-649.

Emeis, K.C., Richnow, H.H., and Kempe, S. (1987) Travertine formation in Plitvice-National-Park, Yugoslavia—chemical versus biological-control. *Sedimentology* **34**, 595–609.

Ercole, C., Cacchio, P., Botta, A.L., Centi, V., Lepidi, A., (2007) Bacterially induced mineralization of calcium carbonate: the role of exopolysaccharides and capsular polysaccharides. *Microscopy and Microanalyses,* **13**, 42–50.

Fairchild, I.J., Borsato, A., Tooth, A.F., Frisia, S., Hawkesworth, C.J., Huang, Y., McDermott, F., Spiro, B., (2000) Controls on trace element (Sr–Mg) compositions of carbonate cave waters: implications for speleothem climatic records. *Chemical Geology,* **166**, 255–269.

Fairchild I. J., Smith C. L., Baker A., Fuller L., Spotl C., Mattey D. and McDermott F. (2006) Modification and preservation of environmental signals in speleothems. *Earth Science Reviews,* **75**, 105 – 153.

Fairchild, I.J. and Treble, P.C. (2009) Trace elements in speleothems as recorders of environmental change. *Quaternary Science Reviews*, **28**, 449–468

Fallon, S.J., McCulloch, M.T.,van Woesik, R. and Sinclair, D.J. (1999) Corals at their latitudinal limits: Laser ablation trace element systematic in Porites from Shirigai Bay, Japan, *Earth and Planetary Science Letters,* **172**, 221– 238.

Fallon, S.J., McCulloch, M.T., Alibert, C., 2003. Examining water temperature proxies in Porites corals from the Great Barrier Reef: a cross-shelf comparison. *Coral Reefs* **22**, 389–404.

Ferguson, J.E., Henderson, G.M., Kucera, M., Rickaby, R.E.M. (2008) Systematic change of foraminiferal Mg/Ca ratios across a strong salinity gradient. *Earth and Planetary Science Lett*ers, **265**, 153–166.

Fleitmann, D. and Matter, A. (In press). External geophysics, climate and environment The speleothem record of climate variability in Southern Arabia. *G.R. Geosciences,* **341**, 633-642.

Flemming, H.C. (2011) The perfect slime. *Colloids and Surfaces and Biointerfaces,* **86(2)**, 251-259.

Flemming, H., Szewzyk, U. and Griebe, T. (2000) *Biofilms:Investigative methods and applications.* Technomic publishing company, Pennsylvania, USA.

Flemming H. C. and Wingender J. (2001) Relevance of microbial extracellular polymeric substances (EPSs) - Part I: structural and ecological aspects. *Water Science and Technology*, **43**, 1–8.

Flemming, H. C., Neu, T.R., Wozniak, D.J. (2007) The EPS matrix: the "house of biofilm cells." *Journal of Bacteriol*ogy, **189**, 7945-7947.

Flemming H. C., Wingender J. (2010). The biofilm matrix. *National Review of Microbiology* **8**, 623–633.

Folk, R.L., Chafetz, H.S. and Tiezzi, P.A., (1985) Bizarre forms of depositional and diagenetic calcite in hot-spring travertines, central Italy. In: N. Scheidemann and P. Harris, eds., *Carbonate Cements*. Society of Economic Palaeontologists and Mineralogists Special Publication 36, Tulsa, Oklahoma. pp. 349-369.

Ford, D.C., Williams, P.W., (2007) *Karst Hydrogeology and Geomorphology*. Wiley, London.

Ford, T.D. and Pedley, H.M. (1996) A review of tufa and travertine deposits of the world. *Earth-Science Reviews,* **41**, 117-175.

Fuhr Dal Bo, P.F., Basilici, G., Angelica, R.S. and Ladeira, F.S.B. (2009) Paleoclimatic interpretations from pedogenic calcretes in a Maastrichtian semi-arid eolian sand-sheet palaeoenvironment: Marı́lia Formation (Bauru Basin, southeastern Brazil). *Cretaceous Research,* **30**, 659 – 675.

Gabitov, R.I. and Watson, E.B. (2006) Partitioning of strontium between calcite and fluid. *Geochemistry, Geophysics, Geosystems,* **7(11)**, 1525-1537.

Gabitov, R.I., Gaetani, G.A., Watson, E.B., Cohen, A.L., Ehrlich, H.L. (2008) Experimental determination of growth rate effect on U^{6+} and Mg^{2+} partitioning between aragonite and fluid at elevated U^{6+} concentration. *Geochimica et Cosmochimica Acta*, **72**, 4058–4068.

Gagan, M.K., Ayliffe, L.K., Beck, J.W., Cole, J.E., Druffel, E.R.M., Dunbar, R.B., Schrag, D.P. (2000) New views of tropical palaeoclimates from corals. *Quaternary Science Review,* **19**, 45–64.

Gagnon, A.C., Adkins, J.F., Fernandez, D.P. and Robinson, L.F. (2007) Sr/Ca and Mg/Ca vital effects correlated with skeletal architecture in a scleractinian deep-sea coral and the role of Rayleigh fractionation. *Earth and Planetary Science Letters,* **261**, 280–295.

Garnett, E.R., Andrews, J.E., Preece, R.C., Dennis, P.F. (2004). Climatic change recorded by stable isotopes and trace elements in a British Holocene tufa. *Journal of Quaternary Science,* **19**, 251–262.

Gascoyne M. (1983) Trace element partition coefficients in the calcite–water system and their palaeoclimatic significance in cave studies. *Journal of Hydrology,* **61**, 213–222.

Gautret, P. and Trichet, J. (2005) Automicrites in modern cyanobacterial stromatolitic deposits of Rangiroa, Tuamotu Archipelago, French Polynesia: Biochemical parameters underlaying their formation. *Sedimentary Geology,* **178**, 55-73.

Geesey, G.G., Jang, L. (1989) Interactions between metal ions and capsular polymers. In: Beveridge, T.J., Doyle, R.J. (Eds.), *Metal ions and bacteria*. Wiley, New York, pp. 325–357.

Genty, D., Baker, A. and Vokal, B. (2001) Intra- and inter-annual growth rate of modern stalagmites. *Chemical Geology,* **176**, 191–212.

Goller, C.C. and Romeo, T. (2008) Environmental influences on biofilm development. *Current Topics in Microbiology and Immunology*, **322,** 37-66.

Gonzalez-Munoz, M.T., Rodriguez-Navarro, C., Martinez-Ruiz, F., Arias, J.M., Merroun, M.L., Rodriguez-Gallego, M. (2010) Bacterial biomineralization: new insights from *Myxococcus-* induced mineral precipitation. In: H.M. Pedley and M. Rogerson (Editors), *Speleothems and Tufas: Unravelling Physical and Biological controls*. Geological Society Special Publication. Geological Society of London, London, **336**, pp. 31-50.

Gradzinski, M. (2010) Factors controlling growth of modern tufa: results of a field experiment. In: H.M. Pedley and M. Rogerson (Editors), *Speleothems and Tufas:*

Unravelling Physical and Biological controls. Geological Society Special Publication. Geological Society of London, London, **336**, pp. 143-191.

Green, D. R. H., Cooper, M. J., German, C. R, Wilson, P. A. (2003) Optimization of an inductively coupled plasma–optical emission spectrometry method for the rapid determination of high-precision Mg/Ca and Sr/Ca in foraminiferal calcite, *Geochemistry, Geophysics and Geosystems*, **4(6),** 8404

Groeneveld, J. and Chiessi, C.M. (2011) Mg/Ca of *Globorotalia inflata* as a recorder of permanent thermocline temperatures in the South Atlantic. *Palaeoceanography,* **26**, 12 pp.

Hammer, Ø., Dysthe, D. K., Lelu, B., Lund., H., Meakin, P. and Jamtveit, B. (2008) Calcite precipitation instability under laminar, open-channel flow. *Geochimica et Cosmochimica Acta,* **72**, 5009 – 5021.

Hanas, J.S., Larabee, J.L., Hocker, J.R. (2005) Zinc finger interactions with metals and other small molecules. In: Iuchi, S., Kuldell, N. Eds., *Zinc Finger Proteins: From Atomic Contact to Cellular Function.* New York, Kluwer Academic, pp. 39-46.

Hancke, K. and Glud, R.N. (2004) Temperature effects on respiration and photosynthesis in three diatom-dominated benthic communities. *Aquatic Microbial Ecology,* **37**, 265-281.

Hay, R.L. and Reeder, R.J. (1978) Calcretes of Olduvai Gorge and the Ndolanya Beds of northern Tanzania. *Sedimentology,* **25**, 649 – 673.

Hellstrom, J.C., McCulloch, M.T. (2000) Multi-proxy constraints on the climatic significance of trace element records from a New Zealand speleothem. *Earth and Planetary Science Letters*, **179**, 287–297.

Henderson, G. M. (2002) New oceanic proxies for paleoclimate. *Earth and Planetary Science Letters,* **203**, 1–13.

Henderson, L.M. and Kracek, F.C. (1927) The fractional precipitation of barium and radium chromates. *Journal of the American Chemical Society*, **49**, 739_749.

Hiscock, K. (2005) *Hydrogeology: Principles and practices.* Blackwell Publishing, Oxford.

Hoch, A. R., Reddy, M. M. and Aiken, G. R. (2000) Calcite crystal growth inhibition by humic substances with emphasis on hydrophobic acids from the Florida Everglades. *Geochimica et Cosmochimica Acta,* **64**, 61−72.

Huang, Y. and Fairchild, I.J. (2001) Partitioning of Sr^{2+} and Mg^{2+} into calcite under karst-analogue experimental conditions. *Geochimica et Cosmochimica Acta*, **65**, 47–62.

Hurlbut, C., S., Klein, C. (1977) *Manual of Mineralogy.* 19th edition. New York, Wiley.

Ihlenfeld C., Norman M., Gagan M., Drysdale R., Maas R. and Webb J. (2003) Climatic significance of seasonal trace element and stable isotope variations in a modern freshwater tufa. *Geochimica et Cosmochimica Acta,* **67**, 2341–2357.

Inskeep, W.P. and Bloom, P.R., (1985) An evaluation of rate equations for calcite precipitation kinetics at pCO2 less than 0.01 atm and pH greater than 8. *Geochimica et Cosmochimica Acta,* **49(10),** 2165-2180.

Inskeep, W.P. and Bloom, P.R. (1986) Kinetics of calcite precipitation in the presence of water soluble organic ligands. *Soil Science Society of America Journal* **50**, 1167-1172.

Irving, H. and Williams, R.J.P. (1953) The stability of transition-metal complexes. *Journal of Chemistry Society,* **637**, 3192-3210.

Jacobson, R.L. and Usdowski, E. (1975) Geochemical Controls on a Calcite Precipitating Spring. *Contributions in Mineralogy and Petrology,* **51**, 65-74.

Janssen, A., Swennen, R., Podoor, N., Keppens, E. (1999) Biological and diagenetic influence in recent and fossil tufa deposits from Belgium. *Sedimentary Geology,* **126**, 75–95.

Jimenez-Lopez, C., Ben Chekrounn, K., Jroundi, F., Rodrigues-Gallego, M., Arias, J.M., Gonzalez-Munoz, T. (2011) *Myxcoccus xanthus* colony calcification: An study

to better understand the processes involved in the formation of this stromatolite structure. *Lecture Notes in Earth Sciences,* Volume **131,** 161-181.

Jones, B. (2010) Microbes in caves: agents of calcite corrosion and precipitation. In: H.M. Pedley and M. Rogerson (Editors), *Speleothems and Tufas: Unravelling Physical and Biological controls*. Geological Society Special Publication. Geological Society of London, London, pp. 7-30.

Jroundi F., Gomez-Suaga, P., Jimenez-Lopez, C., Gonzalez-Munoz, M.T., Fernandez-Vivas, M.A., (2012) Stone-isolated carbonatogenic bacteria as inoculants in bioconsolidation treatments for historical limestone. *Science of the total environment,* **425**, 89-98.

Julia, R. (1983) Travertines. In: *Carbonate Depositional Environments.* AAPG, Tulsa, Oklahoma, pages 64-72.

Kano, A., Matsuoka, J., Kojo, T., Fujii, H. (2003) Origin of annual laminations in tufa deposits, southwest Japan. *Palaeogeography, Palaeoclimatology, Palaeoecology* **191**, 243–262.

Katz, A. (1973) The interaction of magnesium with calcite during crystal growth at 25–95 °C and one atmosphere. *Geochimica et Cosmochimica Acta,* **36.** 481–496.

Kawaguchi, T. and Decho, A.W. (2002) Isolation and biochemical characterization of extracellular polymeric secretions (EPS) from modern soft marine stromatolites (Bahamas) and its inhibitory effect on $CaCO_3$ precipitation. *Biochemistry and Biotechnology,* **32**, 51–63.

Kawai, T., Kano, A., Matsuoka, J., Ihara, T. (2006) Seasonal variation in water chemistry and depositional processes in a tufa-bearing stream in SW-Japan, based on 5 years of monthly observations. *Chemical Geology,* **232**, 33–53.

Kawai, T., Kano, A., Hori, M. (2009) Geochemical and hydrological controls on biannual lamination of tufa deposits. *Sedimentary Geology*, **213,** 41–50.

Kazmierczak T. F., Tomson M. B., and Nancollas G. H. (1982) Crystal growth of calcium carbonate. A controlled composition kinetic study. *Journal of Physical Chemistry,* **86,** 103–107.

Kısakürek, B., Eisenhauer, A., Böhm, F., Garbe-Schönberg, D. and Erez, J. (2008) Controls on shell Mg/Ca and Sr/Ca in cultured planktonic foraminiferan, Globigerinoides ruber (white). *Earth and Planetary Science Letters,* **273**, 260–269.

Konhauser, K. (2007) *Introduction to Geomicrobiology*. Blackwell Publishing, Oxford.

Laval, B., S.L. Cady, J.C. Pollack, C.P. McKay, J.S. Bird, J.P. Grotzinger, D.C. Ford, and H.R. Bohm. (2000) Modern freshwater microbialite analogues for ancient dendritic reef structures, *Nature,* **407**, 626-629.

Lea, D., Mashiotta, T., Spero, H., 1999. Controls on magnesium and strontium uptake in planktonic foraminifera determined by live culturing. *Geochimica et Cosmochimica Acta*, **63 (16)**, 2369–2379.

Lear, C., Rosenthal, H.Y. and N. Slowey, N. (2002) Benthic foraminiferal Mg/Ca-paleothermometry: A revised core-top calibration. *Geochimica et Cosmochimica Acta,* **66**, 3375 – 3387.

Lebron, I. and Suarez, D. L. (1996) Calcite nucleation and precipitation kinetics as affected by dissolved organic matter at 25 °C and pH_7.5. *Geochimica et Cosmochimica Acta,* **60,** 2765–2776.

Lemon, K. P., Earl, A. M., Vlamakis, H. C., Aguilar, C., and Kolter, R. (2008) Biofilm development with an emphasis on *Bacillus subtilis*. *Current Topics in Microbiology and Immunology,* **322**, 1-16.

Leng, M.J. and Marshall, J.D. (2004) Palaeoclimate interpretation of stable isotope data from lake sediment archives. *Quaternary Science Reviews*, **23**, 811–831.

Lin, Y.P., Singer, P.C. and Aiken, G.R. (2005) Inhibition of Calcite Precipitation by Natural Organic Material: Kinetics, Mechanism, and Thermodynamics. *Environmental Science and Technology,* **39**, 6420-6428.

Lippard, S.J. and Berg, J.M. (1994) *Principles of Bioinorganic Chemistry*. University Science, Mill Valley, CA, USA.

Liu, Z.,.Svennson, J., Dreybrodt, W., Daoxian, Y. and Buhmann, D. (1995) Hydrodynamic control of inorganic calcite precipitation in Huanglong Ravine, China: Field measurements and theoretical prediction of deposition rates. *Geochimica et Cosmochimica Acta,* **59**, 15, 3087-3097.

Liu, Z. and Dreybrodt, W. (1997) Dissolution kinetics of calcium carbonate minerals in H_2O - CO_2 solutions in turbulent flow: The role of the diffusion boundary layer and the slow reaction $H_2O + CO_2 \rightleftarrows H^+ + HCO_3^-$. *Geochimica et Cosmochimica Acta,* **61**, 2879-2889.

Liu, Z, Li, H., You, C. (2006). Thickness and stable isotopic characteristics of modern seasonal climate-controlled sub-annual travertine laminas in a travertine-depositing stream at Baishuitai, SW China: implications for paleoclimate reconstruction. *Environmental Geology* **51**, 257–265.

Lojen, S., Trkov, A., Ščančar, J., Vázquez-Navarro, Y.A. and Cukrov, N. (2009) Continuous 60-year stable isotopic and earth-alkali element records in a modern laminated tufa (Jaruga, river Krka, Croatia): Implications for climate reconstruction. *Chemical Geology*, **258**, 242–250.

Lorens, R. B. (1981) Sr, Cd, Mn and Co distribution coefficients in calcite as a function of calcite precipitation rate. *Geochimica et Cosmochimica Acta,* **45**, 553–561.

Lowenstam, H.A., (1981) Minerals formed by organisms. *Science,* **211**, 1126–1131.

Luis, J.F. (2007) Mirone: A multi-purpose tool for exploring grid data. *Computers and Geosciences*, **33,** 31-41.

Mann, S. (2001) *Biomineralization: Principles and Concepts in Bioinorganic Materials Chemistry.* Oxford University Press, Oxford.

Manzo, E., Perri, E., Tucker, M.E. (2012) Carbonate deposition in a fluvial tufa system: processes and products (Corvino Valley – southern Italy). *Sedimentology*, **59(2),** 553-577.

Marshall, J.F., and McCulloch, M.T. (2002) An assessment of the Sr/Ca ratio in shallow water hermatypic corals as a proxy for sea surface temperature. *Geochimica et Cosmochimica Acta*, **66**, 3263–3280.

Martin, P. A., Lea, D. W., Rosenthal, Y., Shackleton, N.J., Papenfuss, T.P. Sarnthein, M. (2002) Late Quaternary deep-sea temperatures inferred from benthic foraminiferal magnesium, *Earth* and *Planetary Science Letters,* **198**, 193– 209.

Martínez-Botí, M.A., Mortyn, P.G., Schmidt, D.N., Vance, D., Field, D.B. (2011) Mg/Ca in foraminifera from plankton tows: Evaluation of proxy controls and comparison with core tops. *Earth and Planetary Science Letters,* **307**, 113-125.

Matsuoka J, Kano A, Oba T, Watanabe T, Sakai S, Seto K. (2001) Seasonal variation of stable isotopic compositions recorded in a laminated tufa, SW Japan. *Earth and Planetary Science Letters,* **192**, 31–44.

McDermott, F., (2004) Palaeo-climate reconstruction from stable isotope variations in speleothems: a review. *Quaternary Science Reviews*, **23**, 901–918.

McDonald, J. and Drysdale, R. (2004) The 2002–2003 El Nino recorded in Australian cave drip waters: Implications for reconstructing rainfall histories using stalagmites. *Geophysical Research Letters,* **31**.

McKenna, V.S. and Prell, W.J. (2004) Calibration of the Mg//Ca of *Globorotalia truncatulinoides* (R) for the reconstruction of marine temperature gradients. *Palaeoceanography*, **19**, PA2006.

McMillan, N. F. (1947) The molluscan faunas of some tufas in Cheshire and Flintshire. *Proceedings of the Liverpool Geological Society,* **19**, 240-248.

McMillan, N. F. and Zeissler, H. (1986) The tufa deposit at Caerwys, north Wales, and its molluscan fauna. *The Amateur Geologist,* **11**, 3-11.

Merz-Preiss, M. and Riding, R. (1999) Cyanobacterial tufa calcification in two freshwater streams: ambient environment, chemical thresholds and biological processes, *Sedimentary Geology,* **126**, 103–124.

Misra, K.C. (2012) *Introduction to Geochemistry, Principles and Applications.* Wiley-Blackwell, Chichester, UK.

Mitsuguchi, T., Matsumoto, E., Abe, O., Uchida, T., Isdale, P.J., (1996) Mg/Ca thermometry in coral skeletons. *Science,* **274**, 961–963.

Mitsuguchi, T., Matsumoto, E. and Uchida, T. (2003) Mg/Ca and Sr/Ca ratios of Porites coral skeleton: evaluation of the effect of skeletal growth rate. *Coral Reefs,* **22**, 381–388.

Mitsuguchi, T., Dang, P.X., Kitagawa, H., Uchida, T. and Shibata, Y. (2008) Coral Sr/Ca and Mg/Ca records in Con Dao Island off the Mekong Delta: Assessment of their potential for monitoring ENSO and East Asian monsoon. *Global and Planetary Change*, **63**, 341–352.

Morse, J.W. and Mackenzie, F.T. (1990) *Geochemistry of Sedimentary Carbonates (Developments in Sedimentology).* Elsevier Science, London.

Morse W.J., Arvidson R.S., Luttge A. (2007) Calcium carbonate formation and dissolution. *Chem. Rev*., **107**, 342–381.

Mucci, A. (1987) Influence of temperature on the composition of magnesian calcite overgrowths precipitated from seawater. *Geochimica et Cosmochimica Acta*, **51**, 1977-1984.

Mucci, A. and Morse, J. W. (1983) The incorporation of Mg^{2+} and Sr^{2+} into calcite overgrowths: Influences of growth rate and solution composition. *Geochimica et Cosmochimica Acta,* **47**, 217–233.

Mucci, A. (1987) Influence of temperature on the composition of magnesian calcite overgrowths precipitated from seawater. *Geochimica et Cosmochimica Acta,* **51**, 1977–1984.

Nielsen, P.H., and Jahn, A. (1999). Extraction of EPS. In: J. Wingender, T.R. Neu and H.C. Flemming, Eds. *Microbial Extracellular Polymeric Substances: Characterization, Structure and Function*. Springer-Verlag, Berlin, pp 50-72.

Nehrke, G., Reichart, G. J., Van Cappellen, P., Meile, C., Bijma, J. (2007) Dependence of calcite growth rate and Sr partitioning on solution stoichiometry: non-Kossel crystal growth. *Geochimica et Cosmochimica Acta*, **71**, 2240–2249.

Nolte, J. (2003) *ICP Emission Spectrometry: A practical guide.* Wiley – VCH, Germany.

Novitsky, J.A. (1981) Calcium precipitation by marine bacteria. *Geomicrobiology* **2**, 375-388.

Nurnberg, D., Bijma, D. and Hemleben, C. (1996) .Assessing the reliability of magnesium in foraminiferal calcite as a proxy for water mass temperatures, *Geochimica et Cosmochimica Acta,* **60**, 803– 814.

Oomori T., Kaneshima H., and Maezato Y. (1987) Distribution coefficient of Mg^{2+} ions between calcite and solution at 10–50°C. *Marine Chemistry* **20,** 327–336.

O'Toole, G., Kaplan, H.B., and Kolter, R. (2000) Biofilm formation as microbial development. *Annual Review of Microbiology,* **54**, 49–79.

Palacios-Fest, M.R. and Dettman, D.L. (2001) Temperature controls monthly variation in Ostracode valve Mg/Ca: *Cypridopsis vidua* from a small lake in Sonora, Mexico. *Geochimica et Cosmochimica Acta*, **65(15)**, 2499-2507.

Paquette J., Vali H., and Mucci A. (1996) TEM study of Pt-C replicas of calcite overgrowths precipitated from electrolyte solutions. *Geochimica et Cosmochimica Acta **60, 4689–4699.**

Pazdur, A., Pazdur, M.F., Starkel, L. and Szulc, J. (1988) Stable isotopes of Holocene calcareous tufa in southern Poland as paleoclimatic indicators. *Quaternary Research,* **30***, 177–189.

Pedley, H.M. (1987) The Flandrian (Quaternary) Caerwys Tufa, North Wales: an ancient barrage tufa deposit. *Proceedings of the Yorkshire Geological Society*, **46**, 141-152.

Pedley, H.M (1990) Classification and environmental models of cool freshwater tufas. *Sedimentary Geology,* **68**, 143-154.

Pedley, H.M., Andrews, J., Ordonez, S., Garcia del Cura, M.A., Gonzales-Matrin, J.A., Taylor, D. (1996) Does climate control the morphological fabric of freshwater carbonates? A comparative study of Holocene barrage tufas from Spain and Britain. *Palaeogeography, Palaeoclimatology, Palaeoecology,* **121**, 237-259.

Pedley, H.M., Ordonez, S., Gonzales-Martin, J.A. and Garcia Del Cura, M.A. (2003) The sedimentology of perched springline and paludal tufas: criteria for recognition, with examples from Guadalajara Province, Spain. *Sedimentology,* **50**, 23–44.

Pedley, H. M., Rogerson, M. and Middleton R. (2009) The growth and morphology of freshwater calcite precipitates from in vitro mesocosm flume experiments. *Sedimentology,* **56**, 511 – 527.

Pentecost, A. (2005) *Travertine.* Springer, Berlin, Germany.

Pentecost, A. and Viles, H. (1994) A review and reassessment of travertine classification. *Géographie physique et Quaternaire*, **48 (3),** 305 314.

Pérez-Huerta, A., Cusack, M., Jeffries, T.E., Williams, C.T. (2008) High resolution distribution of magnesium and strontium and the evaluation of Mg/Ca thermometry in Recent brachiopod shells. *Chemical Geology,* **247**, 229-241.

Pingitore, N.E., Eastmen, M.P., Sandidge, M., Oden, K., and Freiha, B. (1988) The coprecipitation of manganese (II) with calcite: An experimental study. *Marine Chemistry,* **25**, 107–120.

Plummer L. N., Wigley T. L. M., and Parkhurst D. L. (1978) The kinetics of calcite dissolution in CO_2 - water systems at 5 to 60°C and 0.0 to 1.0 atm. CO2, *American Journal of Science,* **278**, 537-573.

Preece, R.C., Turner, C. and Green, H. (1982) Field excursion to the tufas of the Wheeler Valley and to Pontnewydd and Cefn caves. *Quaternary Research Association Field Guide,* London, pp 1-9.

Preece, R.C., Day, P., (1984) Comparison of post-glacial molluscan and vegetational succession from a radiocarbon-dated tufa sequence in Oxfordshire. *Journal of Biogeography* **21**, 463–478.

Price, G. (1998) *Thermodynamics of chemical processes.* Oxford Science Publications, Oxford.

Pringault, O., De Wit, R. and Camoin, G. (2004) Functioning of modern marine microbialites built by benthic cyanobacteria. *Recent research developments in Microbiology,* **8**, 1-16.

Quinn, T.M., and Sampson, D.E. (2002) A multiproxy approach to reconstructing sea surface conditions using coral skeleton geochemistry., *Paleoceanography*, **17**, 1062.

Rivadeneyra, M.A., Delgado, R., Del Moral, A., Ferrer M.R, Ramos-Cormenzana, A. (1994) Precipitation of calcium carbonate by *Vibrio* spp. from an inland saltern. *FEMS Microbiology and Ecology,* **13**, 197–204.

Romani, A.M. and Sabater, S. (1999) Effect of primary producers on the heterotrophic metabolism of a stream biofilm. *Freshwater Biology,* **41**, 729-736.

Roberts, M.S., Smart, P., Baker, A. (1998) Annual trace element variations in a Holocene speleothem. *Earth and Planetary Science Letters*, **154**, 237–246.

Reid R. P., Visscher P. T., Decho A. W., Stolz J. F., Bebout B. M., Dupraz C., Macintyre L. G., Paerl H. W., Pinckney J. L., Prufert-Bebout L., Steppe T. F. and DesMarais D. J. (2000) The role of microbes in accretion, lamination and early lithification of modern marine stromatolites. *Nature,* **406**, 989– 853.

Regenberg, M., Silke, S., Nurnberg, D., Tiedemann, R. and Garbe-Schonburg, D. (2009) Calibrating Mg/Ca ratios of multiple planktonic foraminiferal species with δ^{18}O-calcification temperatures: Paleothermometry for the upper water column. *Earth and Planetary Science Letters,* **278**, 324 – 336

Reynaud, S., Ferrier-Pages, C., Meibom, A., Mostefaoui, S., Mortlock, R., Fairbanks, R. and Allemand, D. (2007) Light and temperature effects on Sr/Ca and Mg/Ca ratios in the scleractinian coral Acropora sp. *Geochimica et Cosmochimica Acta,* **71**, 354 – 362.

Riding, R. (2000) Microbial carbonates: The geological record of calcified bacterial – alal mats and biofilms. *Sedimentology,* **47**, 179 – 214.

Rimstidt J. D., Balog A., and Webb J. (1998) Distribution of trace elements between carbonate minerals and aqueous solutions. *Geochimica et Cosmochimica Acta* **62,** 1851–1863.

Roberts, M.S., Smart, P., Baker, A. (1998) Annual trace element variations in a Holocene speleothem. *Earth and Planetary Science Letters* **154**, 237–246.

Roeselers, G., van Loosdrecht, M.C.M. and Muyzer, G. (2008) Phototrophic biofilms and their potential applications. *Journal of .Applied Phycology,* **20**, 227-235.

Rogerson, M., Pedley, H.M., Wadhawan, J.D. and Middleton, R. (2008) New insights into biological influence on the geochemistry of freshwater carbonate deposits. *Geochimica et Cosmochimica Acta,* **72**, 4976 – 4982.

Rogerson, M., Pedley, H.M., and Middleton, R. (2010) Microbial influence on macroenvironment chemical conditions in alkaline (tufa) streams: perspectives from *in vitro* experiments. In: H.M. Pedley and M. Rogerson (Editors), *Speleothems and Tufas: Unravelling Physical and Biological controls*. Geological Society Special Publication. Geological Society of London, London, pp. 65-81.

Romani, A. M., Fund, K., Artigas, J., Schwartz, T., Sabater, S., Obst, U. (2008). Relevance of polymeric matrix enzymes during biofilm formation. *Microbial Ecology* **56**, 427–436.

Rosenthal, Y., Boyle, E.A. and Slowey, N. (1997) Environmental controls on the incorporation of Mg, Sr, F and Cd into benthic foraminifera shells from Little Bahama Bank: Prospects for thermocline paleoceanography. *Geochimica et Cosmochimica Acta,* **61**, 3633– 3643, 1997.

Rosenthal, Y. and Lohmann, G. P. (2002) Accurate estimation of sea surface temperatures using dissolution-corrected calibrations for Mg/Ca palaeothermometry, *Paleoceanography*, **17(3),** 1044.

Rosenthal, Y. and Linsley, B. (2006) Mg/Ca and Sr/Ca Paleothermometery from Calcareous Marine Fossils. Chapter in the Encyclopedia of Quaternary Sciences, Elsevier Ltd.

Russell, A., Hönisch, B., Spero, H., Lea, D., 2004. Effects of seawater carbonate ion concentration and temperature on shell U, Mg, and Sr in cultured planktonic foraminifera. *Geochimica et Cosmochimica Acta,* **68(21)**, 4347–4361.

Rusznyák, A., Akob, D.M**.,** Nietzsche, S., Eusterhues, K., Totsche, K.U., Neu, T.R., Frosch, T., Popp, J., Keiner, R., Geletneky, J., Katzschmann, L., Schulze, E.D. and Küsel, K. (2012) Calcite biomineralization by bacterial isolates from the recently discovered pristine karstic Herrenberg cave. *Applied Environmental Microbiology,* **78(4)**, 1157–1167.

Salleh, S. and McMinn, A. (2011) The effects of temperature on the photosynthetic parameters and recovery of two temperate benthic microalgae, amphora cf. coffeaeformis and cocconeis cf. sublittoralis (bacillariophyceae). *Journal of Phycology,* **47**, 1413-1424.

Santschi, P.H., Bower, P., Nyffler, U.P., Azevedo, A., Broecker, W.S. (1983) Estimates of the resistance to chemical transport posed by the deep-sea boundary layer. *Limnology and Oceanography, 28, 899-912.*

Savin, S. M. and Douglas, R. G. (1973) Stable isotope and magnesium geochemistry of recent planktonic foraminifera from the south Pacific. *Geological Society of America Bulletin,* **84,** 2327–2342.

Schopf, W.J., Kudryavtsev, A.B.,Czaja, A.D. and Tripathi, A.B. (2007) Evidence of Archean life: Stromatolites and microfossils. *Precambrian Research,* **158**, 141–155.

Schrag, D. P. (1999) Rapid analysis of high-precision Sr/Ca ratios in corals and other marine carbonates. *Paleoceanography, 14*, 97–102.

Sekar, R., Nair, K.V.K., Rao, V.N.R., Venugopalan, V.P. (2002) Nutrient dynamics and successional changes in a lentic freshwater biofilm. *Freshwater Biology,* **47**, 1893-1907.

Sen Gupta, B.K. (2002) *Modern Foraminifera.* Kluwer Academic Publishers, Dordrecht, Germany.

Shannon, R.D., and Prewitt, C.T. (1969) Effective ionic radii in oxides and fluorides. *Acta Crystallographica*, **825**, 925-946.

Shen, C.C., Edwards, R.L., Cheng, H., Dorale, J.H., Thomas, R.B., Moran, S.B., Weinstein, S.E. and Edmonds, H.N. (2002) Uranium and thorium isotopic and concentration measurements by magnetic sector inductively coupled plasma mass spectrometry. *Chemical Geology,* **185**, 165– 178.

Shirai K., Kusakabe M., Nakai S., Ishii T., Watanabe T., Hiyagon H. and Sano Y. (2005) Deep-sea coral geochemistry: implication for the vital effect. *Chemical Geol*ogy, **224**, 212–222.

Shiraishi, F., Bissett, A., de Beer, D., Reimer, A., Arp, G. (2008a) Photosynthesis, respiration and exopolymer calcium-binding in biofilm calcification (Westerhöfer and Deinschwanger Creek, Germany). *Geomicrobiology Journal,* **25**, 83–94.

Shiraishi, F., Reimer, A., Bissett, A., de Beer, D. and Arp, G. (2008b) Microbial effects on biofilm calcification, ambient water chemistry and stable isotope records in a highly supersaturated setting (Westerhöfer Bach, Germany). *Palaeogeography, Palaeoclimatology, Palaeoecology,* **262**, 91–106.

Shiraishi, F., Okumura, T., Takahashi, Y., Kano, A., (2010) Influence of microbial photosynthesis on tufa stromatolite formation and ambient water chemistry, SW Japan. *Geochimica et Cosmochimica Acta,* **74**, 5289–5304.

Sinclair, D.J., Kinsley, L.P.J.,McCulloch,M.T. (1998) High resolution analysis of trace elements in corals by laser ablation ICP–MS. *Geochimica et Cosmochimica Acta*, **62**, 1889–1901.

Singh, L. and Singh, L. (1972) Chemical and morphological composition of kankar nodules in soils of the Vindhyan region of Mirzapur, India. *Geoderma,* **7**, 269 – 276.

Soetaert, K., Hofmann, A.F., Middleburg, J.J., Meysman, F.J.R., and Greenwood, J., (2007) The effect of biogeochemical processes on pH: *Marine Chemistry*, **105,** 30–51,

Stal, L.J. (2010) Microphytobenthos as a biogeomorphological force in intertidal sediment stabilization. *Ecological Engineering,* **36(2)**, 236-245.

Stephensen, A.E., Hunter, J.L., Han, N., DeYereo, J.J., Dove, P.M. (2011) Effect of ionic strength on the Mg content of calcite: Toward a physical basis for minor element uptake during step growth. *Geochimica et Cosmochimica Acta*, **75(15)**, 43404360.

Stoodley P., Sauer, K., Davies, D.G., Costerton J.W. (2002) Review. Biofilms as complex differentiated communities. *Annual Review of Microbiology,* **56**, 187-209.

Suarez, D.L. (1983) Calcite Supersaturation and Precipitation Kinetics in the Lower Colorado River, All-American Canal and East Highline Canal. *Water Resources Research,* **19(3)**, 653-661.

Sutherland, I.W. (1999) Biofilm exopolysaccharides. In: Wingender J, Neu TR, Flemming H-C, editors. *Microbial extracellular polymeric substances: Characterization, structure and function*. Berlin: Springer. pp 73–92.

Sutherland, J.W. (2001) Biofilm exopolysaccharides: a strong and sticky framework. *Microbiology,* **147**, 3–9.

Takashima, C. and Kano, A. (2008) Microbial processes forming daily lamination in a stromatolitic travertine. *Sedimentary Geology,* **208(3-4)**, 114-119.

Tang, J., Dietzel, M., Böhm, F., Köhler, S.J., Eisenhauer, A. (2008) Sr^{2+}/Ca^{2+} and $^{44}Ca/^{40}Ca$ fractionation during inorganic calcite formation: I. Sr incorporation. *Geochimica et Cosmochimica Acta*. **72**, 3733–3745.

Terakado, Y. and Taniguchi, M. (2006) A new method for the study of trace element partitioning between calcium carbonate and aqueous solutions: a test case for Sr and Ba incorporation into calcite. *Geochemistry Journal*, **40**, 161–170.

Teranes, J.L., McKenzie, J.A., Lotter, A.F., Sturm, M., (1999) Stableisotope response to lake eutrophication: calibration of a highresolution lacustrine sequence from Baldeggersee, Switzerland. *Limnology and Oceanography,* **44**, 320–333.

Tesoriero, A. and Pankow, J. (1996) Solid solution partitioning of Sr^{2+}, Ba^{2+}, and Cd^{2+} to calcite. *Geochimica et Cosmochimica Acta*, **60**, 1053–1063.

Tourney, J. and Ngwenya, B.T. (2009) Bacterial extracellular polymeric substances (EPS) mediate $CaCO_3$ morphology and polymorphism. *Chemical Geology,* **262(3-4)**, 138-146.

Toyofuku, T., Kitazato, H., Kawahata, H., Tsuchiya, M., Nohara, M. (2000) Evaluation of Mg/Ca thermometry in foraminifera: comparison of experimental results and measurements in nature. *Paleoceanography,* **15**, 456–464.

Tucker, M.E. and Wright, V.P. (1990) *Carbonate Sedimentology.* Blackwell Science Publications, London.

Turner, E.C. and Jones, B. (2005) Microscopic calcite dendrites in cold-water tufa: implications for nucleation of micrite and cement. *Sedimentology,* **52**, 1043–1066.

Verheyden S., Keppens E., Fairchild I.J., McDermott F. and Weis D. (2000) Mg, Sr and Sr isotope geochemistry of a Belgian Holocene speleothem: implications for paleoclimate reconstructions. *Chemical Geology*, **169**, 131-144.

Visscher, P.T., Stolz, J.F. (2005) Microbial mats as bioreactors: populations, processes, and products. *Palaeogeography, Palaeoclimatology, Palaeoecology* **219**, 87–100.

Vu, B., Chen, M., Russell, J.C., and Ivanova, E.P. (2009) Bacterial Extracellular Polysaccharides Involved in Biofilm Formation. *Molecules* **14,** 2535-2554.

Walter, L.M., 1986, Relative efficiency of carbonate dissolution and precipitation during diagenesis: A progress report on the role of solution chemistry. In: Gautier,

D.L., ed., *Roles of Organic Matter in Sediment Diagenesis: Society of Economic Paleontologists and Mineralogists Special Publication* 38, pp. 1–11.

Wang, Y. and Xu, H. (2001) Prediction of trace metal partitioning between minerals and aqueous solutions: a linear free energy correlation approach. *Geochimica et Cosmochimica Acta* **65**, 1529–1543.

Wang, D.B., Wallace, A.F, De Yoreo, J.J., Dove, P.M. (2009) Carboxylated molecules regulate magnesium content of amorphous calcium carbonates during calcification. *Proceedings of National Academy of Sciences U.S.A.,* **106**, 21511–21516.

Warren, L.A., Maurice, P.A., Ferris, F.G. (2001) Microbially Mediated Calcium Carbonate Precipitation: Implications for Interpreting Calcite Precipitation and for Solid-Phase Capture of Inorganic Contaminants. *Geomicrobiology Journal,* **18(1)**, 93 – 115.

Watermanm F., Hillebrand, H., Gerdes, G., Krumbein, W.E., Sommer, U. (1999) Competition between benthic cyanobacteria and diatoms as influenced by different grain sizes and temperatures. *Marine Ecology Progress Series,* **187**, 77-87.

Webster, A. and May, E. (2006) Bioremediation of weathered-building stone surfaces. *Trends in biotechnology*, **24**, 6.

Wei, G., Sun, M., Li, X., Nie, B., (2000) Mg/Ca, Sr/Ca and U/Ca ratios of a porites coral from Sanya Bay, Hainan Island, South China sea and their relationships to sea surface temperature. *Palaeogeography Palaeoclimatology Palaeoecology*, **162**, 59–74.

White, W.M. (2007) Geochemistry [Online]. Available from:
http://geoweb.gg.uwyo.edu/geol4490/White%20Geochemistry/Chapter02.pdf
[Accessed 26 May, 2012].

Wilson, R.C.L., Drury, S.A., Chapman, J.L. (2000) *The great ice age: climate change and life.* New York: Routledge.

Wingender, J., Neu, T. R. and Flemming, H. C. (1999) What are bacterial extracellular polymeric substances In: Wingender, J., Neu, T. R..and Flemming, H. C Eds. *Microbial extracellular polymeric substances - Characterization, Structure and Function*. New York, Springer.

Wolfaardt, G.M., Lawrence, J.R., Robarts, R.D., Caldwell, D.E. (1998) In situ characterization of biofilm exopolymers involved in the accumulation of chlorinated organics. *Microbiolial Ecology,* **35**, 213–223.

Wong, C., Banner, J.L., Musgrove, M. (2011) Seasonal dripwater Mg/Ca and Sr/Ca variations driven by cave ventilation: Implications for and modelling of speleothem palaeoclimate records *Geochimica et Cosmochimica Acta,* **75**, 3514-3529.

Wright, V.P. and Tucker, M.E. (1991) *Calcretes.* Blackwell Scientific Publications, London.

Yu, K.F., Zhao, J.X., Wei, G.J., Cheng, X.R., Chen, T.G., Felis, T., Wang, P.X., Liu, T.S. (2006) δ^{18}O, Sr/Ca and Mg/Ca records of Porites lutea corals from Leizhou Peninsula, northern South China Sea, and their applicability as palaeoclimatic indicators. *Palaeogeography, Palaeoclimatology, Palaeoecloogy,,* **218**, 57–73.

Yusuf N. (1980) Magnesium and strontium in Foraminiferen-Schalenas Anzeiger fur Paleosalinitat. Neues Jahrb. *Geology and Paleontology,* **6**, 373–384.

Zhang, D.D., Zhang, Y., Zhu, A. and Cheng X. (2001) Physical Mechanisms of River Waterfall Tufa (Travertine) Formation. *Journal of Sedimentary Research*, **71**, 205-216.

Zhang, X. Q., Bishop, P. L. & Kupferle, M. J. (1998) Measurement of polysaccharides and proteins in bio®lm extracellular polymers. *Water Science Technology,* **37**, 345-348.

Zhang, Y. and Dawe, R.A. (2000) Influence of Mg^{2+} on the kinetics of calcite precipitation and calcite crystal morphology. *Chemical Geology,* **163**, 129-138.

Zhong S. and Mucci A. (1989) Partitioning of rare earth elements (REE's) between calcite and seawater solutions at 25°C and 1 atm and high dissolved REE concentrations. *Geochimica et Cosmochimica Acta,* **59,** 443– 453.